An Investigation of the Equivalence Between Combline and Evanescent-mode Waveguide Filters & of Aspects Related to Reduction of Manufacturing Costs for Combline Filters

by

Shamim O. Nassar

Thesis presented in partial fulfilment of the requirements for the degree of Master of Science in Engineering at the Faculty of Engineering, Stellenbosch University

Supervisor: Prof. Petrie Meyer
Co-Supervisors: Prof. P. W. van de Walt and Dr. Dirk de Villiers

Department of Electrical & Electronic Engineering

December, 2011

Declaration

By submitting this thesis electronically, I declare that the entirety of the work contained therein is my own, original work, that I am the sole author thereof (save to the extent explicitly otherwise stated), that reproduction and publication thereof by Stellenbosch University will not infringe any third party rights and that I have not previously in its entirety or in part submitted it for obtaining any qualification.

Date: December 2011

Signed: _____

Date: 21st November, 2011

Abstract

Keywords *- Combline filter, Evanescent-Mode Waveguide Filter*

An investigation of the functional similarities and differences between a combline filter and an evanescent-mode waveguide filter is presented. The design theory of the two types of filters is outlined. Two filters are designed to operate at a centre frequency of 2 GHz with a 5% bandwidth using similar waveguide dimensions, but using the two different design theories. The bandpass characteristics of the two filters are then compared over the primary passband and over a broad range of frequencies to observe the stopband characteristics. It is shown that a combline filter with a large groundplane spacing behaves like an evanescent-mode waveguide filter but a difference in bandwidth exists between the two.

Different aspects related to the manufacture of coaxial cavity filters are addressed with specific emphasis on cost reduction. The considerations to be made when choosing the right materials, manufacturing techniques and surface finishes for microwave coaxial cavity filters so that good performance is obtained while reducing the overall costs associated with manufacturing are discussed. The concept of Design for Manufacture (DFM) is discussed.

Three combline filters are designed for reduced manufacturing cost, applying different changes in the physical structure to suit the specific manufacturing technique used. Two of these have the same design specifications, operating at a centre frequency of 1.3 GHz with a 10% bandwidth but are designed for manufacture using two different manufacturing techniques: milling and wire-cutting EDM. The third filter is designed for manufacture using a combination of the milling and wirecutting processes to have a bandwidth of 1.8% with the primary passband centred at 2.125 GHz. Problems encountered in manufacturing are explained, one of which results in the use of waterjet cutting for the manufacture of filters initially supposed to be manufactured using wirecutting EDM. Measurement results for the manufactured filters show a good agreement between the bandwidths of the 3D electomagnetic simulation results. The obtained results also show the effects of poor surface finishing and of deformations on the resonant frequency and the unloaded Q of the filters.

Opsomming

Sleutelwoorde: *Kamlynfilter, Golfleier-onder-afknip filter, grondvlak spasiëring*

'n Studie van die funksionele ooreenkomste en verskille tussen kamlynfilters en golfleier-onder-afknip filters word aangebied. Die ontwerpstegnieke van beide tipes filters word aangebied. Twee filters word ontwerp met 'n senterfrekwensie van 2GHz en 'n bandwydte van 5%, met soortgelyke golfleierafmetings maar deur gebruik te maak van die verskillende ontwerpstegnieke. Die gedrag van die twee filters word vergelyk in die deurlaatband sowel as oor 'n wye stopband. Dit word getoon dat 'n kamlynfilter met 'n groot grondvlakspasiëring soos 'n golfleier-onder-afknip filter optree, met 'n verskil in bandwydte.

Verskillende aspekte wat verband hou met die vervaardiging van koaksiale filters, met spesifieke klem op koste vermindering, word aangebied. Die oorwegings wat die keuses van materiaal, vervaardigingstegnieke en oppervlakte afwerking beïnvloed word bespreek. Die konsep van Ontwerp vir Vervaardiging (DFM in Engels) word bespreek.

Drie kamlynfilters word ontwerp vir verminderde vervaardigingskoste deur die fisiese sruktuur aan te pas by die spesifieke vervaardigingstegniek. Twee van die filters het dieselfde spesifikasie, naamlik 'n senterfrekwensie van 1.3GHz en 'n 10% bandwydte, maar word ontwerp vir twee verskillende vervaardigingsprosesse, naamlik frees en draadsny. 'n Derde filter word ontwerp vir 'n kombinasie van hierdie twee prosesse, en met 'n senterfrekwensie van 2.125GHz en 'n bandwydte van 1.8%. Probleme met die vervaardiging word bespreek, onder andere die verandering van draadsny na water-sny tegnieke. Gemete resultate toon goeie ooreenstemming met die teoretiese analise wat die bandwydtes betref, maar swak oppervlak afwerking het 'n verswakking van die onbelaste Q van die resoneerders tot gevolg.

"The Empires of the future are the Empires of the mind."

~ ***Winston Churchill***

~*~*~*~*~*~*~*~*~*~*~*~*~*~*~

"If I have seen further, it is by standing on the shoulders of giants."

~ ***Isaac Newton***

Acknowledgements

- My first words of appreciation go to the Almighty for having granted me the patience and strength to complete my masters degree and for having granted me the opportunity to meet all the people with whom I have worked closely during the two years of my studies.
- I owe my deepest gratitude to my supervisor Prof. Petrie Meyer for the constant words of encouragement and very appreciated advice. The optimism with which he approaches situations has been a great lesson and I can only hope that I have learn't how to apply it well. It has been a great honour to have worked under his supervision.
- To my co-supervisors Prof. P. W. van de Walt and Dr. Dirk de villiers, I am greatly indebted for all the invaluable advice given and the wonderful supervision and patience. I have learn't so much from them and for that I am very grateful.
- I cannot possibly find enough words to express my gratitude to my colleagues in Room 206 (David Prinsloo, David Smith, Phillip Terblanche, Sunelle Otto and Ngoy Mutonkole) for creating just the right environment to work in, for making my stay in South Africa easier for me and for always being ready to help. You are all just wonderful.
- I would also like to thank my other colleagues Theunis Beukman and Rodwell Bakolo for sharing some good pieces of advice every now and then.
- To Mr. Wessel Croukamp, I am very grateful for his assistance in assembling my filters in a very short amount of time.
- I am also thankful to Mr. Stephan Nortje of Reutech Radar Systems for his useful insight into the world of manufacturing, Mr. Willie Lombard of CHG Engineering for the manufacturing of my filters and Mr. Willie Conradie of Executive engineering for advice in regard to manufacturing.
- To my family, I am very thankful for the never ending support. They have always believed in me and supported my choices and I wouldn't ask for anything more than that.
- I would also like to specially thank Abdallah Hatimy for always being very encouraging.
- Much appreciation to my friends for always being willing to listen and to advice and for the laughter that is always welcome.
- Last but not least, much appreciation to Reutech Radar Systems for financial support.

Contents

List of Figures

List of Tables

Chapter 1

Introduction

1.1 Historical Development Of Microwave Filter Design

Modern filter design dates back to early 20th century, prior to the World War II. Since that period, the demand for better communication systems has created a need for more effective filters, enabling transmission of frequencies within defined passbands and having progressively better selectivity at the transition into the stopband.

Even though microwaves now have numerous applications in the communications arena, the initial development of devices operating at these frequencies was motivated by military requirements. In the late 19th century, after experimental verification of the electromagnetic theory of Faraday and Maxwell, the area of electromagnetics suddenly attracted attention from physicists and engineers.

The roots of modern day transmission line theory can be ascribed to work done by Oliver Heaviside in the late 19th century. He was the first to introduce the concept that metallic conductors act to guide an electromagnetic wave [1]. He was convinced that guided waves required two leads as a pair of parallel wires, or if only a single one was used, then it would need earth, or have something equivalent to act as a second conductor. He also considered propagation within a hollow guide, but thought it impossible that a wave could be propagated in such a medium without an inner conductor. Shortly afterwards, J. Larmor investigated the theory of resonant structures such as coaxial metallic cylinders and a single dielectric cylinder [1].

The possibility of propagating electromagnetic waves in hollow guides was later to be confirmed by Lord Rayleigh in 1897 [1]. He defined the concept of propagation of transverse electric and magnetic waves, and found that the existence of such waves was dependent on a cut-off frequency, and on the cross-sectional dimensions of the guide.

In the 1930s, the scientists at Bell Laboratories and the Massachusetts Institute of Technology got involved in more experiment-based research on waveguides [2]. Initially unaware of Rayleigh's earlier paper, their interest was oriented towards investigating the transmission line properties of waveguides as a low-loss alternative to the use of open-wire and coaxial lines.

Work on microwave filters started before World War II. One of earliest papers of the topic was published in 1937 by W.P. Mason and R. A. Sykes in which they used ABCD parameters to derive the image impedance and image phase and attenuation functions of a variety of filter sections[3]. Major advances mainly using image parameters were made at various laboratories in the United States during the World War II years of 1941 to 1945 [3]. At the MIT Radiation laboratory, most of the work was on waveguide filters, whereas the Harvard Radio Research Laboratory focused mainly on broad-band low-pass, bandpass and high-pass filters for ECM (Electronic Counter Measures) applications and also on narrow-band tunable coaxial resonator filters for search

receivers [3]. The Radiation Laboratory and associated microwave laboratories in the USA and in the UK produced some of the the best scientists and engineers in the world. Some of the more commonly known names are: H. A. Bethe, N. A Marcuvitz, E. M. Purcell and J. Schwinger. N. A. Marcuvitz authored the *Waveguide Handbook* during the World War II period, a classic book characterising microwave behavior which is still used in the field of microwave engineering today.

Modern distributed circuit theory may be considered to have begun when Paul I. Richards published a paper on commensurate resistor-transmission-line circuits, in 1948 [3]. In 1955, K. Kuroda published, in a Japanese thesis, a set of transformations, which enable unit elements of characteristic impedance equal to that of the load or generator to be introduced into a network to separate the short- and open-circuited stubs physically [3]. These transformations first appeared in English in 1958, in a paper by Ozaki and Ishii [3].

Initial theories on direct-coupled cavity filters are attributed to Fano and Lawson based on their work in [4]. They argued that a simple resonant cavity does not provide sufficient out-of-band attenuation for a given minimum stopband insertion loss [4]. This led to the investigation of the use of a chain of cavities directly coupled to each other, in an attempt to obtain more satisfactory characteristics. They showed that narrow-band microwave filters, consisting of a chain of cavities all tuned to a single frequency, could be derived from corresponding lumped-element filters [4]. However, even though their theory revolved around a low-pass prototype, the implementation was tedious. It required a difficult synthesis technique at an era without computers. Specific formulas were later defined for the Butterworth and Chebyshev low-pass prototypes in [36, 35], and extensive look-up tables were established in the *Handbook of Filter Synthesis* by Anatol Zverev.

Developments to the theory of direct-coupled cavity filters followed in a paper by Cohn [5]. Apart from extending the range of applicability to broader bandwidths, this paper also presented very simple specific equations for the low-pass prototypes, lumped-constant filters, waveguide filters and strip-line filters. He introduced the idea of inter-cavity couplings by means of impedance inverters, a theory that was later on further extended by Levy [6].

Parallel-coupled filters were first introduced in 1958. Theory on these was first published by Cohn in April 1958[7] and also appeared in a paper by Ishii and Ozaki in June of the same year [8]. Research on these established the foundation for interdigital and combline filters.

In 1962, George Matthaei published design procedures permitting direct design of bandpass filters using interdigital arrays of resonator line elements between parallel ground planes, from lumped-element, lowpass prototype filters [9]. The following year, he proceeded on to publish a paper on the theory and realisation of combline filters [10].

Around the same period, waveguide filter design was challenged by the concept of transmission using below cut-off waveguide filters, otherwise termed evanescent-mode filters. The filter consisted of a finite length waveguide with axially-spaced screws, a configuration which exhibits bandpass characteristics below the cut-off frequency of the guide, arguably due to the evanescent form of the TE_{10} mode [11]. Owing to similarities in response and construction, it has been argued that evanescent-mode filters are merely waveguide-coupled versions of the combline filter [11].

Microwave circuits are modelled using commercial electromagnetic solvers based on well-established numerical methods for solving Maxwell's equations. Computer Aided Design (CAD) from a strictly circuit point of view only gained momentum in the 1970s with the wide availability of mainframe computers [12]. Numerical electromagnetics began to emerge at around the same period, with access to computers being easier than before. The commercial field solvers were made a practical reality only in the 1990s using the UNIX workstation and personal computers (PCs) [12]. They are often used in concurrence with circuit-theory-based CAD.

Full-wave 3D Electromagnetic simulation has become an important part of a microwave engineer's workflow. 3D EM field simulation of microwave and RF circuit designs allows the engineer to consider many higher order effects such as complex 3D discontinuities, interaction of components with the layout, unwanted coupling, box

resonances, parasitic radiation etc [38]. *Sonnet Software* was one of the earliest commercial suppliers of EM simulation software. They offer a three-dimensional (3D) planar EM simulator that is an intelligent blend of analysis power and processing speed, usually trade-offs for most EM simulators [39]. Other key EM tools are: HFSS from *Ansoft*, CST Microwave Studio from *Computer Simulation Technology*, and Momentum from *Agilent Technologies*. These assist designers in tackling almost any high frequency EM analysis problems. A unique 3D EM/circuit co-simulation enables a designer to even include highly non-linear components into a circuit layout, providing reliable results in time and frequency domain.

Other examples of proffessional design tools used in the RF and microwave industry are *Microwave Office* and *AXIEM*, both from *AWR Corporation*. Built on the unique AWR high-frequency design environment platform with its unique unified data model, Microwave Office offers unparalleled intuitiveness, powerful and innovative technologies, and unprecedented openness and interoperability, enabling integration with best-in-class tools for each part of the design process [41]. Microwave Office design suite encompasses all the tools essential for high-frequency IC, PCB and module design, including: linear circuit simulators, non-linear circuit simulators, electromagnetic (EM) analysis tools, and integrated schematic and layout Statistical design capabilities [41]. AWR's AXIEM electromagnetic (EM) software benefits designers most by helping to diagnose issues early, thereby significantly shortening the design process due to its speed, capacity and accuracy. The AXIEM product was developed specifically for three-dimensional (3D) planar applications such as RF PCBs and modules, LTCC, MMIC, and RFIC designs [41].

The main aim of recent advances in filter design has been to reduce the physical size of the devices, whilst retaining or improving the electrical characteristics. Current design techniques, with the aid of computer simulation technology, boast reduction of design and manufacture time and cost.

1.2 Aims and Objectives

This thesis addresses two major topics. The first topic is that of the equivalence between evanescent-mode waveguide filters and combline filters, and the conditions under which the use of one is preferred over the other. The second topic addresses the issue of cost reduction in the manufacture of the combline and evanescent-mode waveguide filters. The main aims of the thesis can therefore be outlined as follows:

1. To investigate the functional differences between Evanescent-mode filters and Combline filters.
2. To investigate the aspects affecting the cost of manufacture of these types of filters and strategies that can be employed to reduce these costs.

To meet these main aims, the approach to be taken in this thesis can be summarised to encompass:

- The design of Combline filters.
- The detailed design of Evanescent-mode filters.
- A discussion of the relevant results pertaining to the operation of the two filters.
- A comparison of their responses, and an analysis of their functional differences.
- An investigation of factors related to manufacturing of the filters.
- Recommendations for necessary changes relevant to cost reduction.
- The design of filters in accordance to the recommendations for cost reduction.

The Electomagnetic Simulation tools used here are CST (Computer Simulation Technology) and MWO (Microwave Office).

1.3 Overview of the Thesis

This document is structured into seven chapters, the contents of which are outlined below.

Chapter 2: Design of Combline Filters

This chapter discusses the different characteristics of coaxial line filters that are important in the design of combline filters and covers the design process of both the circuit model design of a combline filter and the 3D physical model design of the filter.

Chapter 3: Design of Evanescent-Mode Waveguide Filters

Chapter 3 covers the design of evanescent-mode waveguide filters, with discussions on evanescent-mode waveguides, characteristics of evanescent-mode resonators and the detailed design process for circuit model of the filter and the 3D physical model.

Chapter 4: The Equivalence Between Combline and Evanescent-mode Waveguide Filters

In this chapter, combline filters and evanescent-mode waveguide filters are designed using a similar set of specifications. Both the circuit-based design and physical realisation using 3-D electromagnetic solvers are outlined. A detailed discussion of their performance and a comparison of the two based on the performance and structure is also included.

Chapter 5: Manufacture of Microwave filters and Cost-related aspects

This chapter investigates different aspects related to the manufacturing of filters, and also investigates the effects that these have on the accumulated costs of manufacture. The chapter discusses different manufacturing technology used, choice of materials and coatings, a break-down of costs and also addresses the concept of Design for Manufacture (DFM).

Chapter 6: Design of Combline Filters for reduced manufacturing costs

In this chapter, Combline filters are designed in accordance with the recommendations given in chapter 4. The design process is outlined in detail, discussing the options available at each stage of design and the decisions made in order to minimise the costs of manufacture. The chapter also includes the measurement results for the filters designed for reduces manufacturing costs.

Chapter 7: Conclusion

The final chapter gives a conclusive discussion and relevant recommendations in accordance with the work outlined in the preceding chapters.

Chapter 2

Design of Combline Filters

2.1 Introduction

Combline bandpass filters are some of the most commonly used bandpass filters owing to their compactness, ease of design, good unloaded Q factors and because very broad stopbands can be achieved with this type of filter.

Combline filters are constructed from parallel coupled transmission lines all shorted at the same end, forming a comb-like structure, hence the name. A typical construction of the filter is shown in figure 2.1.

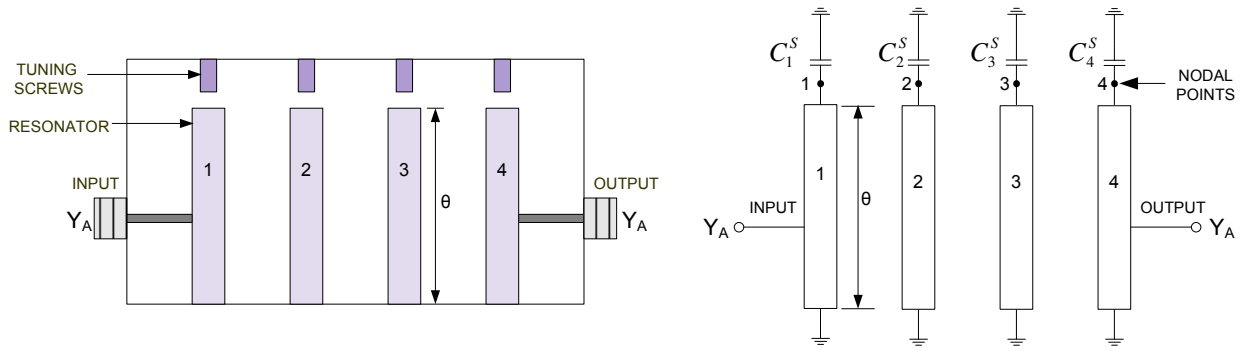

Figure 2.1: A combline Bandpass filter

In figure 2.1 (b) the capacitance between the transmission lines and enclosure, C_j^S, for each of the four resonators, is a capacitance due to the gap between the end of the resonator post and the tuning screw in figure 2.1 (a). The port admittances have been labelled Y_A and θ is the electrical length of the transmission lines.

This chapter focuses on the design of these filters, with subsequent sections discussing the design of the circuit model of such filters and their physical implementation. Different characteristics defining the performance of these filters will be discussed, with relevant plots to support the discussions. The chapter also includes the design of a fourth order combline filter with a Chebyshev characteristic, operating at a frequency of 2GHz and having a passband ripple of 0.5dB. The circuit is modelled in Microwave Office (MWO) and the physical structure is modelled in Computer Simulation Technology (CST) software, a 3D electromagnetic field solver. The discussions and designs in this chapter act as a basis for investigations in Chapter 4 on the characteristics of this type of filter in relation to an evanescent-mode waveguide filter (to be discussed in chapter 3) and for the designs to be covered in later chapters.

2.2 Circuit Model for a Combline Filter

The main aim of this section is to design a circuit model for a 2GHz, 4th order combline filter. The section begins with a discussion on transmission line resonators, focusing mainly on coaxial type resonators which are used in a combline filter. The section then discusses the circuit model for a single combline resonator, before focusing on the coupling of two such resonators. To end the section, the realisation of a full filter is discussed and a 2GHz, 4th order combline filter is designed to have a fractional bandwidth of 5 % and a passband ripple of 0.5dB.

2.2.1 Characteristics of Transmission-line resonators

In microwave filter designs, a length of transmission line terminated in either an open-circuit or a short-circuit is often used as a resonator. Figure 2.2 illustrates some typically used resonators of this type. Each of these resonators can be represented by a lumped element circuit equivalent to the resonator at centre frequency.

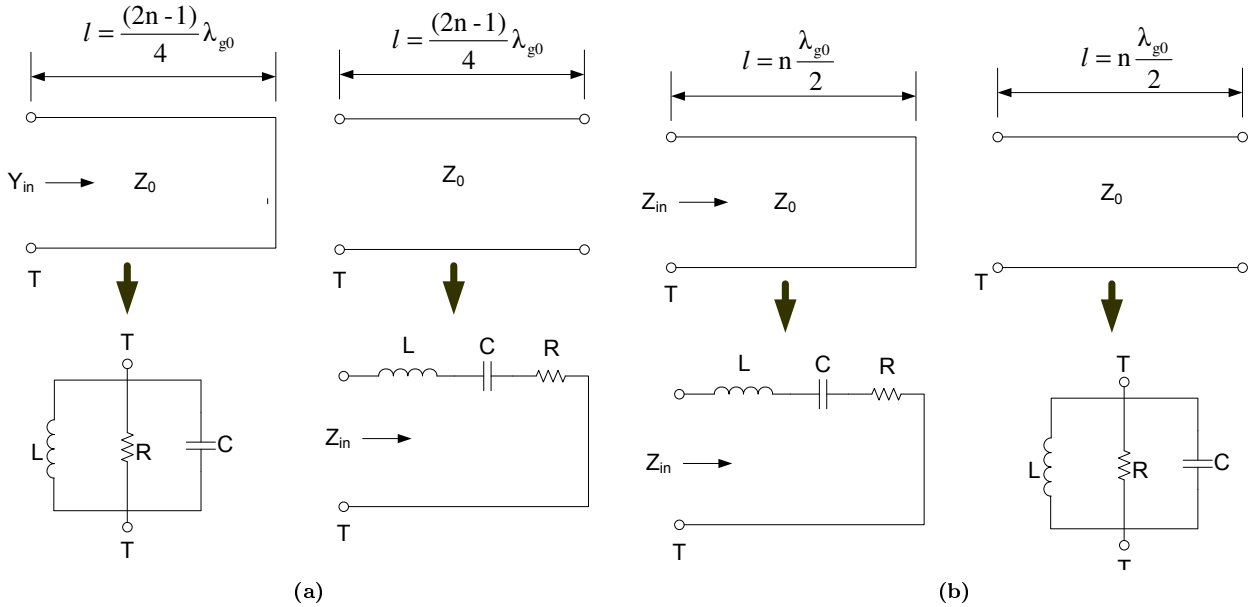

Figure 2.2: Transmission line resonators and their lumped-constant equivalents

The resistance, R, in the lumped equivalent circuits of figure 2.2 is dependent on the loss factor of the transmission lines at resonance. For lossless lines, both would be zero. The reactive elements in the lumped equivalent circuits are determined by equating the *slope parameters* of the lumped element circuits to those of the transmission line circuits, exhibiting the same type of resonance (series or parallel). For resonators with a series type of resonance, the *reactance slope parameter*, which is the slope of the reactance as a function of frequency, is used. It is generally defined as [15]

$$\chi = \frac{\omega_0}{2}\frac{dX}{d\omega}\bigg|_{\omega_0} \Omega \tag{2.1}$$

For resonators with a parallel type of resonance, the *susceptance slope parameter* is applied and is given by

$$\flat = \frac{\omega_0}{2}\frac{dB}{d\omega}\bigg| S \tag{2.2}$$

Combline filters have resonator lines that are less than $\frac{\lambda_0}{4}$ long at resonance. These are short-circuited at one end, with the other end terminated in a capacitance to ground. This capacitance can be realised by a gap at

the end of the transmission line and the ground housing resulting in the standard combline resonator shown in figure 2.3.

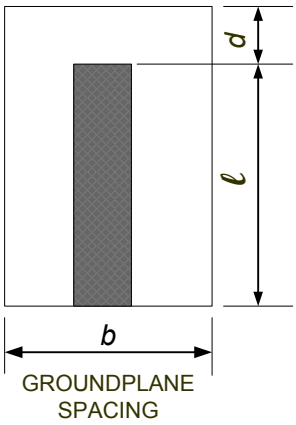

Figure 2.3: Representation of a Combline Resonator

Three characteristics of resonators are of prime importance in filter design: the impedance, the Q-factor and the filter's higher order resonances.

Characteristic Impedance of a Coaxial-Line Resonator

The characteristic impedance of a coaxial resonator is a function of the cross-sectional dimensions of the line and the dielectric constant of the dielectric between the conductors. For a combline structure, the resonator forms the inner conductor and the surrounding enclosure forms the outer conductor of coaxial lines, typical examples of which can be seen in the cross-sectional views shown in figure 2.4. The cross-section of the inner conductor can take up different shapes, but the more common ones are circular and rectangular or square. The outer conductor can also be either circular, square or rectangular in cross-section.

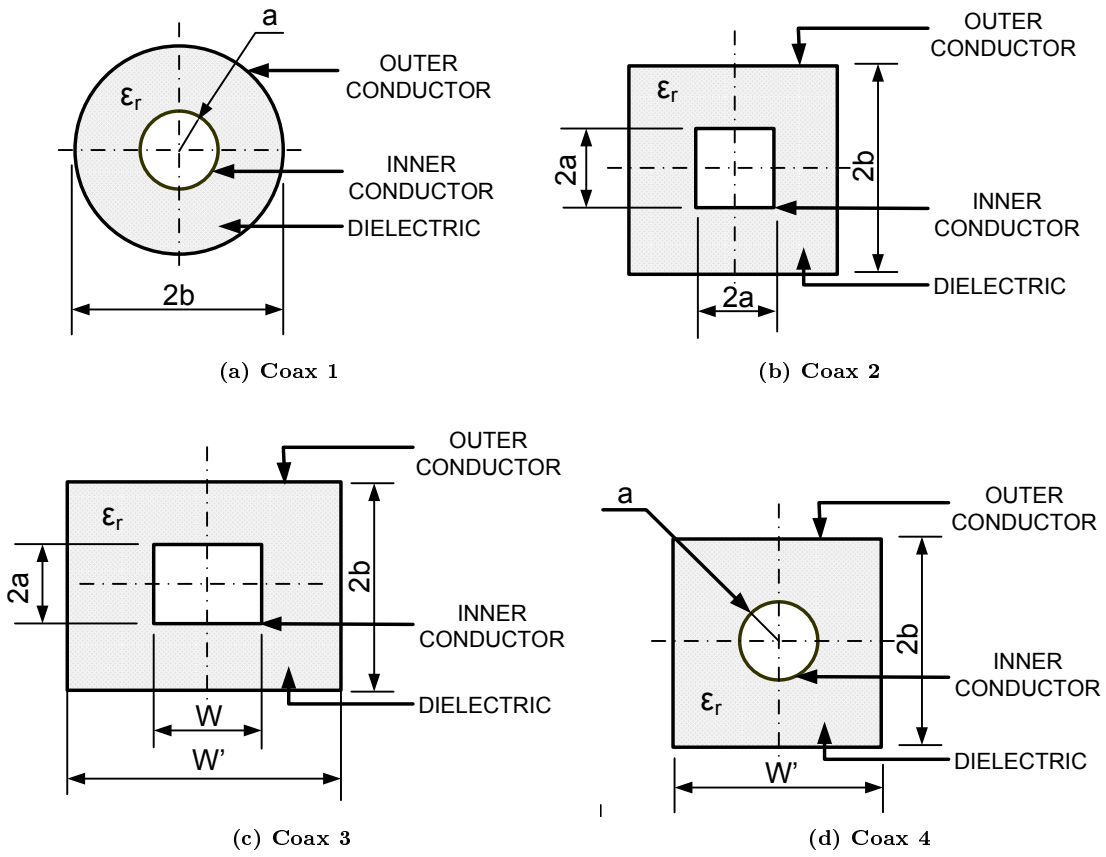

(a) Coax 1 (b) Coax 2

(c) Coax 3 (d) Coax 4

Figure 2.4: Coaxial Transmission lines

The characteristic impedances for the coaxial line in figures 2.4 (a), (b) and (c) are given as [31]

$$Z_{0\,Coax\,1}\sqrt{\varepsilon_r} = 59.952 \ln \frac{b}{a} \text{ Ohm} \tag{2.3}$$

$$Z_{0\,Coax\,2}\sqrt{\varepsilon_r} = 136.7 \log_{10}\left(0.9259\frac{b}{a}\right) \text{ Ohm} \tag{2.4}$$

$$Z_{0\,Coax\,3}\sqrt{\varepsilon_r} = 59.952 \ln\left(\frac{1 + {}^{W'}/_{b}}{{}^{W}/_{b} + {}^{t}/_{b}}\right) \text{ Ohm} \tag{2.5}$$

The characteristic impedance of the coaxial line in figure 2.4 (c) [Coax 3] is plotted below in figure 2.5.

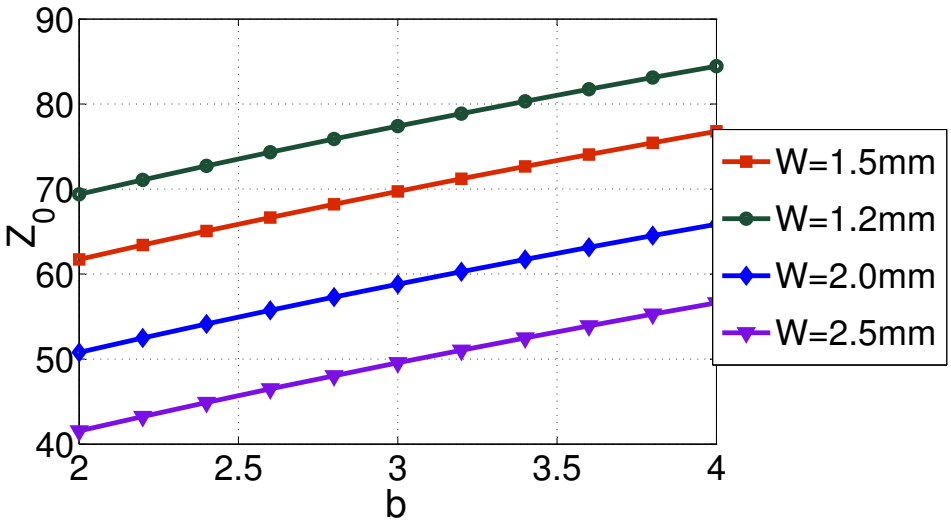

Figure 2.5: Characteristic Impedance of the Coaxial Line in Figure 2.4 (c) for Different W, when W'=5mm and a=0.5mm

Lower impedances are obtained for larger values of the dimension W when W' is maintained. The characteristic impedance can also be decreased by decreasing 'b'.

For the coaxial line in figure 2.4 (d), when $W' = 2b$ so that the outer conductor is a square, the characterisitic impedance is given as [31]

$$Z_{0\,Coax\,4}\sqrt{\varepsilon_r} = 59.952 \ln\left(1.0787\frac{b}{a}\right) \text{ Ohm} \tag{2.6}$$

Analysis of this line for $W' > 2b$ is difficult with few numerical solutions for the computation of the characteristic impedance. In [31], a table of impedance data for this type of line (figure 2.4 (d)) is provided, based on Cristal's Analysis. The data is used to plot a graph of the characteristic impedance of the line varied against the ratio $\frac{a}{b}$ for different $\frac{W'}{b}$. The graph is shown below in figure 2.6.

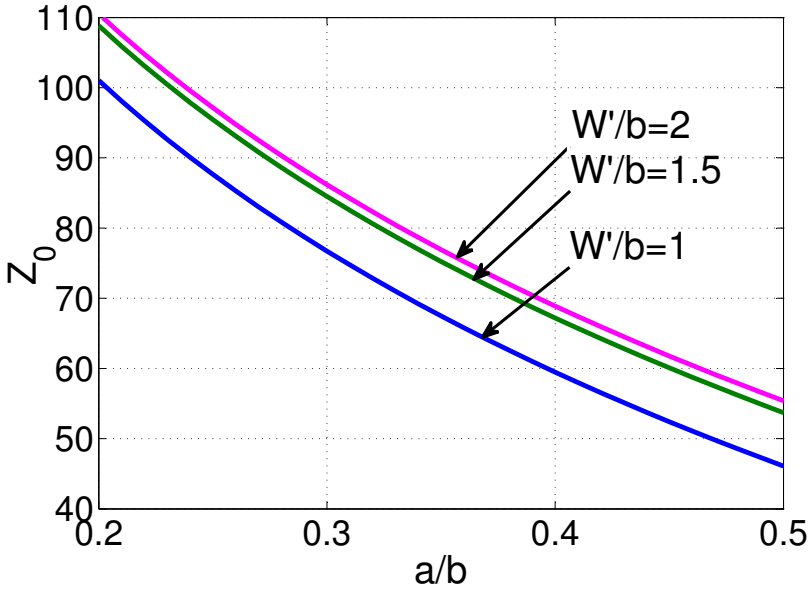

Figure 2.6: Variation of the Characteristic impedance of the Coaxial Line in Figure 2.4 (d) with Changes in $\frac{a}{b}$

By increaing the ratio $\frac{W'}{b}$, by increasing the length of the longer rectangle edge, the characteristic impedance

of the line is increased, so that a square coaxial line ($\frac{W'}{b} = 1$) gives the lowest characteristic impedance for the provided range of $\frac{a}{b}$. Notable also is the decrease in characteristic impedance with either and increase in the dimension 'a' or a decrease in the dimension 'b'.

A plot comparing the characteristic impedances of the all the coaxial lines shown in figure 2.4 is given in figure 2.7.

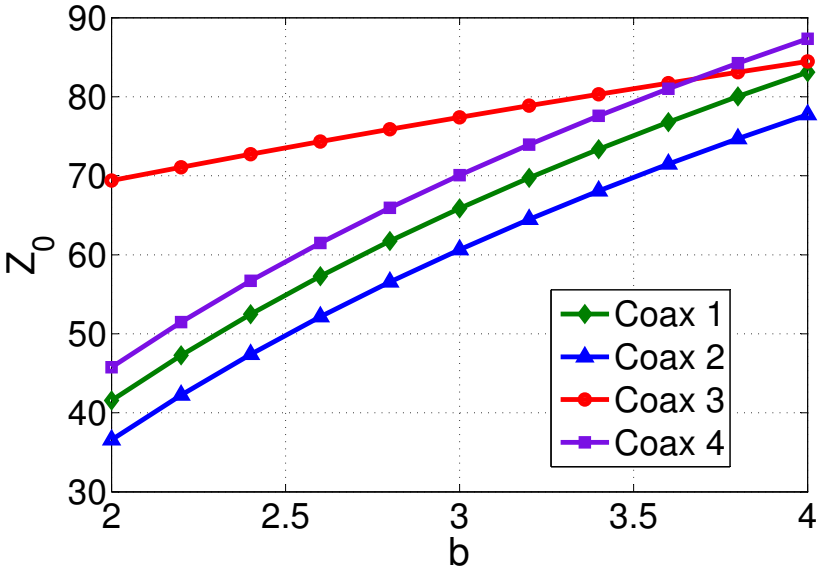

Figure 2.7: Characteristic Impedances of the Coaxial Lines, Coax 1, Coax 2, Coax 3 and Coax 4 in Figure 2.4 (a), (b), (c) and (d) respectively. [Coax 1: a=1mm], [Coax 2: a=1mm] [Coax 3: W'=5mm, W=1.2mm, a=1mm] [Coax 4: Cristal's Impedance data used [31]]

The variation of the characteristic impedance of the coaxial line in figure 2.4 (c) i.e. Coax 3 is less sensitive to changes in 'b' in comparision with the characterisitc impedance of the other three configurations in figure 2.4, which appear to have parallel sensitivities.

In the design of combline filters, rectangular outer conductors, with either circular, rectangular or square inner conductors are usually used for the coaxial resonators. A number of such resonators located in close proximity to each other can be coupled electromagnetically through the interraction of their electric or magnetic fields. Such an arrangement is shown in figure 2.8. An important parameter in combline filter design, the *groundplane spacing*, which is a spacing between the two conductor walls shielding the posts on either side of axis along which the posts are aligned, is also defined in figure 2.8. This parameter will be referred to in the designs of the combline filters the the chapters that follow.

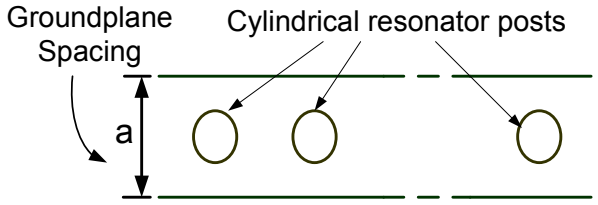

Figure 2.8: Ground Plane for Coupled Resonators

The end walls of the resonators between the adjacent posts are removed to allow for interraction of the electromagnetic fields or in some instances, they are re-structured in the form of irises leaving enough space for the right amount of electromagnetic energy to be coupled from one resonator to the next. Coupled resonators are discussed in section 2.2.3, where the impedance properties of such will also be discussed.

Q-Factor of a Coaxial Resonator

Another property of a coaxial lines that is important to consider when designing a combline resonator is the attenuation of the line which determines the Q-factor of the resonator and the cutoff frequencies of higher modes likely to propagate in the coaxial line.

The attenuation of cylindrical coaxial lines due to ohmic losses in the conductors is [15]

$$\alpha_c = 1.898 \times 10^{-4} \sqrt{\varepsilon_r} \sqrt{f_{GHz}} \left(\frac{1 + b/a}{b \ln b/a} \right) db/unit\,length \tag{2.7}$$

and is plotted in figure 2.9 as a function of the characteristic impedance.

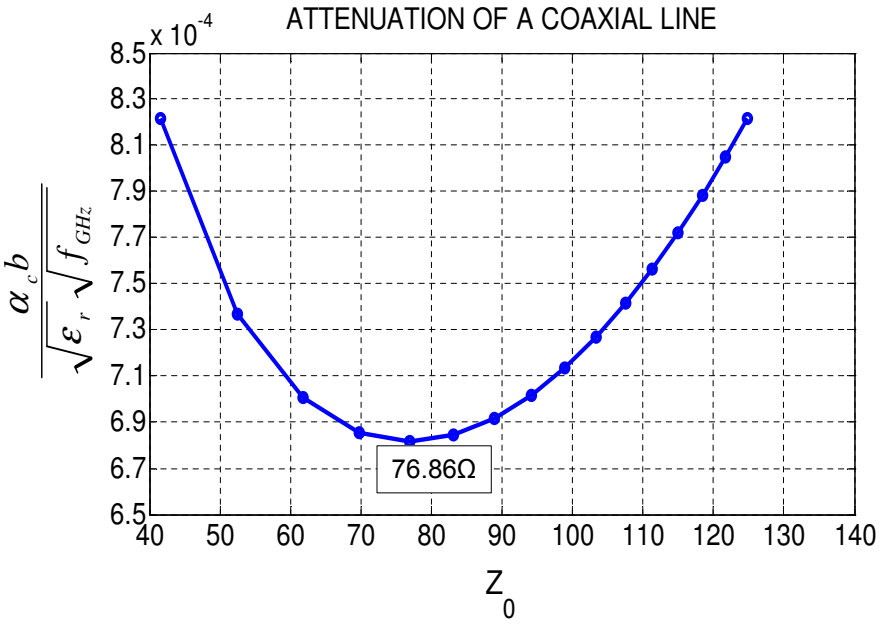

Figure 2.9: Attenuation of a coaxial line

As can be seen, minimum attenuation is obtained when the line has a characteristic impedance of approximately 77Ω. Using figure 2.7, the ratio of b to a needed to obtain this characteristic impedance for coax 1 for instance, is approximately 3.6. With this knowledge, the size of the inner or outer conductor can be chosen in relation to the size of the other, as long as this ratio is maintained.

The Q-factor of a coaxial line with a lossless dielectric is a function of only the line loss, and is given by

$$Q_C = f(\alpha_c) \tag{2.8}$$

A plot of the Q-factor as a function of characteristic impedance is shown in figure 2.10. Maximum Q occurs when the attenuation is minimum, which is where the line has a characteristic impedance of approximately 77Ω.

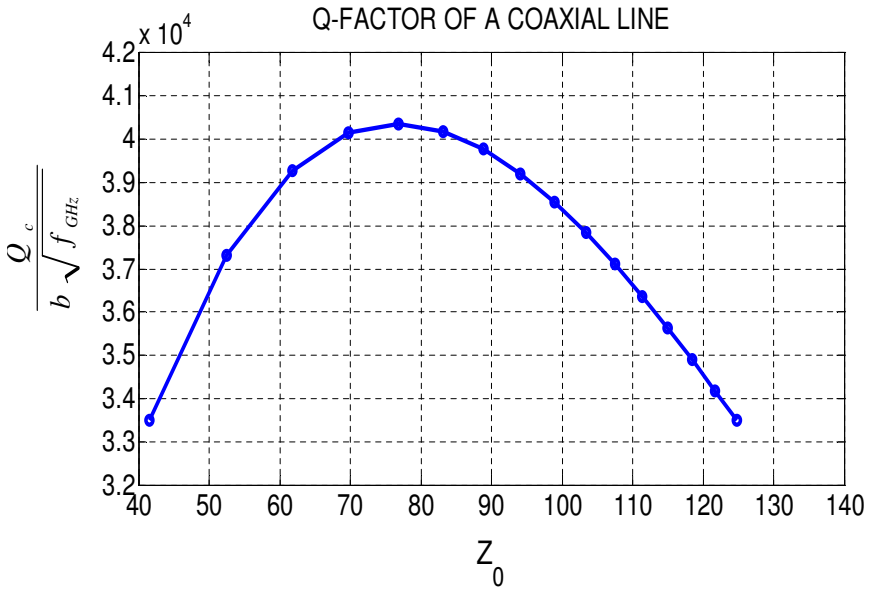

Figure 2.10: Q-factor of a Coaxial line

For the filters designed in this thesis, the dielectric is air, therefore, the assumption made is that there are no losses in the dielectric, so that the attenuation is only due to the losses in the conductors. In practice, the end-gap capacitance of a transmission-line resonator in a ground housing also contributes in a lesser way to the Q-factor of the resonator. However, in this instance, the change in Q is not dependent on Z_0. The total stored energy in a cavity is dependent on the volume of the cavity. A reduction in the volume of the cavity results in a decrease in the total stored energy, in turn resulting in a decrease in the Q-factor of the cavity. By increasing the length, l (see figure 2.11) of a transmission line resonator in a ground housing, the end-gap size, d, in figure 2.11 is reduced. The increase in length also results in a decrease in the volume of the resonator. Figure 2.11 below shows an increase in Q-factor with an increase in the end-gap size, an therefore, also an increase in the volume of the resonator.

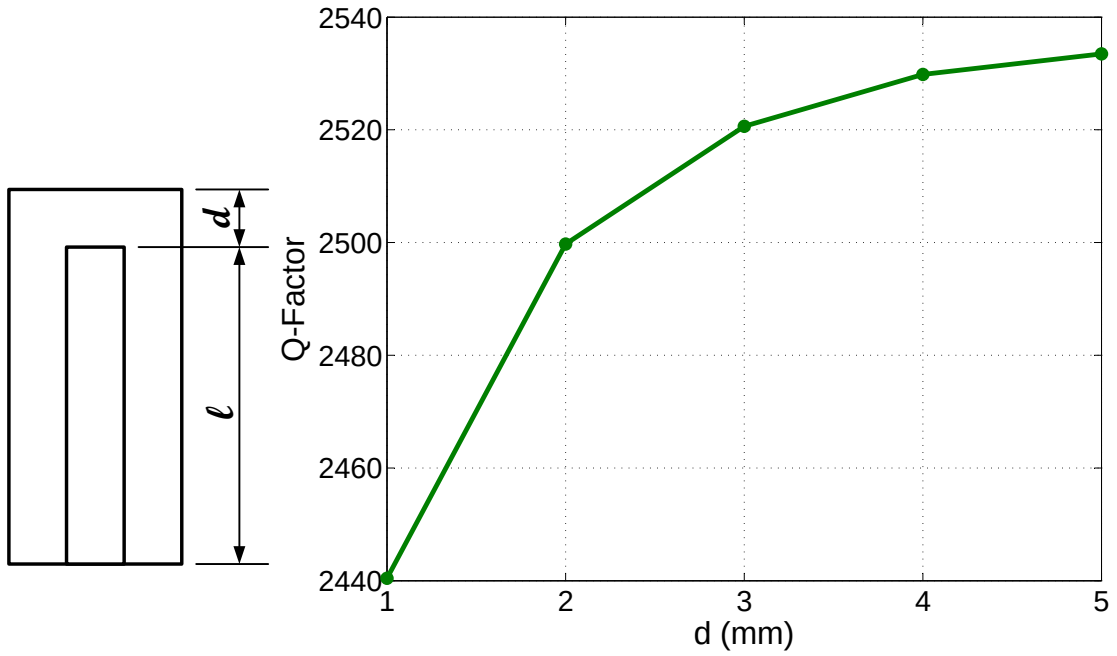

Figure 2.11: Change in Q-factor due to changes in end-gap capacitance

Higher Order Modes

In addition to the TEM mode, a coaxial line can also support TE and TM waveguide modes. These higher order modes are usually suppressed, however, it is important to be aware of the cutoff frequencies of the lowest order modes to avoid propagation of these modes. When the cross-section of a coaxial line is appreciable relative to the wavelength, the waveguide modes can be expected to propagate. This therefore limits the size of coaxial line that can be used if the higher order modes are to be avoided, especially in applications where power handling capacity and attenuation are both major considerations. An air-filled coaxial line had a minimum attenuation for a characteristic impedance of 77Ω , and maximum power handling capacity occurs at a characteristic impedance of 30Ω [13]. Most commonly used coaxial cables and connectors have a 50Ω characteristic impedance as a compromise between minimum attenuation and maximum power handling capability. The first higher order mode is expected to propagate when the average circumference of the line is approximately equal to the wavelength in the medium filling the line and its cutoff frequency is given by [15]

$$(f_c)_{GHz} = \frac{7.51}{\sqrt{\varepsilon_r}} \frac{1}{a+b} \tag{2.9}$$

with a and b measured in inches. The shift in frequency can be corrected by tuning the depth of the screws. Some mode patterns are shown in section 2.3.1, where the 3D implementation of a coaxial resonator in CST is discussed.

2.2.2 Realisation of circuit model for a combline resonator

A combline resonator of the type shown in figure 2.3 can be represented as a transmission line in parallel with a capacitor and a resistor as shown in figure 2.12.

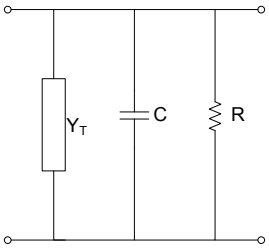

Figure 2.12: Circuit model of combline resonator

The capacitive susceptance is given by

$$B_C = \omega_0 C \tag{2.10}$$

and the susceptance of the transmission line is

$$B_T = -Y_0 cot\beta l \tag{2.11}$$

where l is the physical length of the line and Y_0 is the characteristic impedance of the line. At resonance, the susceptance due to the capacitance should be equal to that due to the transmission line, so that they cancel each other and the resonator's impedance is real. Therefore, at resonance

$$\omega_0 C - Y_0 cot\beta l = 0 \tag{2.12}$$

so that

$$C = \frac{Y_0}{\omega_0} cot\beta l = \frac{Y_0}{\omega_0} cot(\theta_0) \tag{2.13}$$

with θ_0 being the electrical length of the line at ω_0, the resonant angular frequency. The recommended Y_0 for maximum Q is approximately $\frac{1}{77}$ as was shown in figures 2.9 and 2.10.

The circuit model for a single loss-less resonator at 2GHz capacitively coupled to the input and output ports is shown in figure 2.13, with the cprresponding S-Parameter response as calculated by MWO. The capacitance represents probe coupling. In case loop coupling is preferred instead of probe coupling, the capacitor can be replaced with an inductor for a positive reactance. These types of coupling will be discussed in chapter 6. The resonant point is clearly visible.

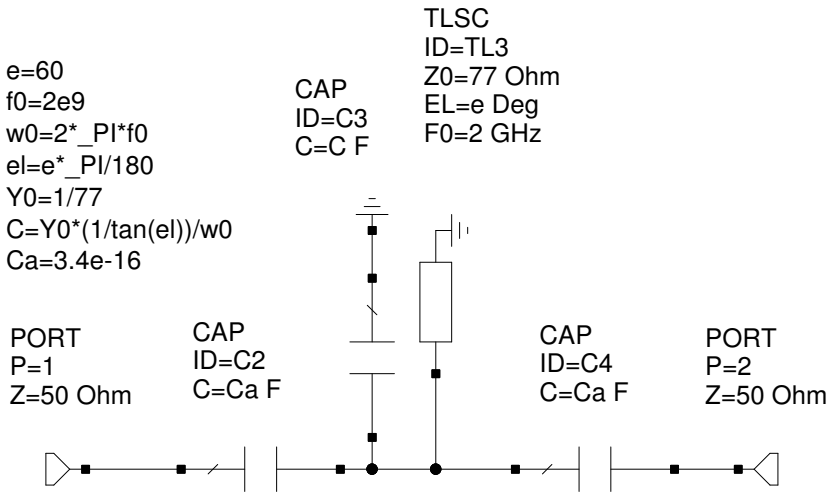

(a)

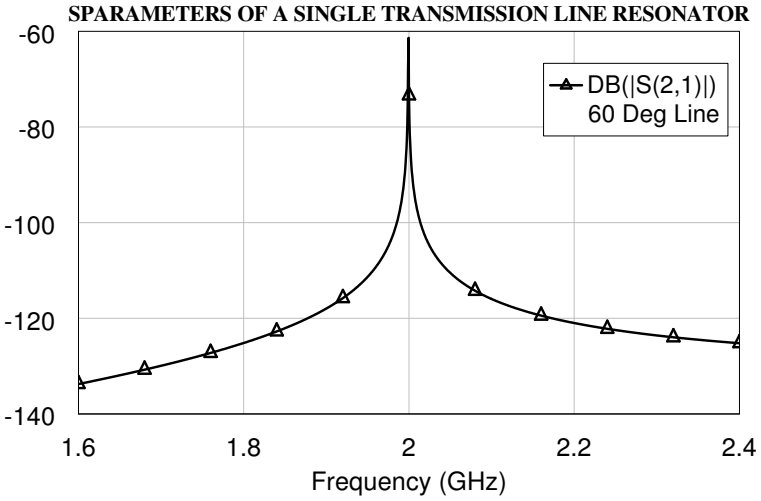

(b)

Figure 2.13: Single resonator MWO circuit model and S-Parameter response

The choice of the electrical length of the resonator line will not only affect the size of the resonator (the shorter the line, the smaller the filter), but also the position of the second passband. For a combline resonator, typical electrical lengths of resonator lines range between 45^0 and 60^0 at ω_0. The second passband is expected to occur when the length of the line is approximately over a half-wavelength long [15] at midband. Figure 2.14 shows the frequencies at which the second resonances are expected to occur if different lengths of lines are used for the resonator in figure 2.13.

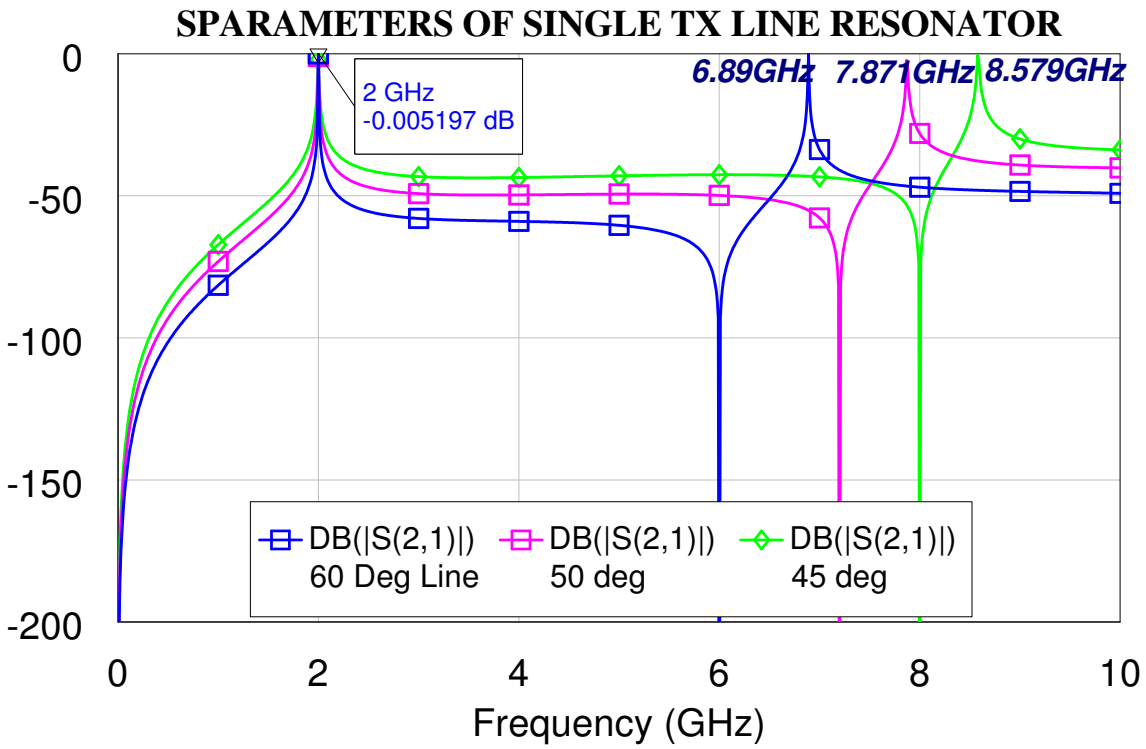

Figure 2.14: Position of second resonance for different electrical lengths of transmission lines

As is expected, the shorter lines have the second resonant frequencies further out. This is a significant advantage, but has to be considered against the lower Q obtained for shorter resonators.

2.2.3 Narrowband Coupled Resonators

The term *coupling* is widely used in engineering and scientific applications. Regardless of the application, the keyword common to all these applications is *energy*. In the context of electrical circuits, coupling refers to the transfer of power/energy between resonators due to the interaction of the electromagnetic fields of each of the resonators. Resonator coupling is one of the most significant factors affecting the performance of a filter. In [15], Matthaei proposes the use of impedance and admittance inverters as coupling elements for resonators to permit the use of identical resonators.

An impedance inverter (K inverter) operates like a quarter wavelength line of characteristic impedance K at all frequencies and an admittance inverter (J inverter) operates like a quarter wavelength line of characteristic admittance J at all frequencies [15]. The basic K and J inverter definitions are shown in figure 2.15.

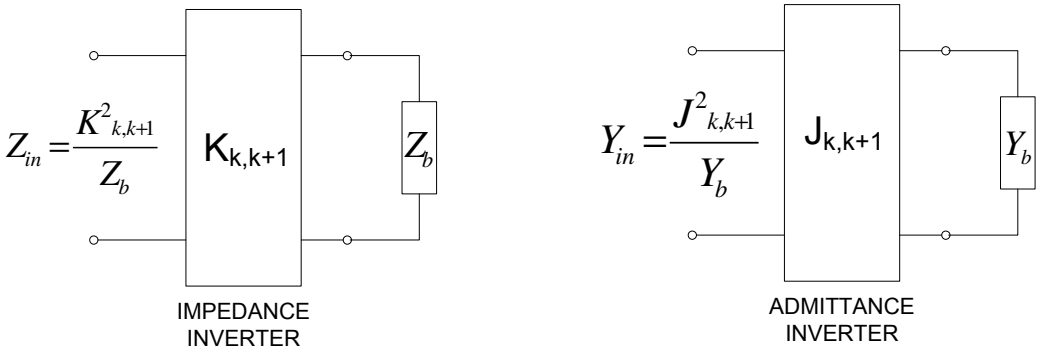

(a) K Inverter **(b)** J Inverter

Figure 2.15: Definition of Impedance Inverters and Admittance Inverters

The inverting property of the inverter makes it possible to represent a series inductor as a capacitor with inverters on either side, and in a similar manner, a shunt capacitor can be represented by a series inductor sandwiched between two inverters. This property allows for simplicity of circuit implementation so that a circuit can have only either shunt resonator elements or series ones. The ability to scale the value of the inductance and capacitance also allows for the use of identical resonators which can be chosen for optimal use of space and for the obtaining of an optimum Q-factor. Having a common type of resonator and coupling method also makes manufacturing and tuning of filters easier.

Combline filters use shunt resonators and therefore employ the use of J inverters as coupling elements. There are a couple of ways in which a J-inverter can be physically implemented, some of which are given in figure 2.16.

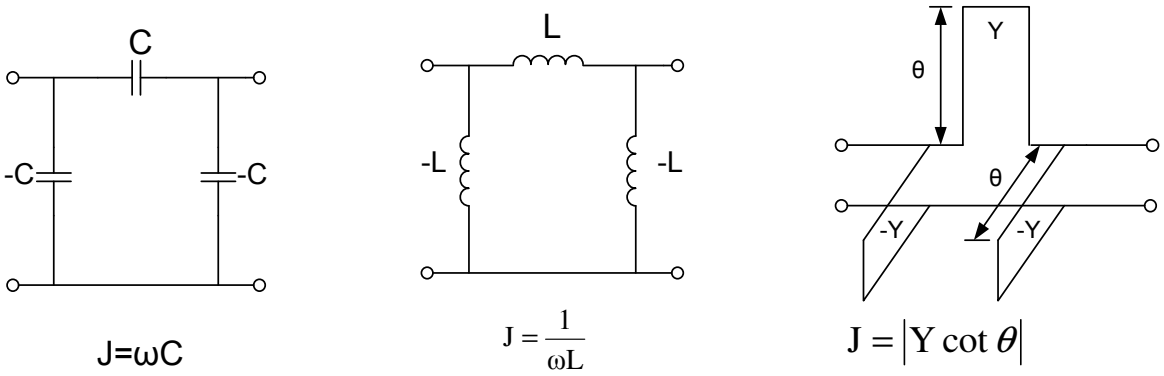

(a) **(b)** **(c)**

Figure 2.16: Implementation of a J Inverter

When used between two shunt resonators as shown in figure 2.17, the negative elements in the inverters in figure 2.16 get absorbed into the adjacent shunt element of the same type so that the resulting filter has only positive elements.

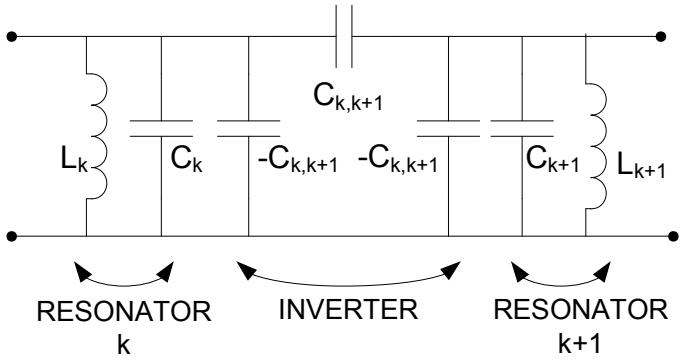

Figure 2.17: Inverter Between Two Resonators

The general expression for the coupling between the resonators, when J inverters are used as the coupling elements can be mathematically represented as [15]

$$k_{k,k+1}|_{k=1\ to\ n-1} = \frac{J_{k,k+1}}{\sqrt{\flat_k, \flat_{k+1}}} \tag{2.14}$$

where $\flat_k$ and $\flat_{k+1}$ represent the susceptance slope parameters of adjacent resonators, $J_{k,k+1}$ is the admittance of the J inverter representing the coupling between adjacent resonators and $k_{k,k+1}$ is a general expression of the usual definition of *coupling coefficient*. Combline filters can be designed using parameters computed from first principles or from pre-determined k and q values provided in tables in [24]. Design using the two approaches is outlined in sections 2.2.4 and 2.2.5.

In designing such filters, the degree of coupling, either specified or computed, is required to determine the line physical dimensions and the spacing necessary to achieve the right amount of coupling. This can be effected when the even- and odd-mode characteristic impedances, Z_{0e} and Z_{0o}, of a pair of coupled lines are known.

Even- and Odd-Mode Characteristic Impedances

'Even-mode' and 'odd-mode' are terms used to refer to the two possible ways in which commensurate electromagnetically coupled lines can be excited. The two modes of excitation are illustrated in figure 2.18 for two circular conductors between groundplanes.

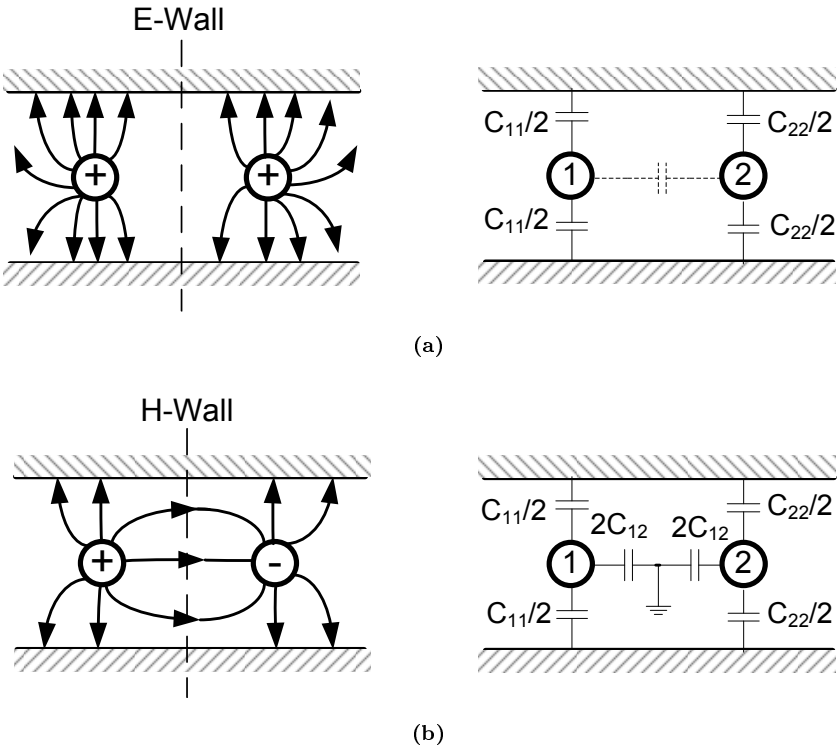

Figure 2.18: Representation of even- and odd-mode voltage excitation for a pair of coupled transmission lines indicating the polarity of the lines involved and the approximate form of the electric field lines. (a) Even-mode, (b) Odd-mode

The capacitances C_{11} and C_{22} represent the capacitance between either of the commensurate coupled lines and the ground, where as the third capacitance, C_{12}, is the capacitance between the two commensurate coupled lines. For the even mode, the two lines are driven using two in-phase voltages of equal magnitude, such that the current flowing in the lines are in the same direction and are of equal magnitudes. The electric field has even symmetry about the symmetry line labelled 'E-wall' in figure 2.18 and no current flows between the two lines. An equivalent circuit representation shows C_{12} open circuited in effect. The resulting capacitance of either line to ground, is therefore

$$C_e = C_{11} = C_{22} \tag{2.15}$$

Conversely, for the odd mode, the two voltages, even though they still have the same magnitude, are out-of-phase. The currents are therefore in opposite directions, but still similar in amplitude. In this case, due to the odd symmetry about the symmetry line, there's a voltage null, so that there's a virtual 'H-wall' represented in the equivalent circuit representation in figure 2.18 as a ground in the middle of C_{12}. The resulting effective capacitance between either line and ground for the odd mode is therefore

$$C_o = C_{11} + 2C_{12} = C_{22} + 2C_{12} \tag{2.16}$$

Using these capacitances, the characteristic impedances of the of the even- and odd-mode are computed as [13]

$$Z_{0e} = \sqrt{\frac{L}{C_e}} = \sqrt{\frac{LC_e}{C_e}} = \frac{1}{\nu_p C_e} \tag{2.17}$$

$$Z_{0o} = \sqrt{\frac{L}{C_o}} = \sqrt{\frac{LC_o}{C_o}} = \frac{1}{\nu_p C_o} \tag{2.18}$$

where ν_p is the propagation velocity which is given as $\nu_p = \frac{1}{\sqrt{\mu\varepsilon}}$. In free space, $\nu_p = \frac{1}{\sqrt{\mu_0\varepsilon_0}}$ = speed of light, $c = 2.998 \times 10^8$ m/sec [13].

2.2.4 Design from First Principles

Using shorted transmission-line resonators and J-inverters as coupling elements and ommiting losses, a general circuit model for the combline structure of figure 2.1 is shown in figure 2.19.

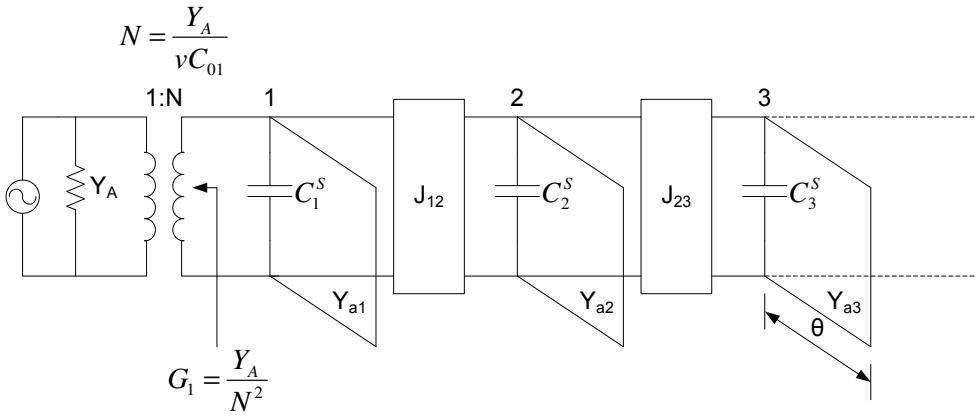

Figure 2.19: Circuit representation of a Combline bandpass filter using J inverters

The transformer at the input can be replaced by an additional J inverter as shown in figure 2.20. The admittance G_1 looking into the transformer from the right is related to the admittance of the inverter by

$$G_1 = \frac{J_{01}^2}{Y_A} \tag{2.19}$$

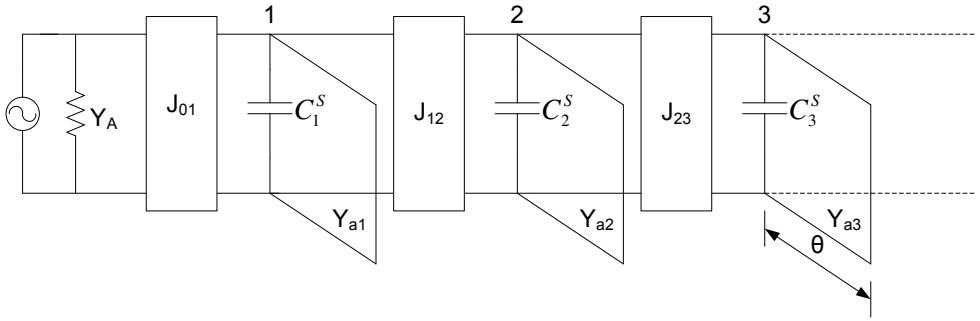

Figure 2.20: The circuit in figure 2.19 with input coupling inverter

The bandpass properties of the combline bandpass circuits in figures 2.19 and 2.20 are derived from the lowpass prototype elements, g_n, shown in figure 2.22. These prototype values can be found in [15] for different types of filter responses and for different orders of the filters. A lowpass to bandpass transformation is then used to obtain the bandpass characteristics and is given by

$$\frac{\omega'}{\omega_1'} = \frac{1}{\Delta}\left(\frac{\omega}{\omega_0} - \frac{\omega_0}{\omega}\right) \tag{2.20}$$

where ω_1' and ω' are defined in figure 2.21 for a lowpass prototype response,

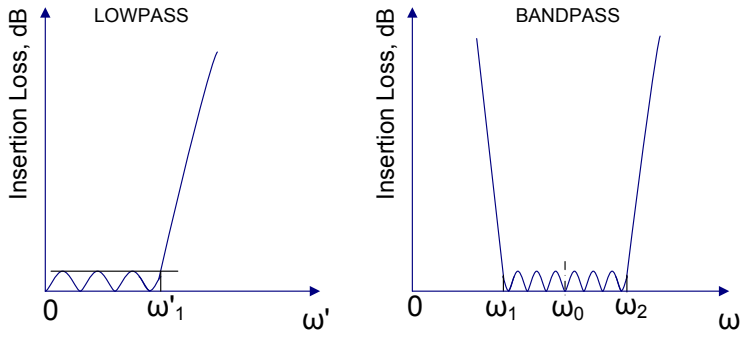

Figure 2.21: Lowpass prototype Response and Corresponding Bandpass Filter Response

and Δ is the desired fractional bandwidth which is given by

$$\Delta = \frac{\omega_2 - \omega_1}{\omega_0} \tag{2.21}$$

and ω, ω_0, $\omega_1$and ω_2 are defined for the corresponding bandpass filter response also shown in figure 2.21. The centre frequency, ω_0, is computed as

$$\omega_0 = \frac{\omega_2 + \omega_1}{2} \tag{2.22}$$

The admittance values of the inverters in figure 2.20 normalised to the port admittance, Y_A, are computed as follows [15]

$$\frac{J_{01}}{Y_A} = \sqrt{\frac{\flat_1 \Delta}{g_n g_{n+1} \omega_1'}} \tag{2.23}$$

$$\left.\frac{J_{j,j+1}}{Y_A}\right|_{j=1\ to\ n-1} = \frac{\Delta}{\omega_1'} \sqrt{\frac{\left(\flat_j / Y_A\right)\left(\flat_{j+1} / Y_A\right)}{g_j g_{j+1}}} \tag{2.24}$$

$$\frac{J_{n,n+1}}{Y_A} = \sqrt{\frac{\flat_n \Delta}{g_n g_{n+1} \omega_1'}} \tag{2.25}$$

where the g_n values are the lowpass prototype element values shown in figure 2.22,

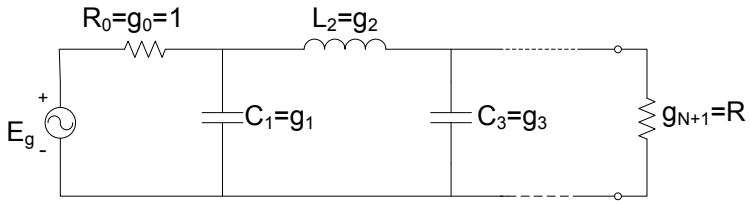

(a)

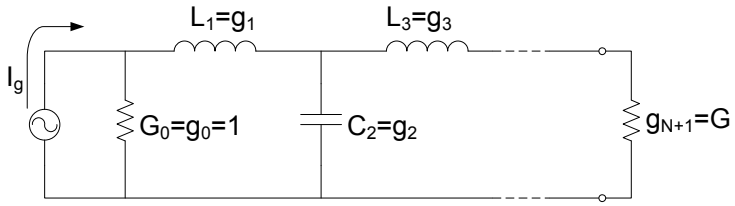

(b)

Figure 2.22: Lowpass filter prototypes

and Δ is the fractional bandwidth of the filter. The susceptance slope parameter, $\flat_j$ is for the individual resonators is given by

$$\left.\frac{\flat_j}{Y_A}\right|_{j=1\ to\ n} = \frac{Y_{aj}}{Y_A}\left(\frac{\cot\theta_0 + \theta_0 \csc^2\theta_0}{2}\right) \tag{2.26}$$

where θ_0 is the electrical length of the line at resonance and Y_{aj} is the characteristic admittance of the resonator line. From section 2.2.1, it was seen that for minimum attenuation and therefore optimal Q-factor, the recommended characteristic admittance is $\frac{1}{77}\Omega$.

The shunt capacitances C_j^S are obtained as

$$C_j^S\big|_{j=1\ to\ n} = Y_A\left(\frac{Y_{aj}}{Y_A}\right)\frac{\cot\theta_0}{\omega_0} \tag{2.27}$$

2.2.5 Design from k and q Values

A different approach to the design combline filters is by the direct derivation of the admittances of the inverters from normalised $\boldsymbol{k}$ and $\boldsymbol{q}$ values which are provided in tables in [24]. The normalised coupling coefficient, $\boldsymbol{k}$, defines the coupling between two adjacent resonators and is related to the admittance of the inverters by equation 2.46. The $\boldsymbol{q}$ values are the normalised loaded Q-factor values which are defined, for the input and output respectively, as the Q-factor of the end resonator coupled by the inverters J_{01} and $J_{n,n+1}$ respectively, to the terminations Y_A. The normalised $\boldsymbol{k}$ and $\boldsymbol{q}$ values can be denormalised by the factor Δ; where Δ is the fractional bandwidth. The denormalised values are then [24]

$$Q_1 = \frac{q_1}{\Delta} \tag{2.28}$$

$$K_{n,n+1} = \Delta k_{n,n+1} \quad n = 1, 2.., N-1 \tag{2.29}$$

$$Q_n = \frac{q_n}{\Delta} \tag{2.30}$$

The denormalised Q-factor at the input, Q_1, and at the output, Q_n, respectively, are related to the admittances of the inverters by [15]

$$Q_1 = \frac{\flat_1}{\left(J_{01}^2/Y_A\right)} \tag{2.31}$$

$$Q_n = \frac{\flat_n}{\left(J_{n,n+1}^2/Y_B\right)} \tag{2.32}$$

where as the denormalised coupling coefficients are related to the inverter admittances by

$$K_{n,n+1}|_{n=1\ to\ N-1} = \frac{J_{n,n+1}}{\sqrt{\flat_n, \flat_{n+1}}} \tag{2.33}$$

with Y_A being the terminating admittance at the input and Y_B being the terminating admittance at the output. The susceptance slope parameter, b_j, can be calculated from equation 2.26.

The subscript N refers to the order of the filter. The inverter values can then be derived from equations 2.46, 2.31 and 2.32 to get

$$J_{01} = \sqrt{\frac{\flat_1 Y_A}{Q_1}} \tag{2.34}$$

$$J_{n,n+1}|_{n=1\ to\ N-1} = K_{n,n+1}\sqrt{\flat_n, \flat_{n+1}} \tag{2.35}$$

$$J_{n,n+1} = \sqrt{\frac{\flat_n Y_A}{Q_n}} \tag{2.36}$$

The two design approaches are completely equivalent and one can easily be derived from the other.

2.2.6 Design of a 2GHz combline filter

In this section, a combline filter is designed using the normalised k and q values obtained from the tables in [15], for the following specifications

Order of the filter	4th Order
Fractional Bandwidth	5%
Centre Frequency	2GHz
Response type	Chebyshev
Passband Ripple	0.5dB

Table 2.1: Design specifications for combline filter

The chosen electrical length for the lines is 60 degrees and the characteristic impedance is chosen to be 77Ω for optimal Q-factor.

The element values for equiripple lowpass prototype of a 4th order chebyshev lowpass filter with a 0.5dB ripple were obtained from [15] and are given in table 2.2.

g_0	g_1	g_2	g_3	g_4	g_5
1	1.6703	1.1926	2.3661	0.8419	1.9841

Table 2.2: Element Values for a 4th Order Equiripple Chebyshev Low-Pass Filter with 0.5dB Ripple

and the normalised $\boldsymbol{k}$ and $\boldsymbol{q}$ values obtained from [24] are:

q_1	1.8258
q_4	1.8258
k_{12}	0.6482
k_{23}	0.5446
k_{34}	0.6482

Table 2.3: Normalised k and q Values for a 4th Order Equiripple Chebyshev Filter with 0.5dB Ripple

The denormalised values are then computed from equations 2.28, 2.29 and 2.30 to get

Q_1	36.516
Q_2	36.516
K_{12}	0.0324
K_{23}	0.0272
K_{34}	0.0324

Table 2.4: Denormalised k and q Values for a 4th Order Equiripple Chebyshev Filter with 0.5dB Ripple and 5% BW

If both the input and output ports have an impedance of 50Ω, the susceptance slope parameter can be calculated using equation 2.26 to get

$$♭_j = 0.0128$$

which is equal for all the resonators since the resonators are all identical. The admittance values for the inverters can then be computed using equations 2.34, 2.35 and 2.36 to get

J_{01}	0.0026
J_{12}	4.148e-4
J_{23}	3.485e-4
J_{34}	4.148e-4
J_{45}	0.0026

Table 2.5: Admittance values for the J-Inverters

The capacitance of the shunt capacitors is computed from equation 2.27 to get

$$C_j^S = 0.5967pF$$

Using the calculated parameters, the circuit model is shown in figure 2.23, with the MWO analysis in figure 2.24.

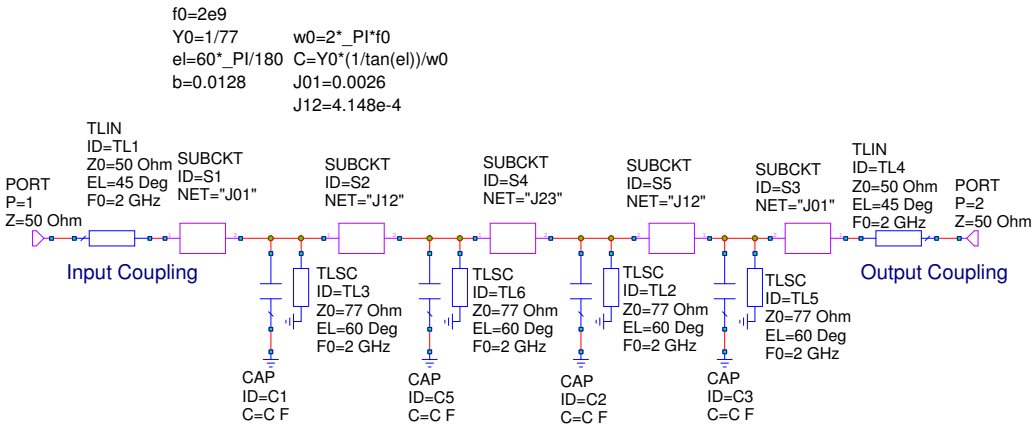

Figure 2.23: MWO model of 2GHz 4th order Chebyshev combline filter

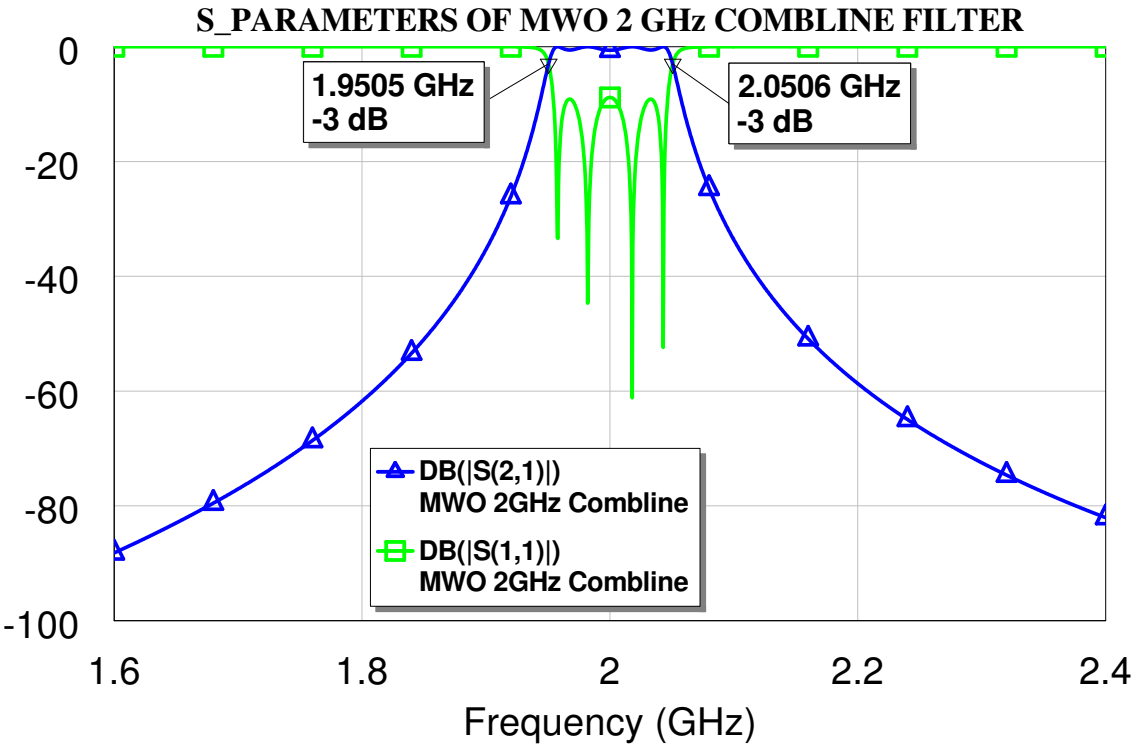

Figure 2.24: S-Parameters of the filter in figure 2.23

The filter has a 3dB bandwidth of 100MHz and a maximum passband return loss of 9.635dB corresponding to a minimum insertion loss of 0.5dB.

2.3 Realisation of Physical 2GHz Combline Filter

In designing the physical combline filter, there are a number of factors to consider. The characteristic impedance of the line is chosen with regard to the Q-factor required for the design, the resonators have to be modelled so that they resonate at the right frequency and the length of the resonator is chosen with the desired size of the filter in mind. In certain cases, when the performance at higher frequencies is also of importance, it is also important to know how wide the stopband should be before the occurrence of the second passband. If the filter

is to be manufactured, the shape of the resonator is also to be chosen carefully to facilitate ease of manufacture. To obtain the right loaded Q-factor, the right type of input and output coupling techniques have to be chosen. The choice of the input and output coupling technique must also consider ease of fabrication and the tuning of the input coupling should also be easy.

Coupling between the resonators in this type of filter is due to fields between adjacent resonators, therefore the inter-resonator spacings also have to be calculated to obtain the right amount of coupling.

This section starts with the modelling of a single resonator to obtain the right resonant frequency and characteristic impedance. It then discusses the incorporation of input and output coupling to obtain the required loaded Q-factor. Coupling between adjacent resonators is then discussed, prior to the modelling of the full filter. The modelling is done in the 3D electromagnetic simulation software CST (Computer simulation Technology). To obtain the correct loaded Q-factor, the group delays of the reflection coefficient, S_{11}, for the CST resonators are compared to those for the MWO resonator circuit models from section 2.2.6. To conclude the section, a comparison is made of the S-Parameters of the MWO circuit model of the fourth order combline filter and its CST 3D model.

2.3.1 Realisation of a Single Resonator

The simple coaxial line topology shown in figure 2.25, with a square outer conductor and a circular inner conductor is chosen as a starting point.

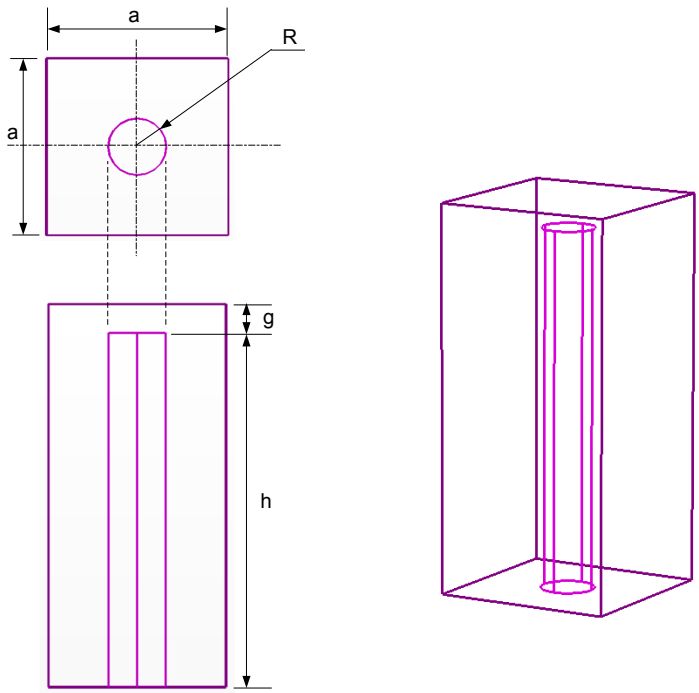

(a) (b)

Figure 2.25: Single Resonator for a Combline Filter

In figure 2.25, h is the length of the resonator line and g is the length of the gap between the roof of the housing and the post. a is the length of one side of the housing and R is the radius of the post.

A characteristic impedance of 77Ω is chosen for optimal Q-factor. From equation 2.6, it is seen that the characteristic impedance is a function of the ratio between the radius/diameter of the outer conductor to the radius/diameter of the inner conductor. For parallel coupled line filters with axially placed posts as resonators,

such as interdigital and combline filters, the spacing between the ground walls of the housing on either side of the parallel posts is referred to as the groundplane spacing and has been shown in figure 2.8.

For combline filters, it is recommended that the size of groundplane spacing be $\leq \frac{\lambda_0}{12}$. If the groundplane spacing exceeds this limit, the designed filters are expected to have bandwidths larger than the ones designed for, due to higher order mode coupling. At 2GHz, if the groundplane spacing, a, is chosen as $\frac{\lambda_0}{12}$, so that, for a midband wavelength of

$$\lambda_0 = \frac{3 \times 10^8}{2 \times 10^9} = 0.15\, m$$

$$a = \frac{\lambda_0}{12} = \frac{0.15}{12} = 0.0125\, m$$

The diameter of the inner conductor can then be obtained through parametric modelling in CST, by plotting a graph representing the variation of the characteristic impedance with changes in the radius of the inner conductor, while the groundplane spacing is fixed at *12.5mm*. Either the Frequency domain solver or the Time domain solver in CST can be used, with the waveguide port set as shown in figure 2.26.

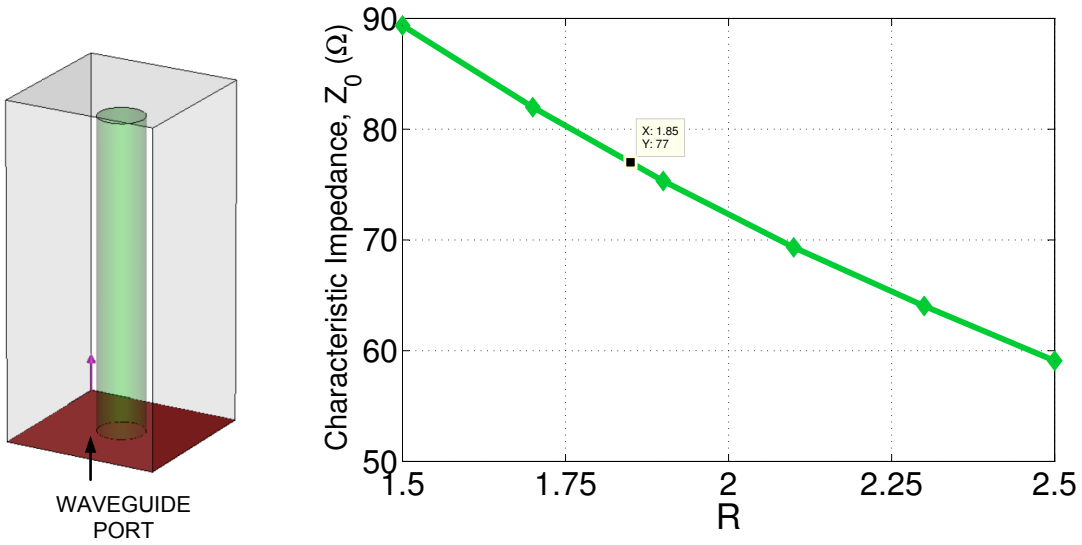

(a) (b)

Figure 2.26: Variation of the Characteristic Impedance of Resonator Line with the Radius of the Resonator Line

A radius, R (see figure 2.25), of 1.85mm will give a characteristic impedance of the coaxial line of 77Ω. By running the simulation with the set-up in figure 2.26, using the Frequency domain or Time domain solvers, the port modes are also computed for a specified port. The electric and magnetic fields for the first two modes are shown in figure 2.27 below.

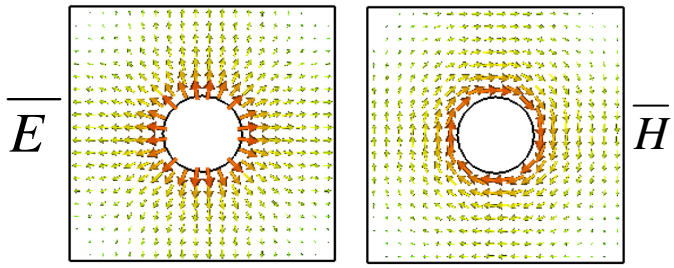

(a) TEM Mode

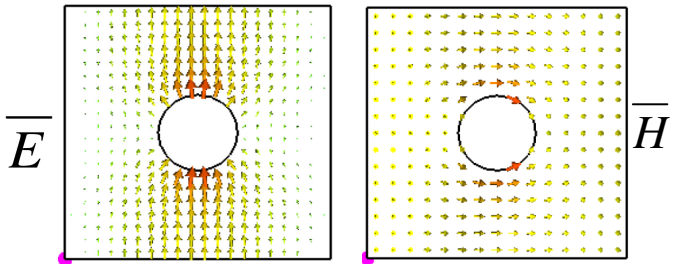

(b) TE_{10} Mode

Figure 2.27: Electric and Magnetic Field Distribution for First Two Port Modes for a Coaxial Line

The cutoff frequencies of the modes are also computed, so that the range of frequencies within which the filter can be used before unwanted higher order waveguide modes can begin to propagate is known. The cutoff frequencies of the first five modes of the coaxial line are

MODE	TYPE	F-CUTOFF (GHz)
1	TEM	0.0
2	TE	10.6
2	TE	10.6
4	TE	16.7
5	TE	23.3

Table 2.6: Cutoff Frequencies of the Modes of Propagation in a Coaxial Line with a=12.5mm and R=1.87mm

The resonator is required to resonate at 2 GHz, so for a chosen electrical length of $60^0 \simeq 1.0472\,radians$ for the resonator lines, the physical length, h (see figure 2.25), is computed as

$$h = \frac{\theta_0}{\beta} \tag{2.37}$$

where

$$\beta = \frac{2\pi}{\lambda_0} = \frac{\omega_0}{\nu_p} \tag{2.38}$$

ν_p is the phase velocity in free-space given by $\nu_p = {}^1/_{\sqrt{\mu_0 \varepsilon_0}} = 3 \times 10^8 \;\; m/sec.$ Therefore,

$$h = \frac{\theta_0 \nu_p}{\omega_0} = \frac{1.0472 \times 3 \times 10^8}{2 \times \pi \times 2 \times 10^9} = 0.025\,m$$

To get the resonator to resonate at 2GHz, the capacitor formed between the post and the housing is varied to obtain the right capacitance, corresponding to the capacitance, C_j^S, in figure 2.20. This capacitance is normally dominated by the parallel plate capacitance between the post and the roof of the housing. Capacitance for a parallel plate capacitor is given by

$$C = \frac{\varepsilon_0 \varepsilon_r A}{d} \tag{2.39}$$

where ε_0 and ε_r are the permittivity of free-space and the dielectric constant of the dielectric between the plates of the capacitor, A is the overlap surface area of the plates and d is the distance between the two plates, in this case g. The capacitance is proportional to the overlapping cross-sectional area and inversely proportional to the gap size, g. Therefore, to increase the capacitance, the gap size, g, needs to be reduced or the cross-sectional area of overlap should be increased.

The correct capacitance for resonance is determined by parametric modelling in CST to obtain a graphical representation of the variation of the resonant frequency with g. The Eigenmode solver is used for this. The results of the simulation for a gap-size range of 0.5mm to 3mm are shown in figure 2.29. The frequency-gap relationship becomes increasingly non-linear as the gap in reduced, so that the sensitivity for small gaps is high compared to that of larger gap sizes. To have a more linear relationship between the gap size and the resonant frequency, a hole is created at the centre of the resonator to a certain depth and a tuning screw is then used to tune the gap size in the manner shown in figure 2.28.

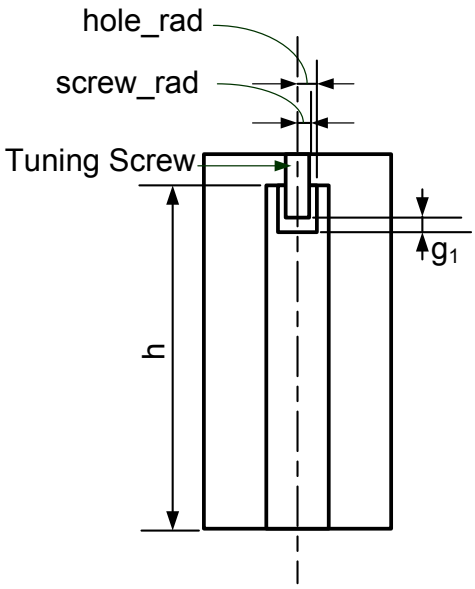

Figure 2.28: Resonator with a Hole or Groove and a Tuning Screw to Tune the Capacitance

For a hole radius, hole_rad, of 1.4mm and a screw radius, screw_rad, of 1mm, a graph showing the variation of frequency with changes in the gap size, $g1$, is also shown in figure 2.29.

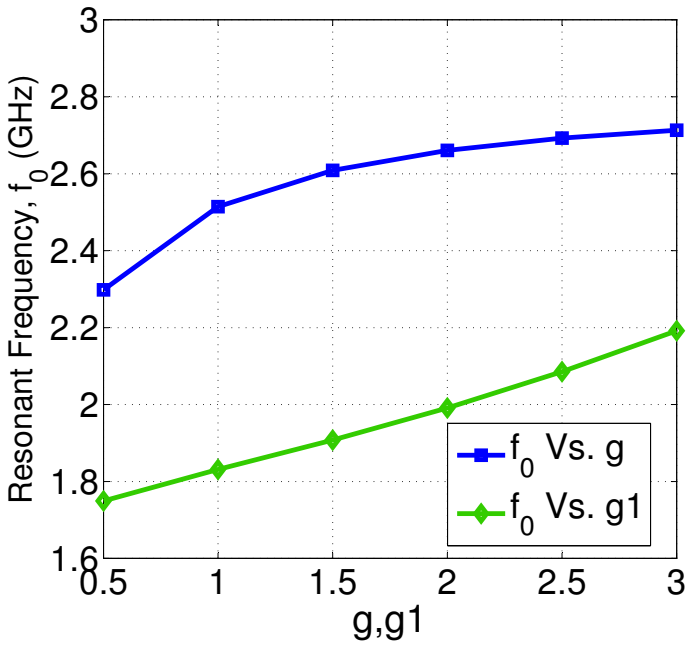

Figure 2.29: Effect of Changing the Gap Sizes, g and $g1$, on the Resonant Frequency of the Resonator Set-ups in Figure 2.25 and 2.28 respectively.

As can be seen, the f_0 versus $g1$ relationship in figure 2.29 is linear and there is a well-defined tuning range for the gap size range of 0.5mm to 3mm. The new set-up (see figure 2.28) also allows for further lowering of the resonant frequency as, because a reduction in gap size, g, in figure 2.25, while leaving provision for ease of manufacturing, could not lower the resonant frequency to the desired 2GHz.

The choice of the radius of the tuning screw to use also has an effect on the capacitance. The tuning screw forms a coaxial line of the form in figure 2.4 (a) with the radius of the inner conductor, a, being that of the screw and the inner radius of the outer conductor, b, being that of the resonator post. The capacitance per unit length of a coaxial line is given by

$$C = \frac{2\pi\varepsilon_0\varepsilon_r}{\ln {}^{b}/_{a}} \tag{2.40}$$

where $\varepsilon_0 = 8.854\times10^{-12}\,F/m$ is the permittivity of free-space and ε_r is the dielectric constant. This relationship is plotted in figure 2.30, with the inner radius of the outer conductor, b, fixed at 1.4mm and the radius of the inner conductor, a, being varied in the range of 1mm to 1.5mm.

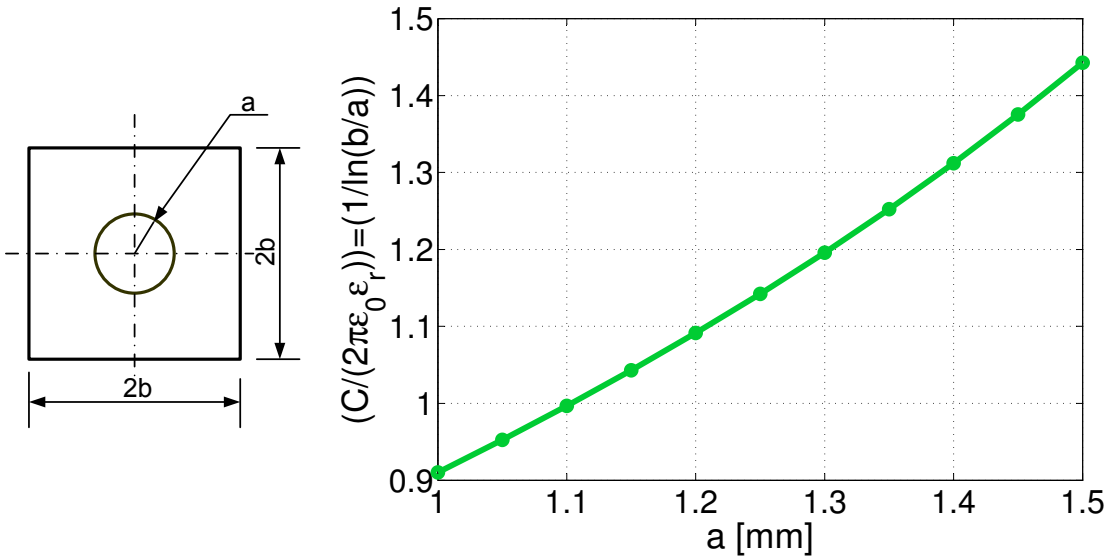

Figure 2.30: Capacitance Per Unit Length of a Coaxial Line Versus the Radius of the Inner Conductor [b=1.5mm]

An increase in the radius of the screw results in a corresponding increase in the capacitance per unit length. An increase in capacitance results in a decrease of the resonant frequency as seen in figure 2.31.

Figure 2.31: Effect of Changing the Radius of the Screw on the resonant frequency for a given insertion length

All of these factors i.e. the length of the resonator post, diameter of the post, groundplane and roof spacing, the tuning screw diameter, the diameter of the cylindrical hole in the end of the post, and the insertion depth of the tuning screw have to be chosen correctly to obtain a high Q resonator with a linear tuning range over the frequency range of interest.

Unloaded Q-Factor

Bandpass filters of narrow and moderate bandwidths can be uniquely defined using their *unloaded Q* factor, their external couplings and their internal couplings. The unloaded Q factor of a resonant circuit is a measure of the loss of the circuit in the absence of any loading effects caused by external circuitry and is defined mathematically as [13]

$$Q = \omega \frac{(Average\ Evergy\ Stored)}{Evergy\ Loss/second} = \omega \frac{W_m + W_e}{P_l} = \omega_0 \frac{2W_m}{P_l}\bigg|_{\omega=\omega_0} \tag{2.41}$$

where W_m is the average magnetic field stored due to the inductance in the resonator and W_e is the average electric energy stored in the capacitor. The lower the loss, the higher the Q factor. At resonance, $W_m = W_e$. The larger the volume of the resonator, the more the energy that is stored in the fields. The choice of material used for the resonator also influences the unloaded Q of the resonator; a material with very good conductivity has less conductor losses and therefore a higher Q. The effect of changing the ground plane spacing of the resonator in figure 2.28 on the unloaded Q, obtained through parametric modelling in CST, is shown in figure 2.32 for a copper resonator and for a silver resonator.

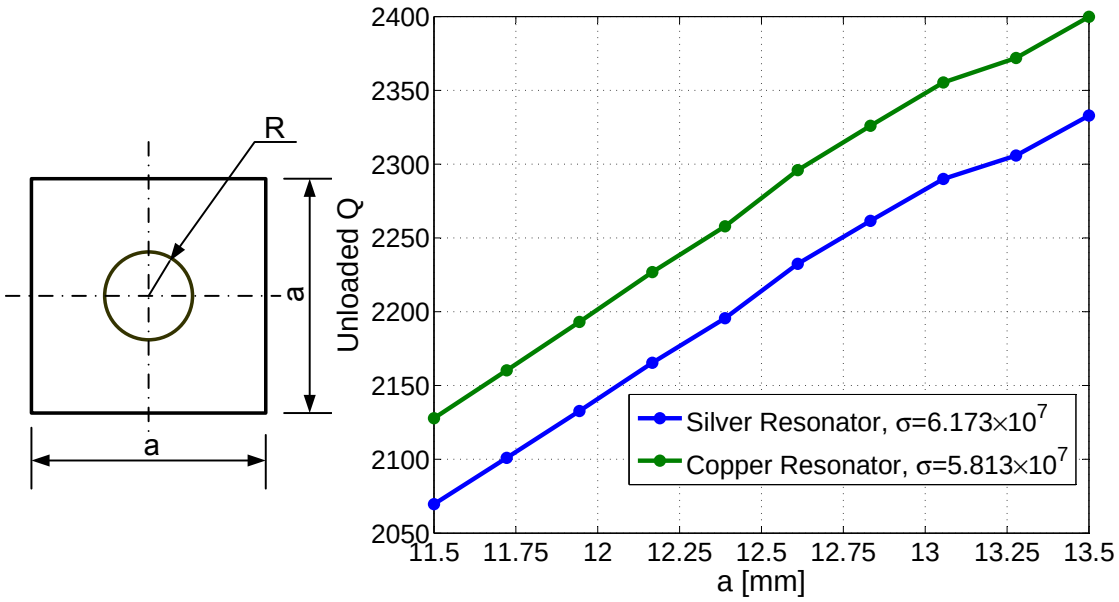

Figure 2.32: Effect of a Change in Groundplane Spacing on the Unloaded Q of a Copper Resonator and a Silver Resonator, [R=1.87mm]

Silver has a higher conductivity than copper and a resonator made of silver for this reason has a higher Q for the same values of *'a'*.

2.3.2 External Couplings

When the circuit is coupled to external circuitry, the overall Q of the resonant circuit is reduced due to resistor losses associated with the external circuitry. This overall Q is referred to as the loaded Q, Q_l, and is expressed as

$$\frac{1}{Q_l} = \frac{1}{Q_E} + \frac{1}{Q} \tag{2.42}$$

where Q_E is the external Q, which defines the coupling between the connecting lines of the external circuitry and the end resonators of a filter. Q_E can be determined from the reflection coefficient, S_{11}, as the resonators of a filter are tuned to resonance. These two parameters are related through a relationship between the external Q and the group delay of S_{11}, τ_{d11}, which reaches a maximum, $\tau_{d11,max}$, at the resonant frequency. The relationship is given by [20]

$$Q_E = \frac{\pi}{2} f_0 \tau_{d11,max} \tag{2.43}$$

The group delay of a reflected signal is the time difference between the input signal and its reflected component and is given by [15]

$$\tau_{d_{11}} = \frac{d\phi_{11}}{d\omega} \tag{2.44}$$

where ϕ_{11} is the phase of the reflection coefficient, S_{11}, and is given by

$$\phi_{11} = \arg\left(S_{11}\right) \tag{2.45}$$

In modelling the resonators of the combline filters in this thesis, the external Q factors of the filters and the inter-resonator couplings are determined using the group delay method. In [27], Ness shows that the group delay of the input reflection coefficients of sequentially tuned resonators contains all the information necesssary to design and tune filters, and that the group delay value at the centre frequency of the filter can be written in terms of the low-pass prototype values, the LC elements of a bandpass circuit and the coupling coefficients of an inverter coupled filter. He outlines a procedure in which, for any given number of elements, a single element (the first) in a lowpass equivalent (see figure 2.22) is considered with the others disconnected from the circuit, to calculate the groupdelay, at the centre frequency, of the single element. The same result can be obtained by considering a single bandpass resonator, obtained by applying a lowpass-to-bandpass transformation on the element values of the lowpass filter, and by disconnecting all the other resonators. A third way of obtaining the same result is by using the external Q for an inverter coupled filter (see figure 2.20). The process can be repeated for the remaining elements or resonators for each type of circuit, by shorting out each added element so that the remaining ones are disconnected from the circuit. The group delays, for a four-element filter are then computed as follows [27]

Number of Elements, n	Lowpass Prototype	Bandpass Filter	Inverter-coupled Filter
1	$\Gamma_{d1} = \frac{4g_0 g_1}{\Delta\omega}$	$\Gamma_{d1} = 4C_1 Z_0$	$\Gamma_{d1} = \frac{4Q_E}{\omega_0};\ Q_E = \frac{g_0 g_1 \omega_0}{\Delta\omega}$
2	$\Gamma_{d2} = \frac{4g_2}{g_0\Delta\omega}$	$\Gamma_{d2} = \frac{4L_1}{Z_0}$	$\Gamma_{d2} = \frac{4}{\omega_0 Q_E k_{12}^2};\ k_{12} = \frac{\Delta\omega}{\omega_0 (g_1 g_2)^{1/2}}$
3	$\Gamma_{d3} = \frac{4g_0(g_1+g_3)}{\Delta\omega}$	$\Gamma_{d3} = 4\left(C_1 + C_3\right) Z_0$	$\Gamma_{d3} = \Gamma_{d1} + \frac{4Q_E k_{12}^2}{\omega_0 k_{23}^2};\ k_{23} = \frac{\Delta\omega}{\omega_0 (g_2 g_3)^{1/2}}$
4	$\Gamma_{d4} = \frac{4(g_1+g_4)}{g_0\Delta\omega}$	$\Gamma_{d4} = \frac{4(L_2+L_4)}{Z_0}$	$\Gamma_{d4} = \Gamma_{d2} + \frac{4k_{23}^2}{\omega_0 Q_E k_{12}^2 k_{34}^2};\ k_{34} = \frac{\Delta\omega}{\omega_0 (g_3 g_4)^{1/2}}$

Table 2.7: Group delay values at the centre frequency in terms of lowpass element values, bandpass element values and inverter-coupled bandpass element values. [27] $\Delta\omega$ = angular bandwidth of bandpass filter

External Q-factors for the circuit model of a 2GHz filter were computed in section 2.2.6, along with the the coupling coefficients defining inter resonator coupling. In modelling the physical combline filter in CST, the external Q factor of a resonator is used to obtain the group delay of S_{11} for the resonator, while tuning for the right filter response.

2.3.3 Internal Couplings

A general expression for the coupling coeffcient, k_{ij}, defining the coupling between two resonators is [21]

$$k_{ij} = \frac{\omega_h^2 - \omega_l^2}{\omega_h^2 + \omega_l^2} \tag{2.46}$$

with ω_h and ω_l being the higher and lower resonant frequencies respectively, separated from the original identical resonant frequency of either resonator, due to coupling. To understand the physical meaning of coupling, in [21], Awai applies the coupled mode theory in an analysis of inter-resonator coupling. He proposes the use of an

overlap integral expression defining the coupling coefficient as the difference between the overlapping integral of the magnetic fields and that of the electric fields, mathematically defined as [21]

$$k = \frac{\int_v \mu \mathbf{H}_1 \cdot \mathbf{H}_2^* d\nu - \int_v \varepsilon \mathbf{E}_1 \cdot \mathbf{E}_2^* dv}{\int_v \varepsilon \left|\mathbf{E}_1\right|^2 dv} \tag{2.47}$$

where $\mathbf{E}_1$ and $\mathbf{E}_2$ are the electric field distributions of the two resonators before coupling, with $\mathbf{E}_1^*$ and $\mathbf{E}_2^*$ as their conjugates, and $\mathbf{H}_1$ and $\mathbf{H}_2$ are the magnetic field distributions of the two resonators prior to coupling, with $\mathbf{H}_1^*$ and $\mathbf{H}_2^*$ as the conjugates. The denominator of the equation is a normalisation factor.

With the knowledge of the coupling coefficients previously computed in section 2.2.6, the spacing between adjacent resonators can be approximated in CST by computing the coupling coefficients for two resonators using equation 2.46. A parametric sweep of the inter-resonator spacings d_{ij} , shown in figure 2.33 dan to dimdnso n mpute the range of coupling coefficients for a given range of d_{ij}.

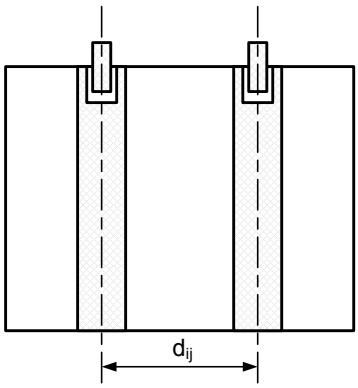

Figure 2.33: Adjacent Combline Resonators

An alternative approach is to use the coupling bandwidths to approximate the distance between resonators. For a set of given k values the relative coupling bandwidth in percentage is computed as

$$CBW_R = k_{ij} \times BW|_{\%} \tag{2.48}$$

CST has a template-based postprocessing application that allows for the computation of relative coupling bandwidths using the Eigenmode solver. Results for both the relative coupling bandwidth given as a percentage and the absolute coupling bandwidth in a preferred unit of frequency canItemizeained.

The combline filter design in this section calls for a bandwidth of 5% for which the calculated coupling bandwidths between adjacent resonators of the filter in percentages are given in table 2.8. The coupling coefficients, k_{ij}, are similar to those used for the MWO circuit model and are obtained from the k and q tables in [24].

ij	k_{ij}	Calculated CBW$_{\%}$
12	0.6482	3.2410
23	0.5446	2.7230
	0.6482	3.2410

Table 2.8: Coupling Bandwidths of Adjacent Resonators

Using the eigenmode solver, the distance between two resonators, d_{ij}, (see figure 2.33), is then varied in a parametric sweep in CST, to obtain the range of coupling bandwidths corresponding to the various d_{ij}. From the resulting plot, the inter-resonator spacings, d_{ij}, corresponding to the computed values given in table 2.8

cost, some of the des. The variation of the relative coupling bandwidth, in %, with changes in d_{ij}, is shown below in figure 2.34.

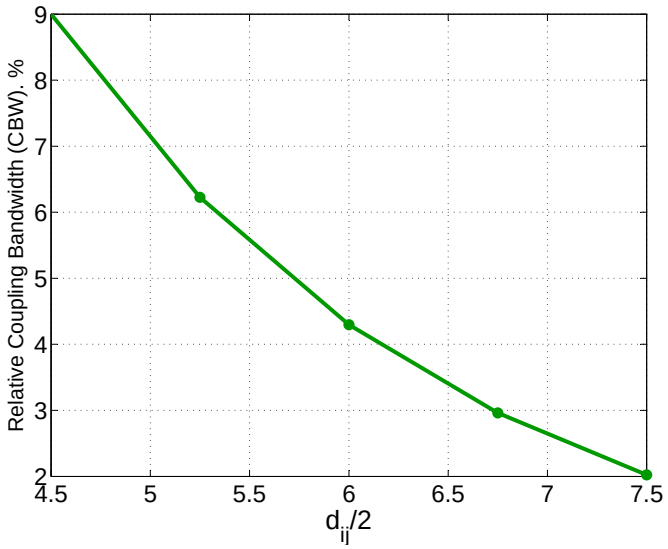

Figure 2.34: Variation of the Relative Coupling Bandwidth with Changes in S_{ij}

The data points in the graph indicate the $\frac{d_{ij}}{2}$ values corresponding to the calculated coupling bandwidths in table 2.8. The d_{ij} values are outlined below in table 2.9.

ij	k_{ij}	d_{ij} (mm)
12	0.6482	13.18
23	0.5446	13.88
34	0.6482	13.18

Table 2.9: Approximate Distances Between the Resonators of a 2GHz Combline Filter

These values serve as a starting approximation for the distances between the resonators so that the full 4th order filter can now be modelled in CST. The right external Q-factor and internal couplings can then be obtained for the 3D model of the filter using the group delay of S_{11} as successive resonators are tuned to resonance, in comparison with those obtained from the MWO circuit model. In doing this, in order to get the right group delay, the distances, d_{ij}, between the resonators might need to be changed, which is why the ones in table 2.9, only serve as estimates.

2.3.4 Tuning of Full Filter

To compute the group delay for the first resonator, the other three resonators are shorted as shown in figure 2.35 and only the first one is tuned. For two resonators, the last two resonators are shorted and the first two tuned so that the right group delay is obtained. The same is done for three resonators, with only the last resonator being shorted and the rest tuned. The computed group delays for S_{11} together with the phase for the two and three resonators respectively are shown below in figures 2.36 and 2.37, comparing the responses from CST to those from MWO. The method used is in line with that outlined by Ness in [27].

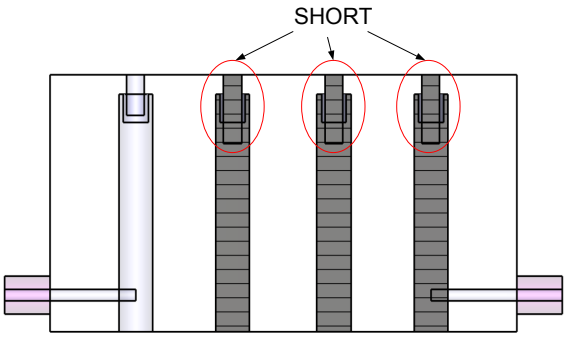

(a) CST Model

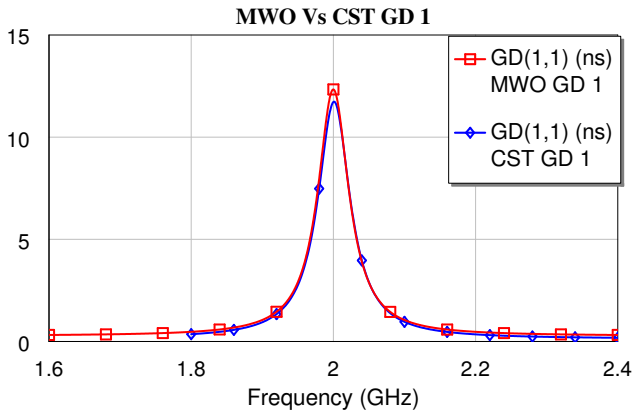

(b) Group Delay for a Single Resonator

Figure 2.35: Computation of the Group Delay and Phase of S_{11} for a Single Resonator

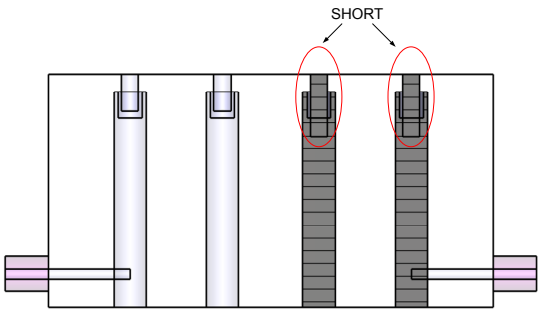

(a) CST Model

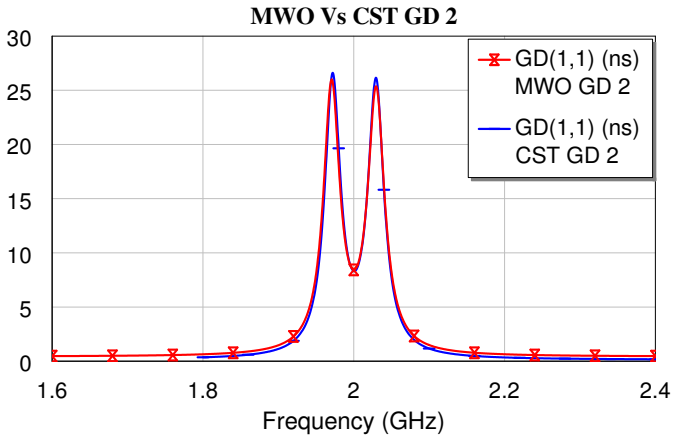

(b) Group Delay Two Resonators

Figure 2.36: Computation of the Group Delay and Phase of S_{11} for Two Resonators

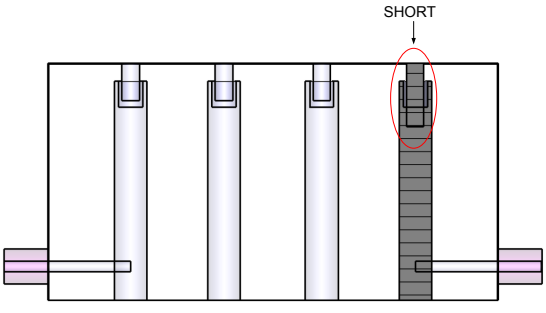

(a) CST Model

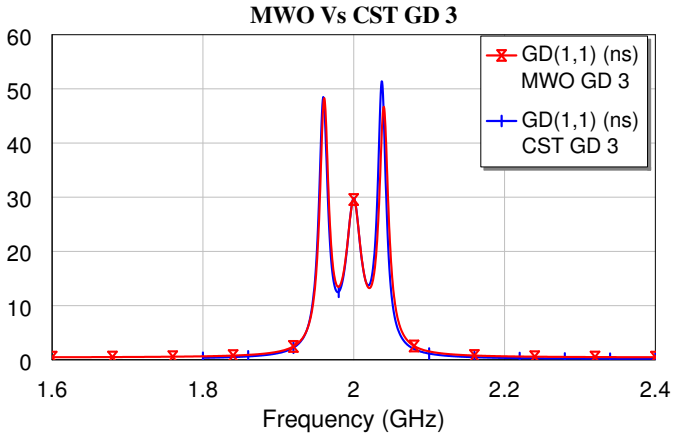

(b) Group Delay Three Resonators

Figure 2.37: Computation of the Group Delay and Phase of S_{11} for Two Resonators

Once this is done, the final resonator can be tuned to obtain the final frequency response. This is given, in comparison with the S-parameters of the MWO circuit model, in figure 2.38 below.

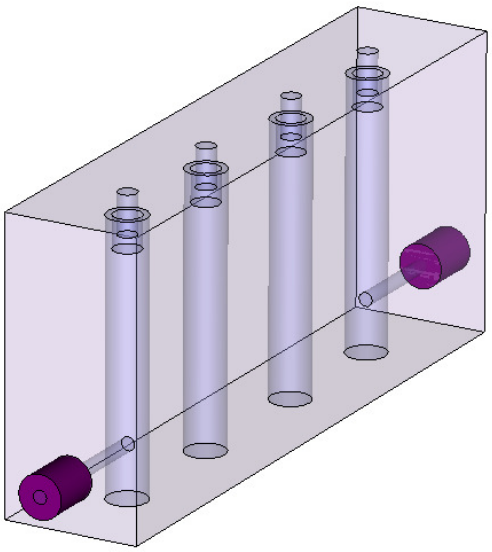

(a)

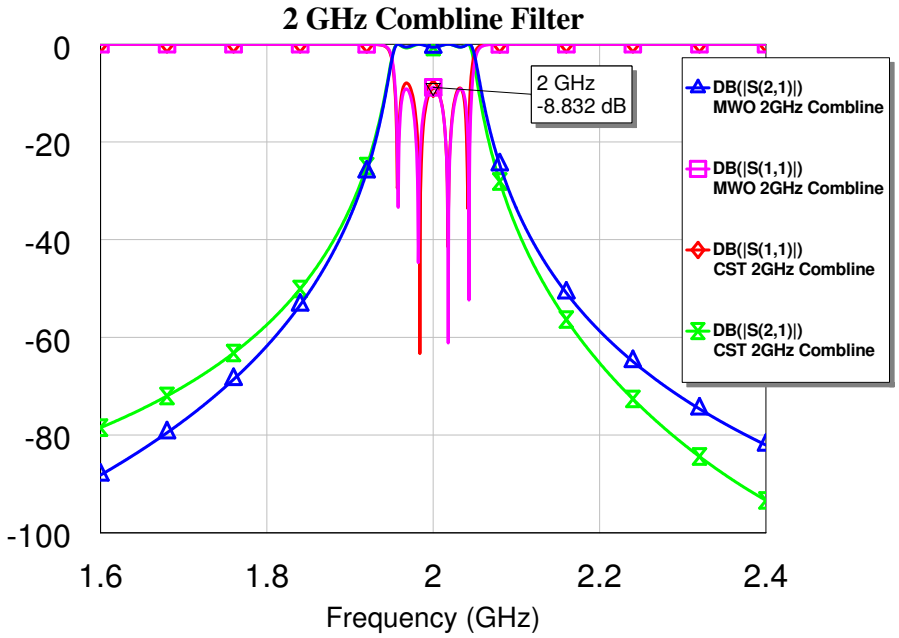

(b)

Figure 2.38: (a) 2GHz Combline Filter (b) S-Parameters of the Combline Filter in *(a)* [The physical dimensions of the filter are given in the Appendix A]

2.4 Conclusion

Different characteristics of combline filters have been discussed in this chapter, and a fourth order filter operating at 2GHz has been designed. The design process outlined, both for the circuit model in MWO and for the 3D implementation of the physical structure in CST, acts as a basis for the designs to be covered in subsequent chapters. The characteristics discussed are also important for discussions in following chapters, starting with Chapter 4 which will cover investigations on the comparison between this type of filter and an evanescent-mode waveguide filter, which is designed in Chapter 3.

Chapter 3

Design of Evanescent-Mode Waveguide Filters

3.1 Introduction

In this chapter, a brief introduction to evanescent-mode waveguides is given followed by a discussion on the design theory used in designing such filters. The design process to be covered entails the realisation of the circuit model for the filter and a discussion of the implementation of the physical structure. The chapter also includes the design of a fourth order evanescent mode filter operating at 2GHz which is designed in both MWO (circuit model) and in CST (3D implementation of the physical structure). The filters designed in this chapter are to be used in Chapter 4 for investigations of the characteristics of an evanescent-mode waveguide filter in relation to those of a combline filter.

3.2 Evanescent-Mode Waveguides

In a paper published in 1965 [16], Cohn states one of the reasons for the continuing attraction of microwave filters as a subject of research, to be their singular appeal for creative study. In another very interesting paper [17], he discusses how scientific laws, rules, theorems or common knowledge, when blindly accepted, can guide us to error and 'wall' us from discovery. Physical 'certainties' can impede progress, but in the past, such barriers have been broken-through, creating lee-way for more technological advancements. The difficulty that presented itself in the acceptance of the concept of possibilities of wave propagation in evanescent-mode waveguides is a good example of such mental obstacles.

Early work done on waveguides by Lord Rayleigh and afterwards by the scientists at Bell Laboratories and Massachusetts Institute of Technology had drawn conclusions about the fact that, below the cut-off conditions defined by derived equations pertaining to the field in the guide, progressive wave propagation could not exist [2]. For this reason, waves existing below cutoff were labelled "evanescent", defined as "fading quickly"[2]. However, these conclusions only hold true as long as the guide is infinitely long, or terminates in matching impedance [2].

Due to the practical nature of engineering, concepts that have not been proven to be useful over a number of years are usually deemed to be useless. Early approximate analyses of waveguide dissipative loss indicated that it was infinite at cutoff, so that the concept of transmission below cutoff was not easy to comprehend. That reluctance was a possible reason for the rejection of an application for a patent on an "evanescent mode" filter in 1967 and its dismissal as an "inoperable device" in one major country [2].

In one of its earliest appearances, the evanescent-mode behaviour was a source of mysterious breakdown in waveguides carrying high power, an occurence leading to the name "ghost mode", implying its extraordinary phenomenon. The term "evanescent mode" was then adopted because the mode has an imaginary wave impedance and a real propagation constant [2].

The useful properties of resonators built in below cutoff waveguide were first predicted by Lebedev and Guttsait [33]. They concluded that the resonators were simple and also likely to be useful for wide-band applications. In [34], Edson proposed the use of evanescent mode resonators in filters.

Evanescent-mode filters utilise the scattering waves resulting from obstacles placed in the guide to form high Q, inductively coupled filters. These obstacles, when introduced into a waveguide, distort the initially unperturbed field in their immediate vicinity [2]. The resultant field can be resolved into: the incident wave and a pair of scattered waves directed towards the source and load respectively, all of which consist of a series of evanescent modes [2]. If the energy stored in the electric field exceeds that stored in the magnetic field, then the obstacle is capacitive. Conversely, should the magnetic field store more energy than the electric field, then the obstacle is inductive [2].

In the design of these filters, a major assumption that is made is that the only mode existing in the guide is an evanescent TE_{10} mode. If a rectangular waveguide of conventional aspect ratio is excited in a pure evanescent TE_{10} mode, the attenuation constant of all other modes likely to be excited in the the guide will be extremely high. For this reason, at moderate distances from the obstacle, the field will be virtually a pure evanescent TE_{10} mode [18]. Under such circumstances, a section of evanescent-mode waveguide can be represented using an equivalent section of transmission line shown in figure 3.2 (a). This transmission line equivalent has a characteristic impedance, Z_0, given by

$$Z_0 = jX_0 + R \tag{3.1}$$

Because the unloaded Q factors of evanescent-mode resonators are high, usually more than 1000, the equivalent transmission line circuit can be modelled with an assumption that it is lossless, so that the characteristic impedance is imaginary, unlike that of a conventional waveguide which is real, and is given by [18]

$$Z_0 = jX_0 \tag{3.2}$$

where

$$X_0 = \frac{120\pi b}{a\sqrt{\left(\frac{\lambda}{\lambda_c}\right)^2 - 1}} \tag{3.3}$$

where λ is the free-space wavelength, λ_c is the guide cutoff wavelength, a is the waveguide width and b is the height of the waveguide, shown in figure 3.1.

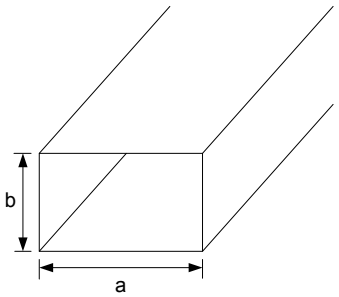

Figure 3.1: Rectangular Waveguide

The propagation constant of an evanescent mode, also dissimilar to that of a conventional waveguide which is a imaginary, is a real function and is given by

$$\gamma = \frac{2\pi}{\lambda}\sqrt{\left(\frac{\lambda}{\lambda_c}\right)^2 - 1} \tag{3.4}$$

The transmission line equivalent circuit can be more conveniently represented by a pi-network or a T-network equivalent of frequency dependent, lumped inductors as shown in figure 3.2 (b) and (c) respectively. Owing to the fact that the propagation constant is real for the range of frequencies from zero frequency to cutoff frequency, the reactance frequency relationship of an evanescent mode waveguide is not of a periodic nature as would be expected of a normal distributed constant network. The behaviour of the elements in the pi-network equivalent therefore approximates the behaviour of a lumped inductance at frequencies between zero and cutoff frequency.

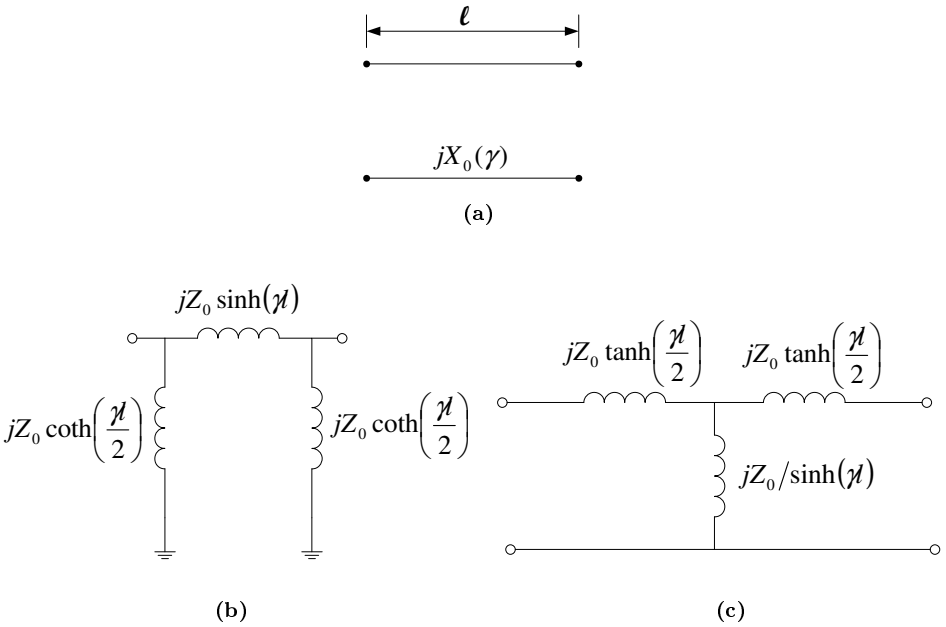

Figure 3.2: (a) Transmission Line Equivalent of an Evanescent-mode Waveguide (b) Pi-Network Lumped Element Circuit Model for Evanescent-Mode Waveguide (c) Equivalent T-section of a Cut-off Guide

For the evanescent-mode waveguide filters designed in this thesis, the pi-section representation is chosen because it is more convenient for filters having shunt resonators. The shunt elements are proportional to the cut-off frequency of the waveguide, whereas the series elements correspond to the length of the waveguide.

Resonating the shunt elements with capacitors as shown in figure 3.3

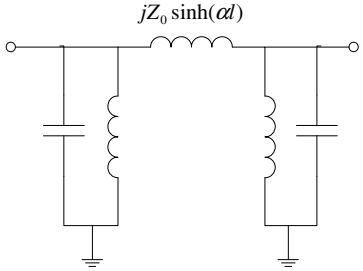

Figure 3.3: Coupled Resonator Filter Formed by Adding a Capacitor

and connecting a number of these sections in cascade results in a lumped-element representation of a multi-order bandpass evanescent-mode filter which is shown in figure 3.4 (b), together with its transmission line equivalent representation in figure 3.4 (a).

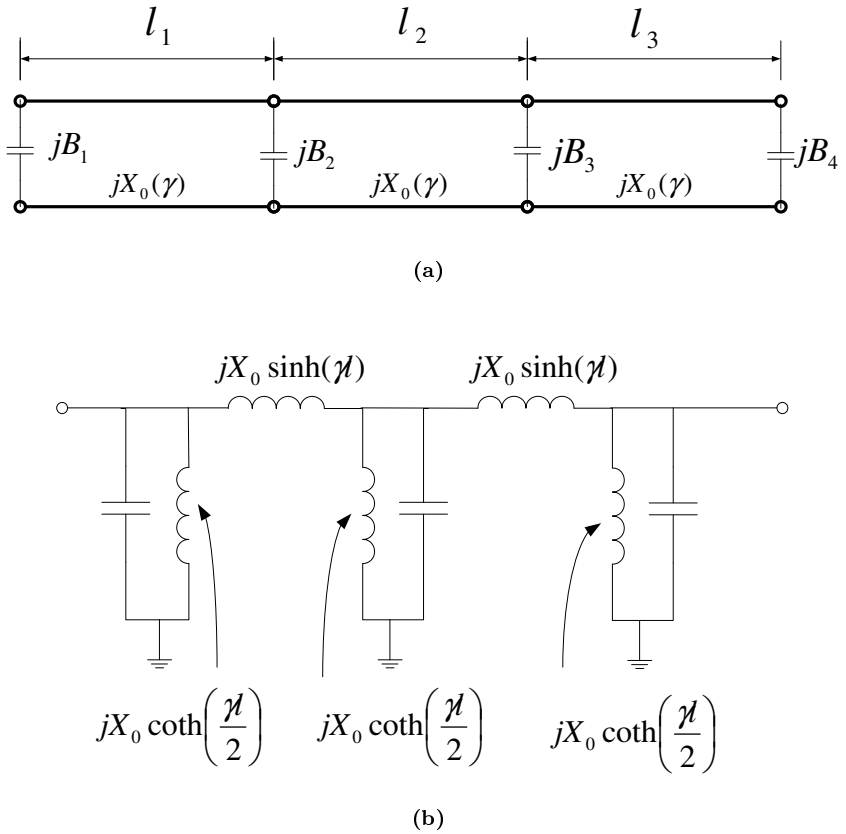

Figure 3.4: Lumped Equivalent Circuit of an Evanescent-mode Waveguide Filter

For moderate bandwidths, the value of γl required results in a value of $\coth(\gamma l/2)$ which is near unity, so that $\coth(\gamma l/2)$ is virtually independent of frequency [18]. The coupling reactance $X_0 \sinh(\gamma l)$ may also be considered a constant over a moderately narrow bandwidth. In such a case, the equivalent circuit in figure 3.4 may be treated as if lumped circuit resonators were involved.

The resemblance of the equivalent elements in figure 3.4 (b) to lumped-circuit elements is more than just representational. As the frequency of operation moves further below cutoff, the approximation to lumped circuits becomes closer, and at a frequency sufficiently far from the cutoff frequency, virtual identity is established.

However, below cutoff the attenuation constant is a function of frequency, so that more losses are incurred when working further from the cutoff frequency. This prevents direct design in terms of lumped-circuit theory, together with the fact that the reactance-frequency slope, if $\coth(\gamma l/2)$ is assumed to be constant, will have a pole at cutoff frequency (see equation 3.1) instead of at infinity like in the case of a lumped inductance. For this reason, the slope of the reactance-frequency characteristic for the equivalent evanescent mode "inductance" will be steeper than that for a corresponding lumped inductance [18]. In order to be able to treat the circuit in figure 3.4 as if it were a lumped circuit, a correction factor given by [18]

$$\Delta = \frac{2}{1 + \frac{1}{1-(\lambda_c/\lambda_0)^2}} \tag{3.5}$$

which takes into account the difference, is used. The correction can also be achieved by the use of the frequency transformation [2]

$$F = \frac{f}{f_0} - \left\{ \frac{(f_c/f)^2 - 1}{(f_c/f_0)^2 - 1} \right\}^{1/2} \tag{3.6}$$

For large values of f_c, the expression reduced to the well-known lowpass-to-bandpass transformation

$$F = \frac{f}{f_0} - \frac{f_0}{f} \tag{3.7}$$

which confirms the essentially lumped-circuit properties of the network in figure 3.4 (b).

For narrowband filters, the capacitive elements in figure 3.4 are achieved using posts introduced perpendicular to the broad dimension of the waveguide.

3.3 Realisation of a Circuit Model

With the conditions under which the equivalence between the inductive elements of an evanescent-mode waveguide filter and those of a lumped-circuit filter having been established, a circuit model of an evanescent-mode filter can now be realised, in terms of the elements of a lumped circuit filter.

As with combline filters, the first design step is to obtain a J-inverter-coupled coupled-resonator filter, repeated here for convenience in figure 3.5.

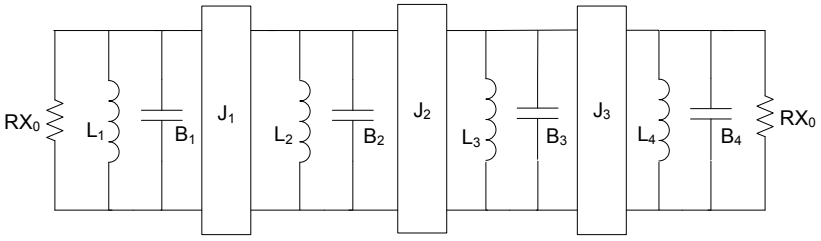

Figure 3.5: J-Inverter-Coupled Coupled-resonator Filter

The standard coupled resonator filter can be re-partitioned as shown in figure 3.6 with the evanescent mode guide sections represented by the pi circuit inside the blue box and the inverters in the pink boxes.

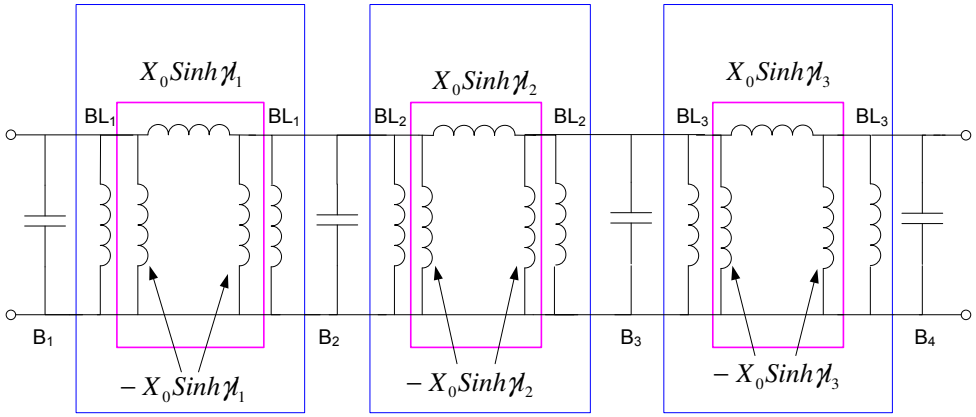

(a)

Figure 3.6: Below Cutoff Waveguide Filter using J-Inverters

The impedance of the inverters is then given by

$$J_j = X_0 \sinh \gamma l_j \tag{3.8}$$

with a 90^0 phase shift.

Once represented in the form in figure 3.5, the resonant properties can be computed easily for the parallel LC resonators. However, for that circuit to be valid, the equivalent shunt inductance on either side of the series inductance within the blue box in figure 3.6 must equal the corresponding single shunt inductance element on either side of the series inductance in figure 3.4 (b).

Therefore, for the shunt elements before the first inverter, we have

$$\frac{1}{X_0 \coth \frac{\gamma l}{2}} = BL_1 - \frac{1}{X_0 \sinh \gamma l_1} \tag{3.9}$$

and for the shunt elements after the nth inverter we have

$$\frac{1}{X_0 \coth \frac{\gamma l}{2}} = BL_n - \frac{1}{X_0 \sinh \gamma l_n} \tag{3.10}$$

where n is the number of inverters in the circuit. In figure 3.6, $n = 3$.

For the inner shunt elements

$$\frac{1}{X_0 \coth \frac{\gamma l}{2}} = BL_{k-1} + BL_k - \frac{1}{X_0 \sinh \gamma l_{k-1}} - \frac{1}{X_0 \sinh \gamma l_k} \; ; \; 1 < k < n \tag{3.11}$$

The inductive reactances in figure 3.5 are given by [18]

$$\omega_0 L_k = \frac{1}{BL_{k-1} + BL_k} = \frac{1}{B_0 \left(\coth \gamma l_{k-1} + \coth \gamma l_k \right)} \; ; \; 1 \leq k \leq n \tag{3.12}$$

where

$$B_0 = \frac{1}{X_0} \tag{3.13}$$

and for resonance

$$\omega_0 L_k = \frac{1}{\omega_0 C_k} \; ; \; 1 \leq k \leq n \tag{3.14}$$

So that, the capacitances in figure 3.5 can be computed as

$$B_i = \omega_0 C_i = B_0 \left(\coth \gamma l_{i-1} + \coth \gamma l_i \right) \; ; \; 1 \leq i \leq n \tag{3.15}$$

To design the evanescent-mode waveguide filter in terms of lowpass prototype elements, g_i, Craven and Mok show in [18] how the inverter coupled filter in figure 3.5 is first converted to an equivalent ladder network as shown in figure 3.7 by expanding the input impedance of the network in figure 3.5 as a continued fraction with the obtained values shown in figure 3.7.

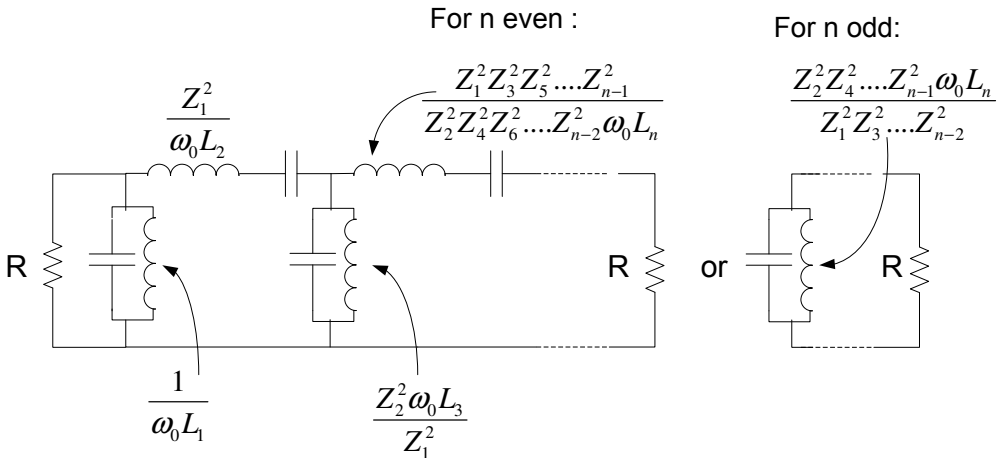

Figure 3.7: Equivalent ladder network of the filter in figure 3.6 (b)

For the ladder networks in figure 3.7 to be equal to the basic lumped network derived from a lowpass prototype and shown in figure 3.8, respective elements in each of the networks must also be equal.

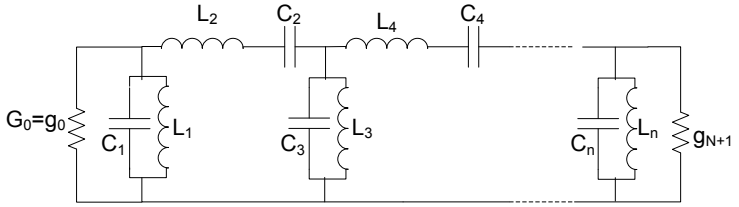

Figure 3.8: Basic lumped element bandpass filter network

Therefore, the first term is

$$\frac{R}{\Delta\omega_0 L_1} = \frac{R_0 g_1 \omega_0}{\omega_2 - \omega_1} \tag{3.16}$$

The correction factor Δ, given by equation 3.5, takes into account the steeper reactance-frequency slope of the evanescent 'inductance' term. For the second term, the equated elements are

$$\frac{\sinh^2(\gamma l_1)}{R\Delta\omega_0 L_2} = \frac{g_2\omega_0}{R_0(\omega_2 - \omega_1)} \tag{3.17}$$

By introducing the fractional bandwidth $\delta = \frac{\omega_2 - \omega_1}{\omega_0}$, and simplifying with the aid of equation 3.16, equation 3.17 can then be solved for $\sinh(\gamma l_1)$ to get

$$\sinh(\gamma l_1) = \frac{\Delta}{\delta}\sqrt{g_1 g_2 \omega_0 L_1 \omega_0 L_2} \tag{3.18}$$

The general expression for the terms between the first and last terms is

$$\sinh(\gamma l_i) = \frac{\Delta}{\delta}\sqrt{g_i g_{i+1} \omega_0 L_i \omega_0 L_{i+1}} \tag{3.19}$$

3.4 Design of a Circuit Model for a 2GHz Evanescent-Mode Waveguide Filter

The design specifications for this filter are chosen to be the same as those for the combline filter in section 2.2.6, and are given again below in table 3.1.

Order of the filter	4th Order
Fractional Bandwidth	5%
Centre Frequency	2GHz
Response type	Chebyshev
Passband Ripple	0.5dB

Table 3.1: Design Specifications for an Evanescent-mode Waveguide Filter

The design process starts with the choice of an appropriate size of waveguide which has a cut-off frequency above the desired frequency of operation. Ordinarily, there is no classified waveguide size for a given frequency band. There is a wide choice. Most choices require trade-offs between the desired physical size of the filter and the required unloaded Q-factor. Depending on the system requirements, the frequency at which spurious responses begin to occur and the required mass of the filter should also be considered.

For this thesis, WR-187 and WR-137 waveguides were chosen. The dimensions of these in inches and cm are given in table 3.2.

EIA Designation (WR-XX)	TE_{10} Cut0ff Frequency (GHz)	Inside Dimensions ($a \times b$) [Inches (cm)]	Outside Dimensions [Inches (cm)]
WR-187	3.152	1.872×0.872 (4.755×2.215)	2.000×1.000 (5.080×2.540)
WR-137	4.301	1.372×0.622 (3.485×1.580)	1.500×0.750 (3.810×1.905)

Table 3.2: Standard guide data for WR-187 and WR-137 waveguides [13]

The unloaded Q-factor of a guide having a capacitive obstacle excited in the evanescent TE_{10} mode is computed as [18]

$$Q_{BC} = \frac{\omega\mu}{R_s}\frac{ab}{2}\frac{1-\frac{1}{2}\left(\frac{f}{f_c}\right)^2}{a\left[1-\frac{1}{2}\left(\frac{f}{f_c}\right)^2\right]+b} \tag{3.20}$$

where R_s is the the surface resistance given by

$$R_s = \sqrt{\frac{\omega\mu}{2\sigma}} \tag{3.21}$$

with σ being the conductivity of the walls of the guide. a and b are in metres. For a guide constructed in copper with $\sigma = 5.813 \times 10^7 S/m$, and with an air dielectric, figure 3.9 shows the Q-factor of the TE_{10} mode at different frequencies both below and above cutoff in a WR-137 waveguide. The unloaded Q computed for the TE_{m0} modes of a waveguide above cutoff with is calculated as [15]

$$Q_{AC} = \frac{1.212 \times 10^4 b\sqrt{f}}{1+\frac{2b}{a}\left(\frac{f_c}{f}\right)^2} \tag{3.22}$$

with a and b measured in inches. The cutoff frequency of a WR- 137 waveguide is 4.301GHz.

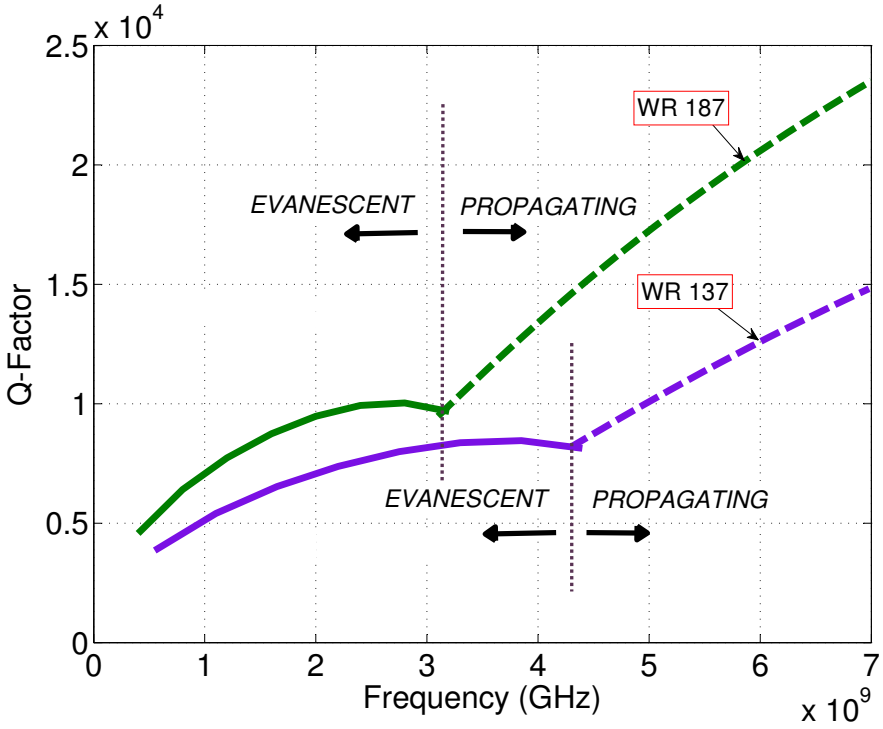

Figure 3.9: Q-Factor of the TE_{10} Mode in a WR137 Waveguide

A high Q-factor of about 7000 can be obtained at 2GHz for the filter designed in WR 137 waveguide. However, the curves only represent the Q of the inductive elements, and exclude losses due to the capacitive elements. If the losses from the capacitive elements are included, this value is expected to decrease. Total Q-factors are commonly two-thirds of the Q-factors obtained due to the inductive elements alone [2]. The inductive element approaches self resonance as cutoff is approached so that the amount of needed capacitance for resonance decreases, and in effect, the amount of loss associated with the capacitve element also decreases. The advantage of this aspect is that the necessary screw penetration is approximately the same as the one that would be required in a conventional above cut-off guide section, so that the Q factor presented in the curves in figure 3.9, both below and above cutoff, is almost the same as the Q-factor of the complete resonator.

For a filter built in a WR-187 waveguide, the plot of the Q-factor, also both below and above cutoff is also given in figure 3.9. Owing to the larger physical dimensions of the cross-section size of a WR-187 waveguide, a larger Q-factor due to the inductive elements of more than 9000 can be obtained at 2GHz.

The characteristic impedance is calculated from equation 3.3 to obtain

$$X_{0_{187}} = 144.2$$

$$X_{0_{137}} = 89.8$$

In [18], Craven and Mok reduce the expression for $\sinh(\gamma l_i)$ in equation 3.19 for filters with narrow bandwidths and shunt resonator terminations to the approximation

$$\sinh \gamma l_i \simeq \frac{1}{2}\frac{\Delta}{\delta}\sqrt{g_i g_{i+1}} \qquad for\ r = 1, ..., n-1 \tag{3.23}$$

For a symmetrical chebyshev response, we also have

$$l_i = l_{n-i}$$

The g_i values are the element values of the lowpass prototype and given in table 3.3 below for a fourth order chebyshev response with a 0.5dB ripple

g_0	g_1	g_2	g_3	g_4	g_5
1	1.6703	1.1926	2.3661	0.8419	1.9841

Table 3.3: Element Values for a 4th Order Chebyshev Equiripple Lowpass filter with 0.5dB ripple

The correction factor can be computed using equation 3.5 to get

$$\Delta_{187} = 0.748$$

$$\Delta_{137} = 0.879$$

For the given fractional bandwidth of $\delta = 5\% = 0.05$, we now have for the WR-187

$$\sinh \gamma l_{1_{187}} = \sinh \gamma l_{3_{187}} = 10.557$$

$$\sinh \gamma l_{2_{187}} = 12.564$$

and for the WR-137

$$\sinh \gamma l_{1_{137}} = \sinh \gamma l_{3_{137}} = 12.403$$

$$\sinh \gamma l_{2_{137}} = 14.762$$

so that the impedances for the J-inverters can now be computed using equation 3.8 to get, for the WR-187 waveguide

$$J_{1_{187}=}J_{3_{187}} = 1.5227e + 003\Omega$$

$$J_{2_{187}} = 1.8123e + 003\Omega$$

and for the WR 137 we have

$$J_{1_{137}=}J_{3_{137}} = 1.1135e + 003\Omega$$

$$J_{2_{137}} = 1.3252e + 003\Omega$$

If the inductors forming the J-inverters are then assigned the notation L_{Ji}, and are computed using the formula

$$L_{Ji} = \frac{Z_i}{\omega_0} \tag{3.24}$$

we then get, for WR-187

$$L_{J1_{187}} = L_{J3_{187}} = 0.1212\mu H$$

$$L_{J2_{187}} = 0.1442\mu H$$

and for the WR-137 we get

$$L_{J1_{137}} = L_{J3_{137}} = 0.0886\mu H$$

$$L_{J2_{137}} = 0.1055\mu H$$

Using equations 3.12 to 3.15 and choosing l_0 so that $\coth \gamma l_0 \approx 1 \approx \coth \gamma l_4$ (l_0 and l_4 are the distances between the end resonators and the end walls of the filter), the inductance and capacitance of the shunt resonator elements are then computed and are given in table 3.4.

WR-XX	L_1(nH)	C_1(pF)	L_2(nH)	C_2(pF)	L_3(nH)	C_3(pF)	L_4(nH)	C_4(pF)
WR-187	5.726	1.106	5.717	1.108	5.717	1.108	5.726	1.106
WR-137	3.566	1.776	3.562	1.778	3.562	1.778	3.566	1.776

Table 3.4: Calculated Inductance and Capacitance of the Shunt Resonator Elements

The terminating impedances, R, can then be computed from equation 3.16 to get

$$R_{187} = 1.798k\Omega$$

$$R_{137} = 1.316k\Omega$$

The circuit model was then simulated in MWO with the elements impedance transformed so that the port impedances are 50Ω

```
wB=0.05
b=2.215
a=4.755
f0=2e9
fc=3.152e9
c=3e8
lamd0=c/f0
lamdc=c/fc
x0=120*_PI*b/a/sqrt((lamd0/lamdc)^2-1)
B0=1/x0
R0=1
w0=2*_PI*f0
coth_alphl1=1
Lj1=x0*sinh_alphl1/w0
Lj2=x0*sinh_alphl2/w0
Lj3=Lj1
R=(R0*g1*w0*delta*BL1/wB)
Rt=50/R
Rr=R*Rt
g0=1
g1=1.67
g2=1.193
g3=2.366
g4=0.8419
g5=1.9841
delta=2/(1+1/(1-(lamdc/lamd0)^2))
sinh_alphl1=(0.5*delta/wB)*sqrt(g1*g2)
sinh_alphl2=(0.5*delta/wB)*sqrt(g2*g3)
alphl1=asinh(sinh_alphl1)
alphl2=asinh(sinh_alphl2)
BL1=1/B0/(1/(tanh(alphl1))+coth_alphl1)/w0
BL2=1/B0/(1/(tanh(alphl1))+1/(tanh(alphl2)))/w0
BL3=BL2
BL4=BL1
B1=1/(w0^2*BL1)
B2=1/(w0^2*BL2)
B3=B2
B4=B1
```

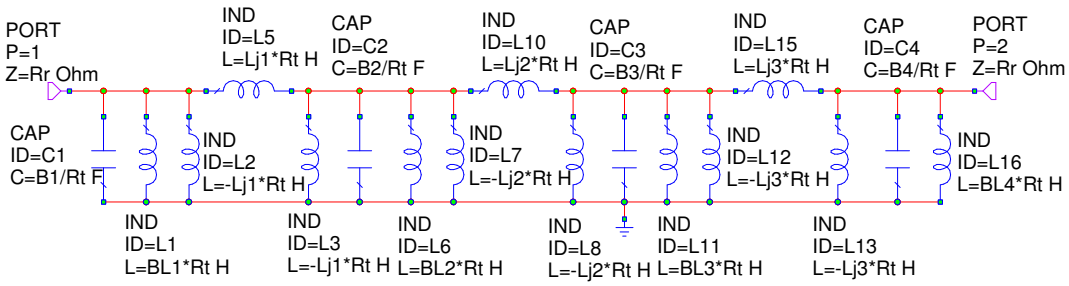

Figure 3.10: Circuit Model of 2GHz Evanescent-Mode Waveguide Filter in MWO

The S-Parameters for the circuit simulated using the computed value of correction factor for the WR-187 waveguide (Δ_{187}=0.748) are shown below in figure 3.11.

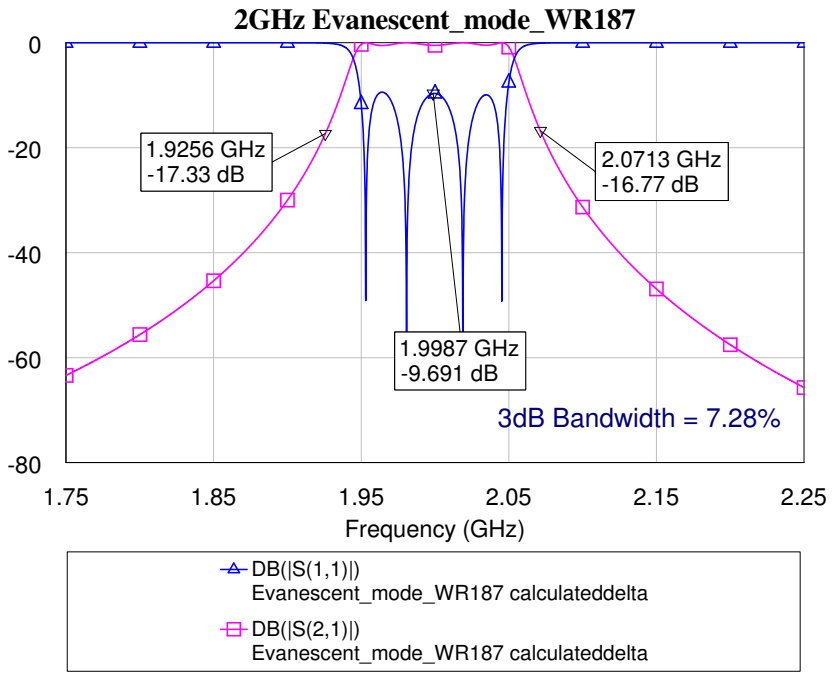

Figure 3.11: S-Parameters of the WR-187 Evanescent-Mode Filter in Figure 3.10

The obtained 3dB bandwidth is 7.28% which is larger than the desired 5% bandwidth. For the filter designed for a WR-137 waveguide, the 3dB bandwidth is 6.21% as shown in figure 3.12.

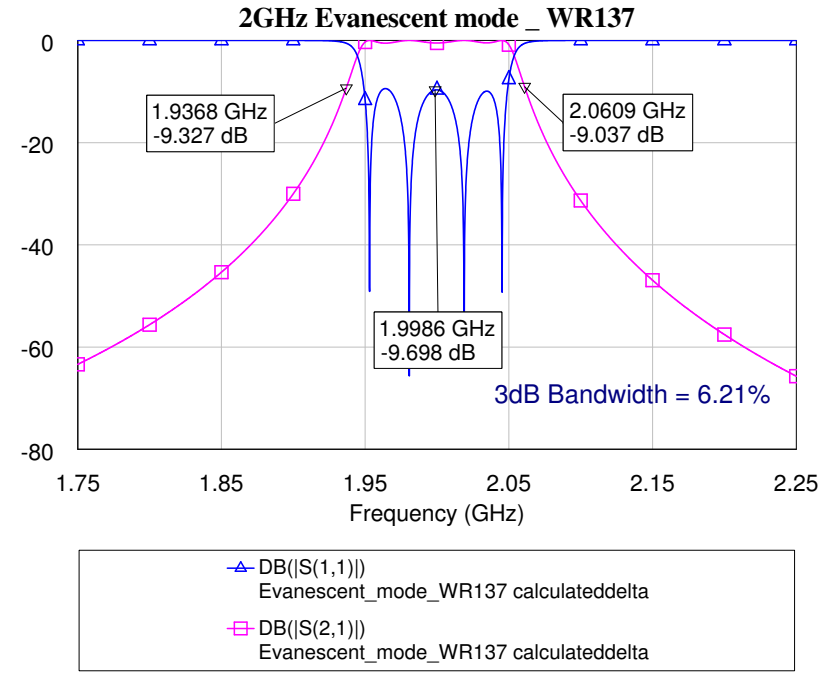

Figure 3.12: S-Parameters of a circuit model for an Evanescent-Mode Waveguide Filter in WR-137 waveguide

The correction factor relates the bandwidth of an evanescent mode resonator to that of a lumped circuit resonator. As was mentioned before, the behaviour of an evanescent mode resonator approaches that of a lumped circuit resonator more as the frequency of operation moves further from cut-off. In the two filters designed from a WR-187 and WR-137, it is evident from figures 3.11 and 3.12 that the bandwidth reduces when working further from cut-off. This behaviour is confirmed by designing additional circuits in WR-112 (cutoff frequency = 5.259GHz) and WR-90 (cutoff frequency = 6.557GHz) waveguides. The resulting S-Parameters

are shown below in figure 3.13 in comparison with responses for the WR-187 and WR-137 filters.

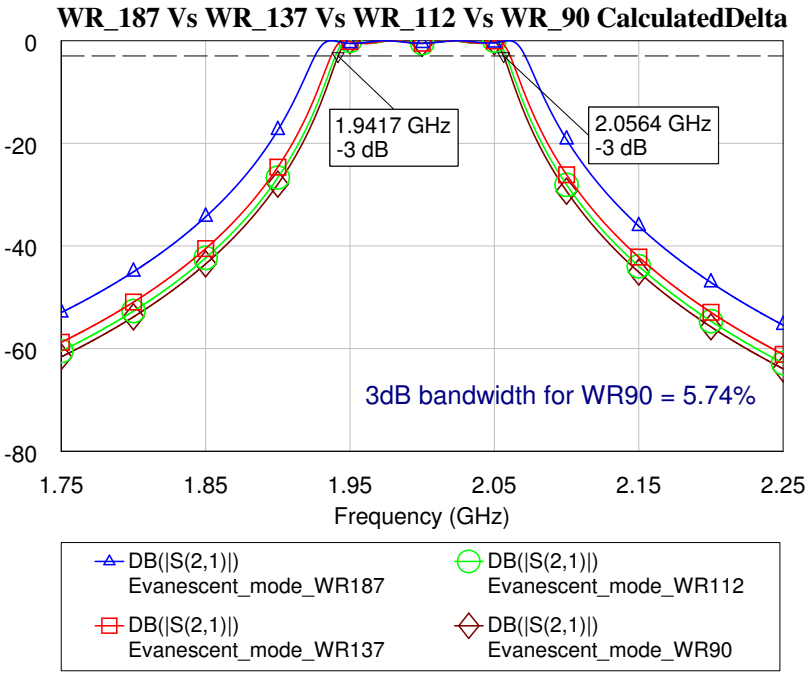

Figure 3.13: S-Parameters of Circuit Models of Evanescent-Mode Waveguide Filters designed in WR-187, WR-137, WR-112 and WR-90

The bandwidth reduces to 5.74% for the WR-90, but still not the desired 5%. It is seen, therefore, that if the operation frequency is moderately below cut-off ($\lambda_c/\lambda_0 = 1.5$), the departure from lumped circuit behaviour is moderate.

If the capacitive screws used as obstacles in the filter are to have a moderate screw-radius to guide-width ratio of about 0.1, they will behave as virtually pure capacitances. If such is the case, Craven and Mok in [18] recommend the use of a correction factor $\Delta_c = 1$. Using this correction factor in the MWO circuit models of the filters designed in WR-187, WR-137, WR-112 and WR-90, it is seen from their S-Parameters in figure 3.14 that they all now have the same bandwidth despite the different sizes of waveguide.

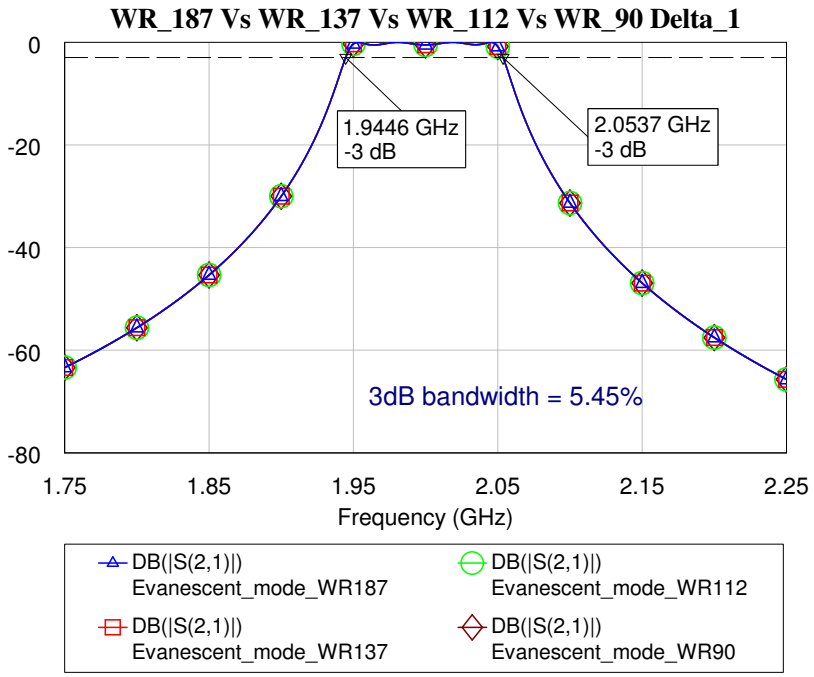

Figure 3.14: S-Parameters of Circuit Models of Evanescent-Mode Waveguide Filters designed in WR-187, WR-137, WR-112 and WR-90 with correction factor $\Delta_c = 1$

The obtained bandwidth is then 5.45%. Therefore, if the ratio of the screw radius to the guide width is maintained at 0.1, any size of waveguide can be used as long as the size and Q-factor requirements are met.

3.5 Realisation of Physical Model for a 2GHz Evanescent-Mode Waveguide Filter

3.5.1 Obstacles in a Waveguide

The simplest elements to use in practical evanescent-mode waveguide filters to simulate lumped capacitances are conventional waveguide obstacles. A variety of capacitive obstacles can be used in waveguide circuit design including capacitive windows, irises and cylindrical screws. However, the equivalent circuit of an obstacle used above cutoff frequency is not necessarily the same as that used below cutoff. In some instances, the effect of the 'imaginary guide wavelength' in below cutoff guides alters the sign of the obstacle susceptance, so that an obstacle can be capacitive above cutoff and yet be inductive below cutoff and vice versa.

A capacitive screw/post/stub (see figure 3.15), is capacitive both above and below cutoff, for moderate insertions into the guide.

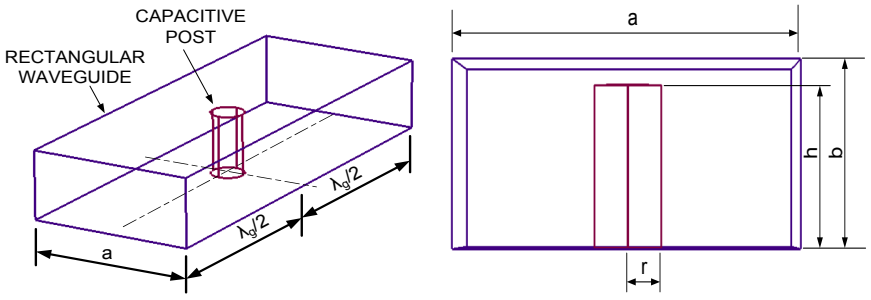

Figure 3.15: Capacitive screw in an evanescent-mode waveguide

It is important because it can be used to realise capacitive susceptances ranging from zero to virtual infinity, at series resonance [2]. When the screw gets in contact with the opposite wall, it results in an inductive susceptance. Screws/stubs/posts of moderate radius (r/a = 0.1 (see figure 3.15 (b))) in a rectangular guide behave as virtually a pure capacitance [2].

Figure 3.16 shows the changes in the magnetic energy of the TE_{10} mode for moderate insertions of the screw into the guide.

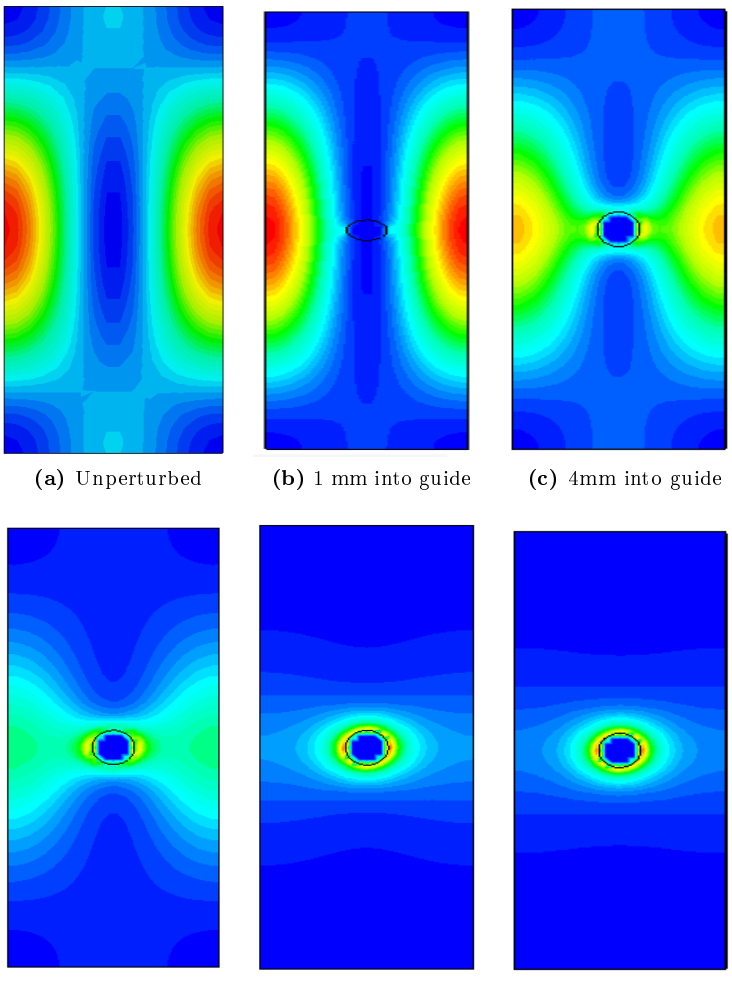

Figure 3.16: Magnetic Energy in a waveguide (a) unperturbed TE_{10} (b), (c), (d) For moderate insertions of a cylindrical post/screw

From figure 3.16 (e) and (f), it can be seen that the perturbation of the field with the increase in the length of

the screw inside the guide eventually results in an energy distribution very similar to that of a TEM field, with the magnetic field lines being concentric about the centrally located post as shown in figure 3.17.

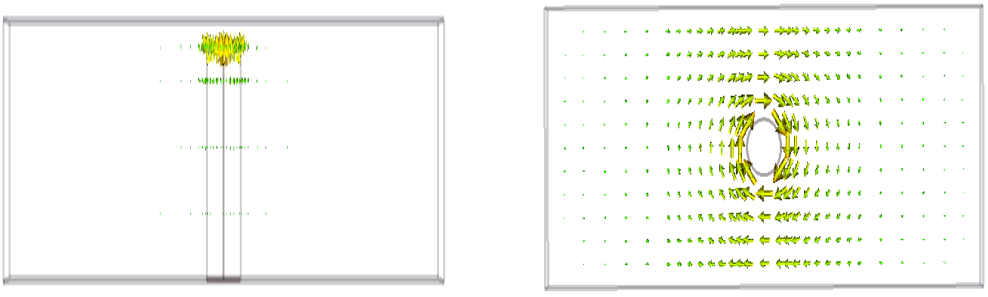

(a) Electric Field **(b)** Magnetic Field

Figure 3.17: Electric and Magnetic Field lines in WR-137 waveguide (a = 34.85 and b = 15.80 mm (see figure 3.15)), with post height, h (see figure 3.15), of 14mm

Visualisation of the distribution of energy in a resonator is important in determining the type of input/output coupling that would be best for that resonator and the positioning of the coupling as will be seen in section 3.5.3.

Given that the guide length is fixed, the required resonant frequency is obtained by adjustment of the penetration of the screw into the guide. For the waveguide in figure 3.15 (a), with a length of 44.69mm and cross-sectional dimensions, a × b, of 34.85mm × 15.80 mm, figure 3.18 (a) shows the variation of the resonant frequency with a change in the height of the screw inside the guide and figure 3.18 (b) shows the change in unloaded Q with the screw penetration depth.

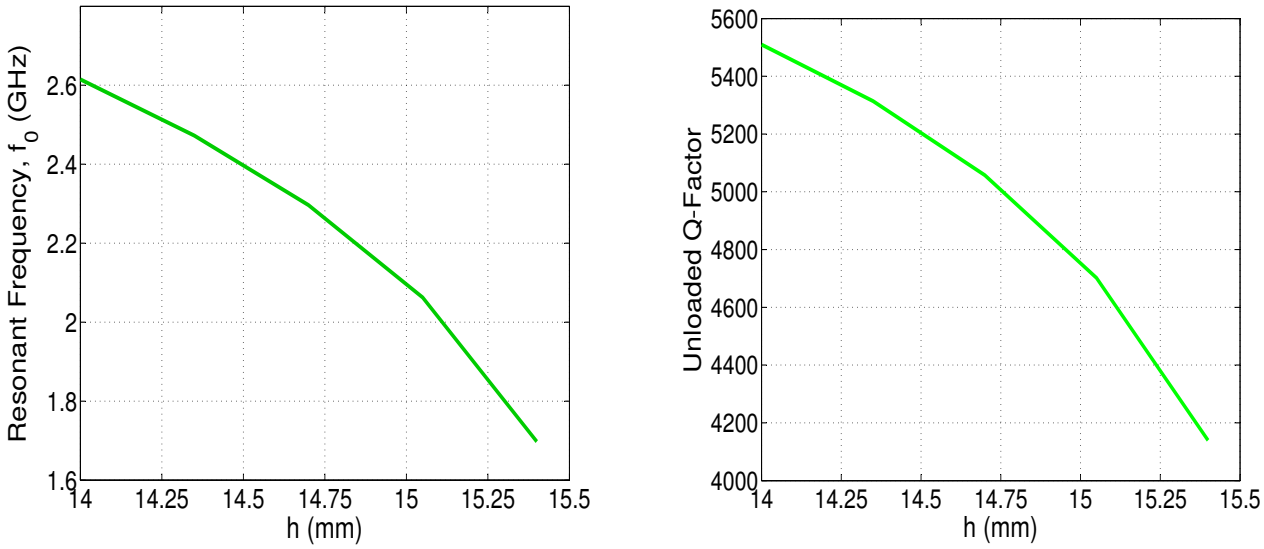

(a) Resonant Frequency vs. h **(b)** Unloaded Q Vs. h

Figure 3.18: Variation of resonant frequency and unloaded Q with increase in screw height, h (see figure 3.15).

The insertion of the screw reduces the overall volume in the guide, and also increases the amount of loss due to the conducting surfaces, therefore the unloaded Q decreases with an increase in h. The unloaded Q over the range of h = 14mm to h = 15.4mm corresponding to a frequency shift of about 0.92GHz ranges from about 4100 to 5500, which is quite high.

The capacitive post can be physically implemented in practical filters using an ordinary machine screw, with the threads turned off except near the head, for narrow-band filters. Bushes inserted into the guide can also be

used, but will create contact problems. For low losses, the screws can be copper- or silver-plated, and for the lowest possible loss, the use of capacitive studs soldered to the wall would be better. Compared to the use of screws, improvements in unloaded Q of up to 15 percent have been obtained with the use of studs [18].

3.5.2 Calculation of Spacings Between Obstacles

Figure 3.19 shows the lengths of the spacings between the capacitive posts in a fourth order filter. l_0 and l_4 represent the length from the first and last posts, respectively, to the guide walls, and are any convenient length necessary to terminate the guide in a short circuit and to achieve the right amount of input/output coupling, depending on the choice of input/output coupling technique.

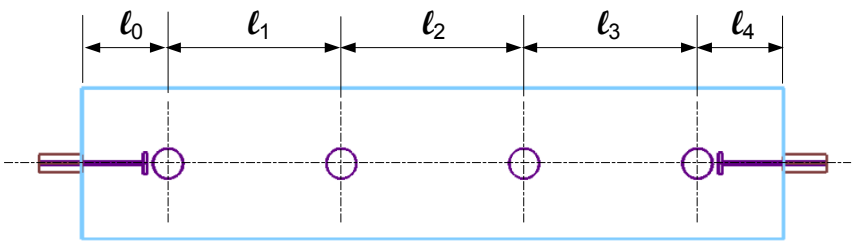

Figure 3.19: Inter-post spacings for an Evanescent-mode Filter with Shunt Resonator Terminations

In section 3.4, the values of $\sinh \gamma l_i$ were computed using equation 3.23 for the calculation of the inverter impedances for a 2GHz filter in both a WR-187 and a WR-137 waveguide. If the propagation constant is known, then the lengths, l_1, l_2 and l_3 can be computed for the 2GHz evanescent-mode filter with specifications given in section 3.4.

The propagation constant, given by equation 3.4, is calculated to get

$$\gamma_{187} = 0.5102$$

$$\gamma_{137} = 0.7975$$

from which the respective lengths are calculated to get

WR-XX	l_1 (cm)	l_2 (cm)	l_3 (cm)
WR-187	5.9819	6.3217	5.9819
WR-137	4.0286	4.2463	4.0286

Table 3.5: Lengths of the spacings between resonators for the 2GHz Evanescent-mode filter in WR-187 and WR-137

3.5.3 Coupling to External Circuitry

For an evanescent-mode waveguide employing the use of shunt resonators, there are several possible external coupling methods. Two of the methods involve coupling posts that are placed in parallel with the shunt inductors of the evanescent mode waveguide on either side of the post as shown in figure 3.20 for one side.

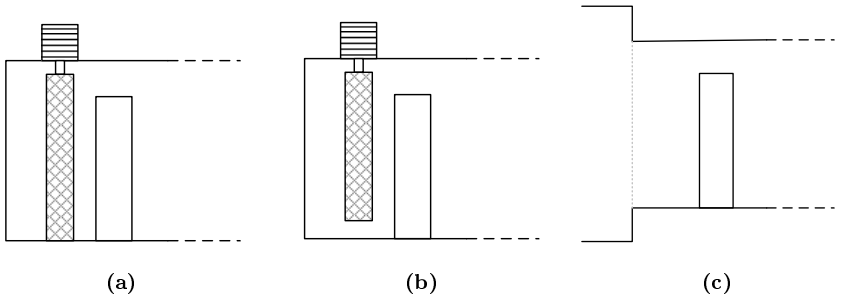

Figure 3.20: External coupling methods

Usually, the type of loading circuit to which the filter is connected determines whether the filter will begin with a shunt or a series resonator. In figure 3.20 (a), a conducting post extends from the centre pin of a coaxial connector to the opposite conducting wall of the waveguide and is actually in contact with that wall, resulting in inductive coupling. The second of these methods, shown in figure 3.20 (b), instead of having the post extending all the way to the opposite wall, allows for a capacitive gap, so that the coupling into the guide is capacitive and can be adjusted using a capacitive screw on the opposite end.

Coupling into the guide can also be achieved by means of a sudden step to propagating waveguide as shown in figure 3.20 (c). The step junction creates a capacitive susceptance which can be compensated by a short length of evanescent mode waveguide between the propagating guide and the 1st loading capacitor [14]. Design details for this kind of external coupling are discussed in [14]. This kind of coupling is for a case where the filter begins with a series resonator.

In this thesis, filters beginning with shunt resonators are being considered and coaxial line loads are used. A few other coupling techniques, different from those in figure 3.20 were considered. In figure 3.21, the input/output coupling techniques used are shown for both capacitive coupling and inductive coupling are shown.

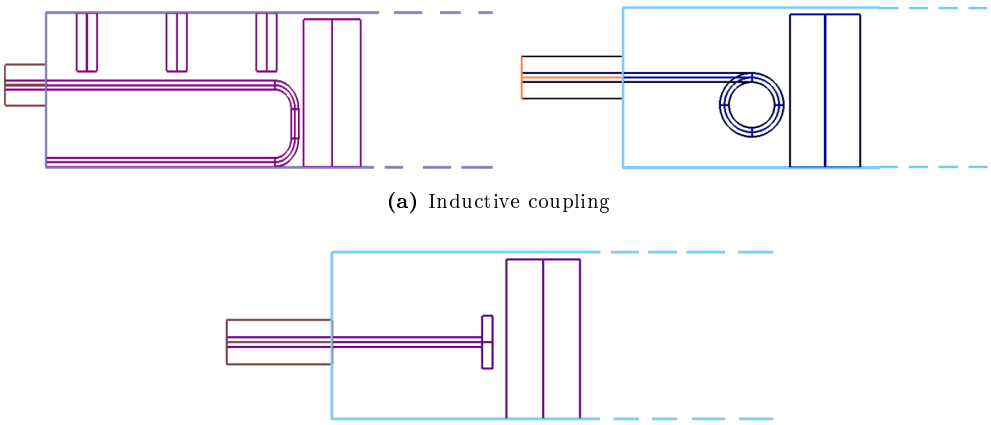

(a) Inductive coupling

(b) Capacitive coupling

Figure 3.21: Input/Output Coupling techniques for Evanescent-mode Filters with Shunt Resonator Terminations

Each of these methods was investigated and worked reasonably well, even though the practical implementation and tuning of some may not be necessarily easy.

3.5.4 Implementation of Full 2GHz Evanescent-mode Waveguide Filter in CST

With all lengths, l_1, l_2 and l_3 now known, a 3D model of an evanescent mode filter, shown in figure 3.22 was simulated in CST with the posts having radius, r (see figure 3.15), being a tenth of the longer dimension of the

guide cross-section, a. Capacitive input/output coupling is used. All the posts have the same height, and were tuned simultaneously until the required resonant frequency was obtained.

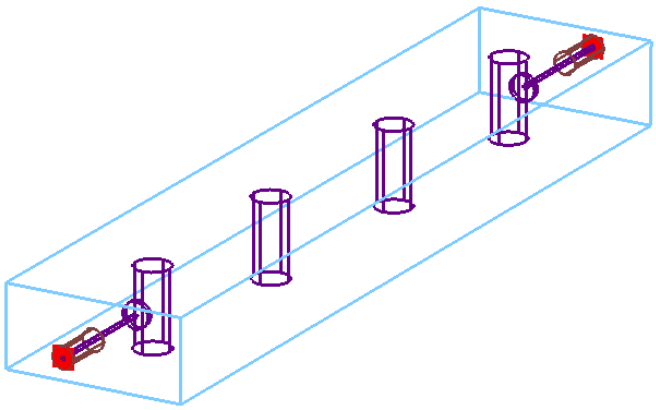

Figure 3.22: 3D model of evanescent mode filter in CST [Dimensions of the full filter are in Appendix A]

The obtained S-parameters for both the filter designed in WR-187 and in WR-137 were then exported into Microwave Office and compared with those obtained for their respective circuit models, with correction factor, $\Delta = 1$, for the circuit models. The results of these are shown in figures 3.23 and 3.24 below.

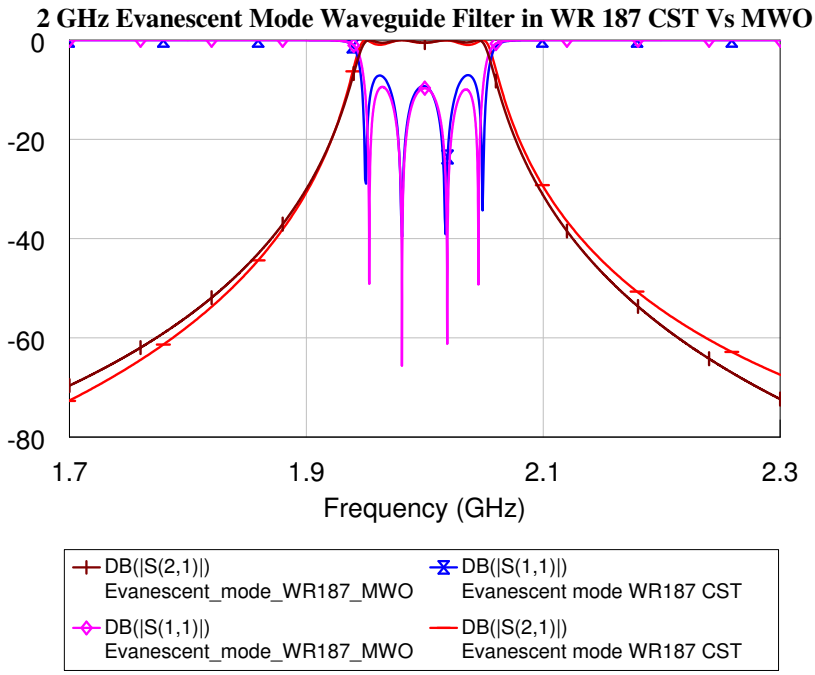

Figure 3.23: S-Parameters of a 2GHz Evanescent-Mode Waveguide Filter in WR-187 waveguide

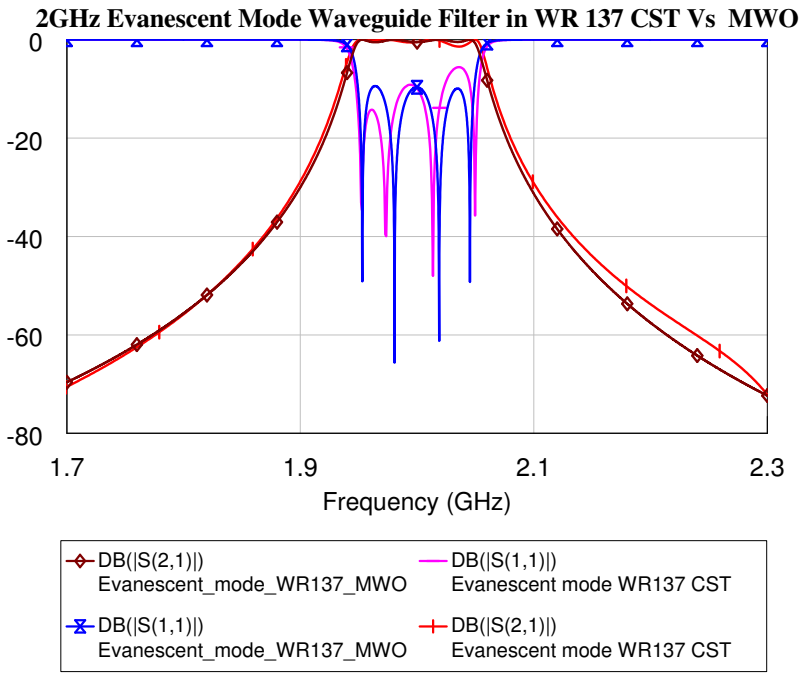

Figure 3.24: S-Parameters of a 2GHz Evanescent-Mode Waveguide Filter in WR-137 waveguide

The CST and MWO models show good agreement, with only a very slight difference in bandwidth .

3.5.5 Parasitic Passbands in the Evanescent-mode Waveguide Filter

At frequencies above the cutoff frequency, normal propagation of waveguide modes is expected to occur. These parasitic passbands occur primarily as a result of the filter behaving like a kind of conventional direct-coupled filter above its cut-off frequency with the capacitive screws acting like end susceptances which couple the half-guide wavelength cavities together [2]. An equivalent circuit of the filter at frequencies above the dominant mode cutoff, that enables the behaviour of the network to be predicted is given in figure 3.25.

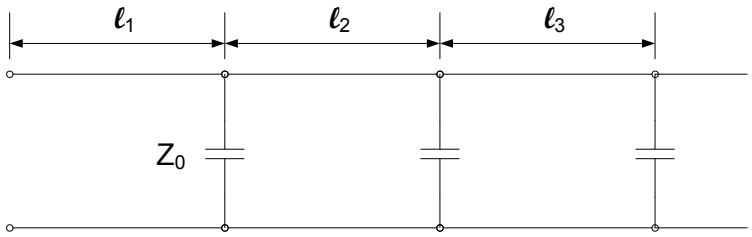

Figure 3.25: Equivalent Circuit for the Prediction of Spurious Passband Behaviour, when $l \approx \frac{\lambda_g}{2}$

Cavity resonance can be expected when the distance between adjacent capacitive obstacles is approximately $\frac{\lambda_g}{2}$ [18], with individual cavity resonances occurring at slightly different frequencies. The frequency at which these passbands occur is dependent on the ratio $\frac{f_0}{f_c}$, the type of obstacle and the bandwidth of the filter [2].

Figure 3.26 shows the S-parameters of two evanescent-mode waveguide filters, one designed in a WR-187 waveguide ($\frac{f_0}{f_c} = 0.635$) and the other in WR-137 waveguide ($\frac{f_0}{f_c} = 0.465$), over a broad range of frequencies.

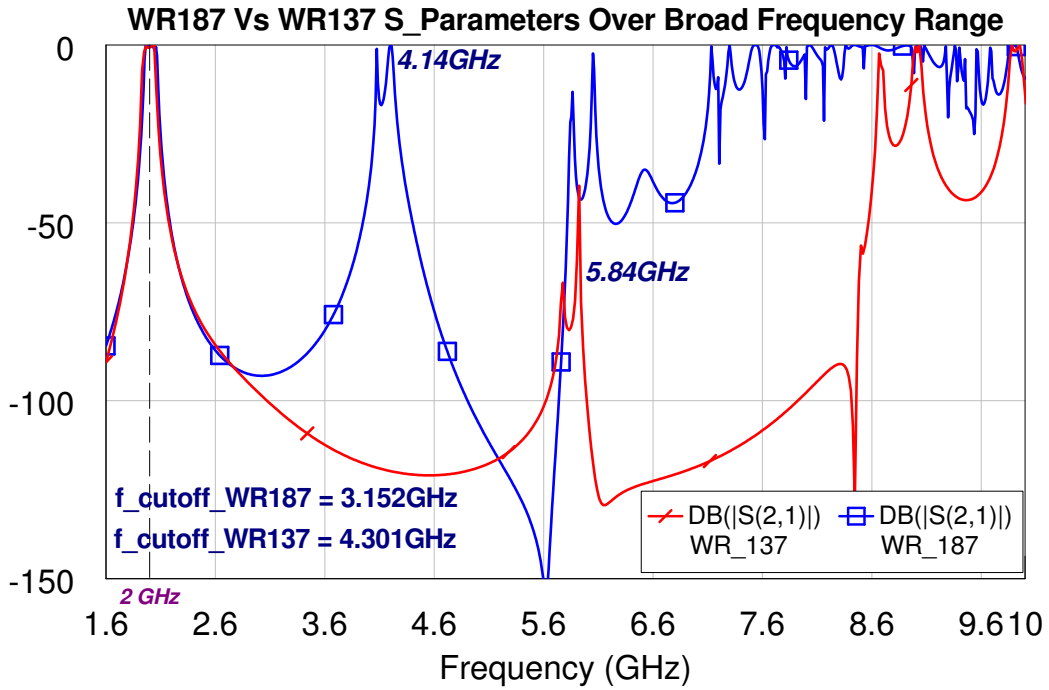

Figure 3.26: Comparison between the S-Parameters of Evanescent-mode Waveguide Filters designed in WR-187 and WR-187 Waveguides

For the WR-137 waveguide, the first passband above cutoff occurs at approximately 5.8GHz, which is about $2.9f_0$, and for the WR-187, the first passband above cutoff occurs at approximately 4.14GHz, corresponding to $2.07f_0$. This is better than the rejection that would be expected in conventional waveguide filters which would have the first spurious passband occurring at about $1.5f_0$.

In a below cutoff guide, the capacitive screws act as highly reflective obstacles to the power being transmitted through so that the first spurious passband occurs primarily as a result of the filter behaving like a conventional directly coupled filter. Even in filters operating fairly close to cutoff, good rejection can be achieved. However, because of the similarity in behaviour to directly coupled filters, narrowband filters such as the ones designed here for a 5% bandwidth are expected to have parasitic passbands at lower frequencies than wider band filters [2].

3.6 Conclusion

As a preparation for discussions on the similarities and differences in performance of evanescent-mode filters and combline filters that follows in chapter 4, this chapter has covered the design process of an evanescent-mode filter. Characteristics of an evanescent-mode waveguide have been discussed and filters designed from these waveguides. The performance of the filter, with the passband and at higher frequencies has also been covered.

Chapter 4

The Equivalence Between Combline Filters and Evanescent-Mode Waveguide Filters

4.1 Introduction

Combline filters and evanescent-mode filters are two types of filters that have very similar bandpass characteristics and construction. Chapters 2 and 3 have covered the design of the two types of filters and as was seen in figures 2.38 (a) and 3.22, the physical structure of both the combline and evanescent-mode waveguide filters has axially placed posts spaced out in the direction of propagation. Figure 4.1 shows the S-parameters of the 2GHz combline filter designed in chapter 2 and of the 2GHz evanescent-mode waveguide filter designed in a WR 137 waveguide in chapter 3.

The plot shows the combline filter response having a steeper rejection on the upper side of the passband as opposed to the evanescent-mode filter which has a near uniform roll-off on either side of the passband. Notable also is the larger bandwidth of the evanescent-mode filter as compared to the combline filter, even though both were designed to have the same percentage bandwidth.

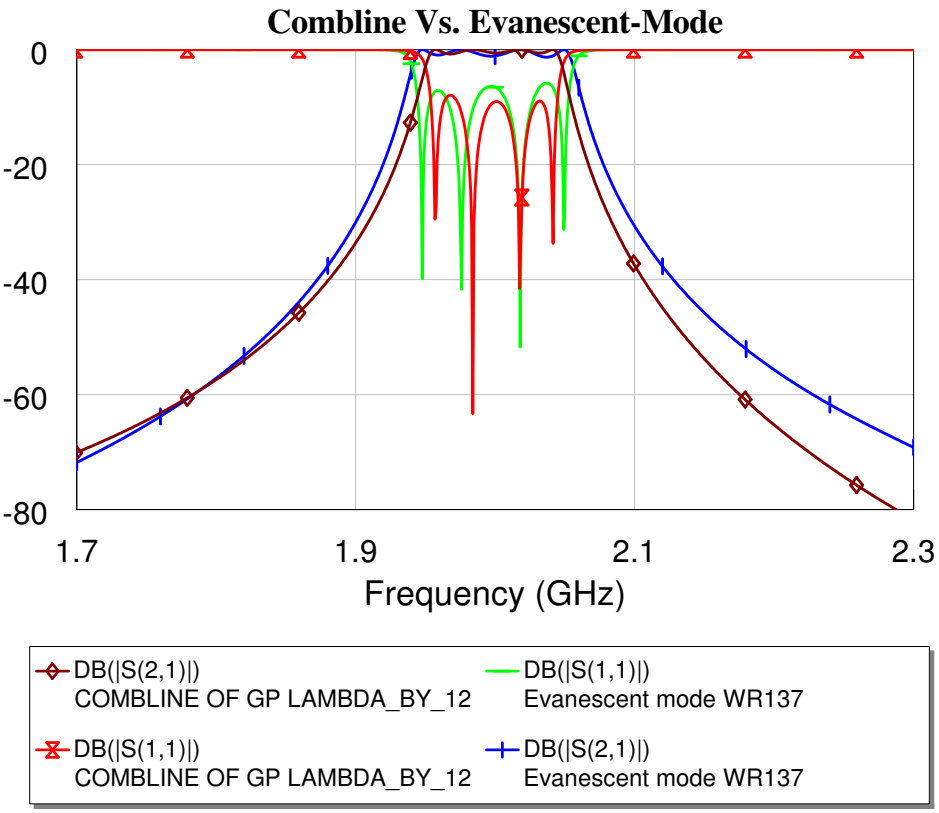

Figure 4.1: S-Parameters of 2GHz Combline Filter and 2GHz Evanescent-mode Waveguide Filter in WR 137

The design process and the manner in which the elements of the two types of filters are implemented differs, despite the similarities in their construction and bandpass characteristics. Combline filters use the concept of transmission line theory, with the dominant mode of propagation being the transverse electromagnetic (TEM) mode whereas evanescent-mode filters are described in terms of waveguides, specifically those propagating an evanescent form of the TE10 mode and operating below the cutoff frequency of the guide.

Various attempts have been made to understand or rather to explain the similarity between the two types of filters and to establish the relationship leading to these near-parallel responses. In [11], Nicholson and Powell infer that the bandpass characteristics of the evanescent-mode filter are as a result of coupled TEM modes supported by the screws inserted in the waveguide to act as obstacles, in a direction perpendicular to the direction of propagation. Craven, in [2], explains why the evanescent-mode filter cannot to considered as a TEM line filter, citing that further work done on suitable obstacles including dielectric rods which cannot support a TEM mode was in favour of the evanescent-mode theory. He further notes that in evanescent theory, it is irrelevant whether the tuning screws are all located on one side or if they are located on opposite sides as in the case of the combline and interdigital filters respectively. For either case, the theory remains the same; yet another subtlety of the microwave art in which two filters designed using a similar theory bear little or no resemblance in their physical realisation. Levy et. al. [22] explain the inter-resonator coupling in a combline filter in terms of evanescent waveguide modes. They state that the dominant TM11 and TE10 modes in the evanescent-mode waveguide filters are similar to TEM modes as long as the ratio of the ground plane spacing, b (see figure 2.3), for the combline filter to the wavelength at mid-band, $\frac{b}{\lambda}$, is small. When the groundplane spacing exceeds a certain value in relation to the wavelength at mid-band, the filter no longer operates as a pure TEM line structure. The coupling between the resonators becomes predominantly due to waveguide modes. This is the basis for which this type of filter has been termed a 'transitional' filter in [22].

This chapter investigates the relationship between combline and evanescent-mode waveguide filters. The characteristics of the filters are compared both within the passband and at higher frequencies. The approach taken

involves the comparison of responses obtained from two fourth order Chebyshev filters, one designed using the combline design theory and the other designed using the evanescent-mode waveguide theory. Both filters operate at 2GHz with a 5 % bandwidth and a 0.5dB ripple. For the evanescent-mode filter, the WR-137 filter designed in chapter 3 will be used. The combline filter will be designed in this chapter to have the same cross-sectional dimensions as the WR-137 evanescent-mode waveguide filter. The approach aims to answer the questions:

- Are the two filters the same?
- If not, what are the inherent differences?

The chapter also investigates the changes associated with designs of a combline filter using different groundplane spacings.

4.2 Design of the Experiment

The sections that follow aim at establishing the similarities and/or differences in the responses obtained from both the two types of filters, both within the passband and over a broad range of frequencies beyond that. Different properties of the two filters are to be investigated in two main experiments:

Experiment 1: Investigation of similarities and/or differences with the passband

The procedure followed for this experiment is to initially design a combline filter based on the cross-sectional dimensions of a WR 137 waveguide. The filter response if then compared to that of an evanescent mode waveguide filter designed in WR 137 waveguide (the design in chapter 3 is used). Based on the initial comparison of their S-Parameters, changes in bandwidth and in resonant frequency due to changes in specified parameters are then investigated. The secitions are divided as follows:

- Design of a Combline Filter in a WR 137 Waveguide
- Comparison of Responses for the Combline and Evanescent-mode Waveguide Filters in WR 137
- Effects of changes in post radius on the bandwidth of an Evanescent-mode waveguide filter
- Effects of Changes in the Size of the Groundplane Spacing on the Behaviour of a Combline Filter

Experiment 2: Investigation of similarities and/or differences over a broad range of frequencies

For this experiment, the effects of the changes in the groundplane spacing of a combline filter over a broad range of frequencies. The secondary passband responses for the combline and evanescent-mode filters in WR 137, under comparison, are then analysed with the aim of establishing whether they give near similar responses, or if the combline response obeys the expectations based on combline theory. The effect of changes in specified parameters on the location of the second passband and on the resonant frequency are then investigated. The breakdown is as follows:

- Effects of Changes in the Size of the Groundplane Spacing on the Behaviour of a Combline Filter over a broad range of frequencies
- Secondary Passbands of the Combline and Evanescent-Mode Filters

4.3 Experiment 1: Investigation of similarities and/or differences with the passband

4.3.1 Design of a Combline Filter in a WR 137 Waveguide

For the design a combline filter with the dimensions of the WR 137 (3.485 × 1.580 cm) evanescent-mode filter in chapter 3, the electrical length of the resonator lines that will be used is also chosen to correspond to the length of the posts that were used for the evanescent-mode filter design. The physical length was $h = 1.512$cm so that the equivalent electrical length, θ_0, is found to be

$$\theta_0 = \frac{2\pi l}{\lambda_0} = \frac{2 \times \pi \times 0.01512}{0.150} = 0.633\, radians\ = 36.23^0$$

The ground plane spacings for the filter correspond to the length of the wider side of the waveguide, 3.485cm. With this value, the radius of the inner posts can be calculated so that a characteristic impedance 77Ω is obtained for optimal Q-factor. For a coaxial line of circular inner conductor and square outer conductor with air-dielectric, the radius of the inner conductor is computed as

$$a = \frac{1.0787b}{e^{Z_0 \varepsilon_r/60}} = 5.2\, mm$$

The radius of the combline post is larger than that of the evanescent-mode waveguide filter which was 3.485mm, so the resonant frequency for the two posts having similar lengths but different cross-sectional areas is obviously different. To tune the frequency back to 2GHz, a tuning screw is used in the combline resonator.

The distances between the posts are only slighter larger than those for the WR 137 evanescent-mode waveguide filter designed in chapter 3. The inter-resonator spacings are given below.

$$l_{1_C} = l_{3_C} = 4.0302\, cm\ [l_{1_{EM}} = l_{3_{EM}} = 4.0286\, cm]$$

$$l_{2_C} = 4.3400\, cm\ \ [l_{2_{EM}} = 4.2463\, cm]$$

The subscripts C and EM stand for combline and evanescent-mode respectively. The designed filter and its S-parameters are given below in figure 4.2.

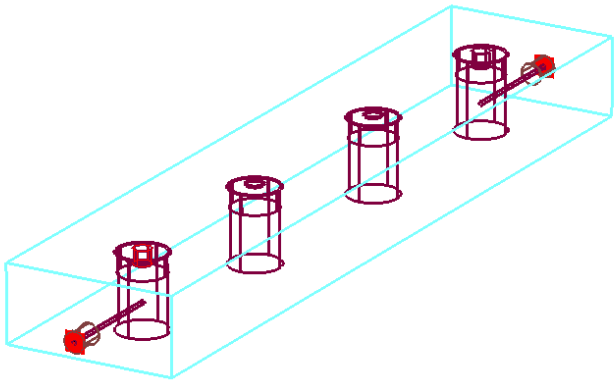

(a)

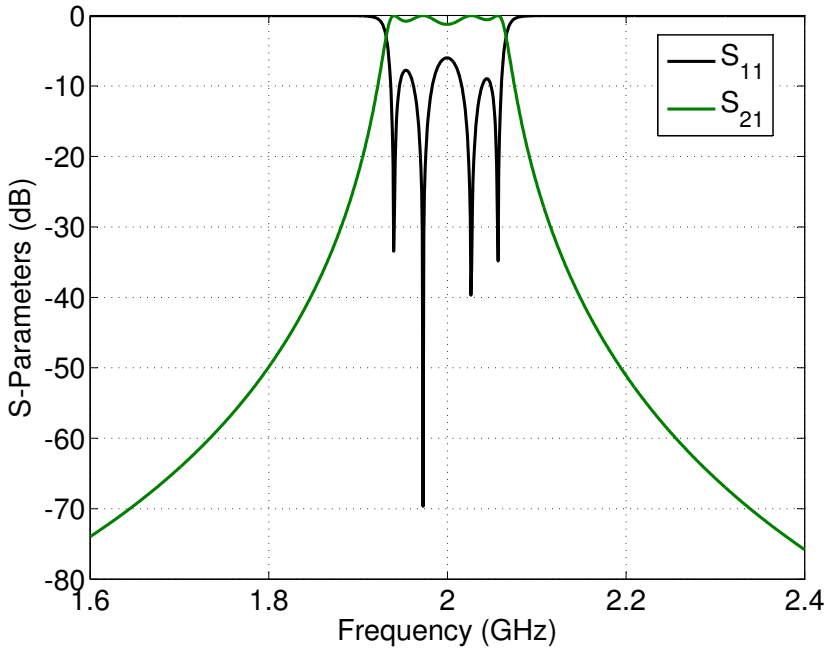

(b)

Figure 4.2: (a) 2GHz Combline Filter Designed in a WR 137 Waveguide (b) S-Parameters of the Filter in *(a)* [Dimensions are given in Appendix A]

The passband ripple is not completely uniform and is more than the desired 0.5dB, but the response can be optimised to obtain a better return loss across the passband.

4.3.2 Comparison of Responses for the Combline and Evanescent-mode Waveguide Filters in WR 137

The S-Parameters of the combline filter designed in the WR 137 waveguide were compared to those of the evanescent-mode waveguide filter designed in a WR 137 waveguide and the plot of these is given below in figure 4.3.

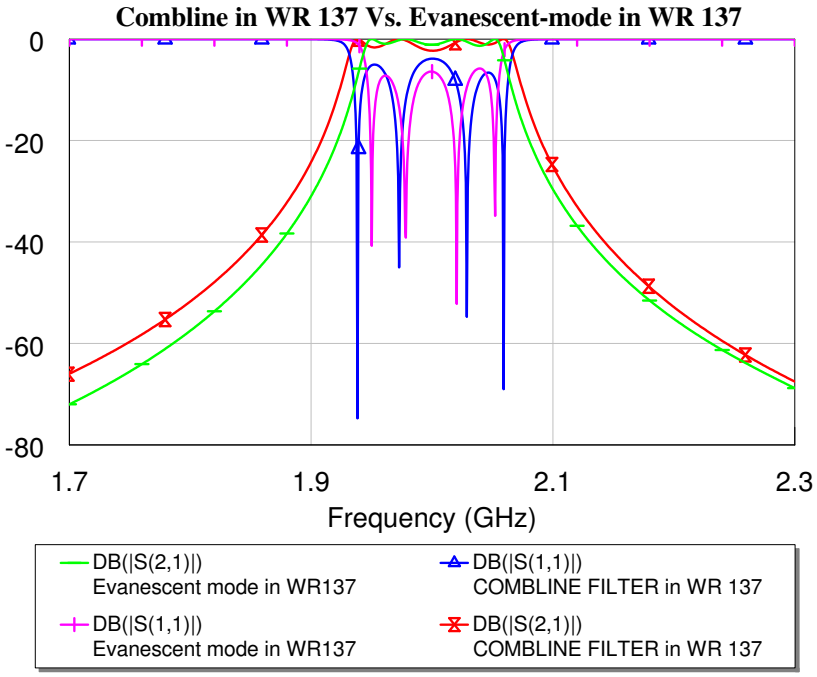

Figure 4.3: Comparison of S-Parameters of Combline and Evanescent-mode Waveguide Filters Designed in WR-137

The filter designed using evanescent mode theory has a bandwidth of 5.78%, which is less than the one obtained for the combline filter, which is about 6.54%. Both are larger than the desired bandwidth of 5%. The circuit model of the evanescent-mode waveguide filter shows a response with a bandwidth of 5.45% for a correction factor of 1 corresponding to a radius of 0.1 times the length of the wider side of the waveguide cross-section, which showed that the bandwidth of the filter designed in CST would also be expected to have a bandwidth larger than 5%. The increase in bandwidth has been attributed to approximations in the design theory [18], especially seeing as the theory only holds as long as it is assumed that the evanescent TE_{10} mode is the only mode that exists in the guide. Other than that, the roll-off for both filters appears to be approximately uniform on either side of the passband. A typical combline response would have a steeper rejection on the upper side of the passband as was shown in figure 4.1 and a typical waveguide filter would have a steeper rejection on the lower side than on the upper side of the passband. This is yet another reason for why the evanescent-mode filter is considered to be a 'transitional' filter.

The difference in bandwidth between the two filters in figure 4.3 prompts the question of whether the difference might be as a result of the difference in the diameters of the posts used in the two constructions, because the guide cross-sectional dimensions were equal. For this reason, the sub-sections that follow aim to investigate:

- the effects that a change in post radius has on the bandwidth of the filters, given that the cross-sectional dimensions of the filters were equal, but the posts in the two filters had different radii of 3.485mm in the evanescent mode filter and 5.2mm in the combline filter.
- the effects that the change in ground plane spacing has on the general response of a combline filter, following the observation of a steeper roll-off on the upper side of the passband in the filter of smaller groundplane spacing (see figure 4.1).

The second investigation also aims to confirm an increase in bandwidth due to an increase in the ground-plane spacing.

4.3.3 Effects of changes in post radius on the bandwidth of an Evanescent-mode waveguide filter

Initial investigations were done on a single resonator filter. For the same cross-sectional dimensions of a WR 137 waveguide, a parametric sweep of the screw radius over a range of 1mm to 6 mm gives a decrease in bandwidth with an increase in radius as shown in figure 4.4.

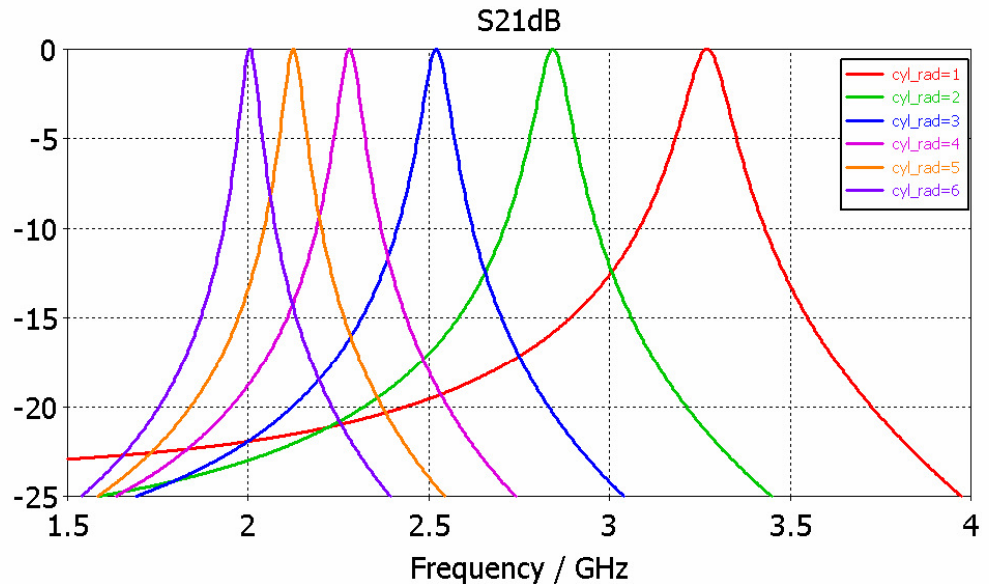

Figure 4.4: Bandwidth change with change in screw radius in WR 137 guide with centred post

The bandwidth changes are larger for smaller radii, but as the radius continues to increase, the change becomes less. For instance, the bandwidth difference for the range of 1mm to 2 mm is approximately 31.2MHz, whereas that computed over the range from 4mm to 5mm is only about 0.4MHz. If considered using combline theory, the near uniformity of bandwidth for larger radii can be explained using the graph illustrating the Q-factor of a coaxial line in relation to the line impedance shown in figure 2.10. The maximum Q-factor is obtained when the line impedance is about 77Ω. The slope of the curve as the Q-factor decreases with an increase in the line impedance beyond 77Ω is not so steep within the range from 77Ω to slightly over 100Ω. Beyond that, the sensitivity increases, so that for small changes in the line impedance, there's a large change in the Q-factor. Figure 4.5 shows the plot of the line impedance obtained for different radii of the post.

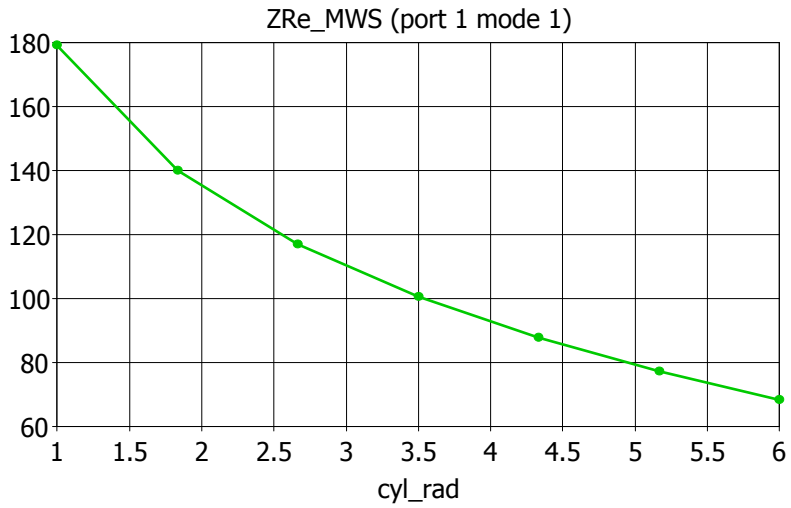

Figure 4.5: Changes in Line impedance with the radius of a post centred within a cavity with cross-sectional dimensions of a WR 137

Notably, the change in the characteristic impedance of the line for the range of radii (variable 'cyl_rad' in figure 4.5) between 3mm to 5.5mm corresponds to the range of frequencies within which the sensitivity of the Q-factor in relation to changes in characteristic impedance does not change much.

The decrease in bandwidth was confirmed through a parametric sweep of the radius of the fourth order evanescent-mode waveguide filter in WR-137, the results of which are given below in figure 4.6.

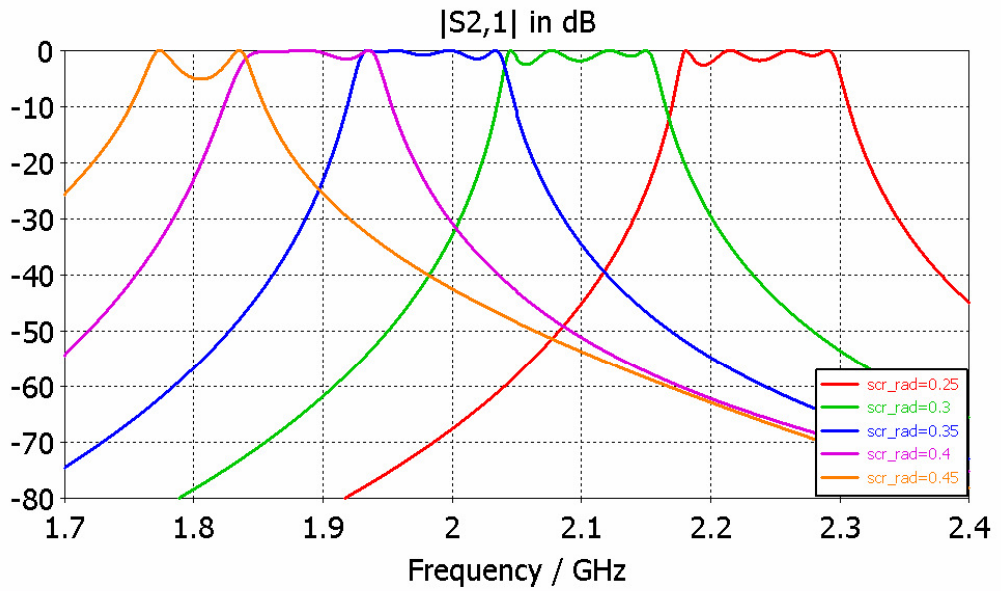

Figure 4.6: Effect of change in the screw size in an evanescent-mode waveguide filter in WR 137

The bandwidth reduces as the radius of the filter increases, so that the difference in bandwidth of the combline filter and the evanescent-mode waveguide filter that was seen in figure 4.3 cannot be attributed to the difference in the diameters of the posts of the two filters. This observation together with the observation that the bandwidth of the combline filter designed for a smaller groundplane spacing was less than that of the combline filter designed in a WR 137 waveguide leads to an investigation of the effect of changing the groundplane spacing of a combline filter. The next sub-section covers this investigation.

4.3.4 Effects of Changes in the Size of the Groundplane Spacing on the Behaviour of a Combline Filter

When the groundplane spacing of a combline filter becomes an appreciable fraction of the wavelength at the resonant frequency, the resonator lines no longer behave like pure TEM lines. It has been recommended that combline filters should be designed with groundplane spacings of less than 0.08λ (where λ is the wavelength at midband) in order for the normal combline theory to be valid [22]. Beyond a certain ratio of the groundplane spacing to the wavelength at midband, filters designed using the combline theory register larger bandwidths than those given by the TEM theory. An increase in the unloaded Q is also achieved with the increase in bandwidth, as would be expected in evanescent-mode waveguide modes.

In the investigations that follow, the line impedance is maintained at approximately 77Ω by adjusting the radius of the post for different groundplane spacings, so that the groundplane spacing is the only variable. Figure 4.7 shows the different bandwidths seen for groundplane spacings of $\lambda/16$, $\lambda/14$, $\lambda/12$ and $\lambda/8$. The obvious increase in bandwidth with an increase in the groundplane spacing can be noted.

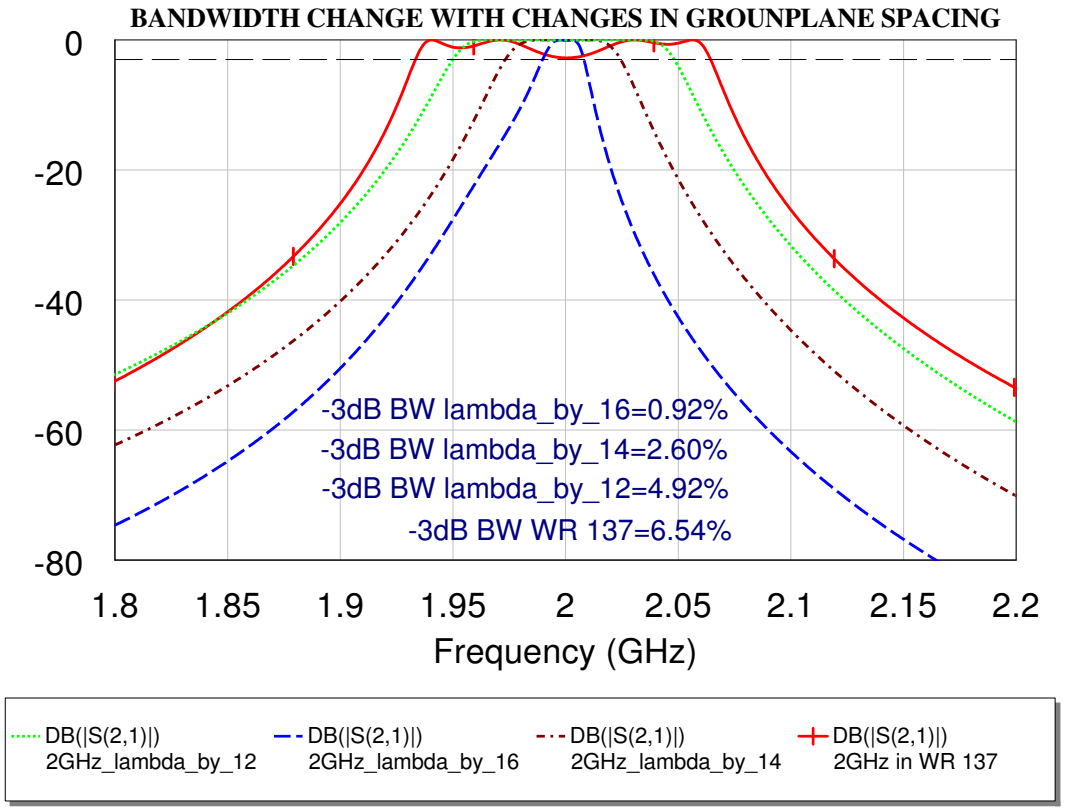

Figure 4.7: Variation of the Bandwidth of a Combline Filter with Changes in the Groundplane Spacing.

For a groundplane spacing of $\lambda/16$, a bandwidth of 0.92% was obtained, and for larger groundplane spacings, larger bandwidths can be seen. However, figure 4.7 only considers the effect of the change in groundplane spacing, with no adjustments of the inter-resonator spacings for the filters with a groundplane spacing of $\lambda/16$ and $\lambda/14$. The filters with groundplane spacings of $\lambda/12$ and 0.232λ (WR 137), however, were fully designed filters for bandwidths of 5%. A comparison of the two confirms the deviation from the design bandwidth of filters with large ground plane spacings ($> 0.08\lambda$ [22]). For filters designed with outer conductors of groundplane spacing larger than 0.08λ, it can be assumed that the coupling is no longer single-mode, but rather multi-mode, so that in order to obtain a bandwidth similar to the design bandwidth, the circuit design should include elements accounting for the other possibly coupled modes.

4.4 Experiment 2: Investigation of similarities and/or differences over a broad range of frequencies

4.4.1 Effects of Changes in the Size of the Groundplane Spacing on the Behaviour of a Combline Filter over a broad range of frequencies

The effects of a change in groundplane spacing on the s-parameters of combline filters with groundplane spacings of $\lambda/16$, $\lambda/12$, $\lambda/11$ and $\lambda/10$ over a broad range of frequencies were also investigated, the results of which are shown below in figure 4.8.

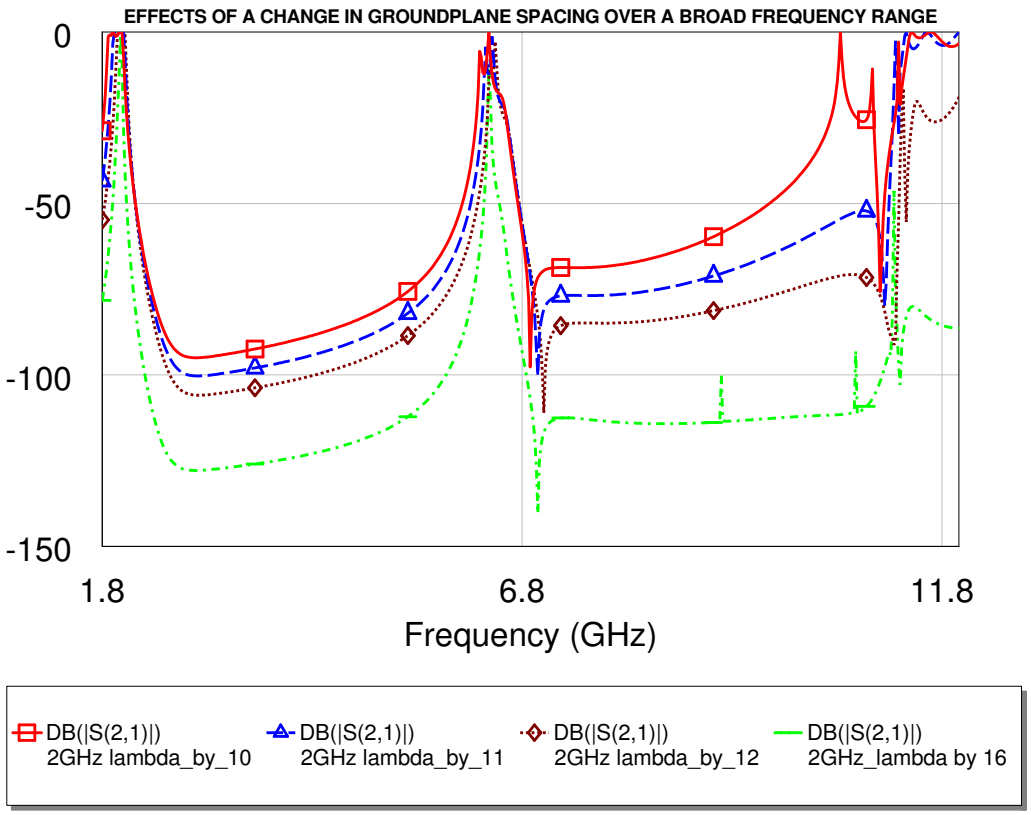

Figure 4.8: Variation of the Bandwidth of a Combline Filter with Changes in the Grounplane Spacing over a Broad Frequency Range.

The primary passbands are centred at 2GHz. The attenuation in the stopband of coaxial line filters has an inverse proportionality to the size of the ground plane spacing. Figure 4.8 confirms this, with the curve for a filter having a ground plane spacing of $\lambda/16$ having a larger attenuation than the curve for the filters with larger ground plane spacings.

The second passband occurs at a frequency of approximately 6GHz, which is expected for the filter having lines with an electrical length of 60^0. A typical combline filter is supposed to have a periodic response, which a circuit model predicts well, but in a physical structure, due to the effects of higher order modes, at higher frequencies, the response is subject to interference. In figure 4.8, the periodic response can be seen for the first three passbands.

In the next section, the behaviour of the combline filter over a broad range of frequencies is investigated to see if it conforms with the combline design theory or if it rather favours predictions based on evanescent-mode waveguide theory.

4.4.2 Secondary Passbands of the Combline and Evanescent-Mode Filters

Up to this point, the evanescent-mode filter designed in a WR 137 waveguide appears to be the same as the combline filter designed in a WR 137 waveguide, except for the difference in bandwidth. For a combline filter, if the TEM line theory is to hold, with the line impedance maintained at 77Ω, the frequency responses are periodic in nature and the position of the second passband can be approximated from the length of line. The second passband is expected to occur when the length of the line is approximately half of the wavelength at midband. The combline filter designed in a WR- 187 waveguide had a line with an electrical length of 36.23^0, so that the second passband for a filter with a resonant frequency of 2GHz would be expected to occur at a

frequency of approximately 10GHz. Figure 4.9 shows the s-parameters of the combline filter in comparison with the ones for the evanescent mode filter in WR 137 over a broad range of frequencies. These are also compared to a response from the circuit model.

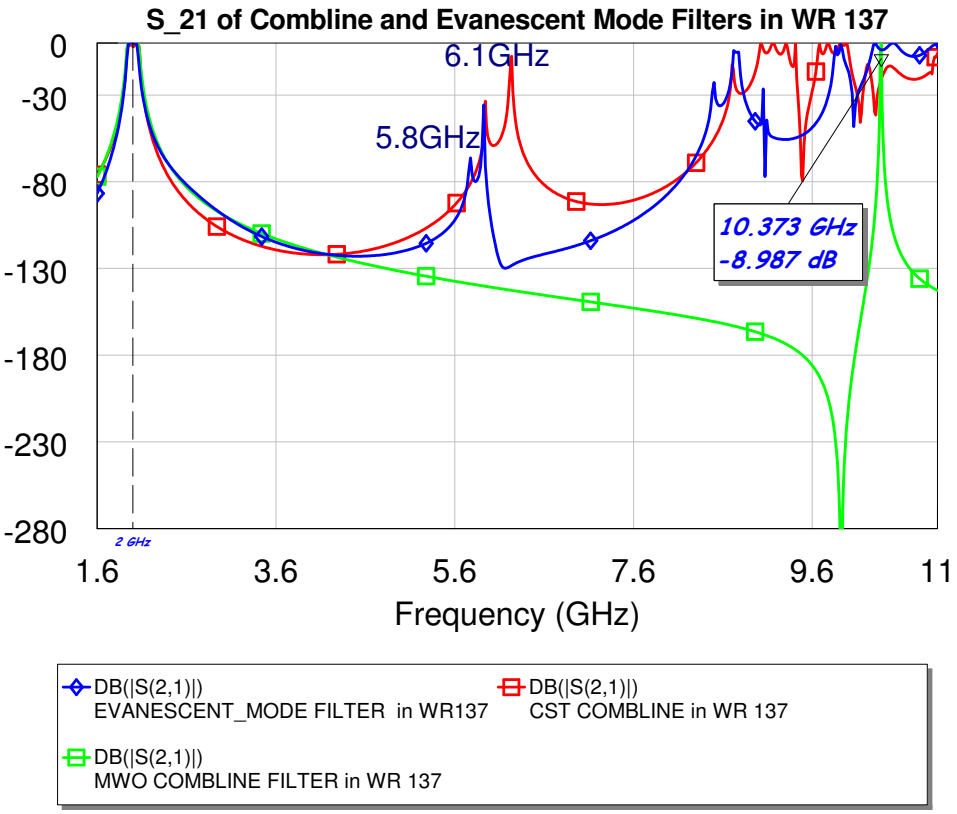

Figure 4.9: S-Parameters of the combline and evanescent-mode waveguide filters designed in WR-187 over a broad range of frequencies

Evidently, the second resonance due the the circuit model (green curve) of the combline filter designed in WR 137 with lines of an electrical length of 36.23^0 has a second resonance at 10.37GHz, as was approximated. However, the response from the 3D model in CST shows its second resonance occurring at about 6.1GHz, and the response is clearly similar to that of the evanescent-mode filter designed in CST, which has its second passband at about 5.8GHz. The difference in location of the second passband of the two filters modelled in CST prompted an investigation of the effects of a change on the screw radius of the length of the stopband before the occurrence of the second passband, the results of which can be seen below in figure 4.10

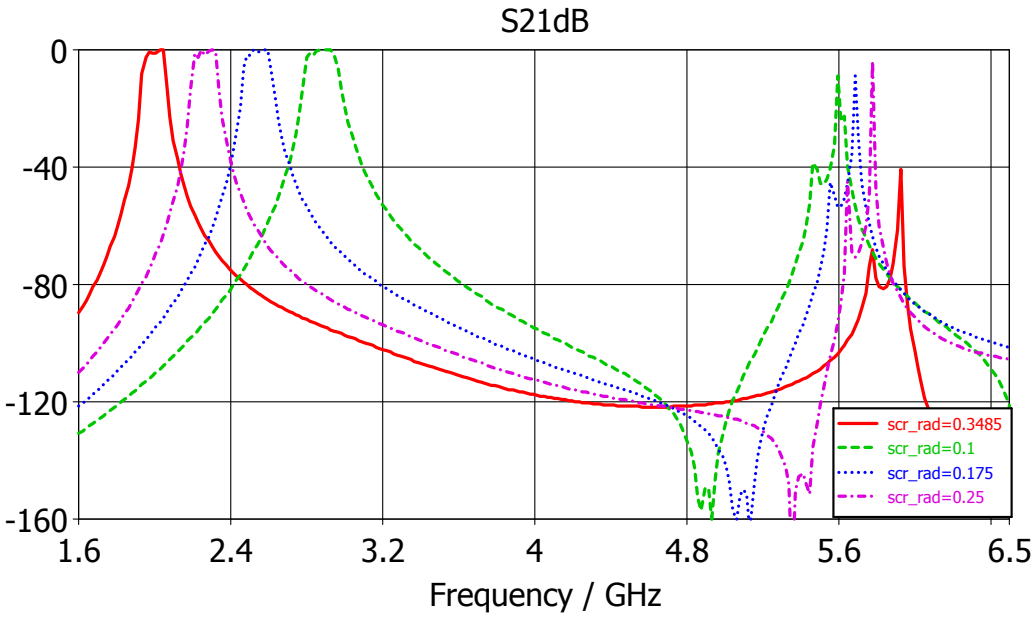

Figure 4.10: Effect of changes in the screw radius on the size of stopband before the second passband for the Evanescent-mode filter in WR 137

In a combline filter, a change in the radius of the screw would result in a shift of the frequency of both the primary and the secondary passbands in the same direction as the resonant frequency changes on account of the change in capacitance as can be seen in figure 4.11. The plot shows the effect of a parametric sweep of the radius of the combline filter designed in chapter 2 with a ground plane spacing of $\frac{\lambda_0}{12}$ on the frequencies of the primary and second passbands.

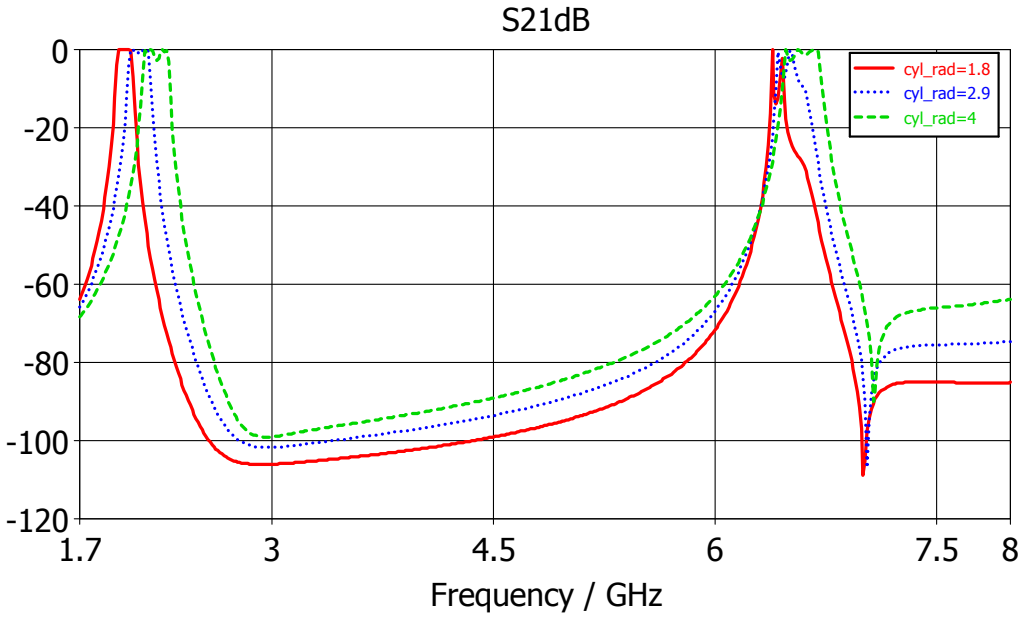

Figure 4.11: Effect of changes in the screw radius on the size of stopband before the second passband for the Combline Filter of Ground plane spacing = $\frac{\lambda_0}{12}$

The shift in frequency for both the primary and second passband is in the same direction as would be expected for a filter obeying TEM line theory.

In figure 4.10, however, the frequency shift of the primary passband is in a different direction to the shift in the secondary passband; the expected decrease in the resonant frequency with increased capacitance is evident

only for the primary passband. It is also evident that there is an increase in the length of the stopband with an increase in the radius of the post. Therefore, an evanescent-mode filter with a larger diameter can be expected to have its second passband occurring further than one with a smaller radius. The same increase in the length of the stopband prior to the occurrence of the second passband is seen in figure 4.12 for the combline filter designed in WR 137.

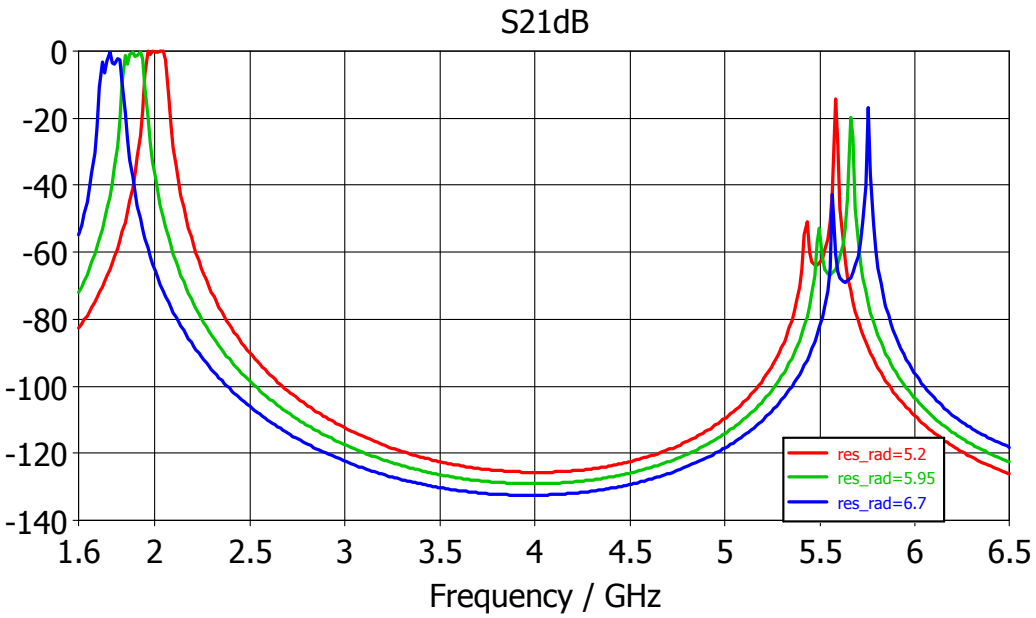

Figure 4.12: Effect of changes in the screw radius on the size of stopband before the second passband for the Combline Filter in WR 137

In figures 4.10 and 4.12, the primary passband can be tuned back to resonate at the required frequency by varying the length of the post or by the use of tuning screws. A parametric sweep of the height of the post to confirm the effect of such a change on the frequency of the primary passband is depicted in figure 4.13 below.

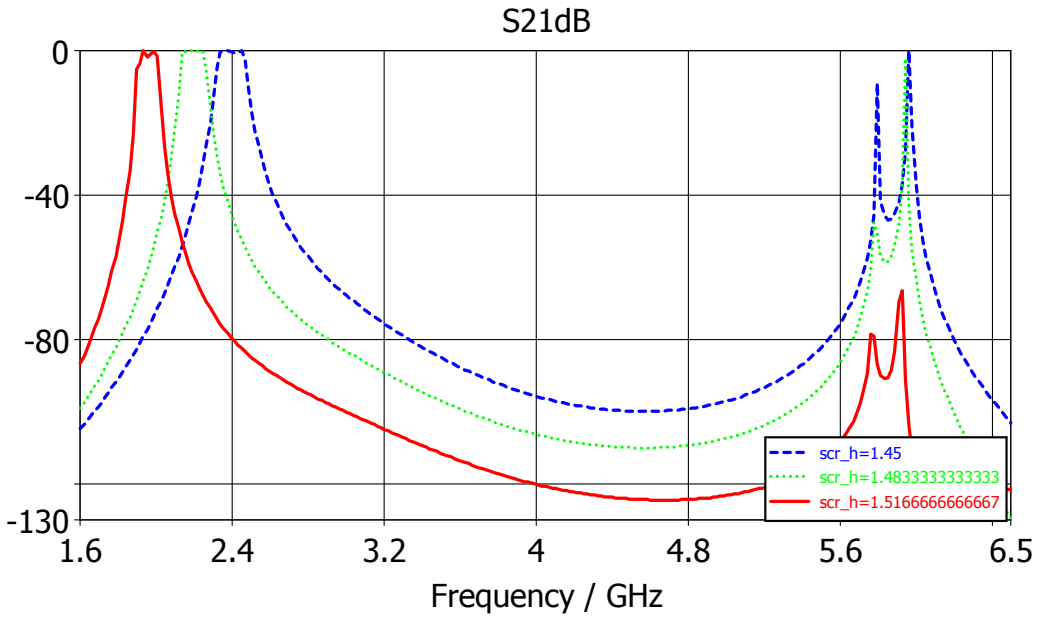

Figure 4.13: Effect of a change in screw height on the S-parameters of the Evanescent-Mode Filter in WR 137 over a Broad Range of Frequencies

The location of the second passband remains unchanged, but the attenuation increases with an increase in the depth of the post inside the guide. This could explain the lower attenuation in the second passband of the combline filter in figure 4.10 in comparison to the evanescent-mode waveguide filter; a post with a wider diameter, equivalent to that of the combline filter, when tuned back to resonate at the same frequency as the filter with a smaller post registers a decrease in the attenuation of the second passband. Figures 4.10 and 4.13 therefore show that the radius of the post can be used to manipulate the position of the second passband in an evanescent-mode waveguide filter. It has also been seen that the combline filter designed in WR 137 has similar characteristics to the evanescent-mode filter, and does not behave like a typical filter designed using TEM line theory should.

4.5 Summary of Characteristics

Posts in combline filters are resonator lines in a TEM line with the main coupling between adjacent posts being magnetic. The proximity of the posts to each other is therefore of importance if the right amount of coupling is to be achieved. The coupling, represented using J-inverters, is dependent on the susceptance slope parameter, which for a given electrical length of the resonator line, is proportional to the characteristic admittance of the line. In section 2.2.1, equation 2.6 gives the characteristic impedance of a coaxial line with a rectangular outer conductor and a circular inner conductor. The characteristic impedance is seen to be dependent on the ratio of the radius of the outer conductor to the radius of the inner conductor, with figure 2.6 (b) showing an increase in the characteristic impedance with an increase in the ratio. Thus, an increase in the characteristic impedance of the line can be achieved in one of two ways: either by increasing the ground plane spacing (shown in figure 2.3) or by reducing the diameter of the inner conductor. These variations are in turn expected to have an effect on the bandwidth of the filter. Such a change will result in situations where the energy is either over-coupled or under-coupled due to the change in cross-sectional dimensions that allows for either more or less energy to be stored in the cavity. Adjustments in the spacing between the posts can then be used to achieve the right amount of coupling.

In the evanescent-mode waveguide filter, the posts are coupled by half-wavelength waveguide sections, which in their lumped circuit equivalents are represented, for the filters in this thesis, as a pi of inductors (see figure 3.2). The coupling between the posts is also in the form of J-inverters in a pi-configuration of inductors, with the series elements relating to the length of the sections and therefore to the coupling. The impedance of the inverters, given in equation 3.8 is a function of the characteristic impedance of the guide section and of the product γl. The impedance of the below-cutoff guide section is imaginary and is proportional to the ratio of the length of narrow side of the waveguide cross-section to the length of the wider side of the cross-section. By increasing the cross-sectional dimensions of the waveguide, more energy can be stored in the cavity resulting in a higher unloaded Q. The cut-off frequency of a waveguide is a function of the guide dimensions so that an increase in guide dimensions results in a decrease in the cut-off frequency. Attenuation in the below cutoff waveguide section is also seen, from equation 3.4, to be dependent on the cut-off frequency so that the further the resonant frequency is from the cut-off frequency the more the attenuation in the below cutoff waveguide section. To adjust the coupling for a changed bandwidth, the length of the guide sections has to be adjusted.

Previous sections also compared the behaviour of the filters at higher frequencies and investigated the aspects that determine how long a stopband can be achieved for either type of filter. For combline filters, the second passband is expected to occur when the resonator lines are about a half wavelength long [15]. Thus, by varying the length of the resonator lines, the frequency at which the second passband occurs can be manipulated. An evanescent-mode waveguide filter is expected to have normal propagation of the dominant mode above the cutoff frequency of the waveguide. Operating at frequencies further from the cut-off therefore results in wider stopbands, but at the expense of unloaded Q, given that attenuation increases as the resonant frequency shifts further from cutoff. Figure 3.26 shows that a 2GHz filter designed in a WR 137 waveguide with a cutoff frequency

of 4.301GHz has a wider stopband than a filter designed in a WR 187 waveguide with a cutoff frequency of 3.152GHz.

4.6 Conclusion

The preceding sections have investigated different characteristics of combline and evanescent-mode waveguide filters in an attempt to establish similarities and differences between the two filters, based on two experiments. To answer the question of whether or not the two filters are the same, it has been seen that a combline filter with a large groundplane spacing behaves like an evanescent-mode waveguide filter, with a difference in bandwidth. It has also been noted that the bandwidth obtained from the filter designed using combline design theory was much larger than the one that is designed for. The evanescent mode filter had a bandwidth close to the one obtained from the circuit model, and the increase from the percentage bandwidth in the specifications has been attributed to the approximations and assumptions made in design. For these reasons, it can be recommended that for the design filters of large groundplane spacings relative to the wavelength at midband, evanescent-mode waveguide theory would be better suited. For smaller sized filters, the combline theory would be the favoured choice for the designs, because the desired bandwidths can be obtained and because for evanescent mode filters, it would mean that the chosen waveguide would have a cut-off frequency far from the operation frequency, so that attenuation would be increased.

Chapter 5

Manufacture of Microwave Filters and Cost-related Aspects

5.1 Introduction

Typical microwave systems comprise of several components. In recent times, the growing complexity of the systems with the aim of satisfying the growing needs of the telecommunication industry has resulted in an increase in the number of parts used in most systems. In projects where fixed amounts of funds are allocated for design and manufacture, the cost distribution for individual components becomes an issue; all the components in the system are vital to its efficient operation, but some are very costly, yet there isn't much room for compromises.

As much as the costs need to be limited, technical requirements need to be met. Many modern systems now require higher power levels, lower noise figures, reduced degradation of service quality in specified environments and they also have weight and size constraints that have to be satisfied.

Microwave filters form an important part of a microwave system. Depending on the frequency of operation of the system and the desired bandwidth specifications, these filters vary in type and in size. For each type of filter, there are several manufacturing techniques that can be employed, with specific considerations taken into account to ensure that the costs are limited while maintaining the technical requirements for the desired functionality.

A typical product development process would follow the cycle outlined in figure 5.1.

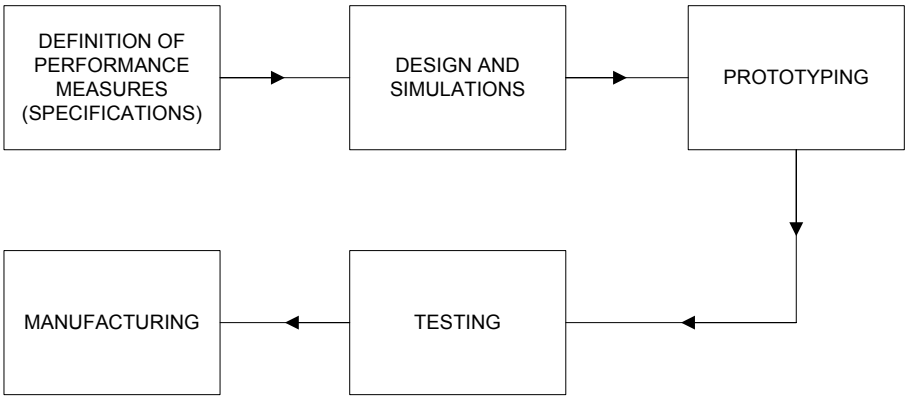

Figure 5.1: Product Development Process

The manufacturing stage requires decision making regarding appropriate choices in materials and fabrication processes, based on the requirements passed on from the designers. Thus, the interaction between the two parties plays an important role in the product development process. If a proper relationship between design and manufacturing should be established at the right stage, it can aid in the reduction of overall development costs.

Manufacturability of a product is measured based on the properties of the materials to be used, the processes to be applied, the manufacturing costs and the assembling costs. For a given material, the manufacturer is tasked with making the decision of which machining technology will be the best for the required design.The choice is largely determined by the properties of the material and the geometrical construction of the work-piece.

The best materials and manufacturing techniques for cost-effectiveness and desired performance are chosen based on the applications of the filters, customer requirements, available manufacturing technology options and the possibility that tuning might be required. There might also be finishing requirements which will need to be taken into account.

This chapter aims to look at microwave filter manufacturing, with specific attention to coaxial cavity filters. In figure 5.2, the different costing elements are shown. The choice of appropriate materials and machining techniques for fabricating the filter enclosure are discussed. A discussion on surface finishing, machining tolerances and coating technologies is also included. The chapter also investigates the factors contributing to the costs of the design and manufacture of the filters, and also includes a section on the concept of Design for Manufacturability (DFM).

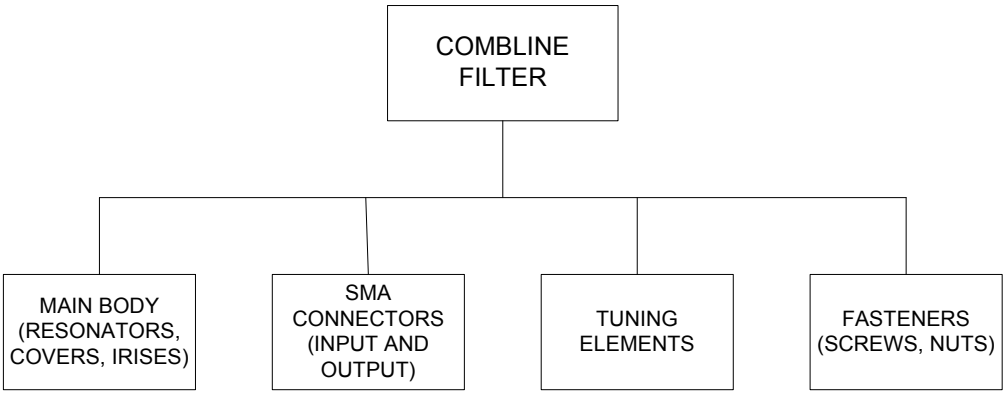

(a)

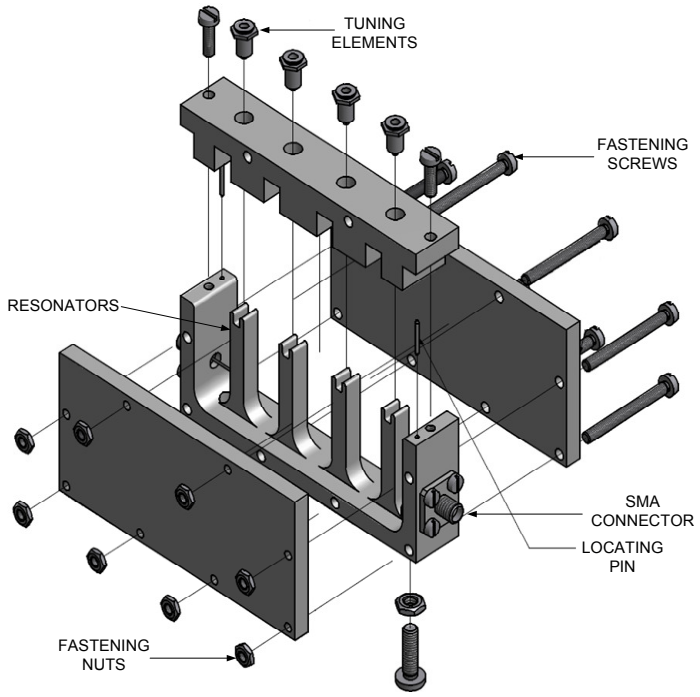

(b)

Figure 5.2: Combline filter Elements

5.2 Appropriate Metals for Microwave Components

The choice of metals to use for microwave components is dictated by the electrical performance of the device, the machinability, the environmental requirements and the cost effectiveness. Because microwave circuits must carry high frequency currents with as little loss as possible, materials with very good electrical conductivity are essential. However, some of these materials may be very expensive, so that in such instances, an alternative option becomes that of using a more affordable material with lesser conductivity to construct the filter and then to use the more desirable metal in terms of electrical conductivity to plate the filter. Due to skin effect, most of the conductive current flows on the surface of a metal. Therefore, at microwave frequencies, because the penetration or skin depth is very small, only a thin plating of a good conductor is required to achieve the low-loss requirements of a component.

The machinability of metals is important because most microwave devices usually have complex shapes; not

many will fit into standard square or rectangular spaces. Therefore, the metals must be generally shaped using some specific manufacturing processes in order to conform to the necessary space within which they are required to fit. For cost effectiveness, the metals must therefore also be easily machinable.

In table 5.1 the electrical conductivities of some of the commonly used materials for microwave applications are outlined.

MATERIAL	CONDUCTIVITY (S/m)
Silver	6.30×10^7
Copper	5.85×10^7
Gold	4.25×10^7
Aluminium	3.50×10^7
Indium	1.11×10^7
Tin	0.877×10^7
Lead	0.456×10^7

Table 5.1: Conductivities of metals

Silver has the best conductivity, but is very expensive, so its use in microwave applications is almost entirely in plating. Waveguides and tuned cavities are usually made of a lightweight and inexpensive material with average conductivity and coated with a thin layer of silver to increase conduction of microwave energy [30]. Copper's conductivity comes only second to silver. It can be drilled, tapped, sheared, sawed and milled, making it a good metal for use in microwaves. However, copper is harder than metals like aluminium and is also very costly. In waveguides, it is not used as extensively as alloys of aluminium, magnesium, brass and silver, because these other metals are cheaper, lighter in weight and also have very good conductivity. Gold is also not used as much because of its price, despite the fact that it has very good conductivity. Aluminium is usually the first on the list of metals used in microwave applications. The majority of enclosures or cases for microwave components are fabricated from aluminium. It has average conductivity, but is very machinable and lightweight, which is why it finds wide usage in the fabrication of most cavity filters. It is not always ideal when higher Q-factors are required, therefore microwave components are routinely coated with silver or gold to improve the Q-factors.

Some properties and applications of commonly used metals at microwave frequencies are summarised in table 5.2 .

Material	Applications
Aluminium	For cases for Microstrip, Stripline and suspended substrates. Cast to be a waveguide which is silver plated for better conductivity (Makes very effecient waveguide: light weight and low cost).
Copper	Used as metallic medium on substrates and laminates. Also used in the fabrication of cavities and filters, but an all-copper structure is heavy, so cannot be used for applications requiring light weight.
Silver	Used primarily in the waveguide regions of the microwave spectrum and higher frequencies. Mostly used only as a coating because even though it is an excellent conductor, it is very costly. Also used in solders.
Gold	Mainly used for plating of cases for microwave circuits . Used to improve conduction as well as to provide protection against oxidation for metals like copper.
Indium	Primarily used in solder compounds for microwave applications (very good conductivity and low-melting point).
Tin	Used in tin-lead solders. Also used for a variety of applications where copper traces in the circuit must be protected from oxidation, and gold-plating is not necessary.
Lead	Used mostly for solders.
Kovar and Invar	Used in high temperature applications in radio and electronic devices, in aircraft controls and for fabrication of high stability cavities and critical resonators. Very difficult to machine, so should only be used in the absence of other alternatives.

Table 5.2: Properties and applications of some common metals used at microwave frequencies

5.3 Manufacturing Technology

Manufacturing is generally a complex activity involving the making of products from certain materials by various processes or operations. Manufacturers can be said to be people with a broad range of disciplines and skills, operating a wide variety of machinery, equipment and tooling with various levels of automation.

The term machining is defined as being a metal cutting process that deals with removal of material, especially metals, using machine tools to obtain a desired shape or form. Machining is classified under two-main categories: Conventional machining and non-conventional machining. The conventional processes are essentially based on the use of mechanical forces to 'cut' away material in the form of chips and these include milling, turning, drilling and grinding. Non-conventional processes employ light, electrical, chemical and sonic energy, superheated gases and high-energy particle beams to shape workpieces. Examples of such processes are Electrical Discharge Machining (EDM), Electro-chemical machining (ECM), water jet cutting (WJ) and laser cutting.

In many microwave applications, very high manufacturing precision is necessary in order to meet performance requirements. Appropriate machining processes are selected with respect to the required geometry, some of which usually have a good level of complexity, and the machining parameters and tools are defined based on the chosen workpiece material. The need for high speed machining for very good quality cannot be met by just any manufacturing technology. Therefore, for microwave engineering applications, only computer-based numerical control (CNC) machines are recommended.

In the manufacture of the filters designed in this thesis, only milling and wire-cutting EDM, one of the types of EDM, are used. As such, only these will be discussed in subsequent sections.

5.3.1 CNC Milling Technology

Based on the orientation of the main spindle, milling machines are classified into two categories: horizontal milling machines and vertical milling machines. The milling process entails the moving of a workpiece radially against a rotating cutter, which cuts on its sides as well as on its tip. A simple illustration of the process is shown in figure 5.3.

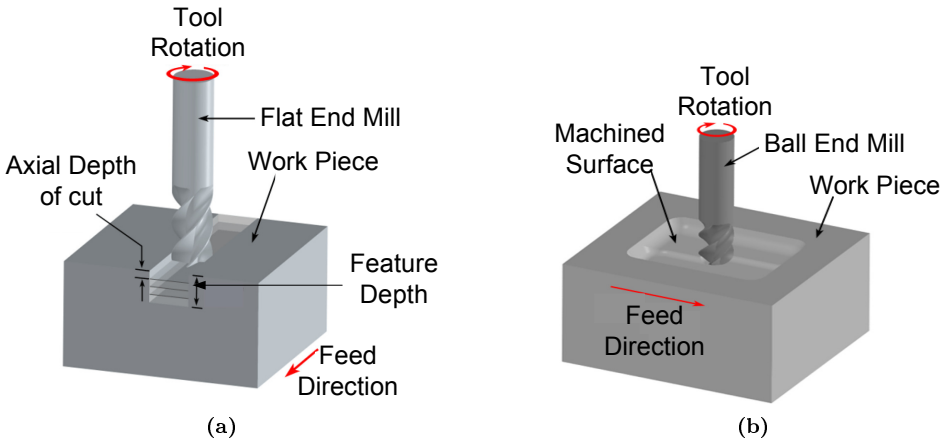

Figure 5.3: Milling Process[57]

Workpiece and cutter movement are precisely controlled to better than 0.001in (0.025mm), usually by means of precision ground slides and leadscrews or analogous technology [45]. Operation of milling machines can be manual, mechanically operated or digitally automated through the use of Computer Numerical Control (CNC).

Also known as machining centers, CNC milling machines are vertical mills, which operate on the Z axis (vertical) and offer precision and speed.

The history of milling machines dates back to as early as the 1810s. However, their evolution into CNC machines was only seen during the 1960s and 1970s[45]. During that period, data storage and input media evolved, and computer processing power and memory capacity increased. The drastic advancement of CNC machines transformed the manufacturing industry.

At some point, the CNC milling machines were quite expensive to purchase and to operate. However, the reduction in the costs of computers and the availability of free operating systems has made the milling machines more affordable.

For most designers wanting to fabricate their devices using milling, it is important to become familiarised with the sizes of milling cutters available to the manufacturing companies being considered. With such knowledge, a designer can then design corner radii of inner geometries based on the cutter sizes. The designer also needs to establish the precision with which the milling can be done and take that into account when choosing the dimensions of the device at the design stage.

The primary cutting tools used in milling machines are called end-mills and examples of these are illustrated in figure 5.4 and figure 5.5.

Figure 5.4: Examples of End-millsing[53]

The gold coloured mills in figure 5.4 have a very thin Titanium Nitrate (TiN) coating that prevents chips from welding to the mill surface.

During the milling process, a variety of operations may be performed in order to get a desired shape of a part. Consider for instance the parts of a combline filter illustrated in figure 5.2. Several operations will be required, some of which are illustrated in figure 5.5.

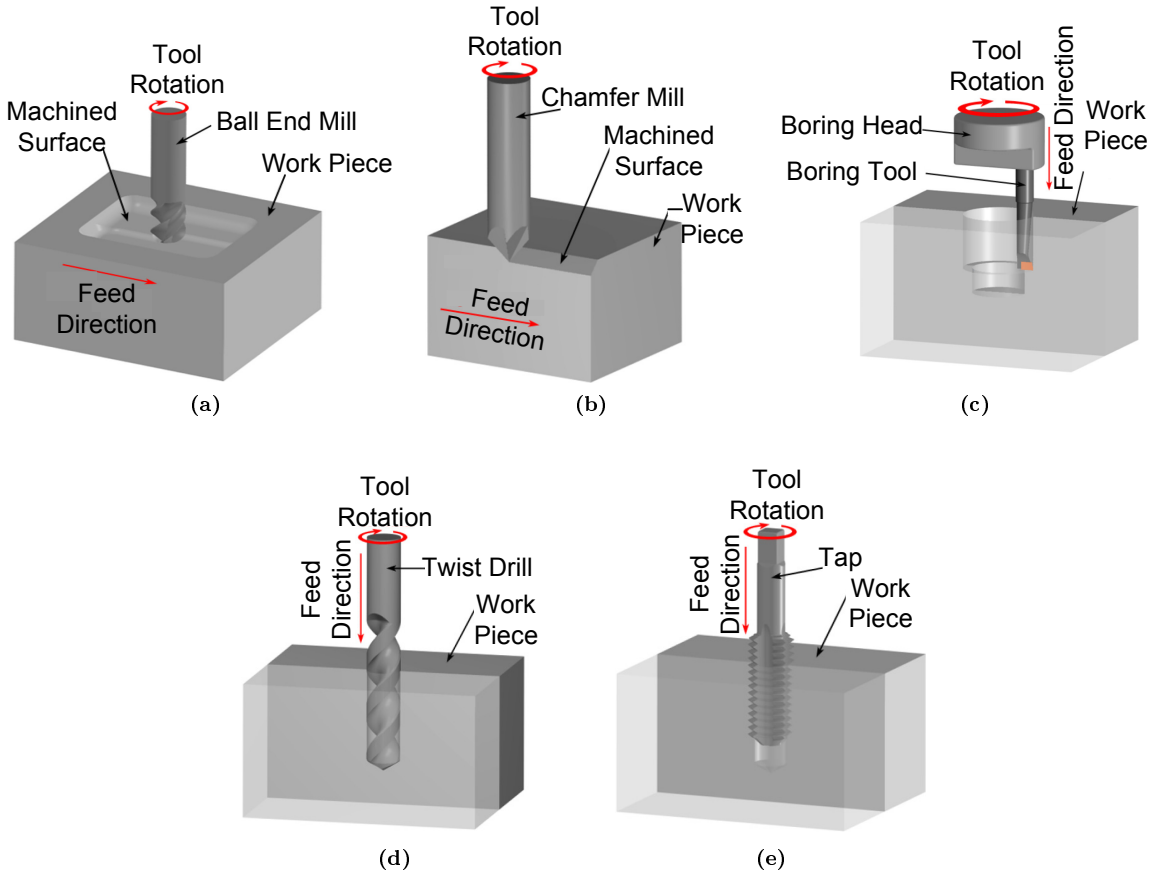

Figure 5.5: Types of cuts and respective end-mills [57]

There are several recommended considerations that a designer should take into account when designing a part to be milled. The most important of these are:

- Milled parts should be designed so that the length-to-diameter ratio of the required end mill is limited to

3:1. Longer end mills are usually necessary for reaching into deep cavities but are prone to breakage and chatter (chatter is the vibration between a workpiece and a tool due to the lack of rigid support for the work-piece or tool), hence leaving a relatively poor surface finish, and require longer machining times. If long end mills cannot be avoided, then the clearances shown in figure 5.6 should be implemented. These clearances prevent friction between the flank of the tool and the part. The flank is the part of the tool that comes into contact with the workpiece.

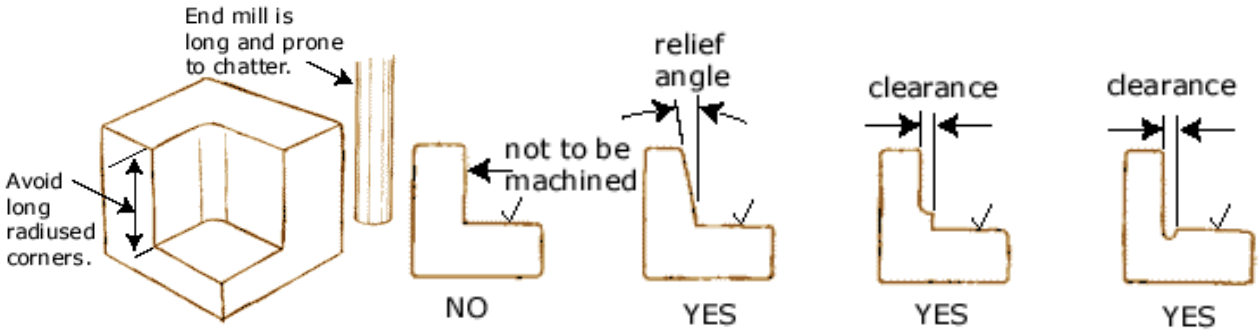

Figure 5.6: Clearances for milling using long end mills[58]

- For designs having three-edge inside corners, one of the inside edges must have the radius of the end mill. Alternatively, a separate hole can also be used to allow relief for a male 90^0corner to fit. These are illustrated below in figure 5.7.

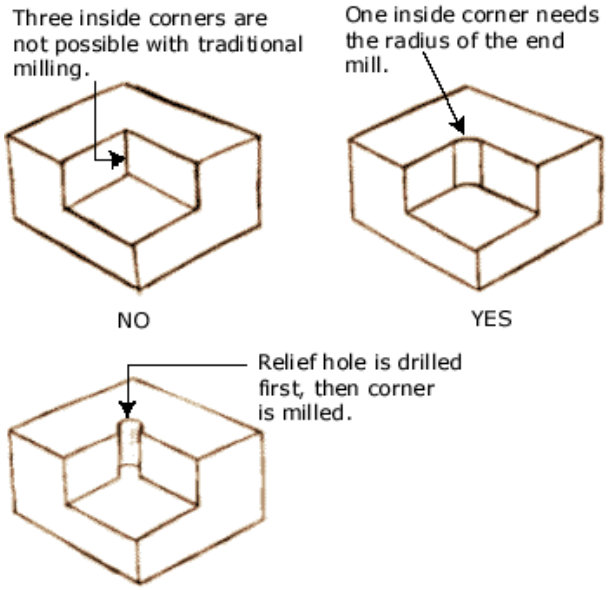

Figure 5.7: Three-edge inside corners for milling[58]

- Chamfers are preferable over fillets for outside corners; a fillet is more expensive to machine than a chamfer.

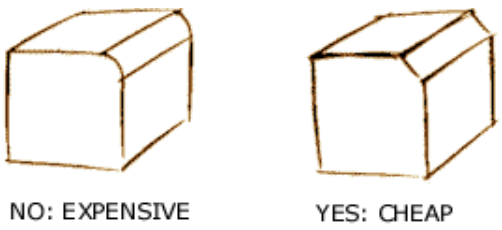

Figure 5.8: Chamfered and filleted outside corners[58]

- Whenever possible, standard tool bit sizes should be used and it is also recommended that, if possible, the inside radii should be determined by the fabrication personnel, to allow for flexibility to use tools that are easy to obtain and maintain. A more extensive discussion on end mill cutter sizes follows.

End mills used with CNC machines vary in sizes ranging from diameters of μ- metres to over an inch. The selection of size depends on the type of application, and is usually done by the machine shop for a specific application. The size of the end-mill also determines how fast you can cut the material and how deep a cavity can be cut; the smaller the diameter, the shallower the cavity. Some of the more commonly used standard diameters are 1mm, 1.5mm and 2.0mm.

A designer usually also needs to specify the surface roughness required in applications where it is of importance. Based on the number of flutes (cutting edges wrapped around the end mill like a spiral (see figure 5.9)), different types of surface finishes can be obtained. A roughing cutter has a smaller number of teeth, cuts away large amounts of material, leaving a poor surface finish, whereas a finishing cutter has a larger number of teeth (four or more), removes smaller amounts of material more carefully and leaves a good surface finish. A more comprehensive discussion on surface finishing is given in section 4.3.3.

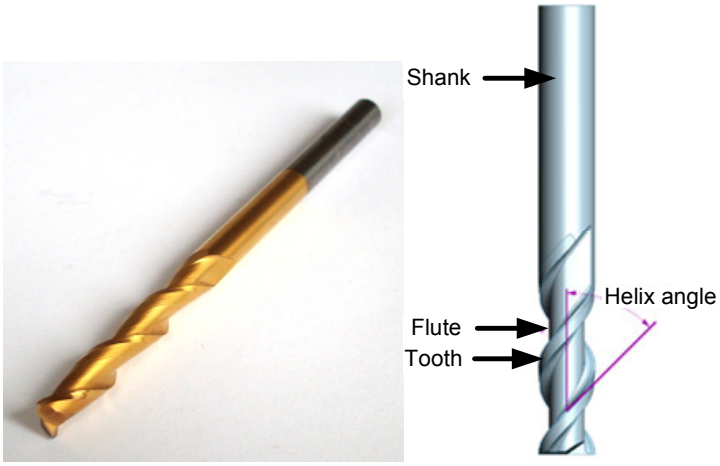

Figure 5.9: End-mill cutter with two flutes [54, 52]

5.3.2 CNC Wire-Cutting Electrical Discharge Machining (EDM) Technology

The term Electrical Discharge Machining (EDM) refers to any machining process that uses an electrode to remove metal (or any other conductive material) from a workpiece by generating sparks between the conducting surfaces [56]. During the process, sparks are created between the electrode and the workpiece and the energy (intense heat with temperatures reaching 8000 to 12000^0C) due to the sparks is dissipated by the melting and vaporising of the workpiece material. The spark is controlled very carefully and localised so that only the surface of the material is affected. In order to prevent pre-mature sparking, the whole process is performed in a dielectric fluid. A simple illustration of EDM is shown below in figure 5.10.

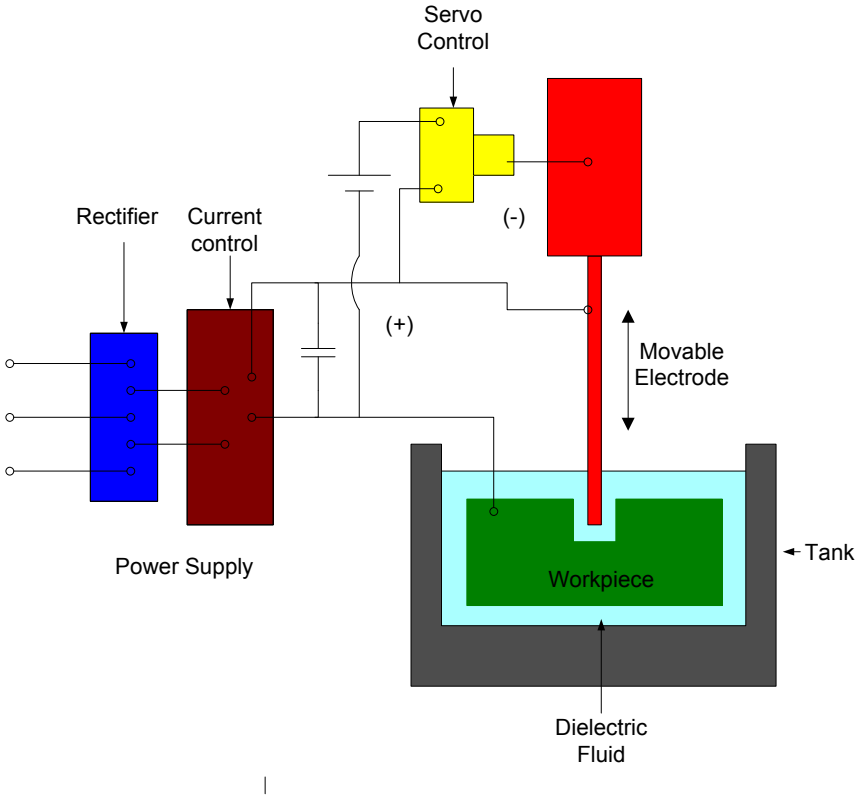

Figure 5.10: Electrical Discharge Machining (EDM)[59]

The two main types of EDM are ram/sinker EDM and Wirecutting EDM. Sinker EDM sinks the shape that is on the electrode part way into the workpiece and is therefore limited in the complexity of shapes that can be created. Wire EDM is more competitive with other more standard machining methods. Therefore, only Wire-cutting EDM is considered here.

Wire-cutting EDM uses a thin metallic wire (electrode) to cut a programmed contour in a conductive material, leaving a path of 0.001" to 0.003" larger than the wire diameter. This programmed path is determined by the relative motion of the machine axis. There is no physical contact between the wire and the machined part; the wire is charged to a required voltage rapidly, while surrounded by de-ionising water. When the correct voltage level is reached, a spark jumps the gap and melt a small portion of the workpiece. The sparking is illustrated in figure 5.11 below.

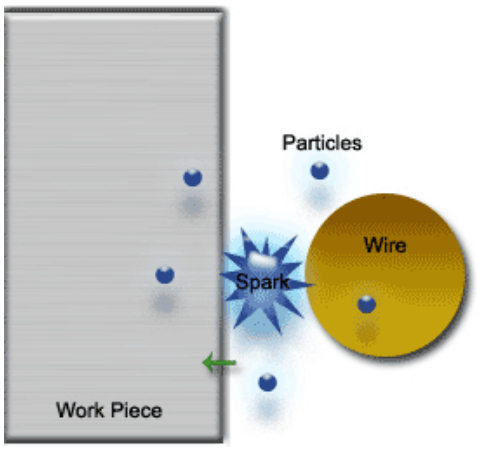

Figure 5.11: Illustration of spark properties for Wire-cutting EDM[61]

The sparks are controlled by the current generating circuit as seen in figure 5.10 and are adjustable for different

material types and desired surface finishes. The de-ionising water, with its conductivity carefully controlled, then cools and flushes away the small particles from the gap.

The wire-cutting process is shown in figure 5.12.

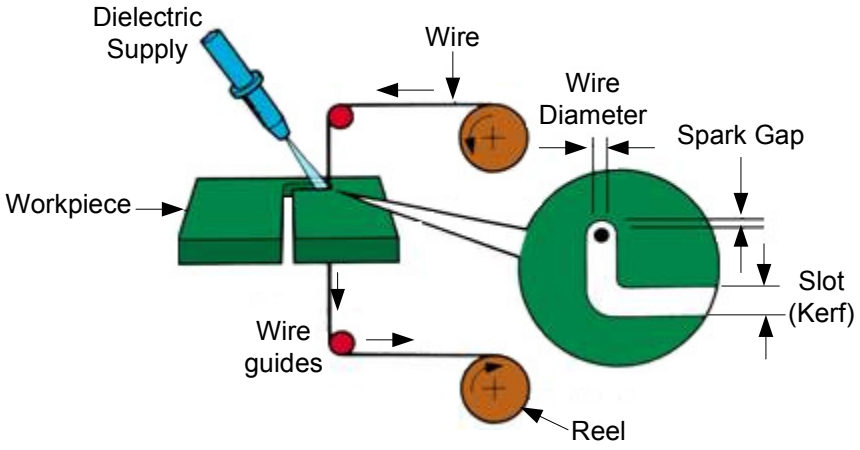

Figure 5.12: Wire-Cutting EDM[59]

CNC wire EDM machines usually operate on all 5 different axes: the Y, X, Z, U, and V axes [51]. The 5 axis CNC machines offer more precise cutting abilities than the 3-axis machines that operate around the normal 3 axes of movement: X, Y and Z. Programming of such machines is hard, but the type of work that can be performed is limitless with the 5 axis machines [51].

The main advantages of Wire EDM are among others:

- Accuracy of up to +/- 0.0001 inches [46].
- It is ideal for delicate parts; low cutting forces are present.
- Allows for tight tolerancing of up to 2 microns due to the low machining forces [46].
- Rapid and economic production, because no tooling is required.
- Pieces over 16 inches thick can be machined [46].
- complex profile capability.
- Tools and parts are machined after heat treatment so dimensional accuracy is held and not affected by heat distortion.
- Hardened materials are easily machined.
- Absolute consistency between machined parts due to no tooling wear as a result of no contact between the cutting wire and surface.

For the microwave designer, it is important to know the wire diameters typically used in the manufacturing industry, so as to work the design around those values. Wire diameters are usually between 0.1mm to 0.3mm. For roughing cuts, the typical wire diameter used is about 0.3mm and for finishing cuts, 0.2mm. Depending on the accuracy and surface finish required, a part can either be one-cut or it can be roughed, then skimmed. Skimming is process where the wire is passed back over the roughed surface again with a lower power setting and low pressure applied [50]. The one-cut is ideal for some applications, but for applications requiring a better surface finish, skimming is essential.

Compared to other CNC machines, CNC wire EDM machines can be said to have ultra high tolerances and precision that cannot be matched [51]. However, as much as wire EDM may have a lot of advantages, it is at times more economical to machine some parts partially by EDM and partially by other means.

5.3.3 Surface Finishing

Microwave fields penetrate only a small distance into a metal. Surface roughness and deformation are thus important and very misleading results may be obtained using surfaces which have been machined or mechanically polished [29]. Surface roughness is just one of the typical characteristics used to describe the surface quality of mechanical microwave components, and in many cases is not sufficient in giving an estimation of the functional properties of the surface. A better estimate requires some knowledge in the following [28]:

- Size and shape of different types of individual irregularities e.g. flaws, scratches, cracks, holes and depressions.
- Directionality of the predominant surface pattern that is characteristic for each manufacturing technology and tooling system.
- Surface roughness.
- Waviness of the surface.
- Dimensional errors of the surface.

Figure 5.13 below shows the surface roughness and waviness (widely spaced irregularities that underlie the roughness [42]), both of which are measures of the surface finish due to tool marks and other machining irregularities.

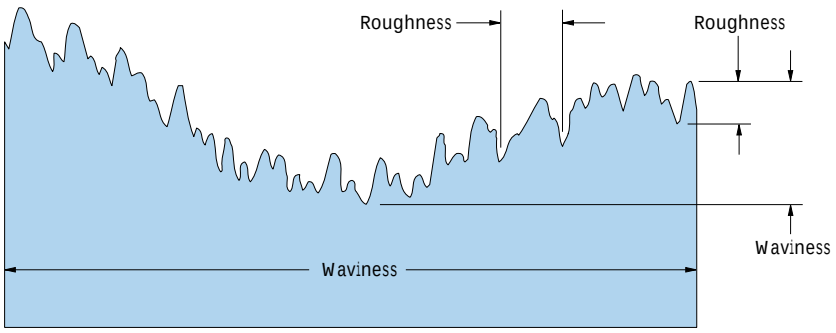

Figure 5.13: Surface roughness vs. waviness [42]

Manufacturing processes usually have an inevitable lack of precision, and surfaces manufactured from the different processes usually have an associated roughness leading to a variation in the device performance. For the designer, the main concern should be the effect of these rough surfaces on the performance of the microwave device being designed, such as the return loss and the insertion loss. The reflected energy and the absorbed energy of electromagnetic waves are dependent on the surface roughness and the working frequency [32]. It is therefore important for a designer to become familiarised with the range of finishes that can be obtained for the manufacturing operations being considered. A full table of these can be found in [29], where the surface texture for milling is approximated to range between 32 to 63 microinches, while that of fine milling ranges between 8 to 32 microinches.

The type of finish required also impacts on the cost of manufacturing. A better finish increases the costs.

5.3.4 Machining Tolerance

Machining tolerance can be said to be one of the most important factors contributing to the cost of manufacturing. Satisfactory performance of a microwave device after manufacture depends a lot on the precision on the machining processes. Most microwave designs have very tight dimensional tolerances and usually need very high precision machining to achieve this. In most cases, special finishing techniques, cutting techniques and care are required. If the dimensional accuracy can be met using a standardised process, the cost would only depend on the manufacturing time. However, if there is a need to change the process to ensure better accuracy, the price rises, because new setups are needed and new measurements are necessary to ensure the quality [28]. Even though the machine is responsible for a lot of the precision, the operator and the programmer also play a huge role, and of course the operating environment is also a contributing factor.

It is important that the drawings and specifications sent to the manufacturer should state the exact manufacturing requirements such as secondary dimensions and tolerances, provisions for chamfers or fillets and the required surface finish. An accurate indication of such can prevent a possible need for redesign due to dimension related manufacturing anomalies.

5.4 Coating Technology

There are several reasons for using coatings on devices. In microwave engineering, the most important ones are: to make it possible to use cost effective base materials with appropriate thin coatings that improve the thermal and electrical conductivity of a device, to prevent surface oxidation or unwanted changes due to the environment within which the device is used and to obtain a higher surface hardness.

There are many different types of coating processes. Some of the more common ones are electroplating, electroless plating, electroforming, organic coating, ceramic coating, hot dipping, vapor deposition, thermal spraying and ion implantation. The quality of the plating process and the surface layer can be evaluated in terms of the following characteristics [28]:

- Thickness variation of the coating layer (including inner and outer corners or other difficult geometries)
- Properties of the surface layer under different load cases (e.g., thermal changes, bending moments, chemical loading)
- Surface roughness of the coating layer
- Hardness profile variation of the coating layer

In mechanical microwave components, the most commonly used coating materials are gold, silver, nickel and tin-lead-alloys. However, out of these, the most favoured choices are usually gold and silver.

Gold is a good conductor of heat and electricity, and is an excellent material for electrical signal transmission. However, gold is very expensive compared to other coating materials.

Silver, as indicated in table 5.1, has the best conductivity of all metals; it can carry a high current load with the least loss at the highest microwave frequencies. It is mostly used for the coating of microwave enclosures and connectors. The most commonly used coating process for silver-plating is silver electroplating, which is discussed in the next sub-section.

5.4.1 Silver Electro-Plating

Electroplating is a process by which an electric current is used to deposit a thin layer of metal over another from a solution containing a dissolved salt of the selected coating material. The plated material is referred to as

the *cathode*, and the plating metal is the *anode*. The salt solution within which the two are suspended is called an *electrolyte* liquid.

The amount of metal deposited at the cathode and dissolved at the anode are directly proportional to the quantity of current passed. The thickness of the coating is a function of the current density, the time and the cathode efficiency.

The variation of the local current density on a part is dependent on the shape of the part and on the arrangement of the anodes. There is a preferred range of current densities for the cathode and also for the anode. Too much current can cause formation of an insulating film on the anode, lowering the current. Too little is also not desirable because it reduces the economic effectiveness of the process.

The current distribution can be increased by using specially designed anodes or by using electroless plating, which is good for narrow slots. However, this produces relatively thick coatings, so it is only applicable when thick coatings are required.

Because of the dependence of the uniformity of the plating on the current distribution, there are certain shape limitations for electroplating. Some of these are noted below:

- Gently curving, convex surfaces are better when trying to obtain a good uniform thickness.
- Corners, edges, fins, ribs and other protuberances tend to 'steal' more than an equal share of the deposited metal.
- Grooves, serrations, holes, concavities and deep recesses often get less plating thickness than other areas.
- Areas with thin coating usually fail first during service that includes a corrosive atmosphere.

Variations in the uniformity of a plating due to the shape of the part being plated can be seen in figure 5.14.

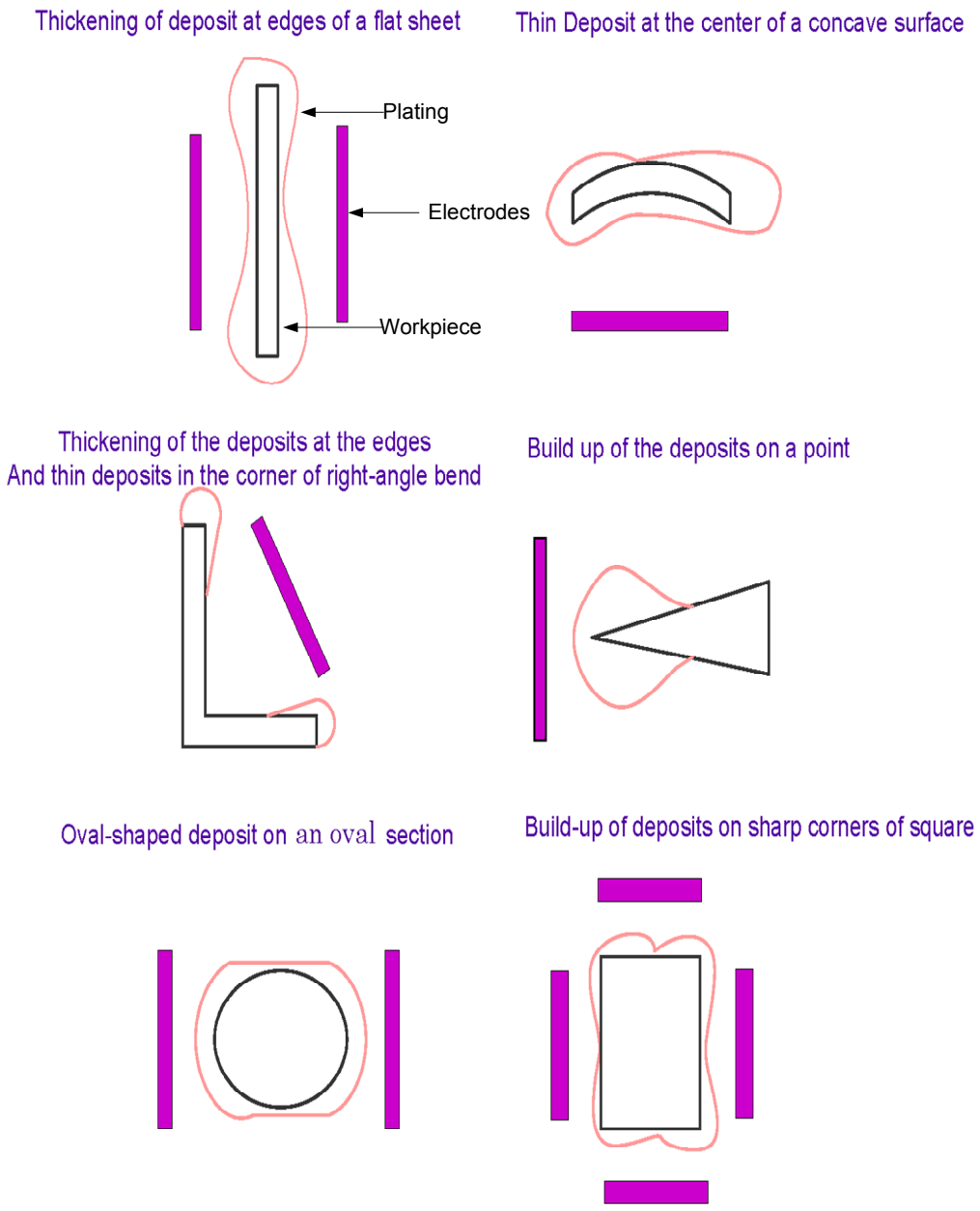

Figure 5.14: Variations in plating thickness due to certain shapes [43]

Therefore, in designing parts to be plated with a good coating at minimum cost, some of the design considerations are as follows:

- Edges should be rounded (See figure 5.15) .
- Flat surfaces should be crowned (See figure 5.15).

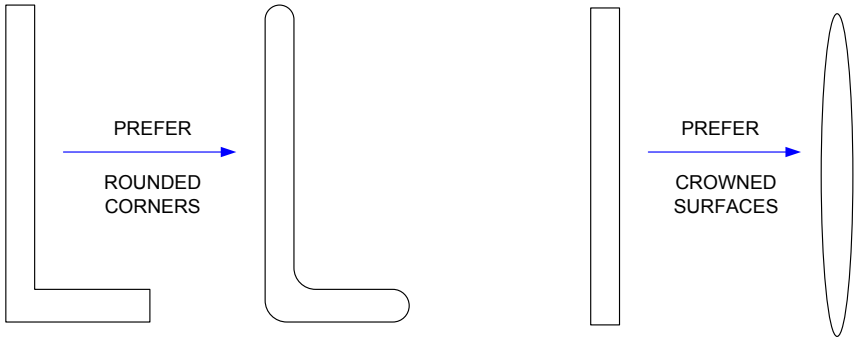

Figure 5.15: Some design considerations

- Convex juts should be generously rounded.
- Blind slots and grooves must not be deeper than they are wide, otherwise thickness of the interior electroplate will be less than the thickness in adjacent areas.

Considerations while choosing specialised anodes are as follows:

- Auxiliary anodes directed to concavities improve uniformity, but costs incurred while using such are higher.
- Internal anodes are needed for electroplating the bore surfaces of round or rectangular, tube-like surfaces with lengths more than two times the diameter or width [43]. Otherwise, thin coatings are inevitable at center areas.
- Such specialises anodes should be conformed to approximate the shape of the contours for more even thickness of the plating. However, such anodes are only used for relatively thick platings of about 2mm or more [43].

Specifications for the thickness of the electro-deposited metal coating are based on the basis metal, the metal deposited, the corrosion protection required, the type of service the finished device or component will encounter and in the case where the major reason for coating is for improved conductivity, the skin depth of the coating metal plays an important role.

Cost estimations are made based on the choice of coating materials, the labor and handling, and the types of equipment used during the process. Most of the cost is due to the choice of the material. Labour and handling do not influence the cost much as long as the same equipment or types of equipment are used.

5.5 Cost Evaluation in the Design and Manufacture of Microwave Filters

5.5.1 Design Costs

Decisions made during the design phase cause roughly 80 percent of the costs during manufacturing stages [28]. It is important to gather and compare different material constructions and manufacturing possibilities at early stages of the design work. It is bound to save money and time later, especially in avoiding re-designing.

5.5.2 Material Costs

Microwave devices use precious and expensive materials such as gold and silver to obtain the required functional requirements. In some applications, extremely good quality grades of alloyed metals are required and these can also be quite costly. At times, the required metals are also difficult to machine using conventional or standardised processes and may need special set-ups, hence introducing added costs. Careful material selection therefore plays a very important role in the estimation of overall costs.

5.5.3 Manufacturing Costs

Manufacturing costs comprise of tooling costs, capital costs, labor costs, indirect labor costs and fixed costs [28]. As has been stated before, most microwave applications require specialised tooling and fixturing systems and quite tight dimensional tolerances. The special set-ups can be quite costly. The costs associated with the long set-up times, use of specialised tools and fixturings can be marginal in high volume production, but in prototyping and in small series production, these can increase the production costs by about 500 to 800 percent [28].

5.6 Design for Manufacturability (DFM)

Manufacturers usually complain that designers don't have enough insight into manufacturing technologies. However, there has also been the observation from the designer's end on the manufacturer's lack of awareness for the related quality requirements of manufactured devices. The trend in most cases has been that of the designer presenting a completed design to the manufacturer with indicated dimensions, some requiring very high precision, which may be very difficult to attain using the available manufacturing technology. After assessing the design, the manufacturer can then go ahead with the design, or recommend that certain changes be made to ease the manufacturing process. Time can be costly, especially when working on projects with time restrictions. Redesigning merely tasks the designer with a usually cumbersome process and if it can be avoided, it can save both money and time.

Design for manufacturability (DFM) is an idea that encompasses aspects such as, the methods utilised for the choice of the most appropriate constructions of an item for production, instructions and/or rules outlined for the design of a device for easier manufacturing and the means to improve the cooperation and integration between the manufacturing and designing parties. DFM mainly aims to reduce costs associated with redesign due to critical feedback from manufacturers, to reduce development time and costs should the design be made with manufacturing capabilities in mind, to improve quality and reliability and in cases where the product is being manufactured to large scale commercial purposes, it aims to increase productivity and improve response time to customer requirements.

In the sub-sections that follow, the roles of the designers and the manufacturers in realising the goals of DFM are addressed and in light of modern requirements, the improvement of DFM due to computer applications is also discussed.

5.6.1 Roles of Designers and Manufacturers in DFM

The norm in design has been to use modular constructions and standardisation with only functional considerations in mind, and not those of manufacturing. Conversely, manufacturers mainly aim to improve their production equipment and enhance the efficiency. They suggest and often implement changes that ensure the ease and flexibility of the manufacturing process, their main focus being on the equipment/tools and not on the products. As has been stated in the preceding section, DFM aims to improve the cooperation and integration

between manufacturing and design stages of product development. One of the recommendations that has been made by researchers is that design engineers of mechanical microwave parts should gain enough knowledge about manufacturing during their tertiary studies, in addition to the traditionally and currently focused on methodologies and computer-aided means, so that they can apply DFM when in industry.

In carrying out the basic steps for DFM, the designer's roles can be outlined to include:

- the use of modular constructions
- the use of parametric design
- trying to select geometries suitable for common standardised tools
- minimising of the number of parts in the construction
- checking for machining allowances prior to design
- leaving enough space for using tools for different machining processes, especially when setting requirements for finishing in closed geometries.
- aiming for symmetrical geometries, if possible, and using constant chamfers and fillets
- selection of corner radii of machined inner geometries according to standardised tools
- clear indications of sensitive parts that require special machining considerations
- proper dimensioning and provision of allowable tolerances
- checking the suitability of a chosen material for the manufacturing methods

The manufacturer on the other hand, is tasked with:

- the development of flexible manufacturing systems
- utilisation of automation
- the use of multiprocessing systems
- using manufacturing methods that are economical inorder to minimise costs
- the development of flexible fixturing systems
- choosing manufacturing methods requiring fewest preparations
- ensuring that the product meets the design requirements and specifications

In the conventional systematic design approach, the cycle places the design and modular construction of a device before the manufacturing documentation and assembly, with a serial interaction rather than a parallel one. With the above outlined roles in mind, DFM ensures the incorporation of manufacturing issues in the design process right from the conceptual stages of design.

DFM may not always be fully applicable in some areas of microwave engineering design, but in most, it provides the attractive advantage of cost reduction. It is therefore highly recommended that both designers and manufacturers adopt the aspects that can improve overall microwave product development.

5.6.2 Computer-Aided DFM

Computer-aided DFM is described in [28] as a design environment which enables the identification of potential manufacturing problems and provides suggestions to eliminate them. It offers the possibility of transferring CAD geometries in drawing interchange/exchange format (DXF) or stereo lithography file format (STL) to computer-aided manufacturing (CAM) or rapid prototyping (RP) software.

A fully computer-based design chain of a filter for instance, would start with the circuit simulation model of the electrical design, then the functional simulation of the filter, which gives the respective simulated behaviour of certain properties in the form of curves, followed by the performance simulation to obtain appropriate dimensions for the physical model. If computer-aided manufacturing software is available, then using the obtained dimensions, manufacturability analysis can be done prior to the 3-D modelling and finally, performance tests and evaluation can also be done. However, the sophisticated manufacturability analysis software are not always available, especially in many academic institutions. The design process in such cases therefore follows a different cycle.

For the filters designed in this thesis, the process starts with the circuit model simulation, then the 3-D modelling of the combline filters which yields the required dimensions that are then sent to the manufacturers with stated tolerances due to the sensitivity of certain sections of the filters. Implementation of DFM in such an instance lies in the discussions made with manufacturers at different design stages to obtain recommendations for the various changes in topology that should be made in light with the available technology for manufacture.

In general, Computer-aided design for manufacture saves a lot of time and costs that might have been incurred otherwise, due to unpredicted problems, which in this case are identified at earlier stages.

5.7 Conclusion

Several aspects of manufacturing have been discussed for coaxial cavity filters like the combline filter. A discussion on material used at microwave frequencies presented the different options for use, concluding that aluminium would be the best option for the enclosure, because of its light-weight, affordability, good conductivity and machinability. Machining techniques were also discussed and milling and wirecutting were considered to be the most viable options for the fabrication of the filter enclosure and the resonators. Surface finishes obtained due to these techniques and their effect of the performance and dimensional tolerances of machined filters have also been outlined. The chapter also included a section on silver-plating of the filters to increase the surface conductivity and Q factor of the filter, since the aluminium will provide a lower Q factor. Aspects related to the evaluation of the design and manufacturing costs are also covered, and the relationship between the design stages and manufacturing stages of production is addressed, with specific emphasis on the concept of design for manufacturability (DFM).

Chapter 6

Design of Combline Filters for Reduced Manufacturing costs

6.1 Introduction

Chapters 2 and 3 discussed the design of combline and evanescent-mode waveguide filters and it was noted that the structure of the two filters was very similar. Filters with that type of structure are some of the most used types of filters at microwave frequencies because they have high unloaded Q factors. The manufacturing of such filters, however, can be quite costly. In chapter 5, different aspects contributing to the cost of manufacturing were discussed, together with recommendations that called for adjustments of filter structures at the design stage of development for easier manufacturing. The chapter discussed the choice of appropriate materials for fabrication of the filters to satisfy the electrical requirements as well as machinability aspects. It also focused on machining techniques and modifications in filter topology that suit the specific techniques, surface properties and ways of obtaining the best surface roughness and machining tolerances. This chapter focuses on design of combline filters for ease of manufacture and for reduced manufacturing costs. The filters are designed for two different sets of specifications. The first filter is a fourth order Chebyshev combline filter operating in the L-Band with a passband between 1235MHz - 1365MHz, with a return loss of less than 20dB in the passband. The second set of specifications calls for the design of an S-Band combline filter with a 40MHz bandwidth centered at 2125MHz and having an insertion loss of more than 80dB at 2GHz. The second filter is also required to have no passbands between 6.375GHz and 9.375GHz. In the subsequent sections, the designs will be discussed in detail, outlining the different changes made to the structures in order to facilitate easier manufacturing and to lower the costs of manufacturing. The chapter also aims to establish the accuracy of the CNC milling and wirecutting EDM processes.

6.2 Filter I: 1.3 GHz Combline Filter

The specifications for this filter are as follows:

Centre Frequency	1.3GHz
Order, N	4
Fractional Bandwidth	10%
Response Type	Chebyshev
Return Loss (RL)	$\leq 20dB$

Table 6.1: Filter Specifications

The subsequent subsections will discuss the design of a circuit model in AWR Microwave Office (MWO), the modelling of the 3D structure in Computer Simulation Technology (CST) software and the manufacturing options used for the manufacture of the filter. The measured results of the manufactured filters are discussed at a later section.

6.2.1 MWO Circuit Model of the 1.3GHz Combline Filter

For this design, short lines with an electrical length of 45^0 are chosen, so that small sized filters can be realised. The filter is designed to have a 4th order Chebyshev response with a passband ripple of 0.01dB and a line impedance of 76.7Ω. The couplings are defined using $\boldsymbol{k}$ and $\boldsymbol{q}$ values obtained from tables in [24]. The circuit is modelled in Microwave Office (MWO) and is shown in figure 6.1 below, and its S-Parameters follow in figure 6.2.

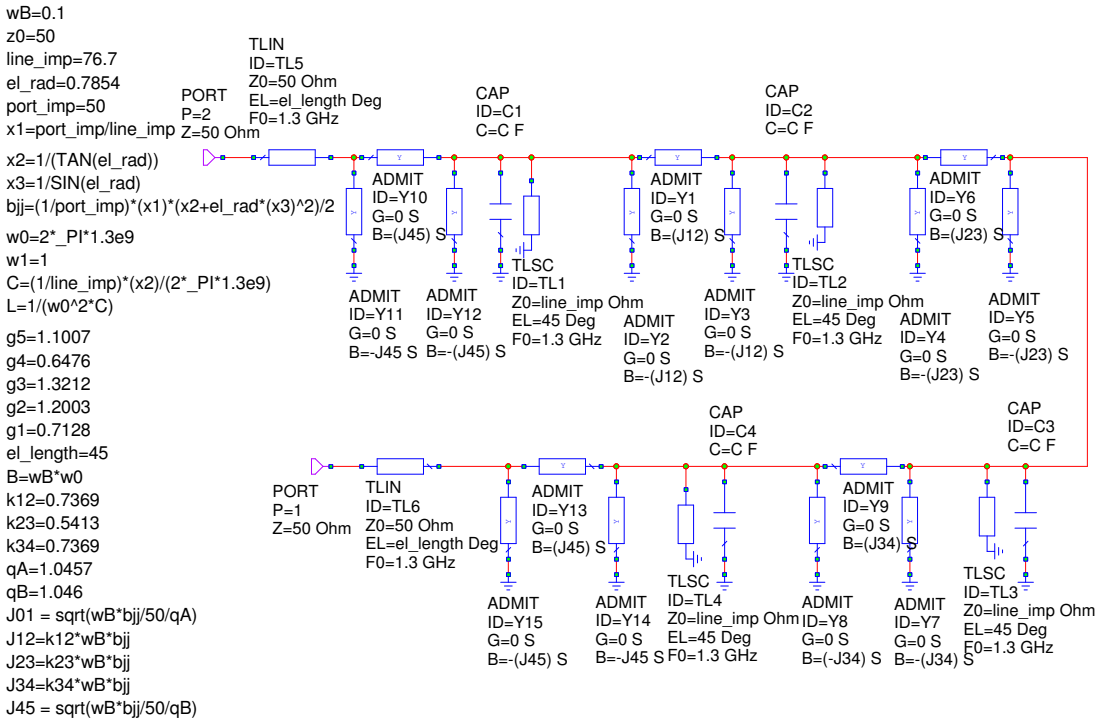

Figure 6.1: Circuit Model of 2125MHz Combline Filter

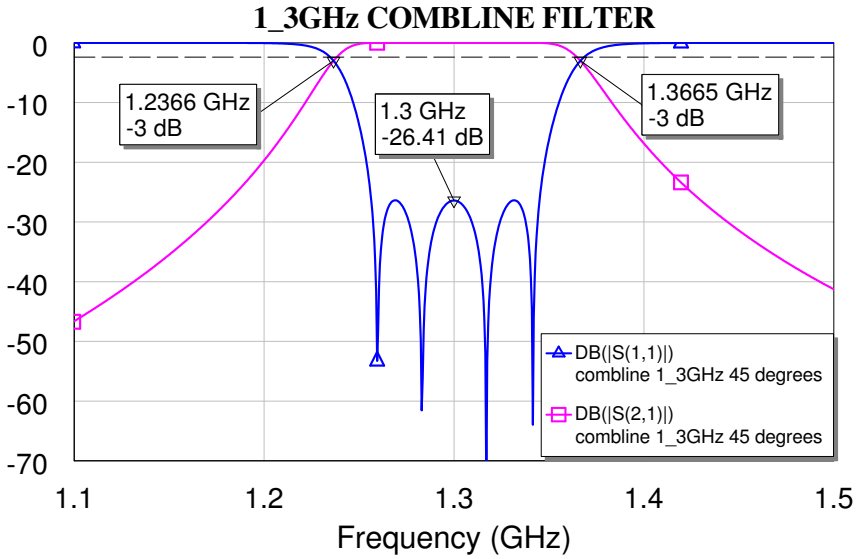

Figure 6.2: S-parameters of the Circuit in Figure 6.1

The filter has a 10% bandwidth centred at 1.3GHz with a reflection coefficient of -26.41dB at resonance. The 3D implementation of the filter in CST (Computer Simulation Technology) is discussed in the subsections that follow.

6.2.2 1.3GHz Combline Filter 3D Electromagnetic Model

The aim of this section is to model a 3D structure of a fourth order 1.3GHz combline filter to meet the specifications outlined in section 6.1, the circuit model of which has been seen in the previous subsection. In creating the model, various aspects that influence the cost of the manufacture of the filter are to be examined at different stages of the design, and with those in mind, relevant changes are to be made in the design with the aim of reducing the overall costs. The main objectives during the design stages will be:

- to incorporate recommended structural changes that make manufacturing using a chosen technique easier.
- to design sections in a way that makes electroplating easier.
- to reduce the number of steps required for the manufacturing.
- to reduce the number of total separate parts that need to be manufactured.

Whilst aiming to meet the above stated objectives, it is also important to note the effects of small changes in dimensions in case of manufacturing anomalies, so that correct tolerancing information can be provided. If very small changes give a considerable change in the response of the filter, then very tight tolerancing is required. On the other hand, if this is not the case, then the tolerancing need not to be so tight; tight tolerancing is very costly.

6.2.3 Resonator Options

Different options exist for the physical implementation of the posts of a combline cavity resonator. The shape of a resonator can be chosen either based on its ease of fabrication or because of the electrical properties that the design aims to achieve. In the case of bandpass filters of the coupled resonator type, the mutual coupling between adjacent resonators, be it capacitive or inductive is of importance, due to the interraction of electric

field (E-Field) lines or magnetic field (H-Field) lines, respectively. Figure 6.3 below shows the interraction of E-Field and H-Field lines between two resonators. The magnetic field is stronger near the shorted end of the resonators and the electric field is stronger on the open circuited end. The shape of a resonator can therefore also be chosen to facilitate either a stronger magnetic coupling in relation to the electric coupling or vice versa.

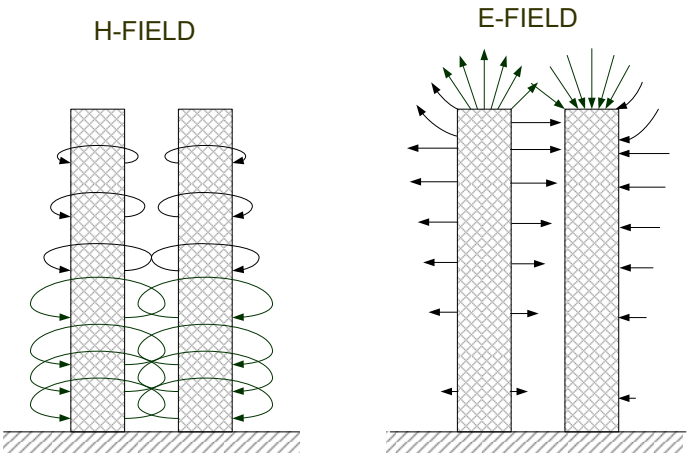

Figure 6.3: Electric and Magnetic Coupling between Two Resonators

A few examples of combline cavity resonators are shown in figure 6.4 below. The more commonly used types of resonators and also the easiest to fabricate are cylindrical and rectangular or square resonators.

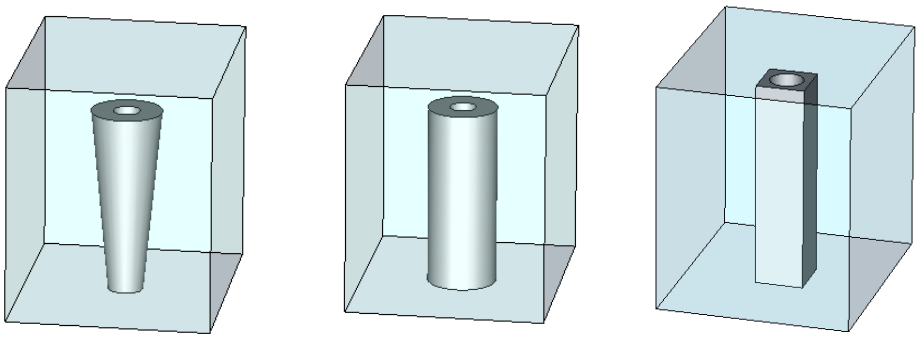

(a) Conical Resonator

(b) Cylindrical Resonator

(c) Rectangular/Square Resonator

Figure 6.4: Different Implementations of Combline Cavity Resonators

In chapter 5, milling and wire-cutting were indicated to be the cheapest options for the fabrication of the type of filters that have been discussed so far. Cylindrical and rectangular posts were considered as viable options for the implementation of combline resonators. For the cylindrical resonator, based on the advice of a consulted manufacturer, the simpler option for manufacture of filters consisting of such resonators would be to fabricate the posts separately from the remainder of the filter body and then to fix them into the base. Flanges will be needed in the base to establish a firm joint. Good electrical contact also needs to be established, so that the flow of current is not disturbed. Using rectangular posts seemed to be the less complicated option, and resonators of the type can easily be milled and wire-cut. For this reason, the filters designed in this chapter have rectangular posts as resonator lines.

To tune the frequency of the filter to the required resonant frequency of 1.3GHz, reduction of the size of the gap between the post and top wall of the cavity was not sufficient. In table 6.2 below, the steps taken to obtain a resonator with a good tuning range and modifications to its structure to enable easier manufacturing are depicted.

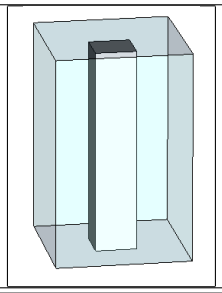	INITIAL RESONATOR POST
ADJUSTMENTS FOR INSERTION OF TUNING SCREW TO ADJUST RESONANT FREQUENCY	
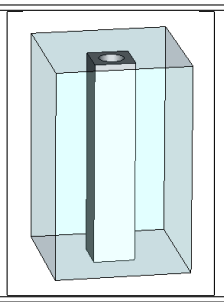	OPTION 1: CYLINDRICAL HOLE
OR	
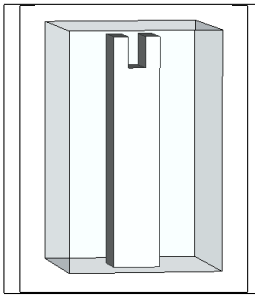	OPTION 2: THROUGH GROOVE
ROUNDING OF CORNERS FOR EASE OF MANUFACTURING	
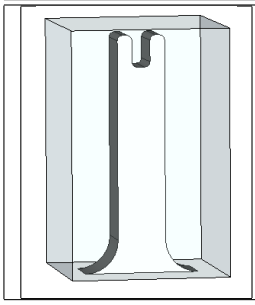	FINAL RESONATOR SRUCTURE

Table 6.2: Adjustments in Resonator for Ease of Manufacturing

By introducing the cylindrical hole or the through groove, a tuning screw extending into the hole or groove can then be used to tune the frequency of the resonator. The cylindrical hole is a better option when milling from the top, the through groove is a better option for wirecutting, but milling can also be used when done from the side. The depth of the hole or groove is chosen such that the length of the tuning screw is sufficient to short the resonator when doing the initial tuning. It is also important to consider, during the design stages, the diameters of the tuning elements that are available to the designer, so that the size of the hole or groove can be chosen appropriately during the 3D modelling of the filter.

In table 6.2, the final resonator structure shows the sharp corners of the resonator curved out to facilitate easier electro-plating. This follows recommendations that were outlined in chapter 5. In designs where the use of a tuning screw with an adjusted structure like that of the 'final resonator structure' in figure 6.2 still does not provide sufficient capacitance to tune the centre frequency to the required resonant frequency, further adjustments can be made to the structure to add the extra capacitance. One such adjustment is shown in figure

6.5. The side caps can be concentric around the post or, in the case of rectangular or square posts, they can just be on either side. The shape should be chosen so that manufacturing is made easy, especially when a specific manufacturing technique is desired.

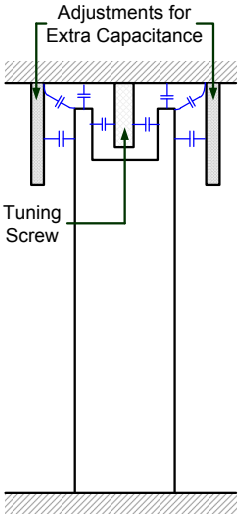

Figure 6.5: Adjustment for extra capacitance

6.2.4 Input/Output Coupling

Different external coupling options have been seen in chapters 2 and 3. All the different options can be used to obtain the right amount of coupling, but the fabrication of some may be very complex and therefore more costly than others. The choice of which coupling technique to use depends on a number of factors, some of which are:

- The field (Electric of Magnetic) by which one aims to couple.
- The bandwidth for which the device is designed to obtain.
- The simplicity of the design with regard to manufacturing.

Figure 6.6 below shows the two options that were considered for the 1.3GHz combline filter.

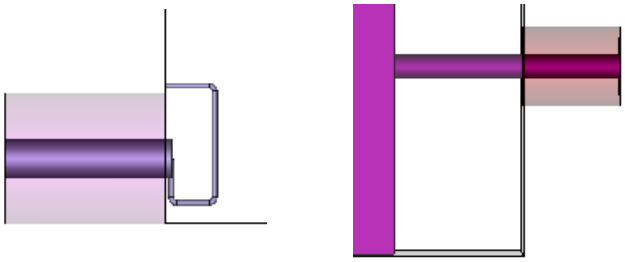

(a) (b)

Figure 6.6: Input/Output Coupling Methods

The loop coupling had two main disadvantages: the first is its complexity compared to a tapped coupling so that its fabrication would be costlier that the tapped coupling and the second drawback, specifically for this filter was that a very large loop would be required to achieve the right amount of coupling, the main reason being that magnetic loops are better suited for applications with very narrow bandwidths [64].

For the filters designed in this chapter, tapped coupling is chosen because it is simple to implement and is a less costly option as compared to the other options. It also produces the strongest coupling compared to probe and loop coupling. The main challenge posed when using tap coupling is the tuning of the input coupling. In the next subsection, the use of a tuning screw inserted from the lower wall of the filter enclosure, is investigated as a potential means to tune the input coupling when a tapped input is used.

6.2.5 Tuning of External Coupling For a Tapped Input

In this sub-section, the possibility of tuning the coupling at the input and output of a resonator coupled to external circuitry using a tapped input and output is investigated. A screw is inserted vertically into the resonator parallel to the resonator post and centrally placed along the axis of propagation as can be seen in figure 6.7. The screw perturbs the interacting magnetic field due to the series inductance of the input tap and the parallel inductance of the post as is seen in figure 6.7. By aligning it in the same axis as the posts, possible excitation of other unwanted modes is prevented.

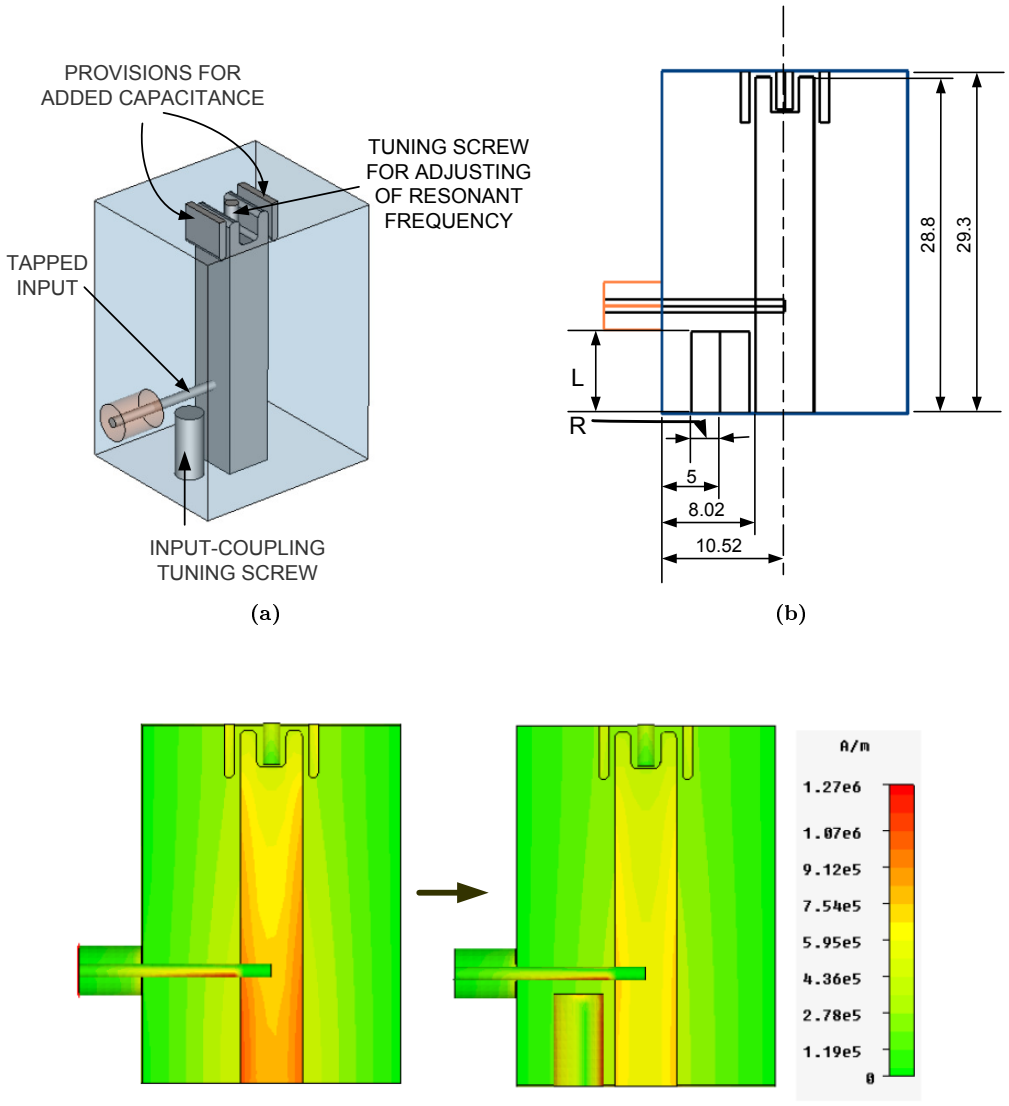

(a) (b)

(c) Perturbation of H-Field

Figure 6.7: Tuning Screw for Input Coupling of Tapped Input

Variations of the loaded Q, the group delay and the resonant frequency of the resonator with changes in the radius, R (see figure 6.7 (b)) of the screw for different depths of the screw, L (see figure 6.7 (b)), as it is inserted into the resonator can be seen in figure 6.8 below.

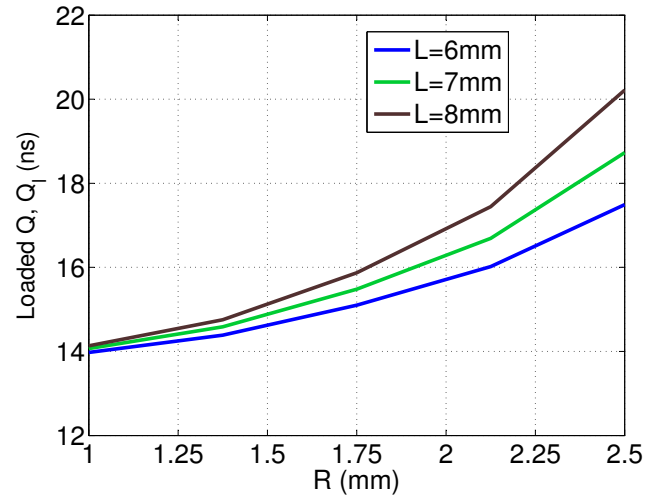

(a)

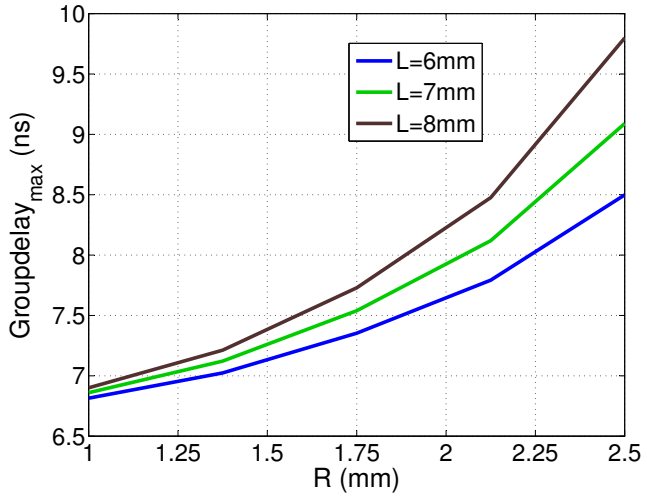

(b)

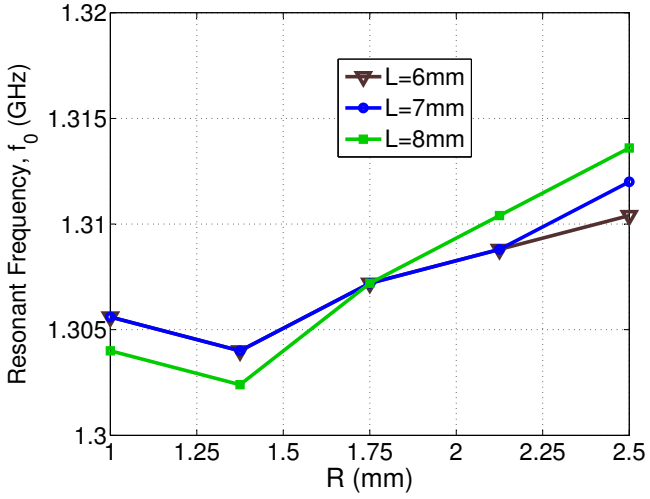

(c)

Figure 6.8: Variation of (a) the Loaded Q and (b) the Maximum Group Delay with Changes in Screw Length

A good tuning range is obtained for bigger radii as opposed to smaller radii, for the different lengths, L, of the screw. For a radius of 2.5mm, a length of 6mm gives a loaded Q of approximately 17.5, which can be increased to just over 20 by increasing the length of the screw inside the resonator to 8mm. A larger change in the group delay, as the length of the screw is varied, can be seen for larger radii. The resonant frequency, however, for any given radius does not vary so much with variations in the length of the screw inside the cavity. It can therefore easily be tuned back to the desired frequency by adjusting the tuning screws. For a radius of 1.75mm, the change in length from 6mm to 8mm has no effect on the resonant frequency. When a resonator or filter using this tuning technique is fabricated, an ordinary brass screw can be used, so that it is not costly and because its sensitivity is much less than that of the resonator tuning screws.

6.2.6 CST Fourth Order Filter

A fourth order filter designed in CST using four resonators of the type illustrated in figure 6.7 is shown in figure 6.9 below.

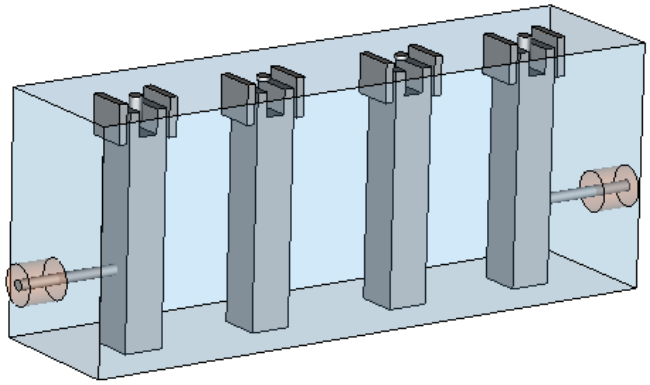

Figure 6.9: 1.3GHz Fourth Order Chebyshev Combline Filter

To reduce the number of cutting steps and hence the manufacturing costs, designing for less cutting steps is recommended. To effect this, the filter in figure 6.9 was further modified by extending the 'side caps' provided for extra capacitance across the spacing between the resonators, leaving out only the desired gap size between the 'side caps' and the resonator posts. The ones beyond the end resonator posts were extended to the end walls of the enclosure. The modified design is shown in figure 6.10.

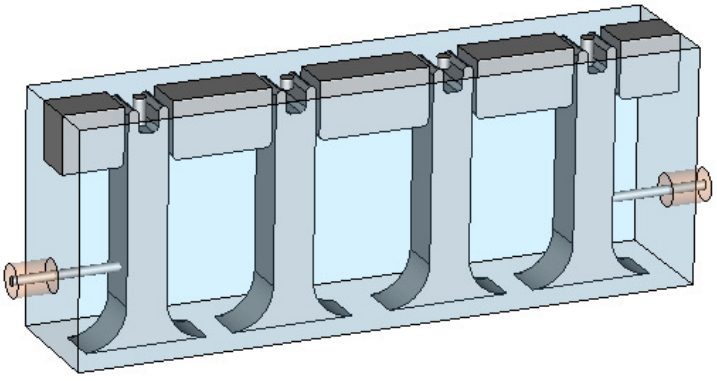

Figure 6.10: Adjustments on the Provisions for Added Capacitance

The S-Parameters of this filter are shown in figure 6.11.

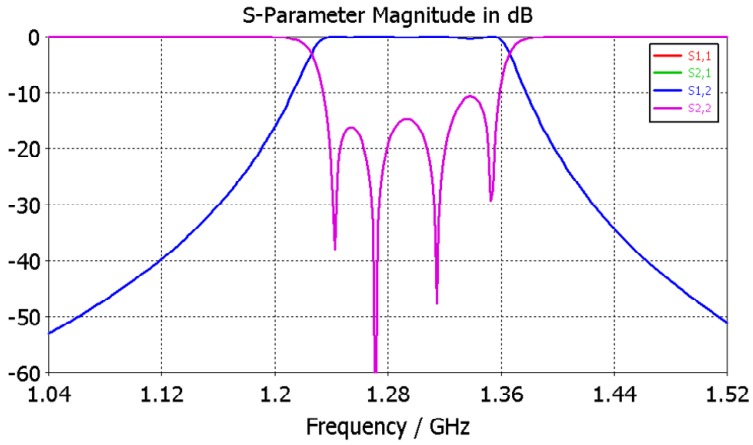

Figure 6.11: S-Parameters of the Filter in Figure 6.9

The design in figure 6.10 has a lot of sensitive areas that would need tight tolerancing. However, the tighter the required tolerance, the costlier the manufacturing. The next sub-section focuses on the sensitivity analysis of various sections in the filter, to see the effect that small changes in dimensions can have of the frequency response of the filter.

6.2.7 Sensitivity Analysis

The sensitivity of a device's performance to small variations in dimensions is a key concern in many design processes. In figure 6.12, sections of the filter for which sensitivity analysis is to be performed are shown. The analysis on the chosen sections aims to identify any possible critical changes in response, supposing an error in manufacturing should occur. By defining face constraints on either of the faces sandwiching the gaps indicated by the coloured ovals labelled 1, 2 and 3, a parametric sweep can be used to investigate the effects that small changes in the dimension would have on the frequency response of the filter. The dimensions are changed in steps of 0.05mm, and both positive and negative changes are considered.

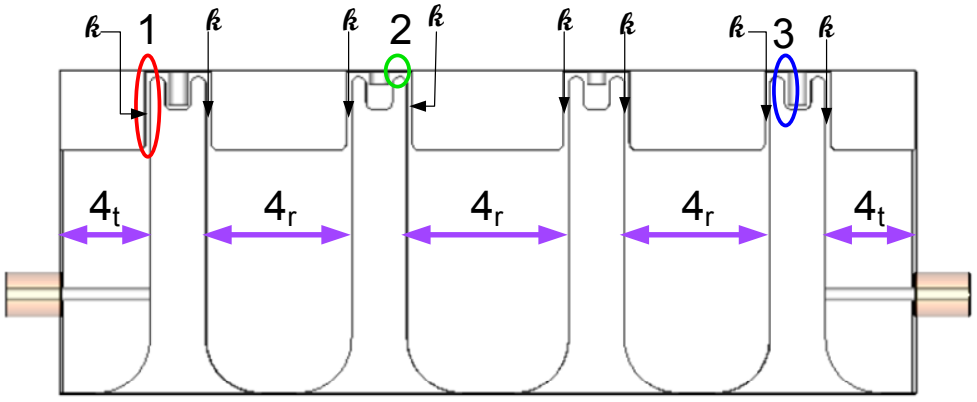

Figure 6.12: Sensitive Sections of a Filter

The sensitivity analysis is done in CST, the results of which are outlined below. The faces considered for each analysis are highlighted and for each analysis, the curves indicating the deviation from the original value by +/- 0.05mm are dashed.

Section 1:

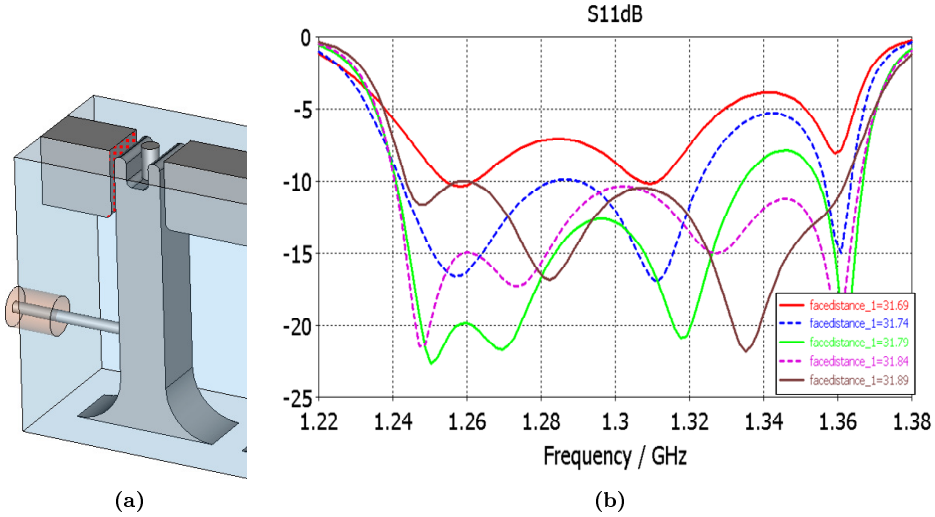

(a) (b)

Figure 6.13: Sensitivity Analysis of Section 1 (see figure 6.12)

Section 2:

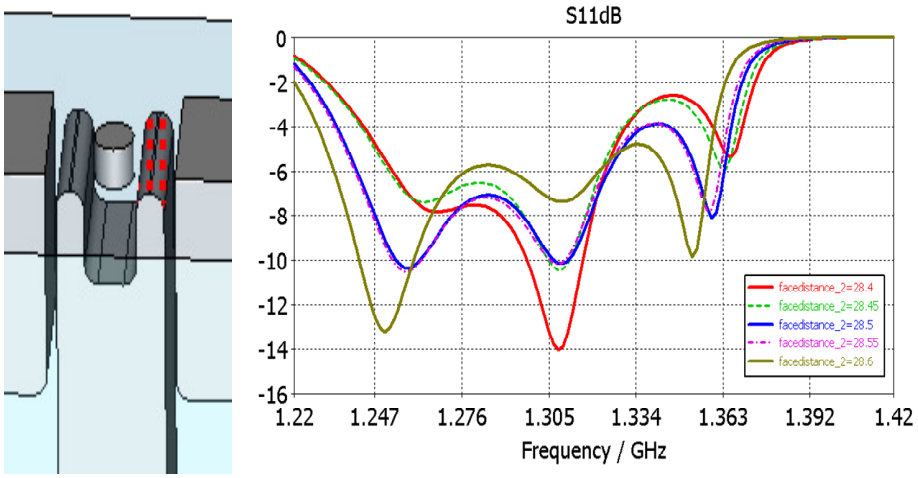

(a) (b)

Figure 6.14: Sensitivity Analysis of Section 2 (see figure 6.12)

Section 3:

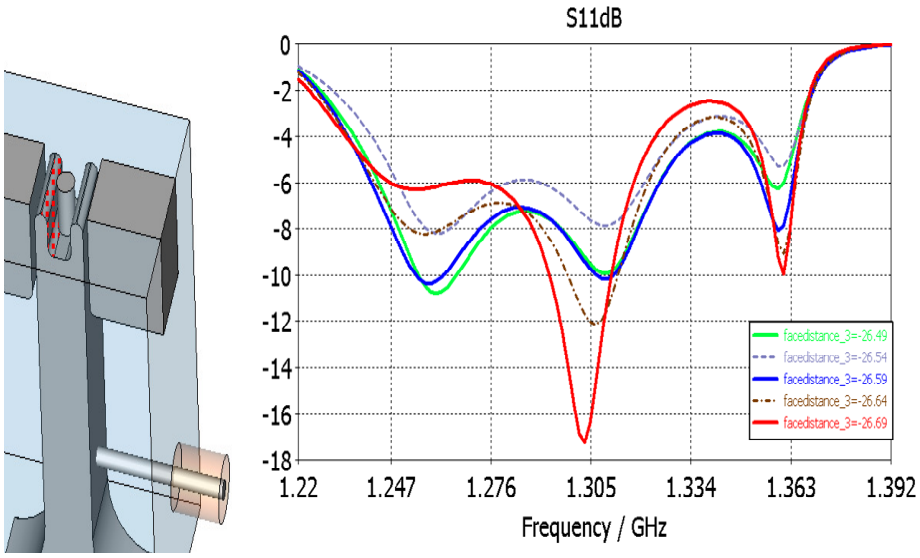

(a) (b)

Figure 6.15: Sensitivity Analysis of Section 3 (see figure 6.12)

Small changes in dimensions in all the areas results in a change in the return loss. The dimensions defining these sections, for all of the resonators are for this reason to have tight tolerances, which for this filter were chosen to be +/- 0.05mm. More detailed tolerancing information for all the dimensions of the filter is provided in Appendix A .

Section 4

In figure 6.12, the distances labelled '4', have been divided into two regions: 4_t and 4_r. A variation of the distance with the subscript t over a range of -0.1mm to 0.1mm over 0.05mm intervals results in a change in the return loss in the passband, affecting one peak more significantly in relation to the other peaks. This result is shown below in figure 6.16 (a). In figure 6.16 (b), the effect of a variation of the distance with the subscript r over a range of -0.1mm to 0.1mm over 0.05mm intervals, while maintaining the gap distances 'k', is shown to have an effect on the bandwidth of the filter, due to changes in the coupling distances. The change in bandwidth for the change of distances '4_r' by +/-0.05mm results in a very slight change of bandwidth. For these reasons, all the dimensions associated with section '4' are chosen to have a tolerance of +/-0.05mm.

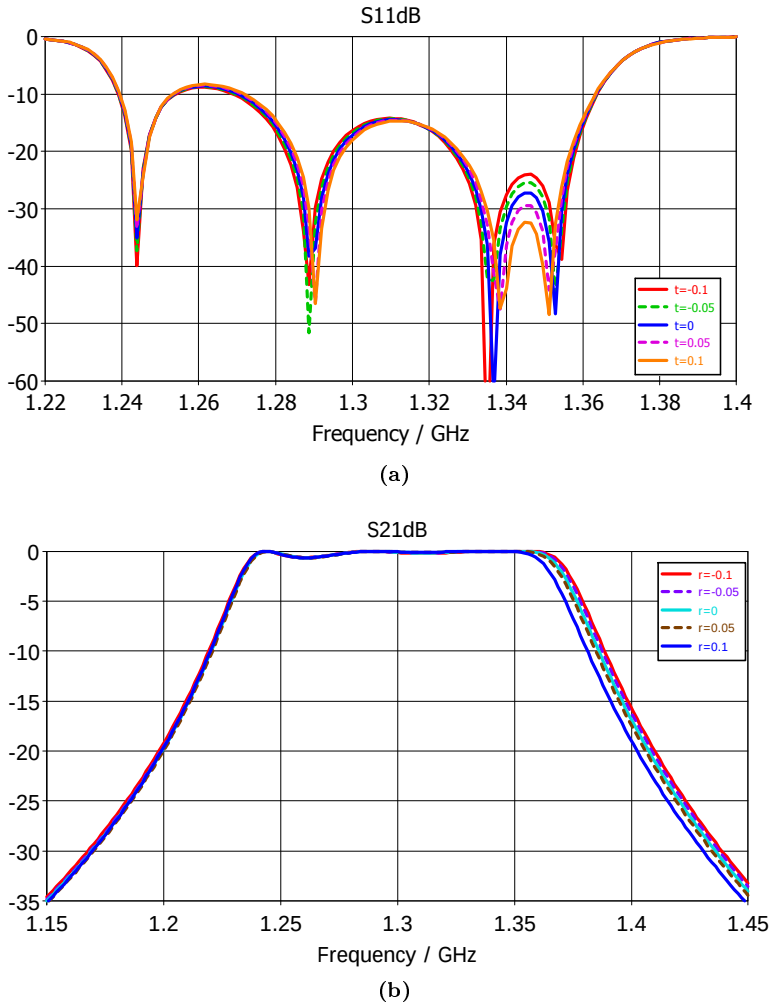

Figure 6.16: Sensitivity Analysis of Sections '4_t' and '4_r' (see figure 6.12)

The effect that slight changes in width of the gaps labelled 'k' is also investigated by varying the gap width in a parametric sweep within the range of -0.1mm to 0.1mm. The main effect is a shift in the resonant frequency due to changes in the capacitance of the resonators, a result which is shown in figure 6.17 below.

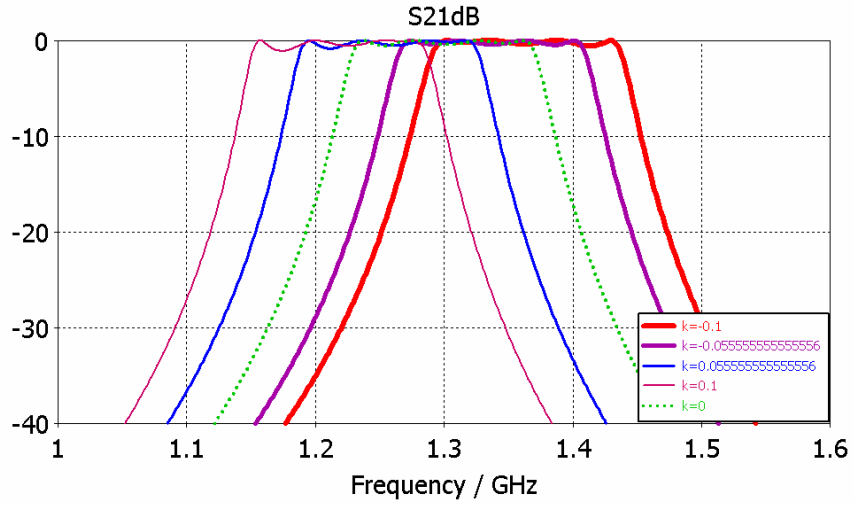

Figure 6.17: Effects of changing distances 'k' (see figure 6.12) on resonant frequency

The dimensions defining the sections labelled 'k' are also chosen to have a tolerance of +/- 0.05mm, so that

incase of an error in manufacturing precision, the centre frequency can be tuned back to 1.3GHz using the tuning screws. It is therefore also important that the depth of the hole or groove into which the tuning screw slides for added capacitance, be chosen carefully so that a good tuning range can be obtained.

6.2.8 Manufacture of the Filters

For the manufacturing of the filter, two machining options were chosen: *Milling* and *Wirecutting EDM*. A detailed description of these processes was given in chapter 5. By manufacturing the filter using the two different machining techniques, the overall costs associated with each can be compared to the other so that the cheaper option can be identified. Using Autocad Inventor, a 3D mechanical design and 3D CAD software, 3D models of the filter were created to enable visualisation of the different parts that would make up the filter. For the two machining techniques, the filter structures in figures 6.20 and 6.18 show the manner in which the filters are to be assembled. The two options are briefly outlined below.

Option I: Wirecutting EDM

In the case of wirecutting, only two covers, labelled side lid 1 and side lid 2 in figure 6.18, are needed, so that the total number of parts when compared to milling (see option II below) is reduced. The wirecutting is done from the side, which is why the widths of the 'side caps' are the same as the widths of the posts. The extra material in the block used for the main body can initially be milled out from either side to leave the middle portion with a thickness corresponding to the width of the posts, after which the wirecutting can be done. Sharp corners along the wirecutting path are rounded so that should be filter be plated, the plating will be relatively better distributed due to the curvature. A clearer view of the wirecutting path can be seen in the side view drawings of the filter included in Appendix A.

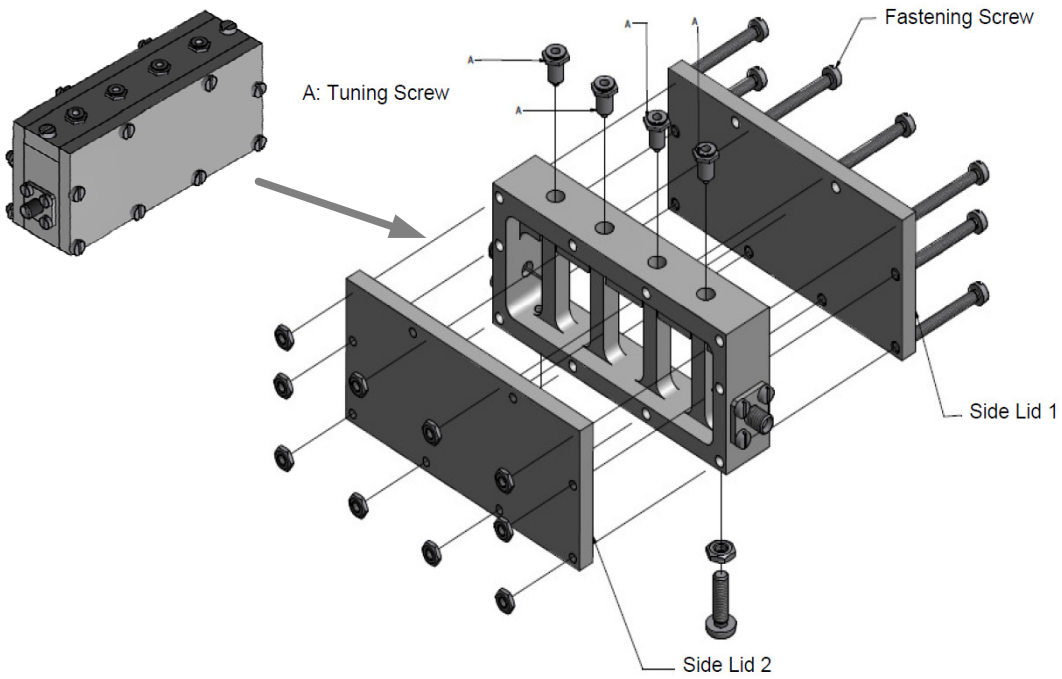

Figure 6.18: Filter to be Wire-cut

Long screws are used here as opposed to using screws on either sides, so that the number of screws used is almost halved. This particular construction becomes difficult to electroplate at the sections with tiny gaps that are not easy accessible, so electroplating would be costly. If the filter can have a good enough unloaded Q-factor

without the electro-plating of these sections, then the approach is a good one. The dimensions of this filter are also given in Appendix A.

Option II: Milling

For milling, the filter ensemble is to consist of three covers; two on either side of the filter main body and a top cover as shown in figure 6.20 (a). The top cover is milled separately from the main body to enable easier coating of the small gap areas around the open end of the posts, that would otherwise be too difficult to plate because they are very narrow. To reduce the number of machining steps the width of the 'side caps' are extended across the groundplane spacing. However, this adjustment results in a reduction of the overall volume of the cavity and therefore a subsequent decrease in the bandwidth of the filter. In CST, adjustment of the bandwidth to regain the desired bandwidth required an increase in the groundplane spacing. Unfortunately, a significant frequency shift away from the desired resonant frequency was also noted with the change in topology. Enough capacitance to shift the centre frequency back to the required one could only be obtained by increasing the height of the 'side caps' which unfortunately in turn results in a decrease in the volume and bandwidth again. For such a design, it would therefore be advisable to model the filter from the first resonator with this change in topology applied; adjustment after design may not yield the required result. The final model in CST had a -10dB bandwidth of 10%, as opposed to the wirecut filter which had a -3dB bandwidth of 10%. A comparision of the insertion loss of the two is shown in figure 6.19 below.

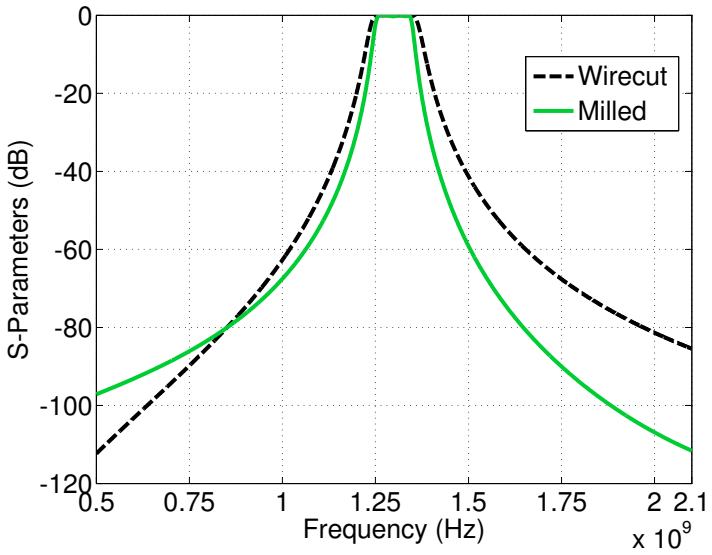

Figure 6.19: Insertion Loss of CST Physical Models of Filters to be Milled and Wirecut. Milled Filter has a -10dB Bandwidth of 10%, Wirecut Filter has a -3dB Bandwidth of 10%

The main body is to be milled from the sides, which is why the corners along the milling path have been rounded. The radii of the rounded corners are consistent with the diameters of the milling cutters that would be best suited for the specific areas, for instance, the post bases have been curved outwards with arc radii of 3mm, as opposed to the smaller radii of the rounded corners at the open end of the posts which are 0.5mm.

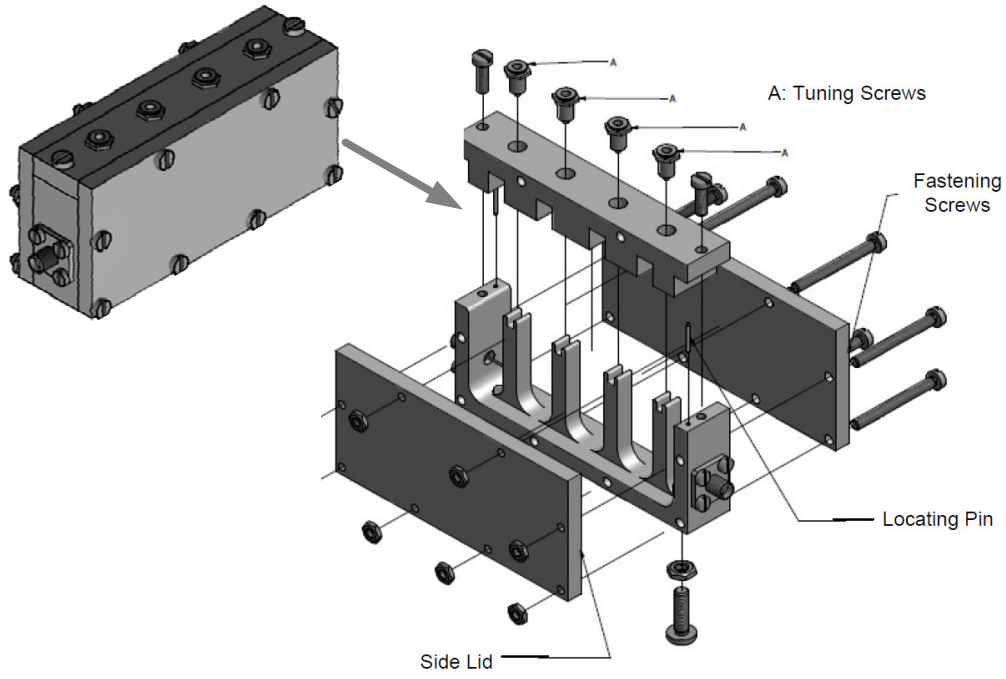

(a)

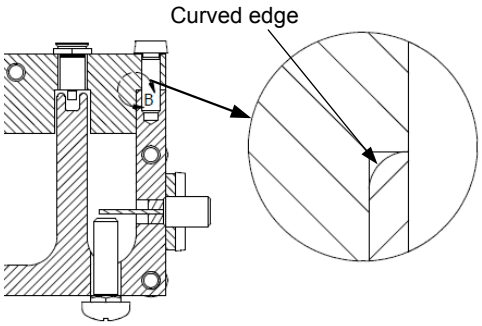

(b)

Figure 6.20: Filter to be Milled

Because the top cover is manufactured separately, silver plating of the groove becomes slightly less complicated than it is in the arrangement chosen for manufacture by wirecutting EDM (see figure 6.18). For good electrical contact, the top cover is fixed to the rest of the filter using two screws, each on either end, and two locating pins are used to ensure that its position is not shifted to the side. Good positioning of the cover also ensures that the right position of the tuning elements is maintained within the groove. The inner edges of the top surfaces of the central part/mainbody (the part with the resonators) are slightly rounded as shown in figure 6.20 (b) to allow the top cover to slide in easily while assembling the parts. A minimal number of fastening screws is obtained by using long screws that extend across from one side lid through the central part and the other side lid and is fastened using nuts for strong fastening. Strong and stable fastening is necessary to prevent the shifting of parts due to mechanical vibrations, incase the filter is used in an environment with such. It also ensures good electrical contact.

The detailed dimensions for the different parts of the filter are given in Appendix A.

6.3 Filter II: 2.125GHz Combline Filter

The specifications for the design of the 2.125GHz Filter are as follows:

Centre Frequency	2.125GHz
Bandwidth	40MHz
Type of response	Chebyshev
$\|S_{21}\| > 80dB$ at 2GHz	
No Passbands between 6.375GHz and 9.375GHz	

Table 6.3: Specifications for Filter Design

In chapter 2, it was stated that by choosing the right length of resonator line, the position of the second passband can be controlled. The specifications for this filter indicate that there should be no passbands between 6.375GHz and 9.375GHz, therefore an appropriate resonator line length has to be chosen to satisfy the requirement. The specifications also call for an insertion loss of greater than 80dB at 2GHz, a specification which is met by choosing the order of the filter that gives a sharp enough roll-off into the stopband. A maximum passband insertion loss of 0.01dB is chosen, so that a return loss of more than 20dB can be obtained in the passband. The approach taken is to initially create the circuit model of the filter in MWO to meet all the desired requirements, then a 3D model can be created in CST, using parameters derived from its circuit model.

6.3.1 MWO Circuit Model for the 2.125GHz Filter

For a Chebyshev equiripple response, shown in figure 6.21 for a lowpass filter,

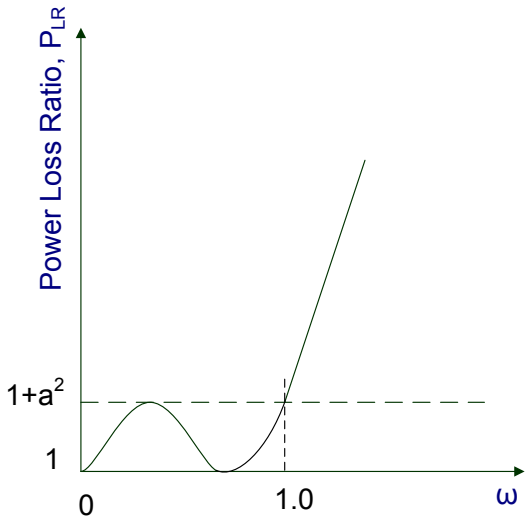

Figure 6.21: Equal-ripple Lowpass Filter Response

the order, N, of the filter can be calculated from the Chebyshev polynomial $T_N(\omega)$, defined mathematically as

$$T_N(\omega) = cos\left\{N\left[cos^{-1}(\omega)\right]\right\} \tag{6.1}$$

for $|\omega| \leqq 1$. For $|\omega| \geqq 1$, it is given as

$$T_N(\omega) = cosh\left\{N\left[cosh^{-1}(\omega)\right]\right\} \tag{6.2}$$

If given the insertion loss, the polynomial can be computed from the chebyshev insertion loss equation

$$IL = 10logP_{LR} = 10log\left[1 + a^2T_N^2(\omega)\right] \tag{6.3}$$

from which a can be calculated when $T_N(\omega) = 1$ ($T_N(\omega)$ oscillates between ± 1 for $|\omega| \leq 1$ so that the passband response has ripples with an amplitude of $1 + a^2$. For a maximum insertion loss of 0.01dB in the passband, we get

$$a = \sqrt{10^{0.01/10} - 1} = 0.048 \tag{6.4}$$

ω is a frequency transformation given as

$$\omega = \frac{2}{\Delta}\left(\frac{f_i - f_0}{f_0}\right) \tag{6.5}$$

where Δ is the fractional bandwidth, which in this case is 0.0188. f_i is the frequency at which the magnitude of transmission coeffcient is specified to meet the specified sensitivity requirement, i.e. $f_i = 2GHz$, and f_0 is the centre frequency, so that $|\omega| = 6.2578$. Since $|\omega| \geqq 1$, from equation 6.3, the chebyshev polynomial is then simplified, for an insertion loss of 80dB to get

$$T_N(\omega) = \sqrt{\left(10^{80/10} - 1\right)/0.048^2} = 2.0833e + 005 \tag{6.6}$$

The order of the filter can then be computed from 6.2 to get

$$N = \frac{cosh^{-1}(2.0833e + 005)}{cosh^{-1}(6.2578)} > 5.1014$$

The order of the filter was therefore chosen to be $N = 6$.

The length of line for the combline filter is chosen so that the second passband occurs at a frequency where the line is about half its wavelength at midband. For this filter, the electrical length was chosen to be 40^0 (0.6981 radians), so that the second passband would be expected to occur at a frequency further than 9.556GHz.

The circuit model of the 6th order Chebyshev combline filter centred at 2.125GHz is shown below in figure 6.22.

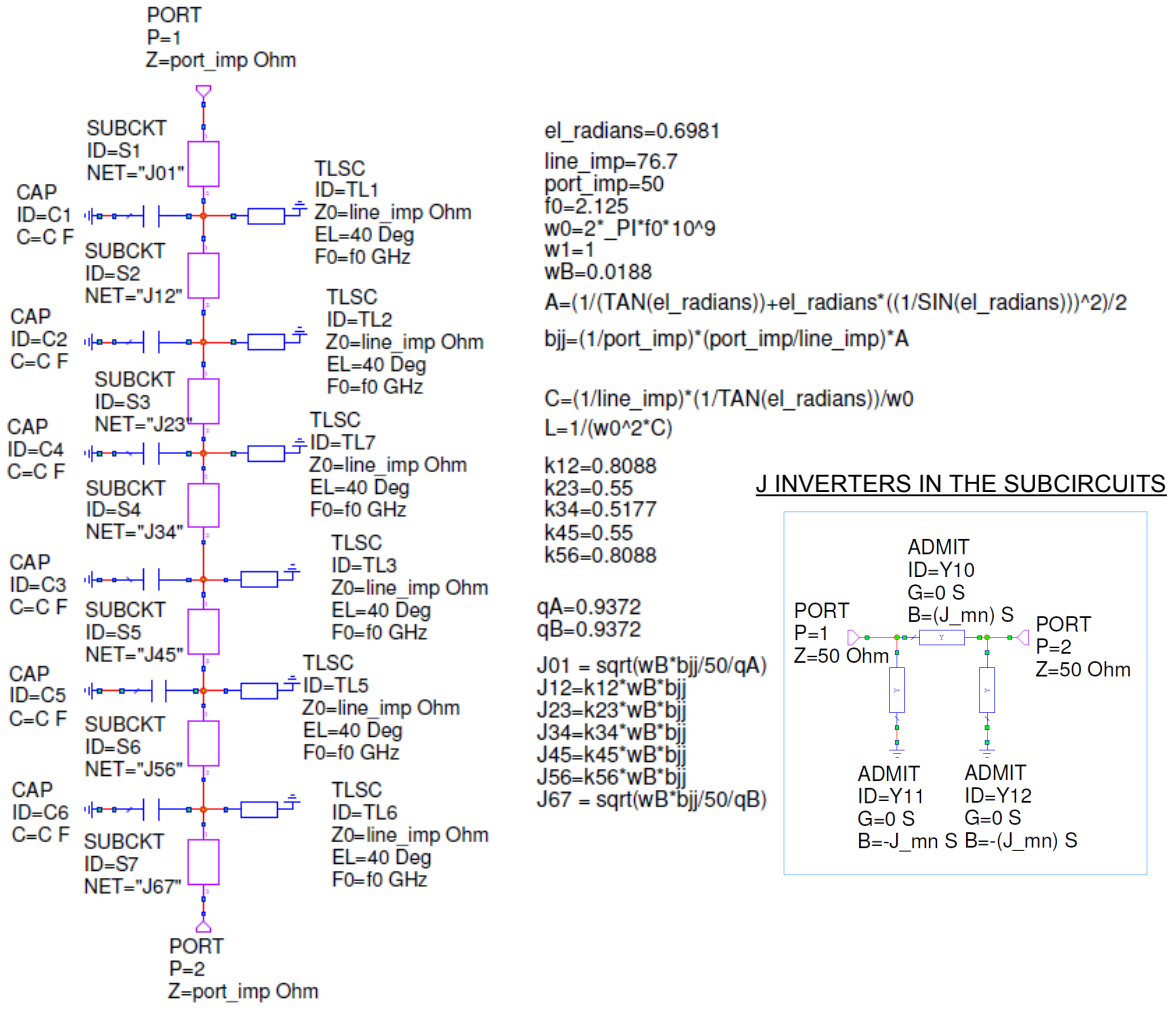

Figure 6.22: 6th Order Chebyshev Combline Filter

The S-Parameters of the filter are shown in figure 6.23 below.

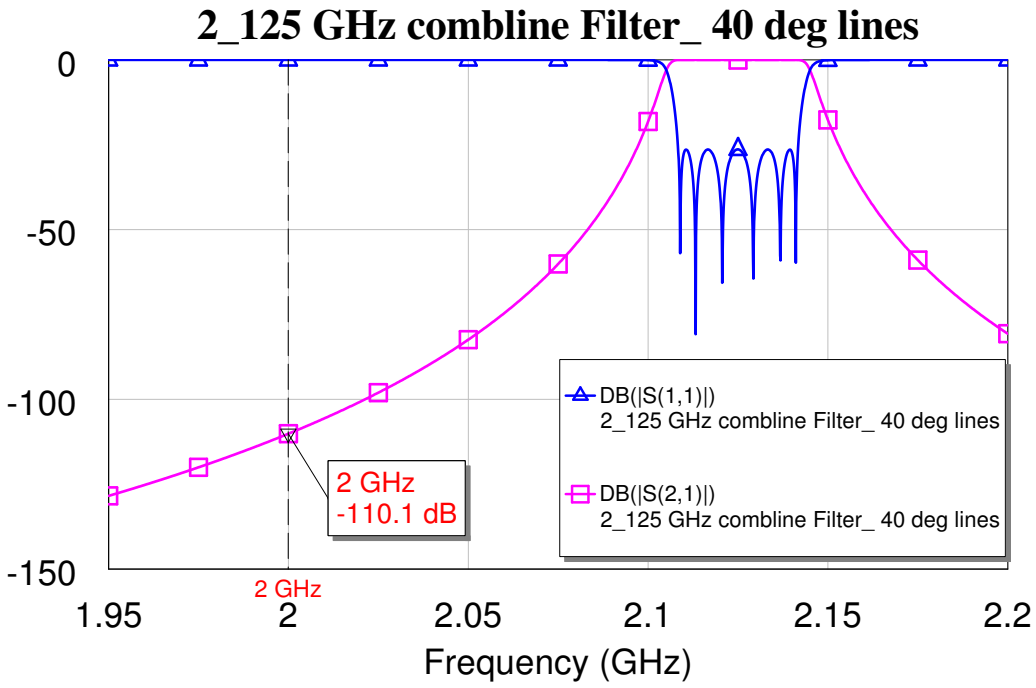

(a) Passband at 2.125GHz

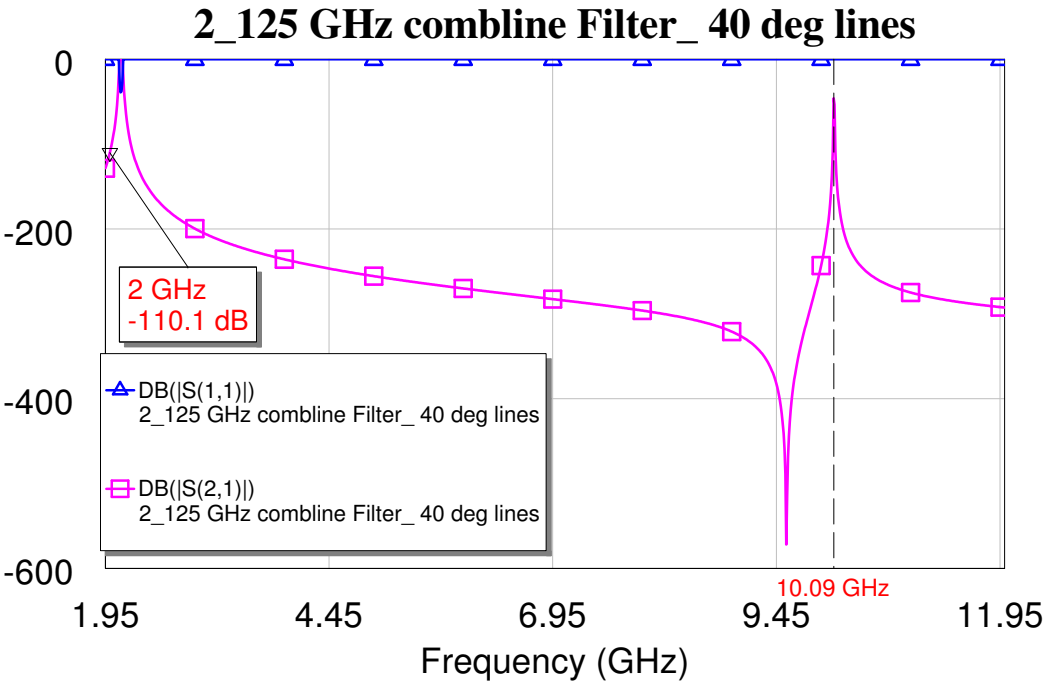

(b) Second Passband at 9.119GHz

Figure 6.23: S-Parameters of 6th Order Chebyshev Combline Filter

The chosen parameters satisfy the specifications with an insertion loss of -110dB at 2GHz and no passbands occuring within the frequency range of 6.375GHz and 9.375GHz. The next section focuses on the realisation of the 3D model of this filter in CST.

6.3.2 CST 3D Model of the 2.125GHz Filter

The resonators of this filter are designed to have a groundplane spacing of $\frac{\lambda}{12}$. The lines are 40^0 long, so a simple resonator structure with just a post enclosed in a rectangular cavity would not suffice if enough capacitance is to be obtained in order to get the resonator to resonate at the required centre frequency of 2.125GHz. For this reason, the structure is modified, as was done for the 1.3GHz filter in the preceding section, with the provisions for the extra capacitance (labelled 'side cap' in figure 6.24) extending to the end walls as shown in figure 6.24. The width of the side cap is the same as that of the resonator post. The through groove used for the 1.3GHz filter, also shown in figure 6.24 (a) proved insufficient, and the side caps would have to extend further downwards to add extra capacitance by increasing the area of overlap with the side of the post. However, the side caps should also not extend too far down because of the possibility of interfering with the magnetic coupling. A Round hole, shown in figure 6.24 (b) was found to be more effective, generally giving an larger increase in capacitance than the through groove.

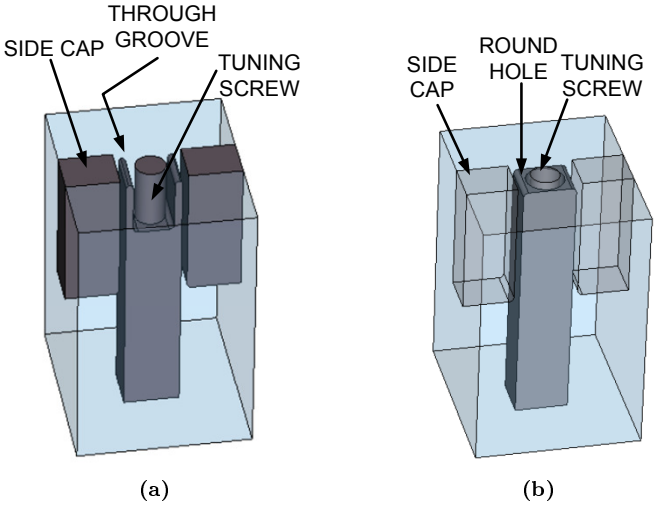

Figure 6.24: Single Resonator of 2125MHz Combline Filter

The tuning screw and the round hole form a coaxial arrangement that acts as a cylindrical capacitor, shown in figure 6.25, with charge residing on the outer surface of the inner conductor (tuning screw) and on the inner surface of the outer conductor (rectangular resonator post with circular hole in this case).

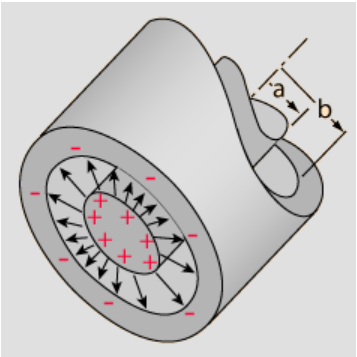

Figure 6.25: Cylindrical Capacitor [63]

The first design for the 6th order filter is shown below in figure 6.26.

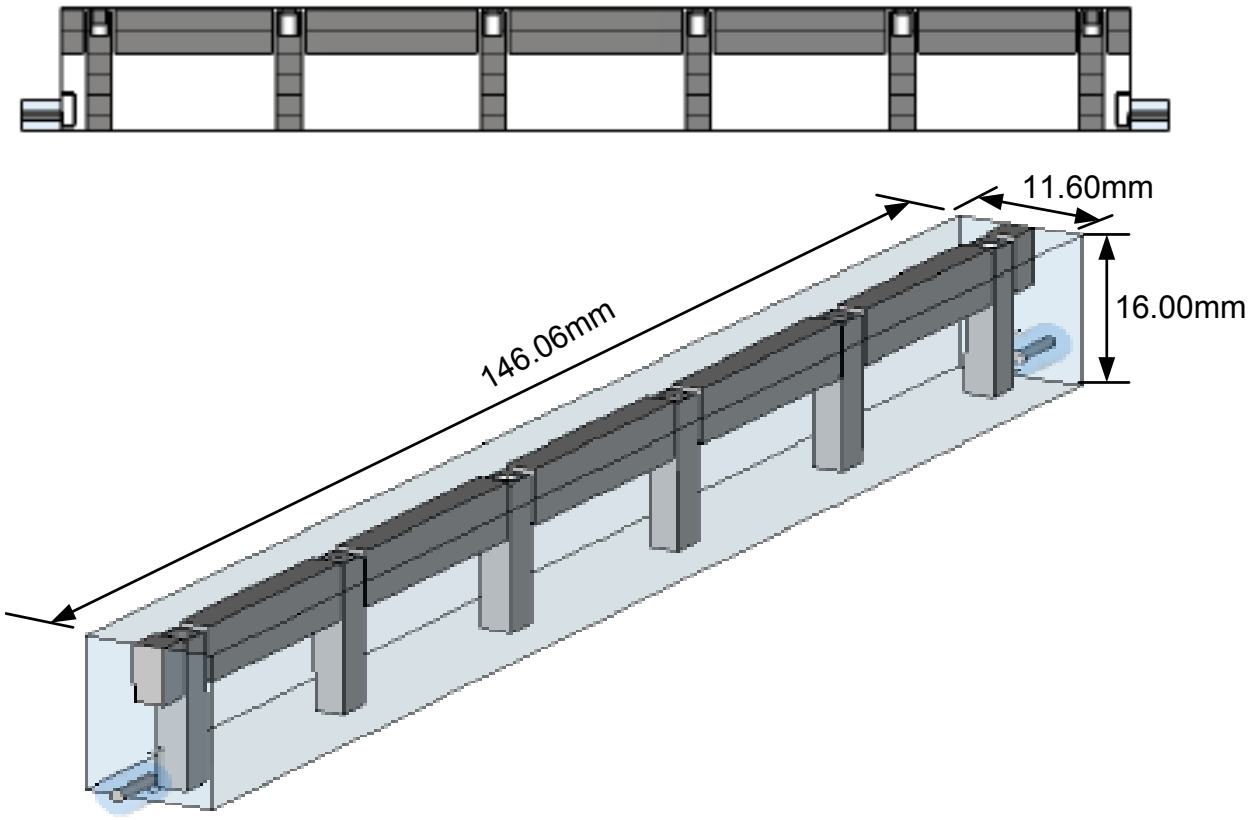

Figure 6.26: First Design of 6th Order Combline Filter]

Two problems were identified for this filter; the first was the length of the filter - a smaller filter of shorter length, possibly close to half the length of this filter, would be more desirable. The second problem was the occurence of a resonance at a frequency between 8.5GHz and 9.0GHz as can be seen in figure 6.27; the specifications called for a design that would have no passbands between the range of 6.375GHz and 9.375GHz.

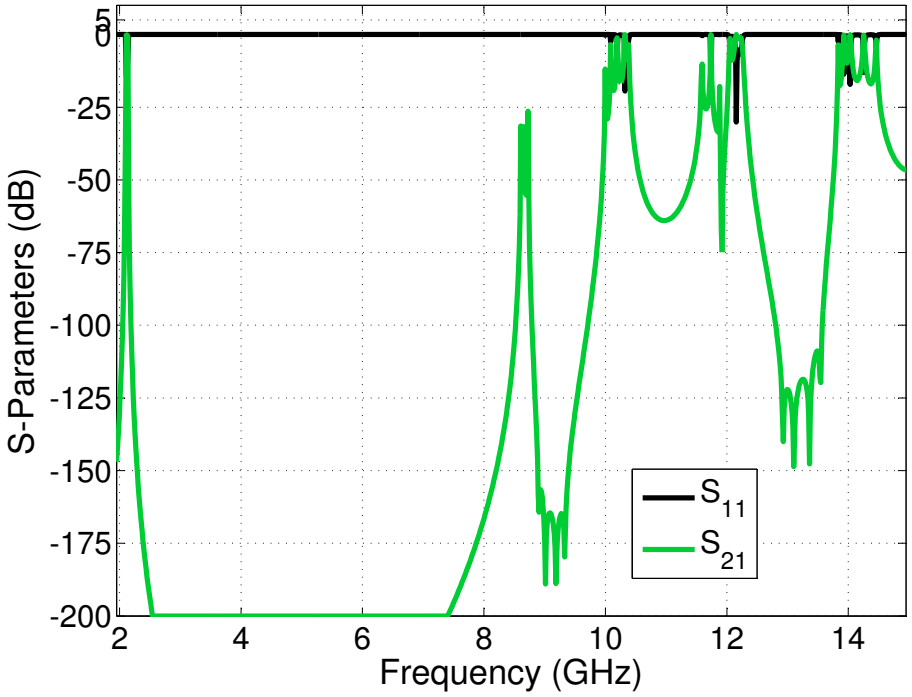

Figure 6.27: S-Parameters of the filter in figure 6.26

The problem of the length reduction can be solved by introducing irises between the resonator posts so that the overall length of the filter is reduced while still obtaining the right amount of coupling. The presence of the passband within the 6.375GHz and 9.375GHz, however, was unexpected, seeing as the resonator lines were 40^0 long. The filter was therefore expected the have its second resonance at a frequency further than 9.556GHz. The third resonance in figure 6.27 occurs at a frequency of just over 10GHz and is assumed to be the second resonance of the coaxial line filter due to its periodicity. A possible reason for the occurrence of the resonance between 8.5GHz and 9.0 GHz could be that the filter rather behaves like a different structure, possibly as a ridge waveguide, because of the modifications to the normally simpler structure with only axially placed posts, to include the 'side caps' for extra capacitance.

The approach taken to find a possible solution was to extend the 'side caps' across from groundplane to groundplane as shown in figure 6.31 (a). The next subsection investigates the effects of such a change on the position of the second resonance in the frequency spectrum, using a single resonator.

Effect of the extension of the extra capacitance for the rectangular coaxial lines

The resonator shown below is expected to resonate at a frequency of 2.125GHz and uses 40^0lines. For a typical combline resonator, the second resonance should occur at a frequency of about 9.556GHz.

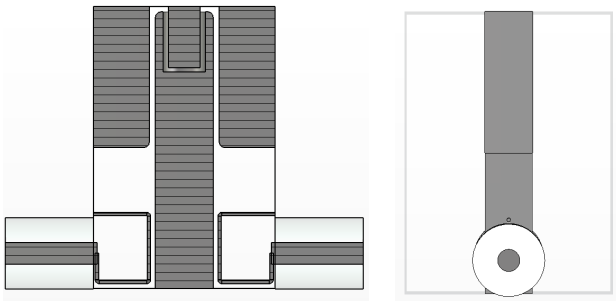

(a) Front View (b) Side View

Port: 1

Port	Mode	Type	Z-Wave	Z-Wave-Sigma	Z-Line	F-Cutoff
1	1	TEM	377	1.96e-005	71.9	0.0
1	2	TE	550	2.33e-005	---	10.8
1	3	TE	364	2.16e-005	---	12.9
1	4	TE	200	1.05e-005	---	19.1
1	5	TE	142	7.12e-006	---	25.4

(c) Cutoff frequencies of waveguide modes

Figure 6.28: First order filter using rectangular coaxial lines and expected cut-off frequencies of propagated modes

The cut-off frequency of the first TE mode is 10.8GHz. The computed S-parameter response over a broad range of frequencies is shown below

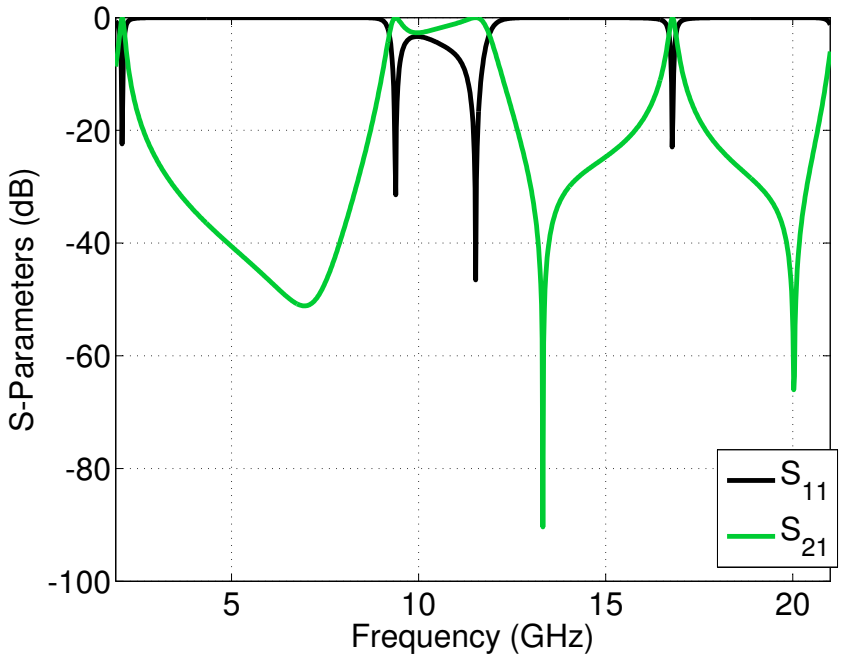

Figure 6.29: The S-parameter response of the filter in figure 6.28.

The first secondary passband starts at a frequency of about 9.519GHz and has a relatively wider passband. The third pasband is centred at about 16.771GHz. From the table shown in figure 6.28, it can be seen that for the coaxial line, the first waveguide mode has a cutoff frequency of 10.8GHz and is therefore only expected to

propagate at a frequency higher than that. In such a case, if the resonator behaves like a pure TEM resonator, then the only resonance occuring below 10.8GHz should be due to the periodic behaviour of the line. However, an eigenmode analysis of the resonator, the results of which are given in figure 6.30 below, shows that there are two resonant modes at frequencies below the expected centre frequency of the second passband for 40^0 line and two modes also occuring above the cutoff frequency of the first waveguide mode and below the cutoff of the second waveguide mode.

```
------------------------------------------------------------------------------
Solver Results:

------------------------------------------------------------------------------
Mode    Frequency             |                    Accuracy
                              |     |(Ax-x)/x|       max(e)         div(e)
------------------------------------------------------------------------------
  1     2.13348072047         |       5.12e-010      6.45e-010      2.85e-016
  2     8.40394641987         |       3.64e-009      1.55e-008      3.67e-016
  3     8.57289234337         |       9.46e-008      3.14e-007      6.34e-016
  4     11.5256866094         |       2.94e-007      9.93e-007      2.63e-016
  5     11.7133427451         |       3.47e-007      1.44e-006      4.38e-016
  6     13.9229210328         |       6.51e-007      3.13e-006      1.89e-016
  7     14.1583537128         |       6.04e-007      2.20e-006      3.83e-016
  8     16.3758788175         |       1.05e-007      3.97e-007      3.32e-016
------------------------------------------------------------------------------
```

Figure 6.30: Resonant frequencies of the modes propagated in the cavity filter in figure 6.28

The second passband therefore is a result of the superposition of several modes.

When the extra capacitance sections are extended across from ground plane to ground plane, the second passband is pushed further to a centre frequency of approximately 11.334GHz and the third to about 19.753GHz. These are shown below

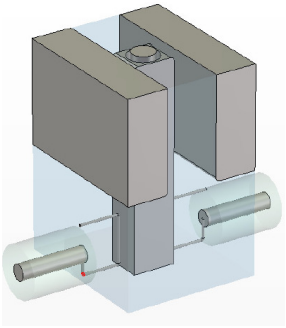

(a)

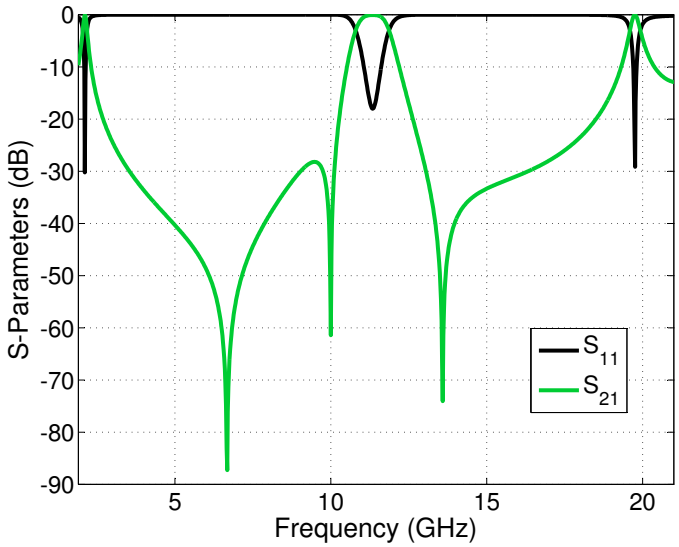

(b)

Figure 6.31: Filter with extra capacitance sections extended from ground plane to ground plane and the s-parameter response

The filter structure was therefore modified to have the 'side caps' extending across the width of the filter between the ground planes. The new design is discussed in the following subsection.

Modifications in the Design of the 6th Order Combline Filter

Figure 6.32 shows the final structure of the filter. The following modifications have also been made to the design:

1. Irises have been included in between adjacent resonator posts. The irises have different heights. [Dimesions of the filter are in Appendix A]
2. The 'side caps' have been extended across the width of the filter.
3. And for ease of fabrication and electro-plating,

- Sharp corners have been rounded and
- A tapped input has been used rather than the more complicated loop used in the first filter (see figure 6.26).

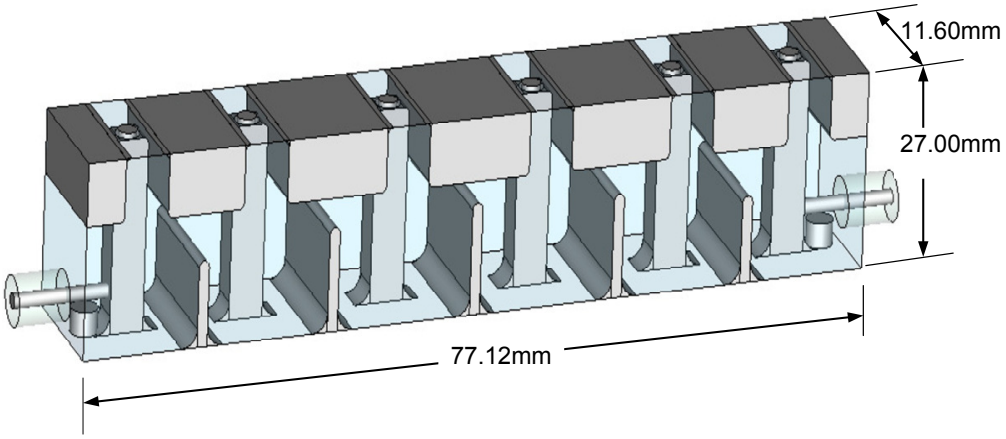

Figure 6.32: 6th Order Combline Filter with Irises

Tuning screws are also included in the structure for the tuning of the input coupling. The length of the filter has been reduced to almost half that of the filter in figure 6.26, so the filter is relatively small sized. The S-Parameters of the filter are shown below in figure 6.33.

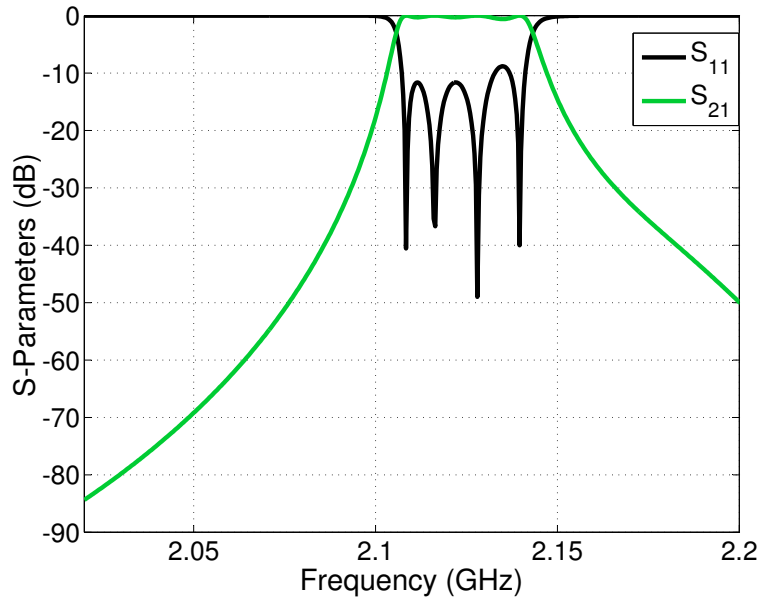

(a)

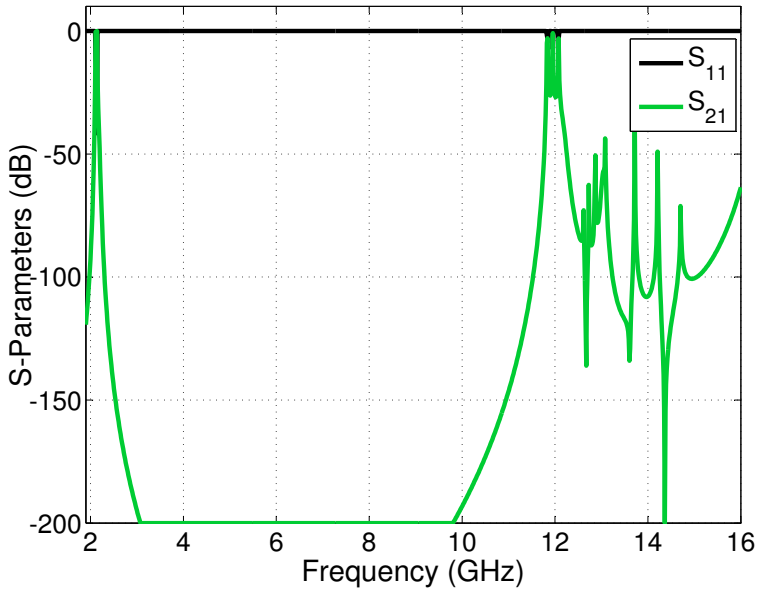

(b)

Figure 6.33: S-parameters of the Filter in Figure 6.32

Figure 6.33 (b) shows that as are a result of the extenstion of the 'side caps' across the width of the filter, the second passband now occurs at a frequency of about 12GHz with a good attentuation in the stopband between the first and second resonances. The next section discusses the manufacturing of the filter.

6.3.3 Manufacturing of the 2.125GHz Filter

For this filter, owing to the complexity of its structure a process combining both milling and wirecutting processes seemed to be the simplest option. The main filter body is to have only three parts, the central body and two side covers. The central body is initially milled out, from either side, leaving a middle piece with the width of the resonator posts, then for the remainder of the structure, wirecutting EDM is used. The two steps are outlined in figure 6.34 below, with the sideviews outlining the cutting paths.

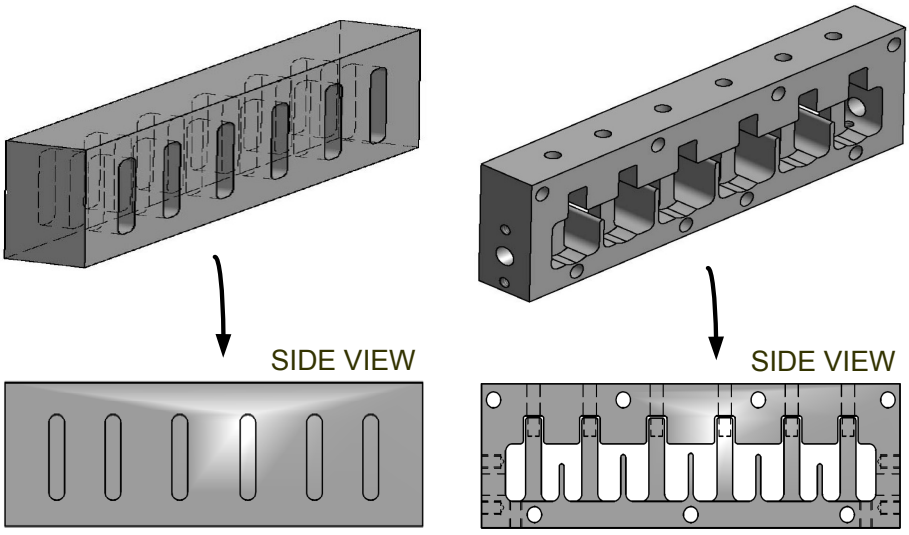

(a) Milling **(b)** Wirecutting EDM

Figure 6.34: Manufacturing Steps for 2.125MHz filter

All the components used to assemble the filter can be seen in an exploded view of the filter shown in figure 6.35 below.

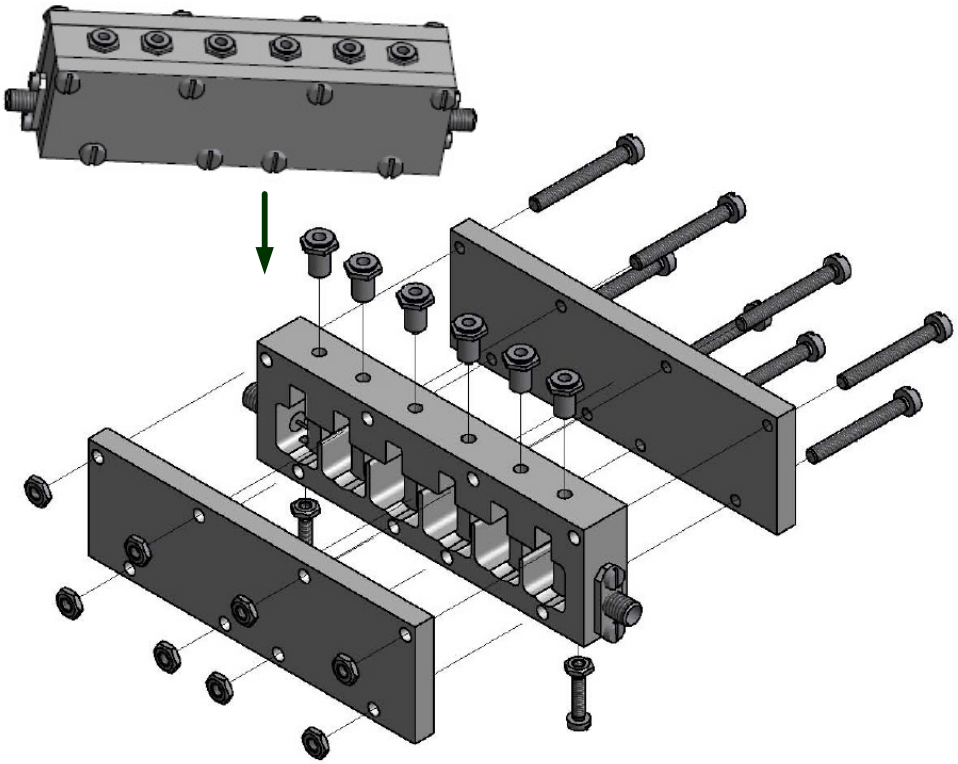

Figure 6.35: Exploded view of the Filter components [Dimensions of the Filter are given in Appendix A]

The two tuning screws used to tune the tapped input coupling are assembled from the bottom. Eight fastening screws are used, extending through the from the end of one side lid to the other end. Six Temex tuning elements are used for the tuning of the resonant frequency, one for each of the six resonators. SMA connnectors are used at the input and output. More detailed dimensioned drawings showing the tolerances can be found in Appendix A.

6.4 Measurement Results

The S-parameter measurements for the manufactured filters were done using the Rohde and Schwarz 4 Port ZVB Vector Network Analyser with a frequency range of 300 KHz to 8GHz and the Agilent HP8510 Microwave VNA which can measure up to 40GHz. The measurement set-up is shown below in figure 6.36. The process involve the tuning of the resonators of the filters until satisfactory results were obtained.

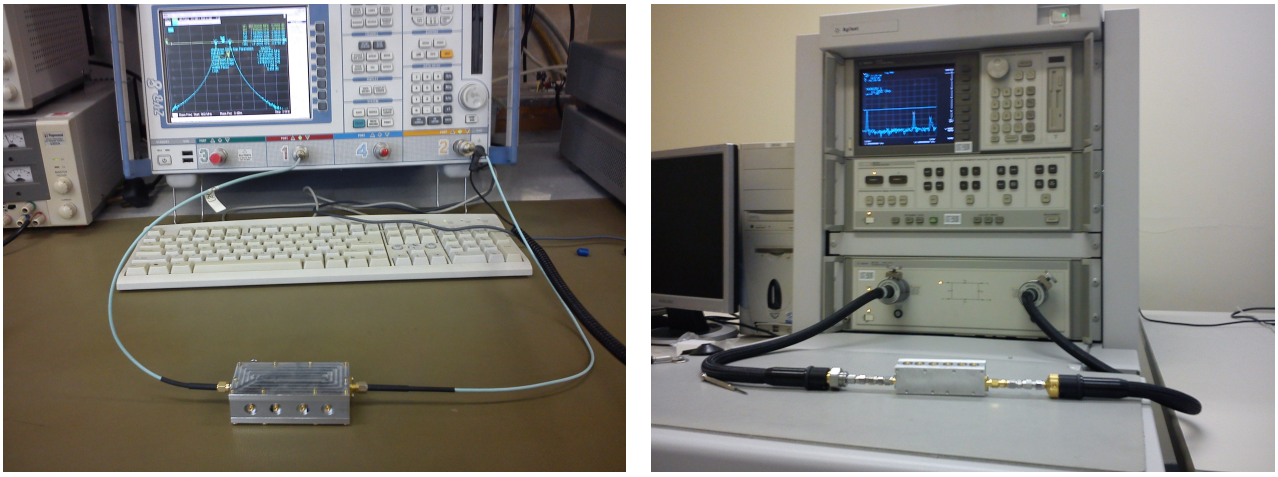

(a) Rohde & Schwarz RF VNA, 4-port **(b)** Agilent HP8510 Microwave VNA

Figure 6.36: Filter Measurements Set-up

Three filters were measured:

Filter I: This was the filter designed for the milling process and the topology is shown in figure 6.20.

Filter II: The topology for the second filter was designed for the wirecutting process, see figure 6.18, which is supposed to have a high accuracy of 0.0001" (0.0025mm) [46]. However, manufacturing of products is always prone to possible difficulties during the process and in this instance, the major problem encountered was that the grade of aluminium used was found not to have uniform conductivity so that the wirecutting process could not be used; marine grade aluminium was used. Marine grade is soft and can cause the clogging of a machine. The other possible reason, therefore, for why EDM could not be used would be a loss of *flushing*. Flushing refers to the removal of the metal particles (chips) from the working gap i.e. the gap between the workpiece, to prevent them from forming bridges that cause short circuits. The better choice would be to use Aluminium 6082 grade which has a higher strength and is a better grade for machining applications.

An alternative process, using ***a waterjet cutter***, was chosen for the manufacturing of the filters. Waterjet cutting is a process that utilises a thin thread of water under high speed and pressure, at times including an abrasive to cut into metal parts with different levels of accuracy depending on the the cutting speed used. Waterjet cutting machines are usually available in most wirecutting machine shops to cut into metals that are non-conductive, but they also cuts conductive metals, with a comparatively lower accuracy that wirecutting EDM. A more detailed description of the process is included in Appendix B.

Filter III: This filter was designed to incorporate both the milling process and the wirecutting EDM process at different stages of manufacturing, see figure 6.34. Due to the similar difficulties incurred for Filter II above with the wirecutting EDM process, the stages involving wirecutting EDM were replaced by waterjet cutting. The physical structure of the filter is illustrated in figure 6.35.

6.4.1 Filter 1: Milled 1.3GHz 4th Order Combline Filter

Figure 6.37 shows the manufactured 1.3GHz 4th order combline filter, fabricated using the milling process.

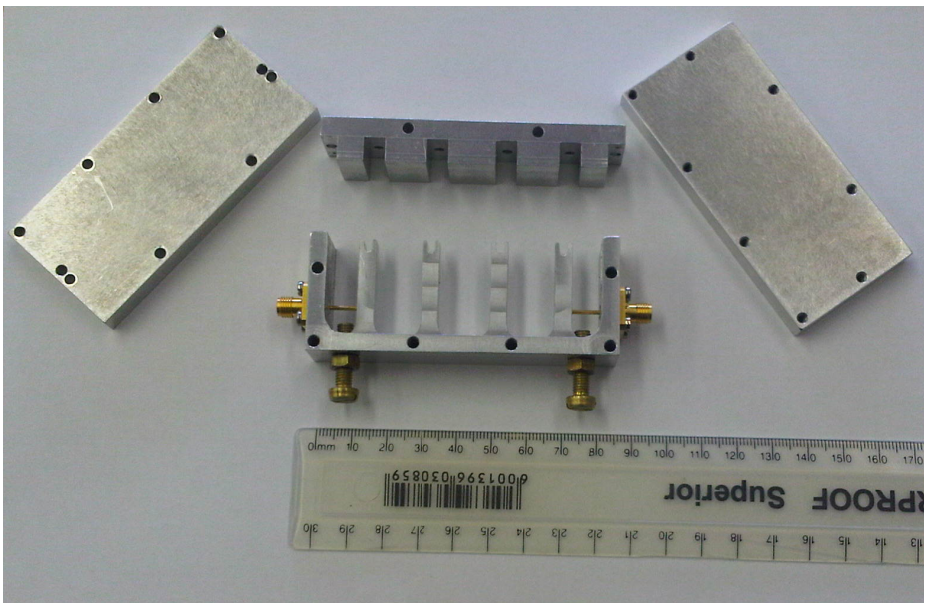

Figure 6.37: Milled 1.3GHz 4th Order Filter

In figure 6.38 and 6.39 below, the measured S-Parameters for the milled filter are compared to those of the CST simulation and the MWO circuit simulation modelled to reflect losses (circuit included in Appendix C). The measured response has an insertion loss of -0.5702dB at midband and a -10dB bandwidth of 3MHz (2.5%) less than the -10dB bandwidth of the CST simulated response. Both the CST and measured results have a relatively lower bandwidth than the MWO circuit model. The reason for this is the adjustment in filter structure to ease the milling process as was explained in section 6.2.8, so that the volume of the cavity is reduced and readjustment of the bandwidth back to the desired bandwidth becomes difficult due to the dependent relationship that different parameters affecting the filter response have. The overall return loss across the passband is less that -14.5dB.

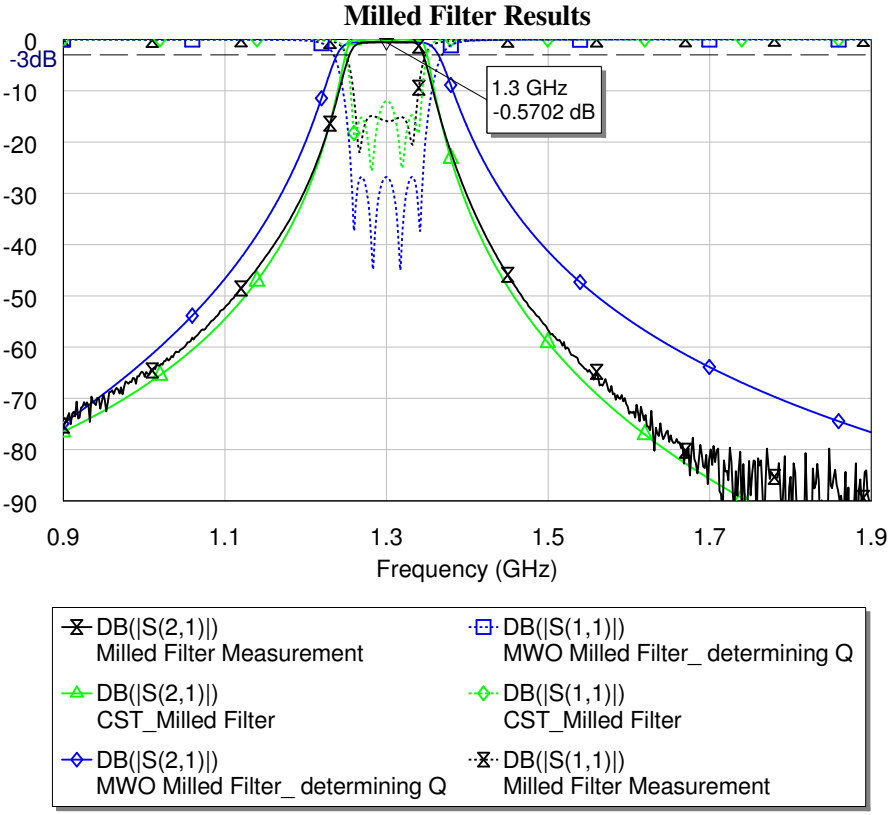

Figure 6.38: CST Results Vs. Measured Results for Filter I; Frequency Range = 0.9GHz to 1.9GHz

The closely comparing CST simulation and measured results show thats the milling process is quite accurate. A considerably low unloaded Q of 510 is obtained for the resonators of this filter. The possible reasons for this are the surface finish which could be smoother and the conductivity of the metal used; aluminium was used and the grade used might have had high resistivity and therefore low conductivity. Different grades of aluminium vary in their levels of resistivity. For a better unloaded Q, the filter can be plated in a metal of a higher conductivity.

When examined over a broader range of frequencies, from 0 to 8GHz, the measured and simulated responses are also seen to compare relatively well, once again showing the accuracy of the milling process. There is a good stopband rejection of less than -80dB across the whole stopband, before the second resonance, which occurs at around 7GHz.

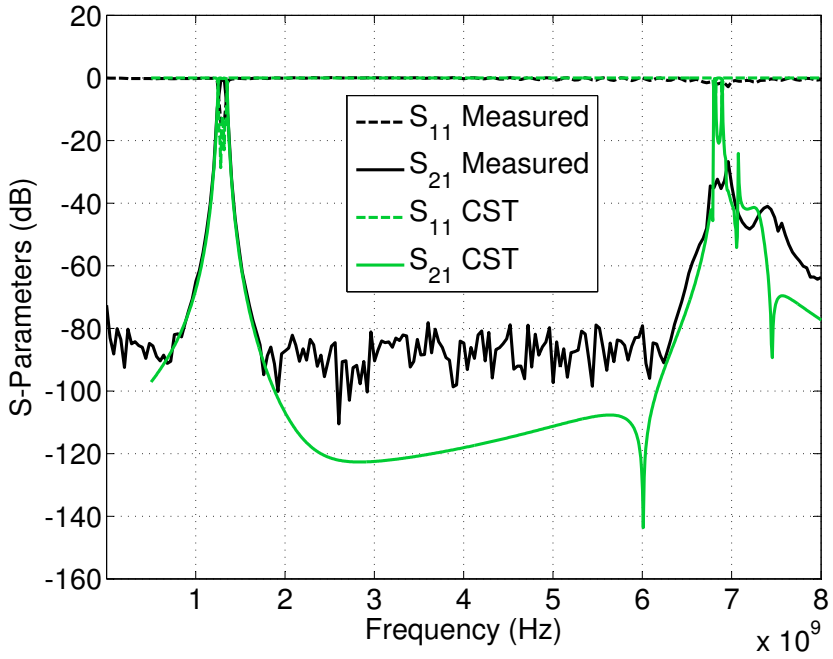

Figure 6.39: CST Results Vs. Measured Results for Filter I; Frequency Range = 0 to 8GHz

6.4.2 Filter II: Waterjet Cut 1.3GHz 4th Order Combline Filter

The filters manufactured using waterjet cutting clearly indicate a relatively low manufacturing accuracy with specific reference to the manufacturing of sensitive microwave components in which slight changes in dimensions can have considerably large changes in performance. Figure 6.40 below shows the deformations in the structure of the filter due to the poor accuracy of the waterjet cutting process. The process also leaves a fairly rough surface finish also shown in figure 6.40 in the boxes labelled '2' .

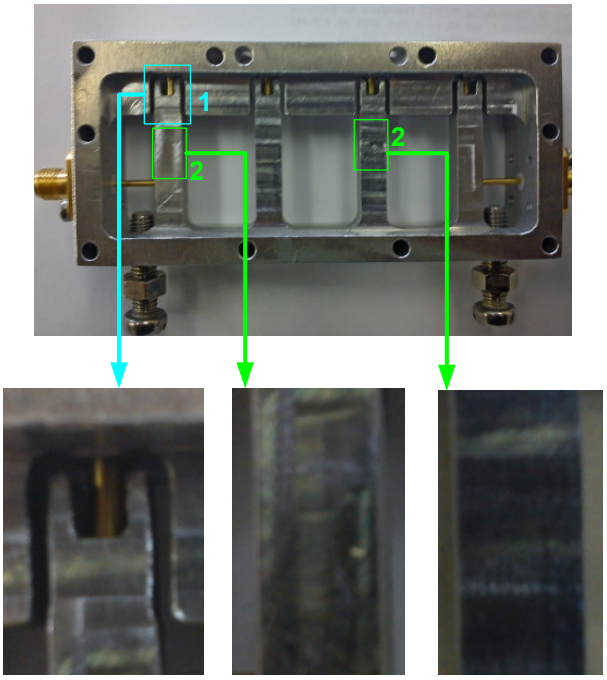

Figure 6.40: Deformations in filter structure due to a lack of accuracy in the waterjet cutting process - Filter II

The measured results obtained for this filter are compared to the MWO circuit simulation and CST simulation S-parameters in figure 6.41 below.

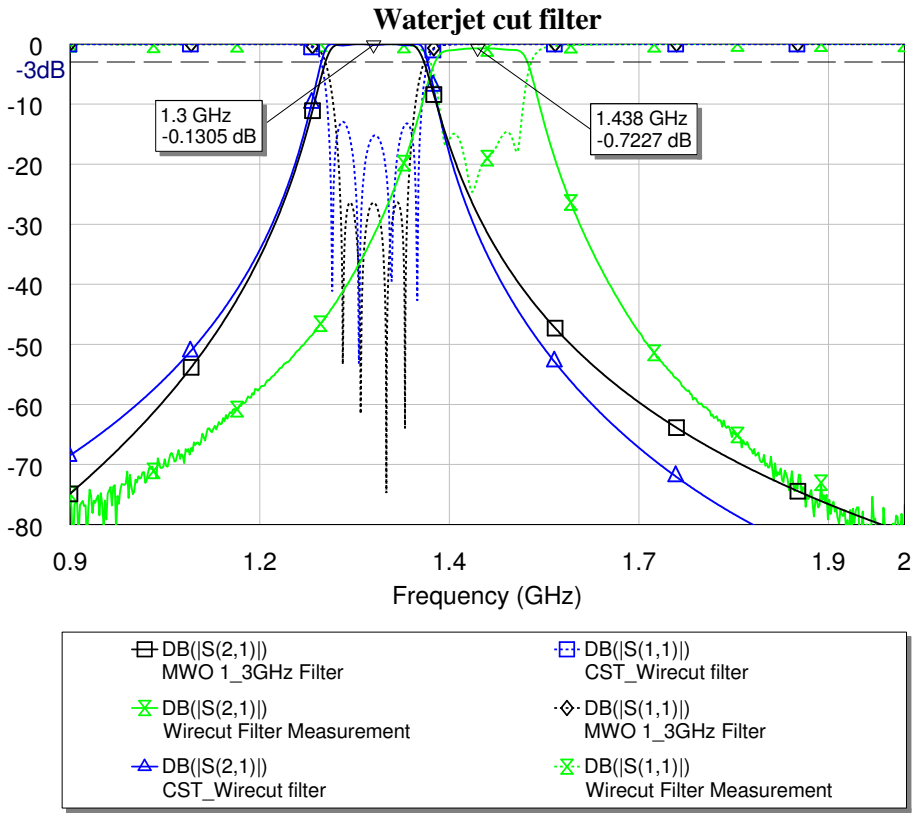

Figure 6.41: MWO Vs. CST Vs. Measured Results for Filter II; Frequency Range 0.9 GHz to 2 GHz

The measured results show that the lowest resonant frequency that could be obtained is approximately 1.438 GHz. The filter was designed to have a centre frequency of 1.3 GHz with a flexible tuning range when using the

tuning screws. However, due to the alterations in the structure shown in figure 6.40 due to the poor accuracy of the manufacturing technique, the overall capacitance was decreased, resulting in the higher resonant frequency. A plot that shows the measured results shifted in frequency down to 1.3GHz for a better comparison of the bandwidth and insertion loss is shown in figure below.

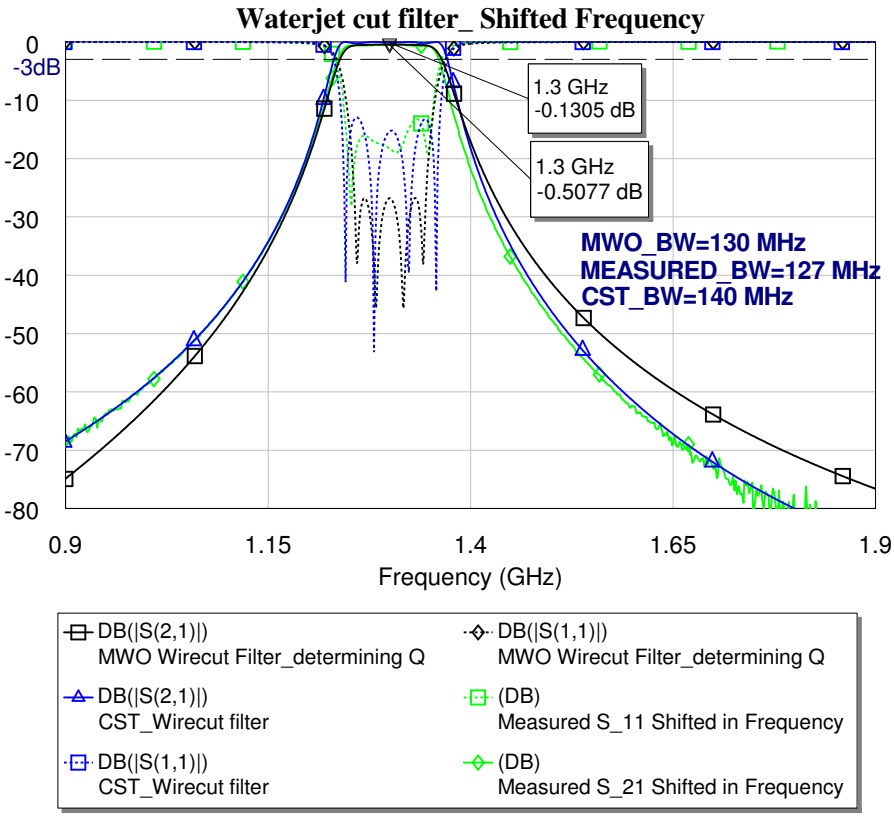

Figure 6.42: MWO Vs. CST Vs. Measured Results for Filter II with Measured Results Shifted in Frequency to 1.3GHz

The insertion loss of the measured filter at midband is -0.5077 dB and the filter resonators have a considerably low unloaded Q of 556. This possible reason for the low unloaded Q obtained is the surface roughness of the filter. A better resonator Q can be obtained for smoother surface finishes and by plating the metal in a metal with a high conductivity e.g. silver plating. The MWO circuit model that accounts for losses in the filter is included in Appendix C.

The measured results show that the manufactured filter has a -3dB bandwidth of 127 MHz which is only 3 MHz less than the desired bandwidth of 130MHz. The stopband response is compared to that of the CST simulation in figure 6.43.

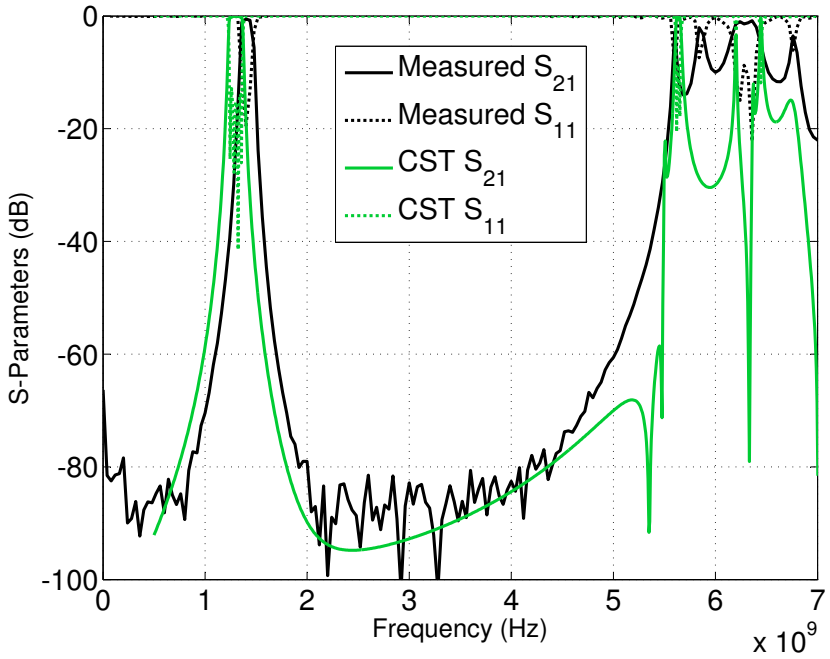

Figure 6.43: CST Vs. Measured Results for Filter II over a Broad Frequency Range

The results show how the measured response compares closely to the CST simulated response. The stopband is shorter than the one obtained for the milled filter by slightly over 1 GHz, due to the difference in structure; the 'sidecaps' of the milled filter extend across the ground plane spacing while those of the waterjet cut filter have a width equal to the width of the posts. The effects of such a change were discussed in section 6.3.1.

6.4.3 Filter III: Milled and Waterjet Cut 2.125GHz 6th Order Combline Filter

Very similar problems in manufacturing seen in Filter II above were incurred for this filter; wider gaps between the resonator posts and the 'sidecaps' were obtained, one of the resonator had a broken section about its open-circuited end and the surface finish was considerably rough. The alterations in design and deformations in structure that resulted from the process are shown in figure 6.44.

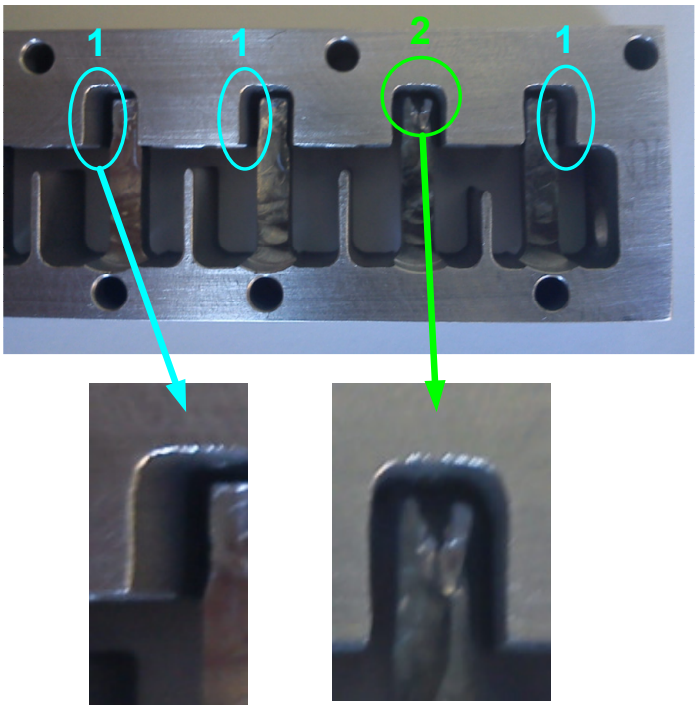

Figure 6.44: Deformations in filter structure due to a lack of accuracy in the waterjet cutting process - Filter III

The ovals labelled '1' indicate the added gap sizes for the capacitances on either side of the resonator posts. This was the case for each of the six resonators. The capacitance was therefore decreased due to that alteration in design resulting in a higher resonant frequency that the one designed for. Figure 6.45 below shows the measured response having a centre frequency of approximately 2.556GHz and the CST simulated response placed over the MWO circuit simulation results having a centre frequency of 2.125GHz which was the desired resonant frequency.

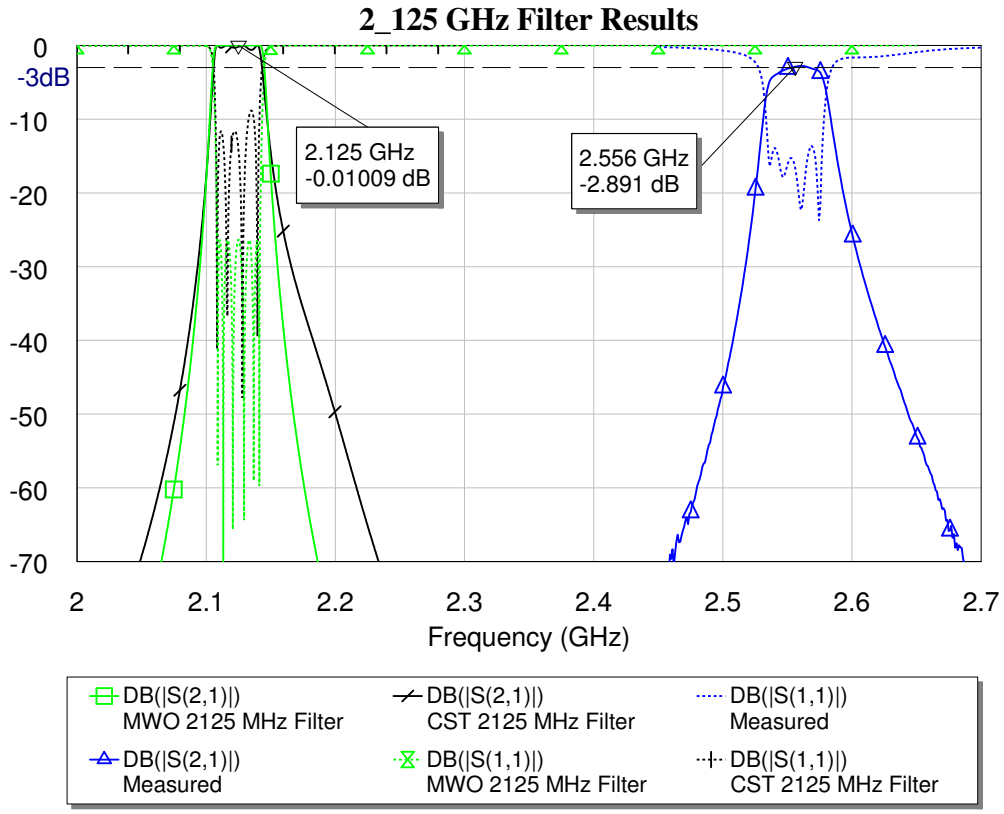

Figure 6.45: MWO Vs. CST Vs. Measured Results for Filter III

For a better comparison of the bandwidth and insertion loss of the responses, the measured response is shifted to the required centre frequency of 2.125GHz and the compared results can be seen in figure 6.46 below.

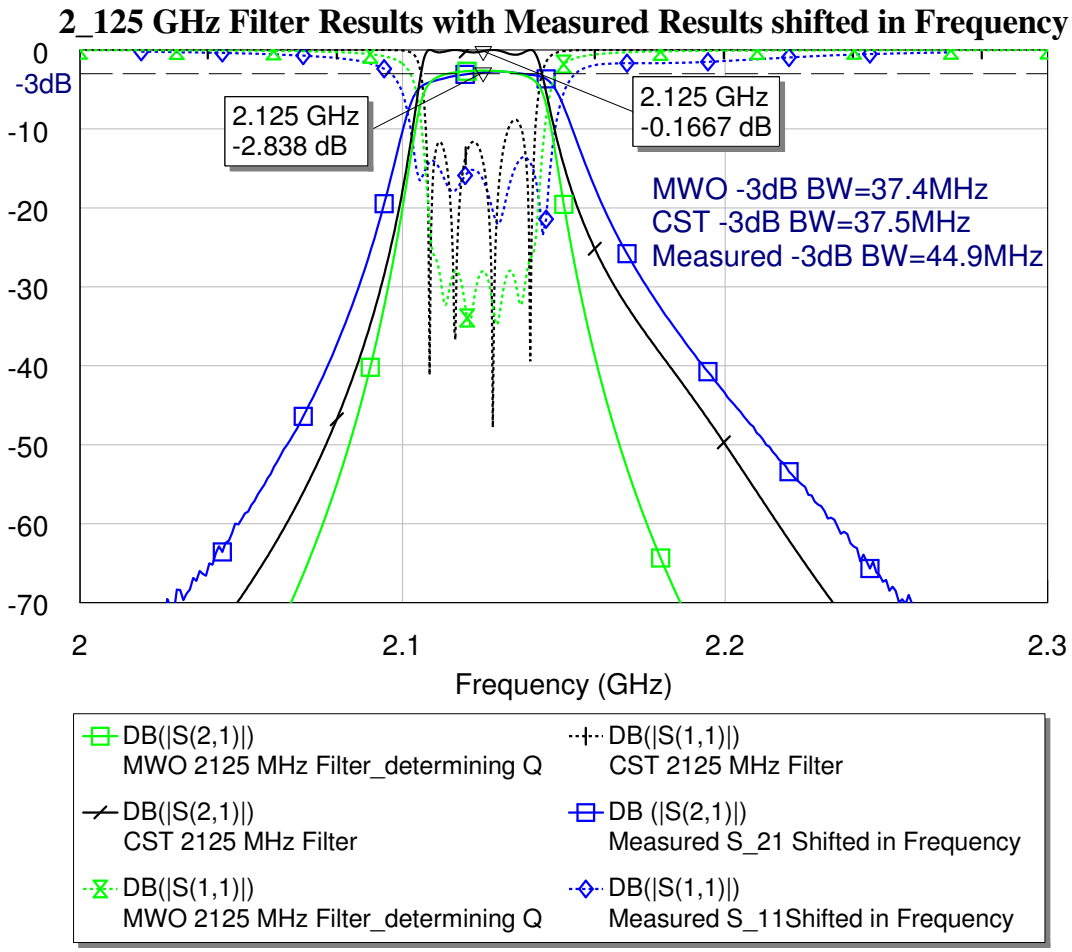

Figure 6.46: MWO Vs. CST Vs. Measured Results for Filter III with Measured Result Shifted in Frequency to 2.125GHz

The MWO office model, given in Appendix C, is modelled to include the effects of losses. An insertion loss of approximately -2.838 dB is obtained for the manufactured filter and the resonator unloaded Q of the filter is found to be approximately 800, which is considerably low, a possible effect of the rough surface finish. A smoother finish and a plating with a metal of a higher conductivity would result in a higher unloaded Q (the filter was manufactured in Aluminium).

A -3dB bandwidth of 44.9 MHz is obtained for the manufactured filter which is higher than the design bandwidth of 37.4 MHz. In figure 6.47 below, the S-Parameters of the manufactured filter are compared to those of the CST simulation over a frequency range of 2 GHz to 13 GHz to observe the stopband response; The specifications called for a response with no passband between the frequencies of 6.375 GHz and 9.375 GHz. In figure 6.47, the dotted black curve shows the original measured response of the filter shifted back in frequency so that the primary passband is centred at 2.125 GHz. From this curve it can be seen that the filter could be tuned down to have the primary resonance centred at 2.125 GHz, the second passband would occur at a frequency of 10.609GHz, therefore having no passbands between 6.375 GHz and 9.375 GHz.

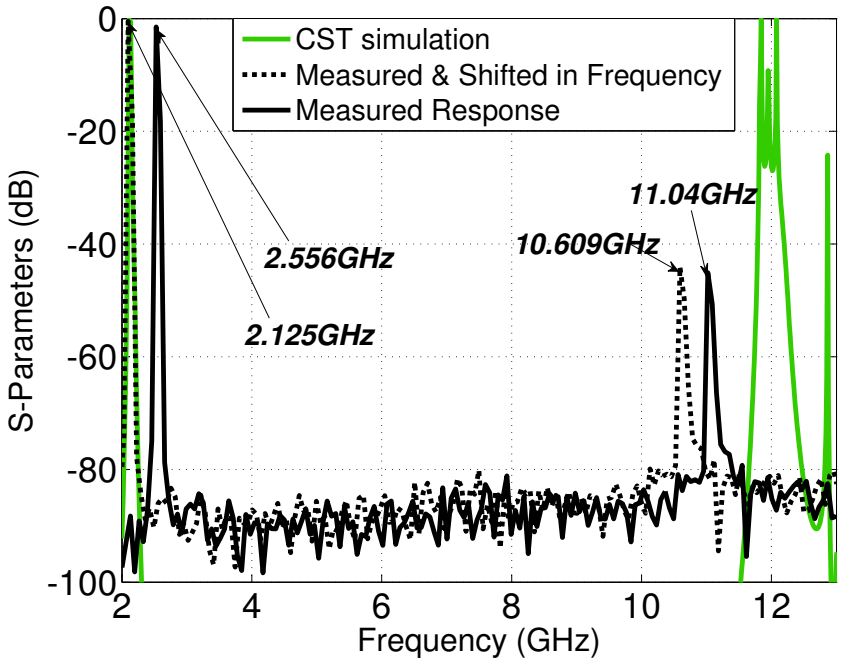

Figure 6.47: Comparison of the CST Simulation and the Measured S_{21} of the Manufactured 2.125 GHz Filter over a Broad Range of Frequencies (2 GHz to 13 GHz).

6.5 Conclusion

This chapter has covered the design of combline filters for ease of manufacture and for reduced manufacturing costs. The filters were designed for two different sets of specifications: The first filter was a fourth order Chebyshev combline filter operating in the L-Band with a passband between 1235MHz - 1365MHz, with a return loss of less than 20dB in the passband. This filter was designed for manufacturing using two different manufacturing methods: CNC Milling and CNC Wirecutting EDM. The main aim of using the two different methods was to establish, through a comparison of the two, which method was costlier, and which method would give a better surface finish for a better performance of the filter. The second set of specifications called for the design of an S-Band combline filter with a 40MHz bandwidth centered at 2125MHz and having an insertion loss of more than 80dB at 2GHz. The filter was also required to have no passbands between 6.375GHz and 9.375GHz. The different changes made to the structures in order to facilitate easier manufacturing and to lower the costs of manufacturing have been clearly indicated, also clearly outlining the problems experienced during manufacturing. A change from manufacturing using wirecutting EDM to the using a waterjet cutter has been explained citing the reasons for this change. The filters resulting from the use of waterjet cutting have been seen to have a very rough surface finish, low dimensional accuracy and a few deformations which have been depicted in the measurements section of the chapter. The results obtained were considerably good despite the manufacturing problems. The milled filter designed to operate at a centre frequency of 1.3 GHz had an insertion loss of -0.5702 dB with a relatively low resonator unloaded Q of 510. The 1.3 GHz waterjet cut filter with a structure similar to that of the milled filter with slight variations in the physical structure had a slightly higher Q of 556 in comparison with the milled filter and an insertion loss of -0.5077 dB. Both of these filters had a measured bandwidth of only 3 MHz less than the bandwidth for their respective CST simulated filters. The final filter, centred at 2.125 GHz was manufactured by a combination of the milling and waterjet cutting processes. The manufacturing also resulted in a number of deformations that were clearly depicted in the chapter. A wider bandwidth of 44.9 MHz, 7.5 MHz higher than the design bandwidth was obtained with the filter having a low resonator Q of 800 and an insertion loss of -2.838 dB.

The cost of milling was found to be cheaper than the cost of wirecutting as per quotes obtained from the

manufacturer. Waterjet cutting was also less costlier than wirecutting. Based on the results in the chapter, recommendations that can become handy to a designer are: to consult with a manufacturer is always be best at the beginning stages of a design process so as to look into the different options available, and to obtain suggestions for possible structural adjustments to make each process easier and possibly to obtain quotes for the costs associated with each. It is also a good idea to specify a grade of metal for a specific use so that the manufacturer does not end up using a lower grade that may not be the best for a specific application. While addressing the issue of cost, performance should not be neglected because if a process results in a filter with poor performance then there might be a need for redesign or for further work which might still add onto the overall costs.

Chapter 7

Conclusion

This thesis has addressed two main research topics: The first topic addressed the equivalence between combline and evanescent-mode waveguide filters, and the second addressed the issue of cost reduction in the manufacturing of combline filters.

Chapter two discussed different characteristics of combline filters and a fourth order filter operating at 2GHz was designed. The design process was outlined, both for the circuit model in MWO and for the 3D implementation of the physical structure in CST, acting as a basis for the designs that were to be covered in subsequent chapters.

Chapter 3 has covered the design process of an evanescent-mode filter as a preparation for discussions on the similarities and differences in performance of evanescent-mode filters and combline filters that followed in chapter 4. Characteristics of an evanescent-mode waveguide were discussed in detail and filters were designed from such waveguides. The performance of the filter, with the passband and at higher frequencies were also discussed.

Following the description of the design processes and characteristics of the combline and evanescent-mode waveguide filters in chapters 2 and 3, chapter 4 brought the two filters of similar physical structure and bandpass characteristics together in an attempt to establish similarities and differences between the two filters, based on two experiments. A combline filter with a large groundplane spacing was found to behave like an evanescent-mode waveguide filter, designed in a waveguide with the same dimensions as the combline filter, but with a difference in bandwidth. It was noted that the bandwidth obtained from the filter designed using combline design theory was much larger than the one that was designed for. The evanescent mode filter had a bandwidth close to the one obtained from the circuit model, and the increase from the percentage bandwidth in the specifications was attributed to the approximations and assumptions made in design. For these reasons, it was recommended that for the design filters of large groundplane spacings relative to the wavelength at midband, evanescent-mode waveguide theory would be better suited. For smaller sized filters, the combline theory would be the favoured choice for the designs, because the desired bandwidths can be obtained and because for evanescent mode filters, it would mean that the chosen waveguide would have a cut-off frequency far from the operation frequency, so that attenuation would be increased.

Chapter 5 covered several aspects of manufacturing specifically addressing coaxial cavity filters like the combline filter. A discussion on material used at microwave frequencies presented the different options for use, concluding that aluminium would be the best option for a filter enclosure because of its light-weight, affordability, good conductivity and machinability. Machining techniques were also discussed and milling and wirecutting were considered to be the most viable options for the fabrication of filter enclosures and the resonators. Surface finishes obtained due to these techniques and their effect of the performance and dimensional tolerances of machined filters were also been outlined. The chapter also included a section on silver-plating of the filters to increase the surface conductivity and Q factor of the filter, since the aluminium will provide a lower Q factor. Aspects related to the evaluation of the design and manufacturing costs were also covered, and the relationship

between the design stages and manufacturing stages of production were addressed, with specific emphasis on the concept of design for manufacturability (DFM).

The main focus of Chapter 6 the design of combline filters for ease of manufacture and for reduced manufacturing costs. The filters were designed for two different sets of specifications: The first filter was a fourth order Chebyshev combline filter operating in the L-Band with a passband between 1235MHz - 1365MHz, with a return loss of less than 20dB in the passband. This filter was designed for manufacturing using two different manufacturing methods: CNC Milling and CNC Wirecutting EDM. The main aim of using the two different methods was to establish, through a comparison of the two, which method was costlier, and which method would give a better surface finish for a better performance of the filter. The second set of specifications called for the design of an S-Band combline filter with a 40MHz bandwidth centered at 2125MHz and having an insertion loss of more than 80dB at 2GHz. The filter was also required to have no passbands between 6.375GHz and 9.375GHz. The different changes made to the structures in order to facilitate easier manufacturing and to lower the costs of manufacturing were clearly outlined. A major problem experienced during manufacturing was that the grade of Aluminium used for the manufacture of the filters did not have unform conductivity and some areas were not conductive enough so that the wirecutting process could not be used for the filters that were to be manufactured by that process. An alternative process, using a waterjet cutter, was opted for, but the filters resulting from the use of the method had a very rough surface finish, low dimensional accuracy and a few deformations which were depicted in the measurements section of the chapter. The results obtained were considerably good despite the manufacturing problems. The milled filter designed to operate at a centre frequency of 1.3 GHz had an insertion loss of -0.5702 dB with a relatively low resonator unloaded Q of 510. The 1.3 GHz waterjet cut filter with a structure analogous to that of the milled filter with slight variations in the physical structure had a slightly higher Q of 556 in comparison with the milled filter and an insertion loss of 0.5077 dB. Due to errors in the manufacturing of the filter, the filter could not be tuned down to the design centre frequency. For both of these filters the bandwidth was only 3 MHz less than the bandwidth for their respective CST simulated filters. The final filter, centred at 2.125 GHz was manufactured by a combination of the milling and waterjet cutting processes. The manufacturing also resulted in a number of deformations that were clearly depicted in the chapter. A wider bandwidth of 44.9 MHz, 7.5 MHz higher than the design bandwidth was obtained with the filter having a low resonator Q of 800 and an insertion loss of 2.838 dB.

The cost of milling was found to be cheaper than the cost of wirecutting as per quotes obtained from the manufacturer. Waterjet cutting was also less costlier than wirecutting. Based on the results in the chapter, it can be concluded that a consultation with a manufacturer would always be best at the beginning stages of a design process, looking into the different options available, possible structural adjustments to make each process easier and possibly to obtain quotes for the costs associated with each. It is also a good idea to specify a grade of metal for a specific use so that the manufacturer does not end up using a lower grade that may not be the best for a specific application. While addressing the issue of cost, performance should not be neglected because if a process results in a filter with poor performance then there might be a need for redesign or for further work which might still add onto the overall costs.

The two topics have been addressed in detail, so that it can be concluded that the objectives of this thesis have been met.

Bibliography

[1] K. S. Packard. "The Origin of Waveguides*: A case of Multiple Rediscovery," *IEEE Transactions on Microwave Theory and Techniques*, Vol. MTT-32, pp. 961-969, September 1984. 1

[2] G. F. Craven and R. F. Skedd. *Evanescent Mode Microwave Components.* Norwood, MA: Artech House, Inc.,1987. 1, 37, 38, 40, 45, 51, 56, 57, 59

[3] R. Levy and S. B. Cohn. "A history of Microwave Filter Research, Design and Development," *IEEE Transactions on Microwave Theory and Techniques*, Vol. MTT-32, pp. 1055-1067, September 1984. 1, 2

[4] A. W. Lawson and R. M. Fano. "The Design of Microwave Filters,". Available: G. L. Ragan, *Microwave Transmission Circuits.*New York: McGraw-Hill Inc., 1948, pp. 613-715. 2

[5] S. B. Cohn. "Direct-Coupled-Resonator filters," *Proceeding of the IRE*, pp. 187-196, 1957. 2

[6] R. Levy. "Theory of Direct-Coupled-Cavity Filters," *IEEE Transactions on Microwave Theory and Techniques*, Vol. MTT-15, pp. 340-348, June, 1967. 2

[7] S. B. Cohn. "Parallel-Coupled Transmission-line resonator filters," *IEEE Transactions on Microwave Theory and Techniques*, Vol. MTT-32, pp. 223-231, April 1958. 2

[8] J. Ishii and H. Ozaki. "Synthesis of a class of Stripline filters," *IRE Transactions on Microwave Theory and Techniques*, Vol. CT-5, pp. 104-109, June 1958. 2

[9] G. L. Matthaei. "Interdigital band-pass filters," *IEEE Transactions on Microwave Theory and Techniques*, Vol. MTT-10, pp. 479-491, November 1962. 2

[10] G. L. Matthaei. "Combline band-pass filters for narrow and moderate bandwidth," *Microwave Journal*, Vol. 6, pp. 82-91, August 1963. 2

[11] B. F. Nicholson and I. L. Powell. "Equivalence between evanescent-mode and combline filters," *Electronic Letters*, Vol. 3, pp. 495-496, November 1967. 2, 59

[12] D. G. Swanson, Jr. and W. J. R. Hoefer. *Microwave Circuit Modeling Using Electromagnetic Field Simulation,* Norwood, MA: Artech House, Inc., 2003. 2

[13] D. M. Pozar. *Microwave Engineering*, 3rd ed. Hoboken, NJ: John Wiley & sons, Inc., 2005. xiv, 13, 18, 30, 44

[14] R. W. Rhea. *HF Filter Design and Computer Simulation*, Atlanta: Noble Publishing, 1994. 54

[15] G. L. Matthaei. *Microwave Filters, Impedance-Matching Networks and Coupling Structures*, NJ: McGraw-Hill, 1980. 6, 11, 13, 14, 15, 17, 19, 20, 21, 22, 32, 44, 71

[16] S. B. Cohn. "Microwave filters, an Advancing Art," *IEEE Transactions on Microwave Theory and Techniques*, Vol. MTT-13, pp. 487-488. 37

[17] S. B. Cohn. "Breaking Through the Mental Barrier," *IRE Transactions on Microwave Theory and Techniques*, pp. 190-191, April 1959. 37

[18] G. F. Craven and C. K. Mok. "The Design of Evanescent Mode Bandpass Filters for a Prescribed Insertion Loss Characteristic," *IEEE Transactions on Microwave Theory and Techniques*, Vol. MTT-19, pp. 295-308, March 1971. 38, 40, 42, 44, 45, 49, 53, 56, 63

[19] R. Levy, R. V. Snyder and G. Matthaei. "Design of microwave filters," Microwave Theory and Techniques, *IEEE Transactions on Microwave Theory and Techniques*, vol.50, no.3, pp.783-793, Mar 2002

[20] P. W. Van de Walt. MN813. "Postgraduate Course in Microwave Networks," Faculty of Engineering, Stellenbosch University, South Africa, 2010. 31

[21] I. Awai and Y. Zhang. "Coupling coefficient of Resonators - An Intuitive Way of Its Understanding," *Electronics and Communication in Japan*, Vol. 90.9, pp. 11-18, 2007. 32, 33

[22] R. Levy, H. Yao, and K. A. Zaki. "Transitional Combline/ Evanescent-Mode Microwave Filters," *IEEE Transactions on Microwave Theory and Techniques*, Vol. 45, pp. 2094-2099, December 1997. 59, 65, 66

[23] G. Craven. "Relationship between direct-coupled waveguide filters and evanescent-mode filters," *Electronics Letters* , vol.4, no.3, pp.44-46, February 9 1968

[24] A. I. Zverev. *Handbook of Filter Synthesis*, 1st ed. John Wiley and Sons, Inc., 1967. 17, 21, 22, 33, 93

[25] M. Politi, G. Macchiarella and G. G. Gentili. "A space-mapping Techinque for the design of comb filters," 3*3rd European Microwave Conference*, pp. 171-173, 2003.

[26] P. Martin and J. B. Ness. "Coupling Bandwidth and Reflected Group Delay Characterisation of Microwave Bandpass Filters," *Appl. Microw. Wireless*, vol. 11, no. 5, pp. 1-10, May 1999.

[27] J. B. Ness. "A Unified approach to the Design, Measurement and Tuning of Coupled Resonator Filters," *IEEE Transactions on Microwave Theory and Techniques*, Vol. 46, pp. 343-351, April 1998. xiv, 32, 34

[28] H. Eskelinen, and P. Eskelinen. *Microwave Component Mechanics*. Norwood, MA: Artech House, Inc., 2003. 84, 85, 88, 89, 91

[29] A. F. Harvey. *Microwave Engineering*. London: Academic Press Inc., 1963 84

[30] T. Laverghetta. *Microwave Materials and Fabrication Techniques*, 2nd ed. Norwood, MA: Artech House, Inc., 1991. 76

[31] M. A. R. Gunston. *Microwave Transmision-Line Impedance Data*. London: Van Nostrand Reinhold Company, 1972. ix, 8, 9, 10

[32] Y. Ning, W. Jiang and J. Deng. "The influence of Conducting Rough Surfaces on the performance of microwave coaxial filter," *Microwave, Antenna, Propagation and EMC Technologies for Wireless Communications, 2009 3rd IEEE International Symposium on* , vol., no., pp.778-781, 27-29 Oct. 2009 84

[33] I. V. Lebedev and e. M. Gutssait. "Resonator of the 'subcritical' waveguide type," *Radiotekh Elecktrom.*, Oct. 1956, p. 1303. 38

[34] W.A. Edson. "Microwave filters using ghost-mode resonance," *IRE Electron. Components Conf.*, 1961, vol. 19, p. 2. 38

[35] H. J. Orchard. "Formulas for ladder filters," *Wireless Engineer*, vol. 30, pp. 3-5, Jan. 1953 2

[36] E. Green. "Synthesis of ladder networks to give Butterworth or Chebyshev response in the passband," *Proc. Inst. Elec. Eng.*, vol. 45, pp. 187-96, Feb. 1957. 2

[37] "All About circuits: Waveguides. " Internet: www://allaboutcircuits.com/vol_2/chpt_14/8.html. [Sept. 10, 2010]

[38] "CST - Leading Technology workshop series 2011." Internet: http://www.cst.com/Content/Events/workshop_documents/workshops_ws2011.aspx [Sept. 9, 2011] 3

[39] "Simulation Tools Build On Electromagnetic Analysis." Internet: http://mwrf.com/Articles/Index.cfm?Ad=1&ArticleID=12743. [Sept. 9, 2011] 3

[40] "Axiem." Internet: http://web.awrcorp.com/Usa/Products/AXIEM-3D-Planar-EM/ [Sept 9, 2011]

[41] "Microwave Office." Internet: http://web.awrcorp.com/Usa/Products/Microwave-Office/ [Sept 9, 2011] 3

[42] "Technical Information. Cutting tools." Internet: http://www.ingersollcuttingtools.com/en/products/uc/0302_Milling_Tech.pdf [Aug. 8, 2011] xii, 84

[43] "Electroplating Explained." Internet: www.samfa.org.za/Library/ electroplating_explained.pdf [May 3, 2011] xii, 87, 88

[44] "Electrical discharge machining." Internet: http://en.wikipedia.org/wiki/Electrical_ discharge_machining [April 26, 2011]

[45] "Milling Machine." Internet: http://en.wikipedia.org/wiki/Milling_machine [April 26, 2011] 78

[46] "What is EDM and the advantages of using it?" Internet: http://www.wire-cut.co.uk/wireedm.htm [April 26, 2011] 83, 120

[47] "EDM Machines." Internet: http://www.sundamachinetools.com/edm-machines/ [April 26, 2011]

[48] "Introduction to Machine Tools." Internet: http://www.mfg.mtu.edu/marc/primers/ machtool/intro.html# types_name [April 26, 2011]

[49] "Electrical Discharge Machining, EDM." Internet: http://www.engineersedge.com/edm.shtml [April 26, 2011]

[50] "Electrode Discharge Machine Wirecut (EDM wirecut)." Internet: http://www.scribd.com/doc/31289146/EDM-Wirecut#archive [April 26, 2011] 83

[51] "CNC Machining Handbook." Internet: http://cncmachiningzone.org/ [July 2, 2011] 83, 84

[52] "Milling Cutter." Internet: http://en.wikipedia.org/wiki/Milling_cutter [April 27, 2011] xii, 81

[53] "End Mills." Internet: http://www.mini-lathe.com/Mini_mill/Accessories/End_mills/end_mills.htm [April 27, 2011] xii, 79

[54] "Some Information about End Mills (Rotational Cutters) for CNC Machines." Internet: http://buildyourcnc.com/endmills.aspx [April 27, 2011] xii, 81

[55] "Coaxial cable." Internet: http://en.wikipedia.org/wiki/Coaxial_cable#Semi-rigid [April 27, 2011]

[56] "What is Wire EDM?" Internet: http://www.jobshop.com/techinfo/papers/ whatiswireedm.shtml [April 26, 2011] 81

[57] "Spindles used in Milling." Internet: http://www.spindlesworld.com/milling-process.html [April 26, 2011] xii, 78, 79

[58] http://www.fs-sourcing.com/Popular%20Technology/Machining/Milling.htm [April 26, 2011] xii, 80

[59] "Electrical Discharge Machining (EDM) of Metals and Alloys." Internet: http://www.themetallurgist.co.uk/articles/electrical_discharge_machining_edm_of_metals_and_alloys.shtml [April 26, 2011] xii, 82, 83

[60] "Milling." Internet: http://www.custompartnet.com/wu/milling [April 26, 2011]

[61] "Basic Wire EDM Principles." Internet: http://www.advancededm.com/edm.htm [April 26, 2011] xii, 82

[62] "What is Wire EDM - A Short History." Internet: http://www.jobshop.com/ techinfo/papers/wireedmshorthistory.shtml [April 26, 2011]

[63] "Cylindrical Capacitor." Internet: http://hyperphysics.phy-astr.gsu.edu/hbase/ electric/capcyl.html [August 12, 2011] xiii, 112

[64] "Loop." Internet: http://www.amateur-radio-wiki.net/index.php?title=Loop [August 12, 2011] 97

[65] "Omax and Wire EDM." Internet: http://www.omax.com/waterjets/omax-wire-edm [October 14, 2011]

[66] "Overview of waterjets." Internet: http://www.webcitation.org/5nWaNTDGA [October 16, 2011]

[67] "B.G. Peck Water Jet Cutting." Internet: http://www.bgpeck.com/waterjet.html [October 16, 2011]

Appendix A

Filter Dimensions and Guidelines for Manufacturing

A.1 2 GHz Combline Filter [From Chapter 2]

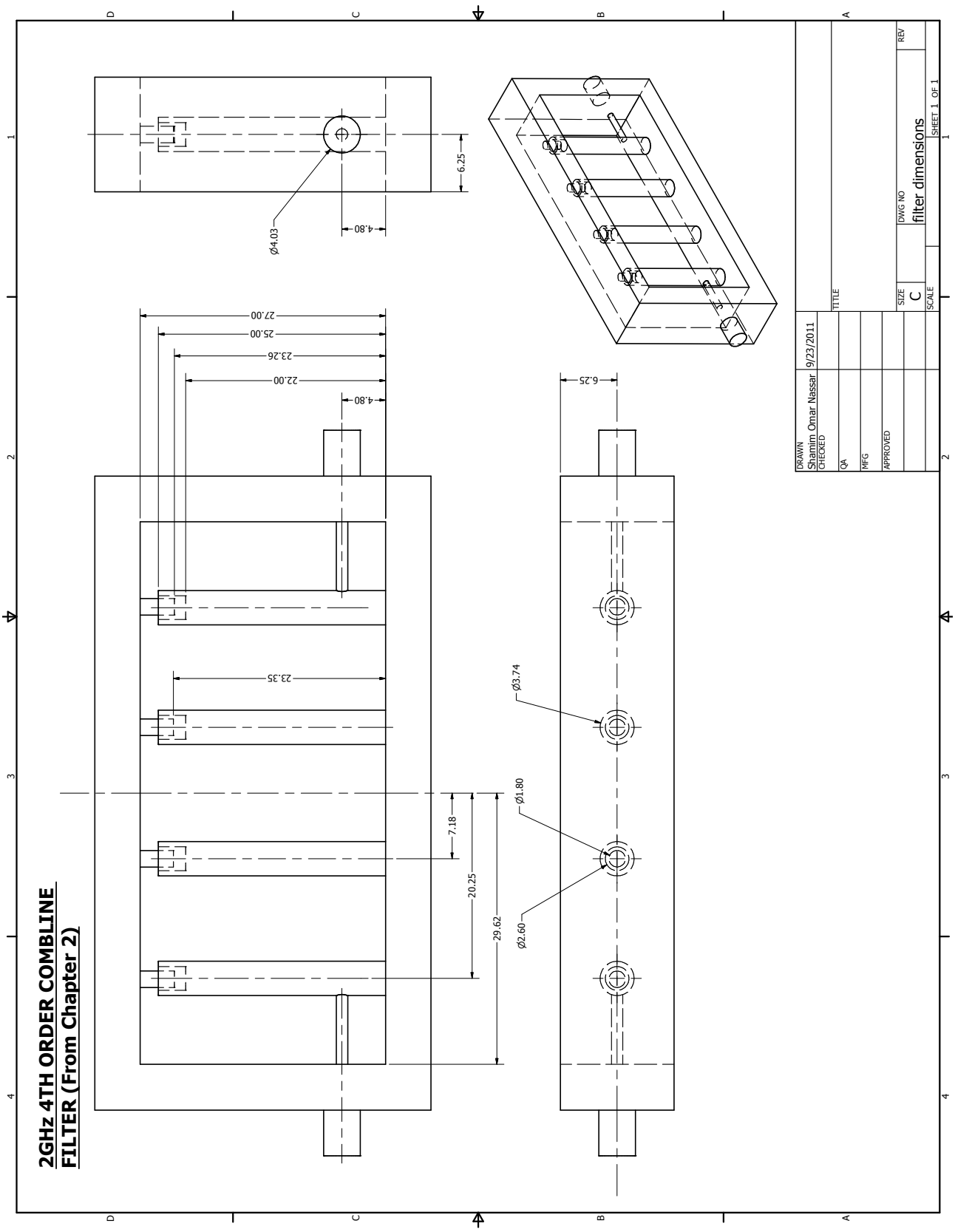

Figure A.1: 2GHz Combline Filter from Chapter 2

A.2 2GHz Evanescent Mode Waveguide Filter in WR137 from Chapter 3

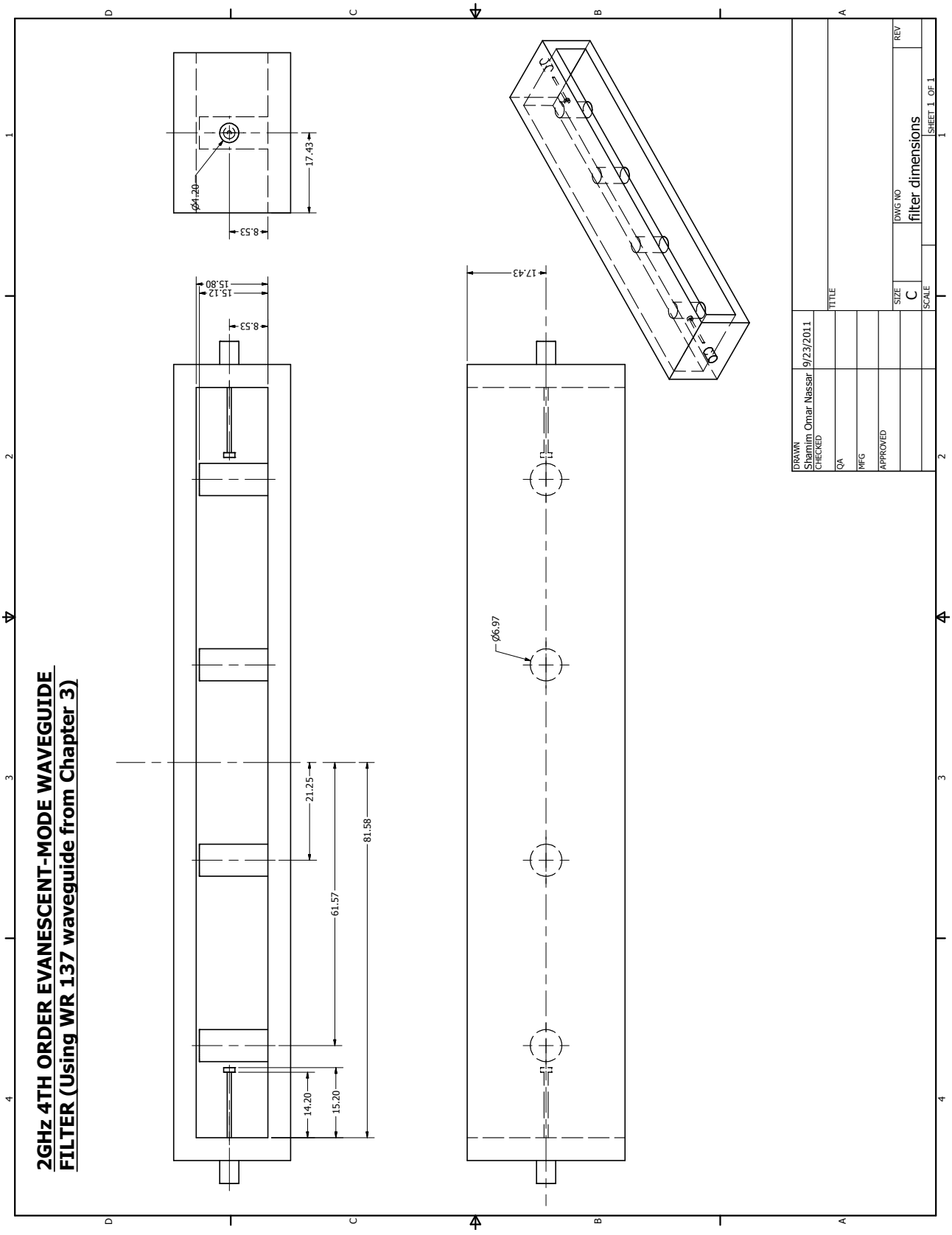

Figure A.2: 2GHz Evanescent Mode Waveguide Filter in WR137 from Chapter 3

A.3 2GHz Combline Filter in WR137 from Chapter 3

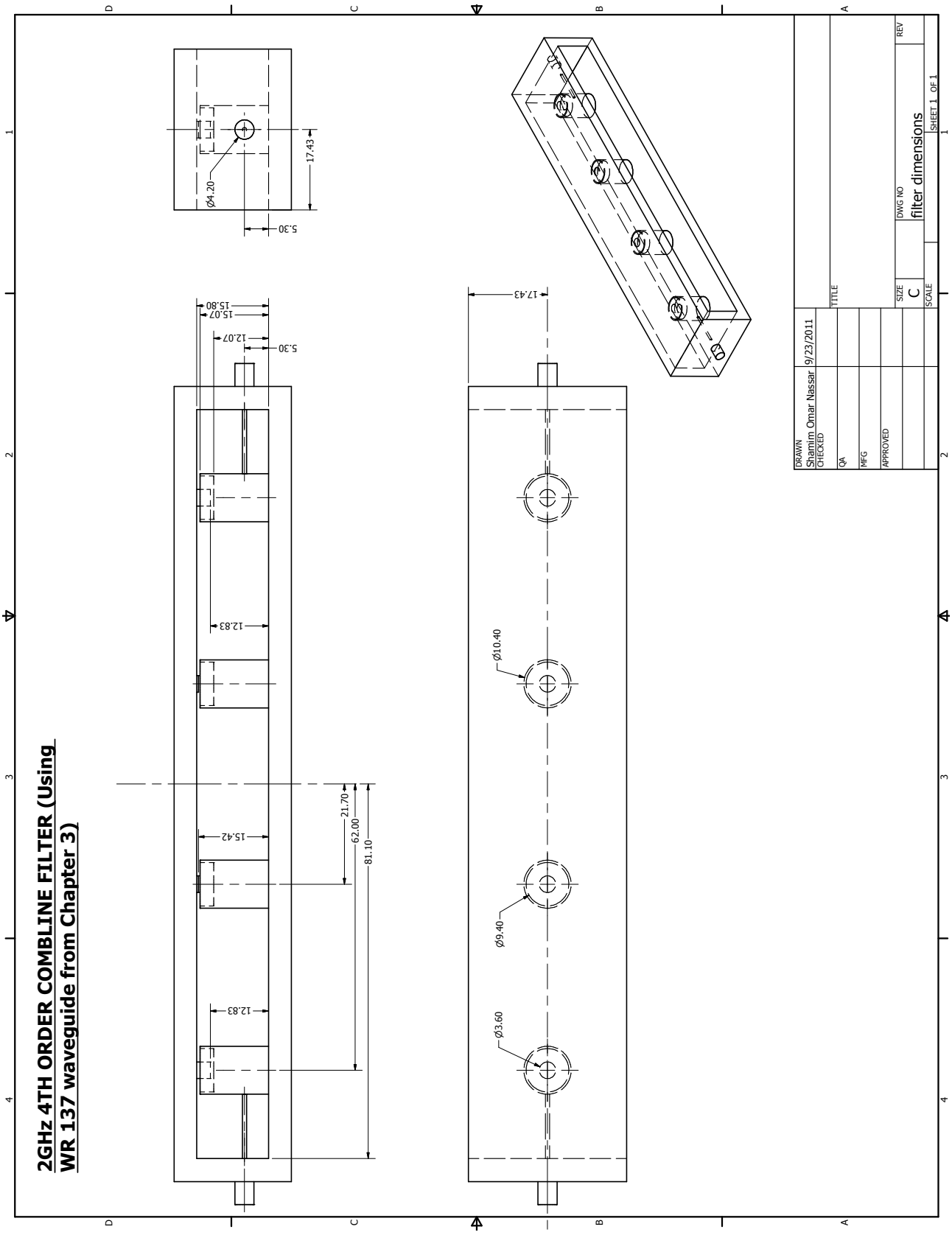

Figure A.3: 2GHz Combline Filter in WR137 from Chapter 3

A.4 1.3GHz Combline Filter

A.4.1 Schematics for Milled Filter

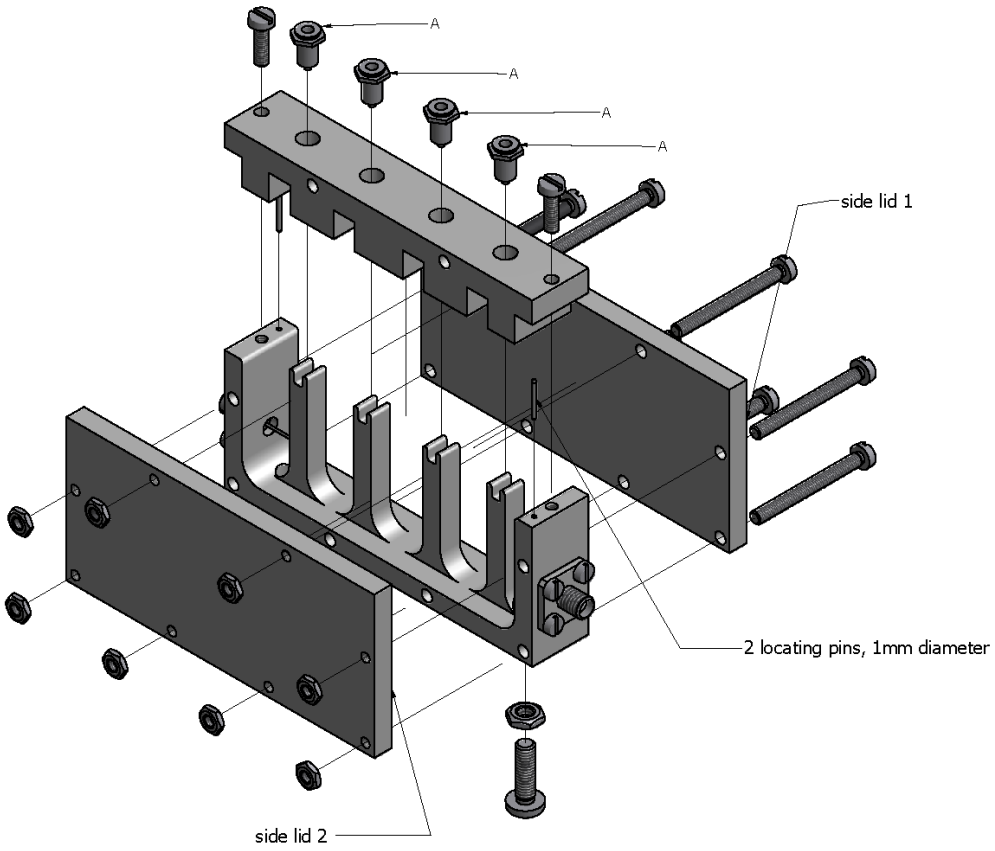

Figure A.4: Exploded View of 1.3GHz Combline Filter - Milling Option

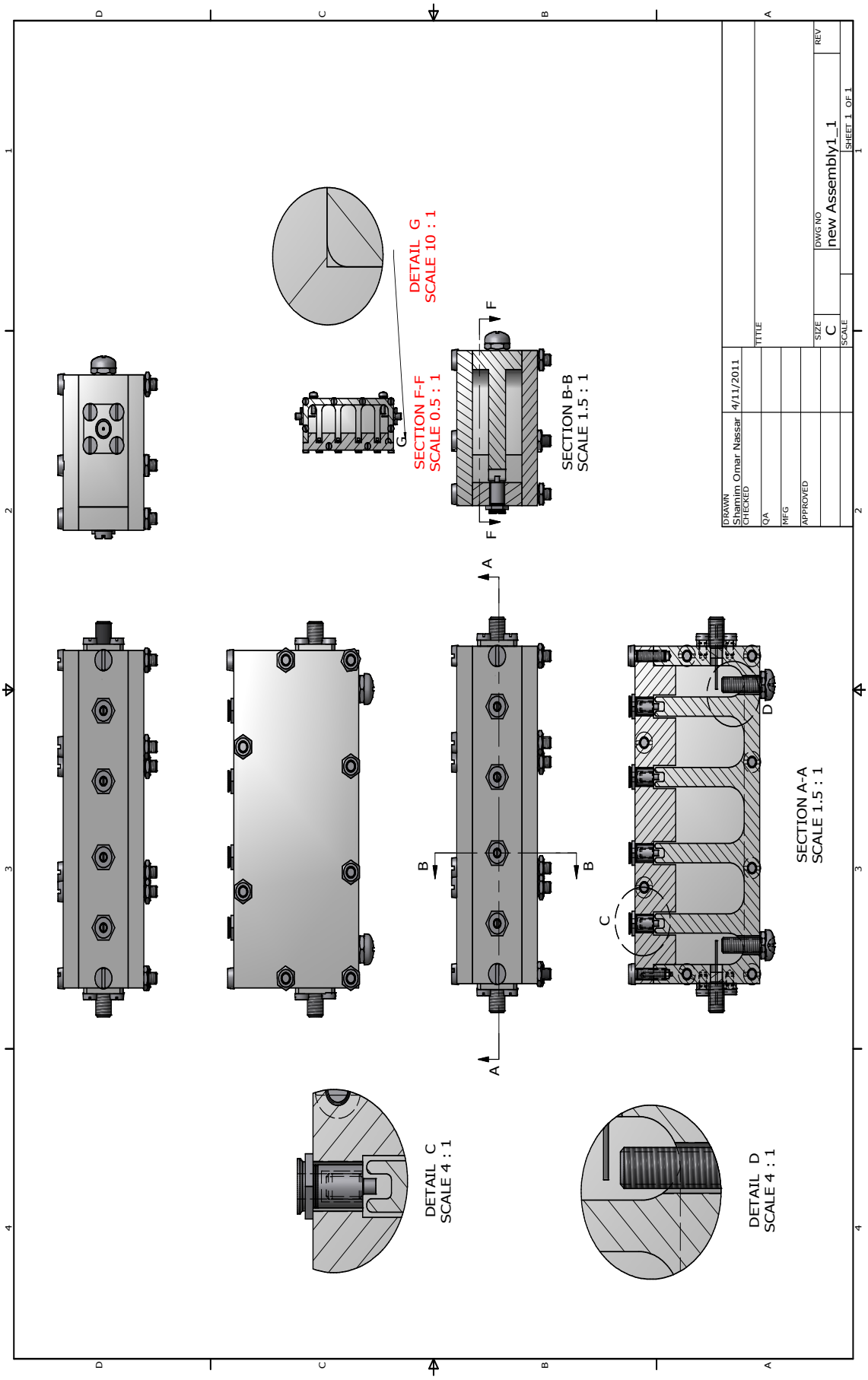

Figure A.5: Sectioned View of 1.3GHz Combline Filter - Milling Option

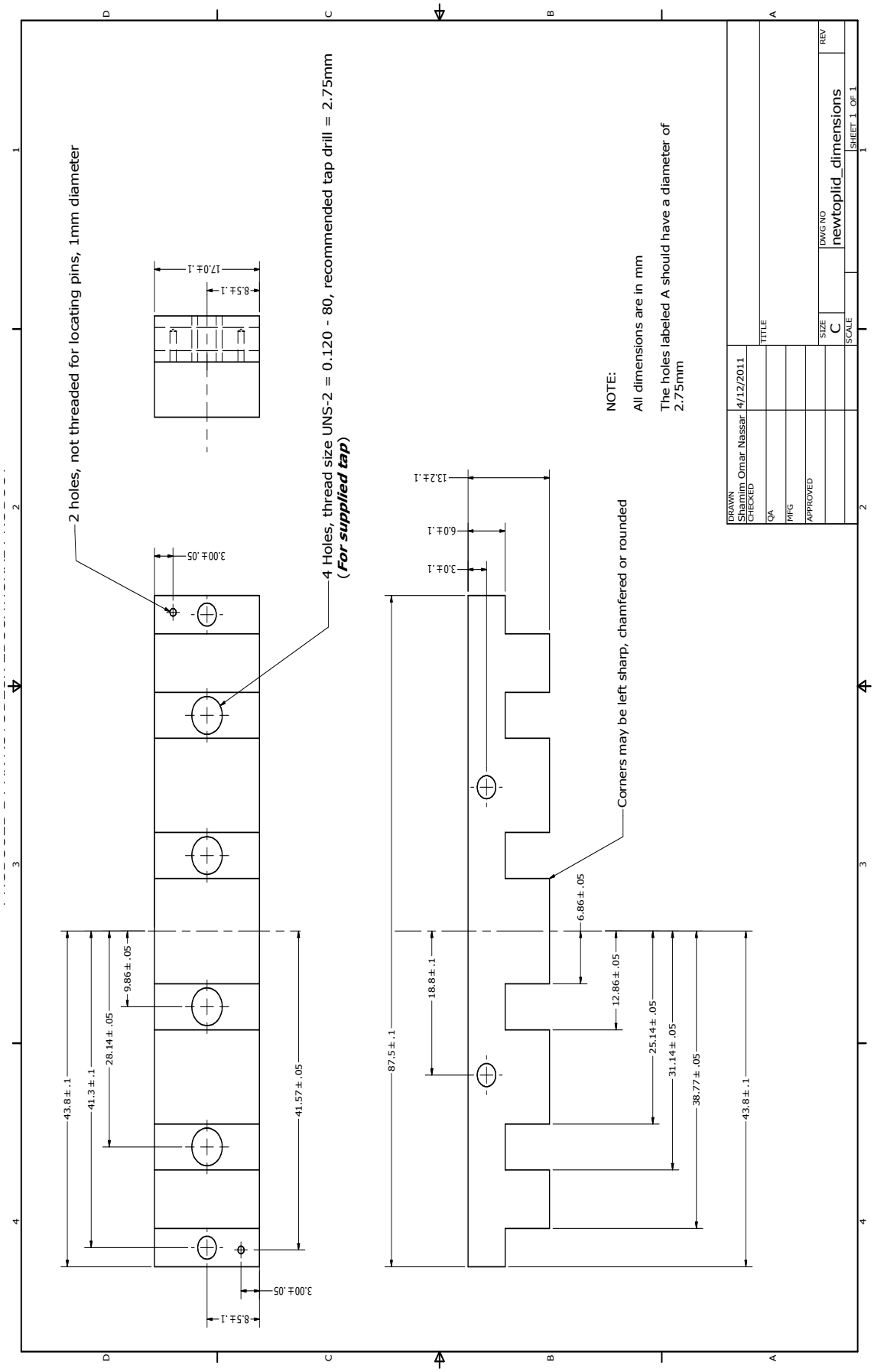

Figure A.6: 1.3GHz Combline filter Toplid Dimensions - Milling Option

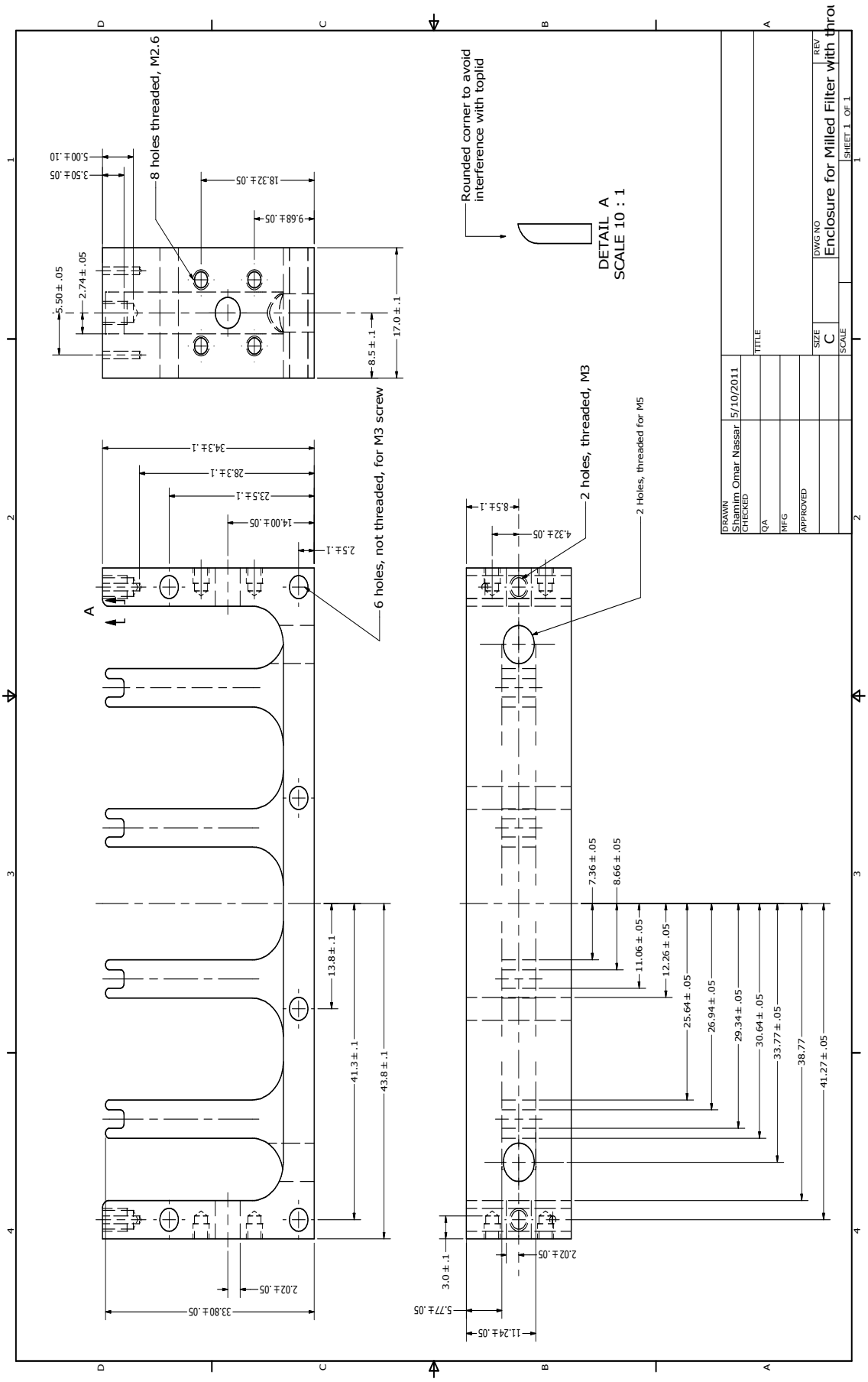

Figure A.7: 1.3GHz Combline Filter Main Body Dimensions - Milling Option

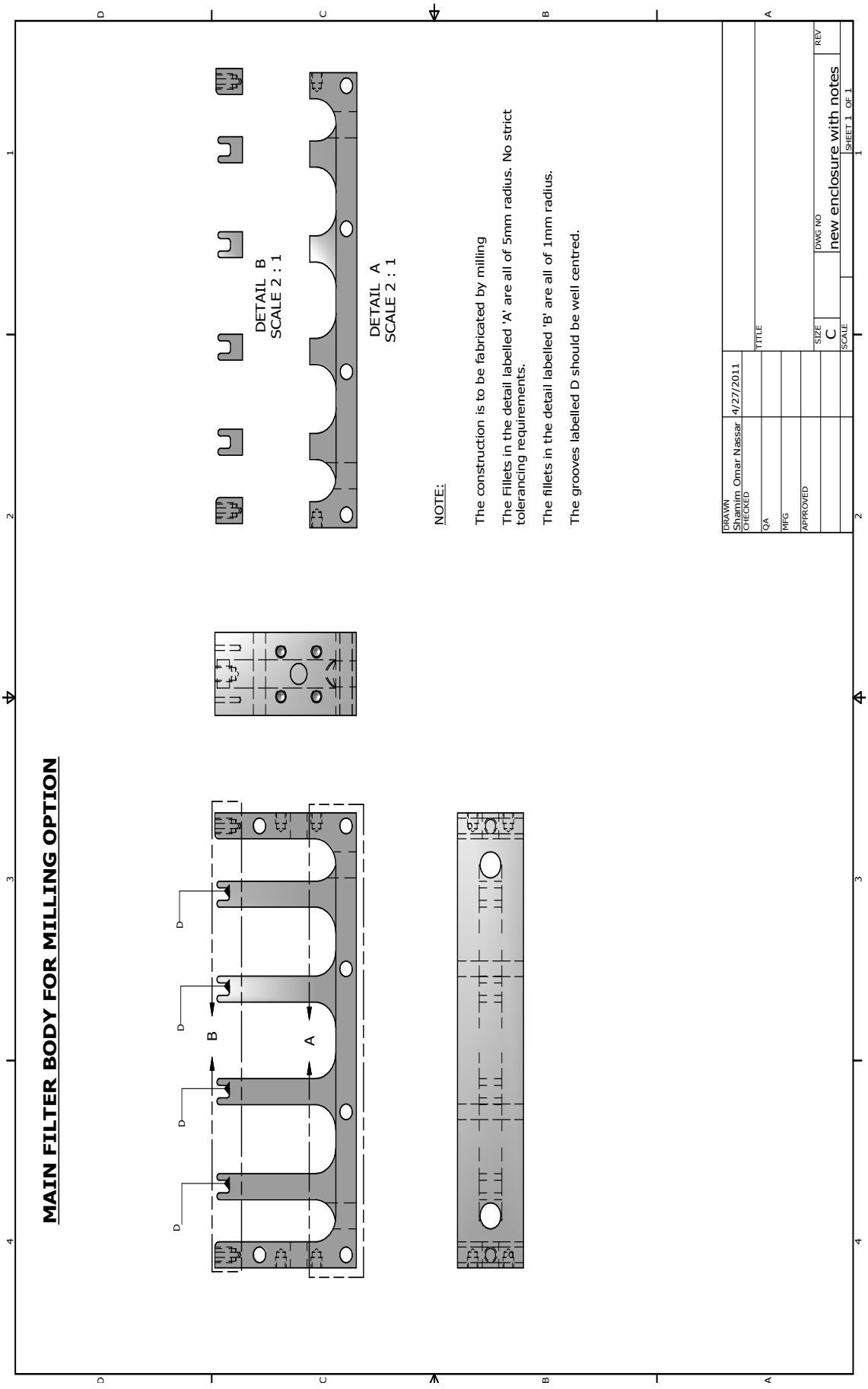

Figure A.8: 1.3GHz Combline Filter Instruction for Milling Rounded Corners

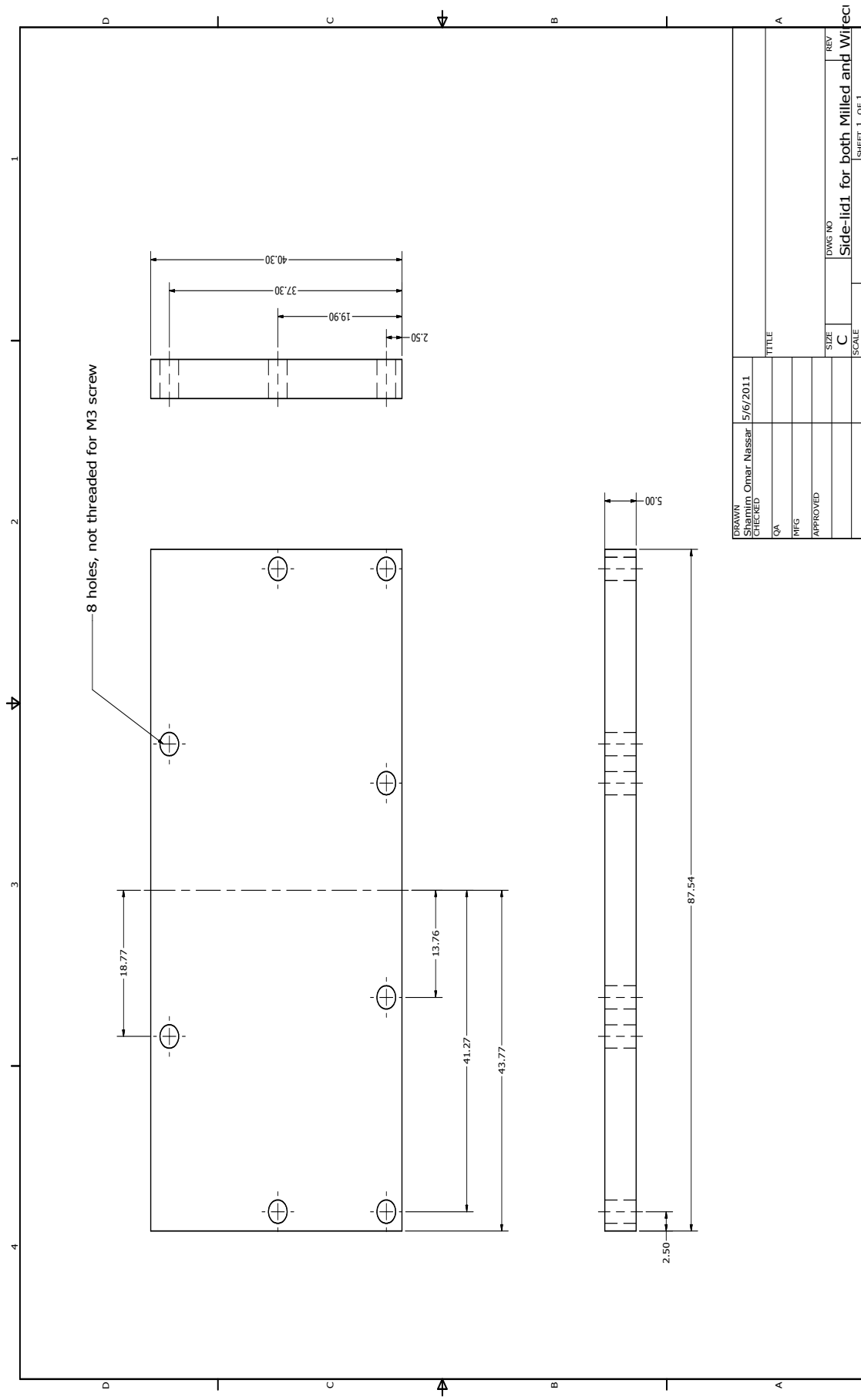

Figure A.9: 1.3GHz Combline Filter Sidelid Dimensions with Unthreaded Holes - Milling Option

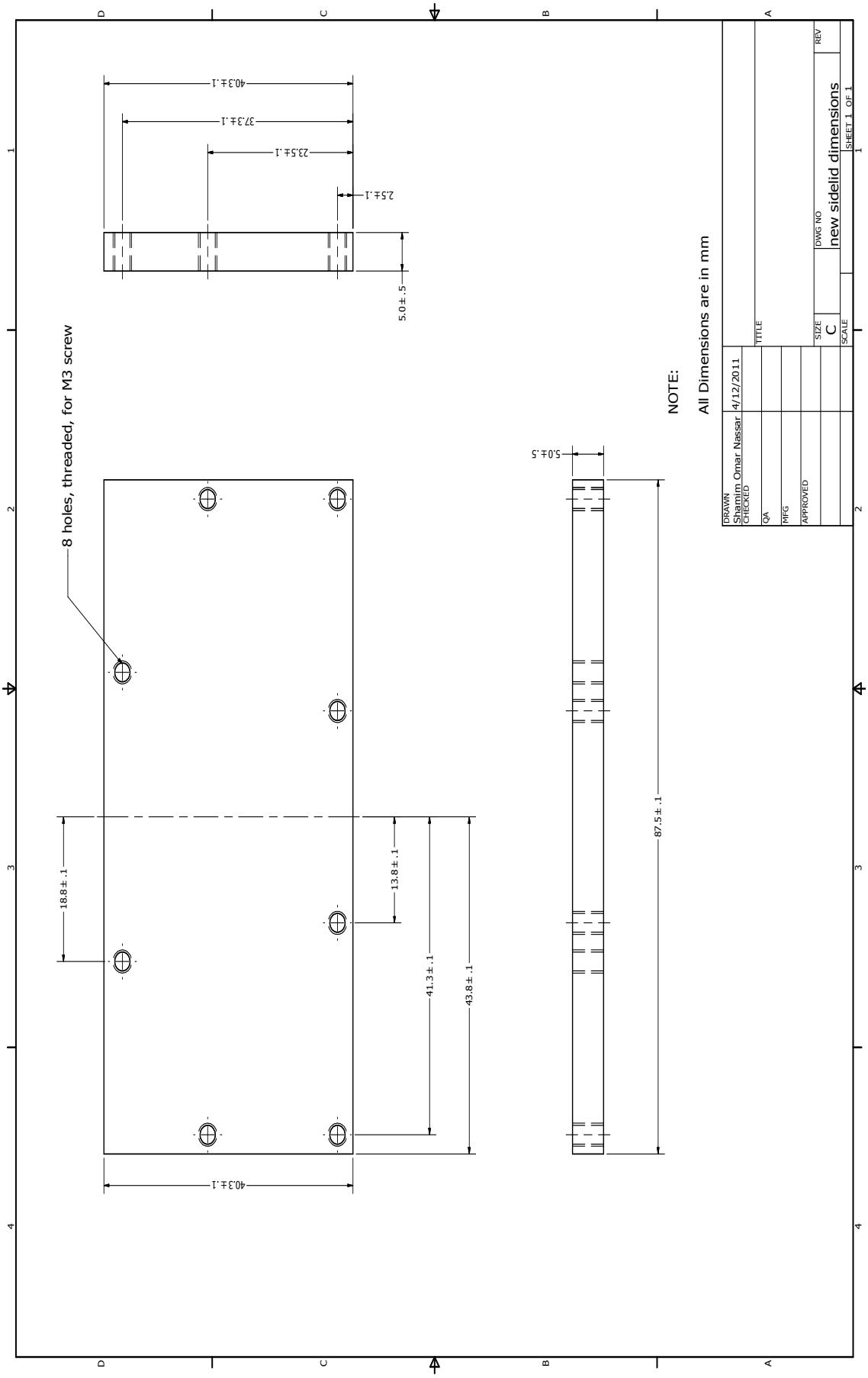

Figure A.10: 1.3GHz Combline Filter Sidelid Dimensions with threaded Holes - Milling Option

A.4.2 Schematics for Wirecut Filter

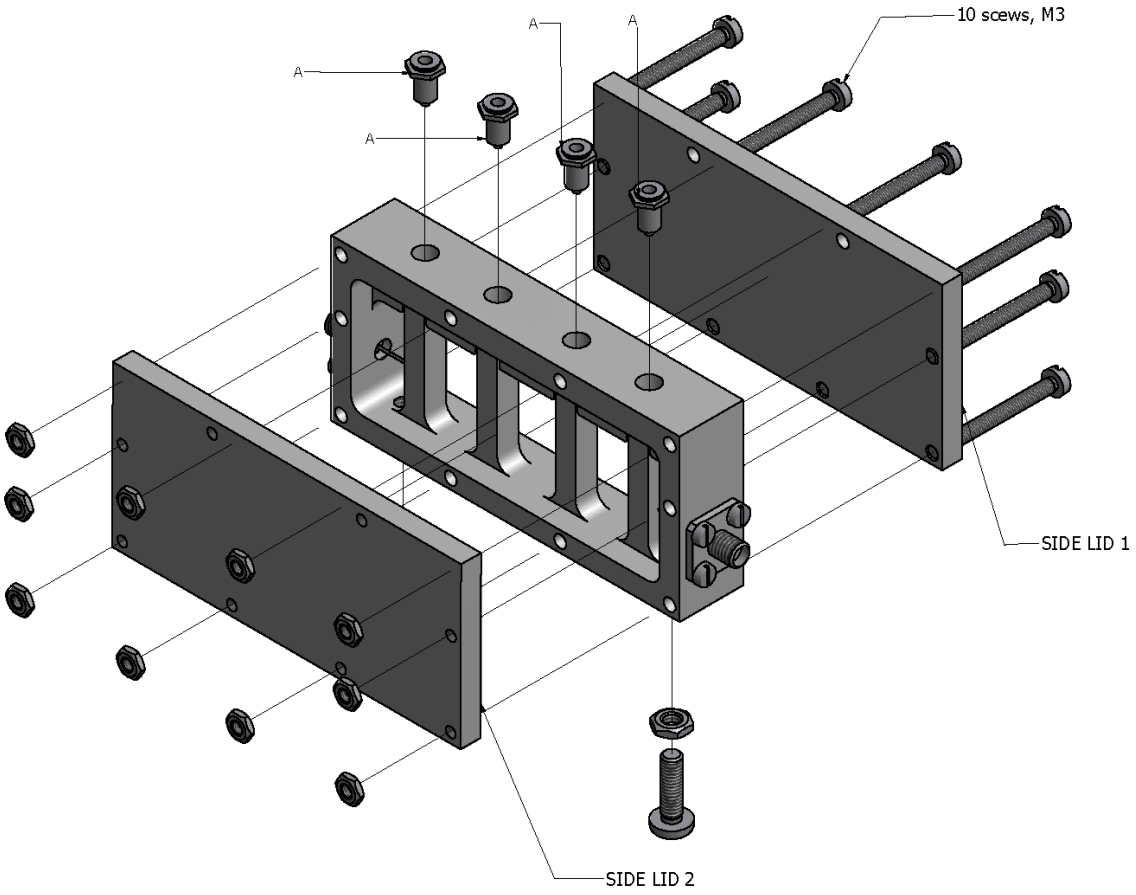

Figure A.11: Exploded View of 1.3GHz Combline Filter - Wirecutting EDM Option

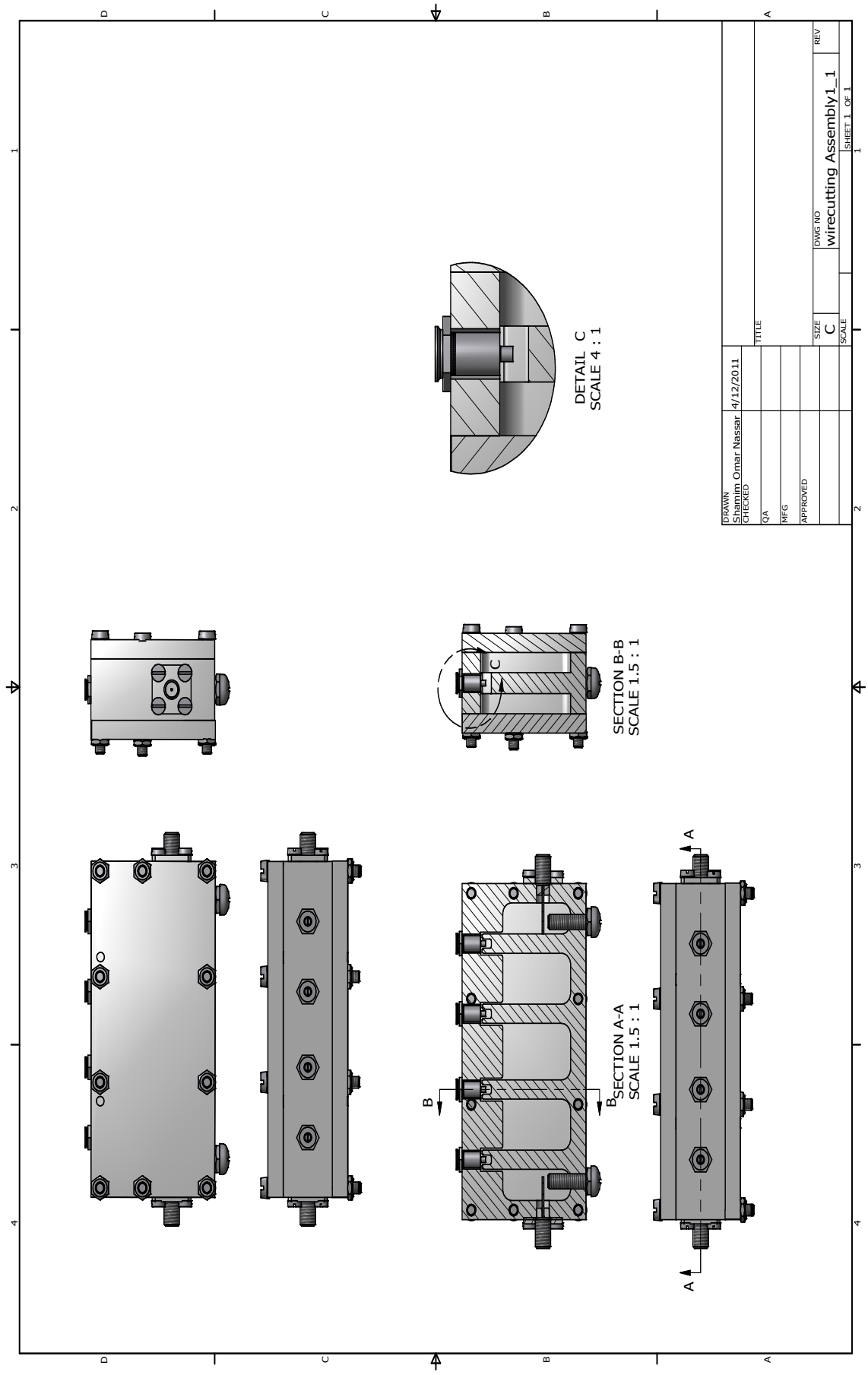

Figure A.12: Sectioned View of 1.3GHz Combline Filter - Wirecutting EDM Option

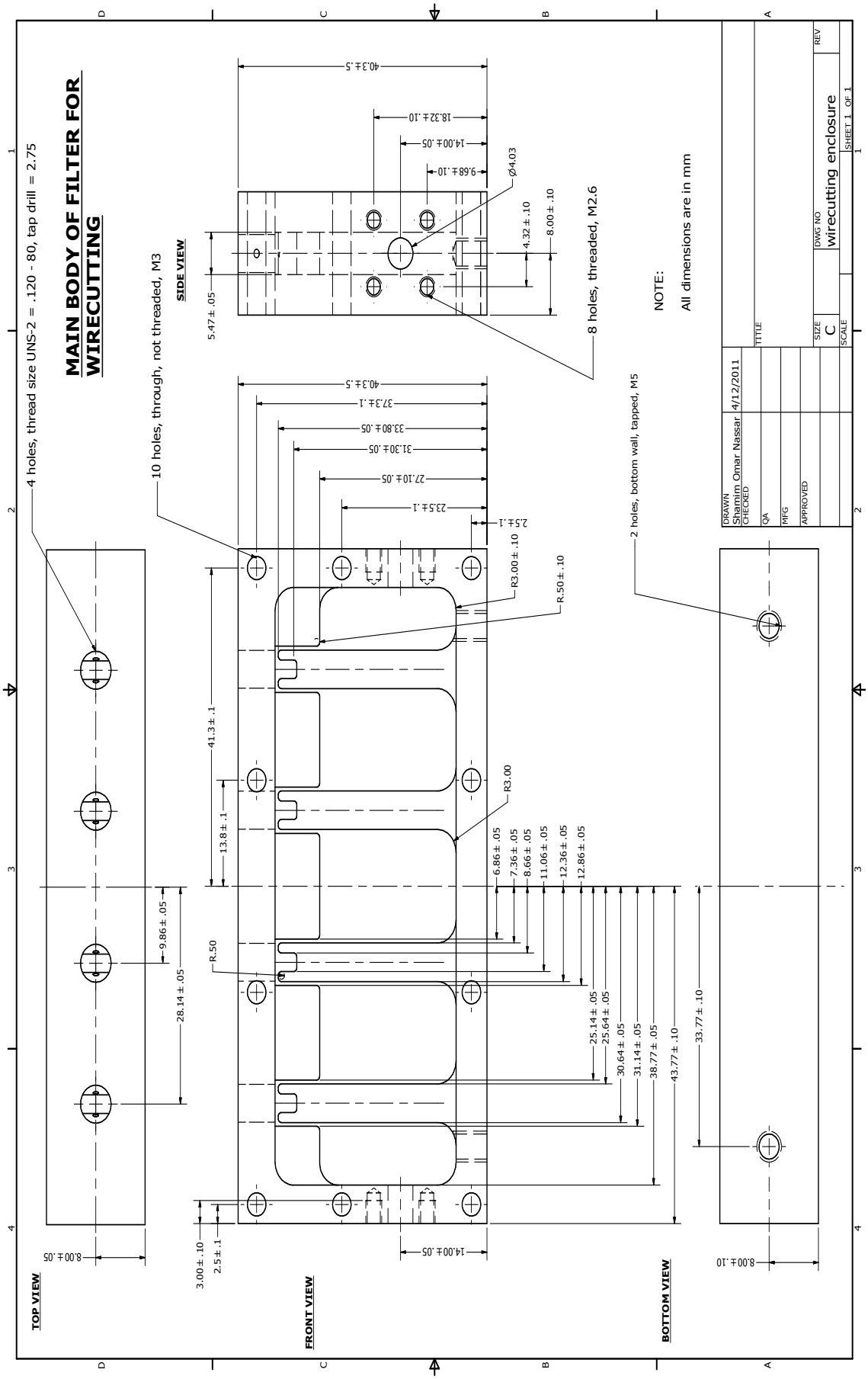

Figure A.13: 1.3GHz Combline Filter Main Body Dimensions - Wirecutting EDM Option

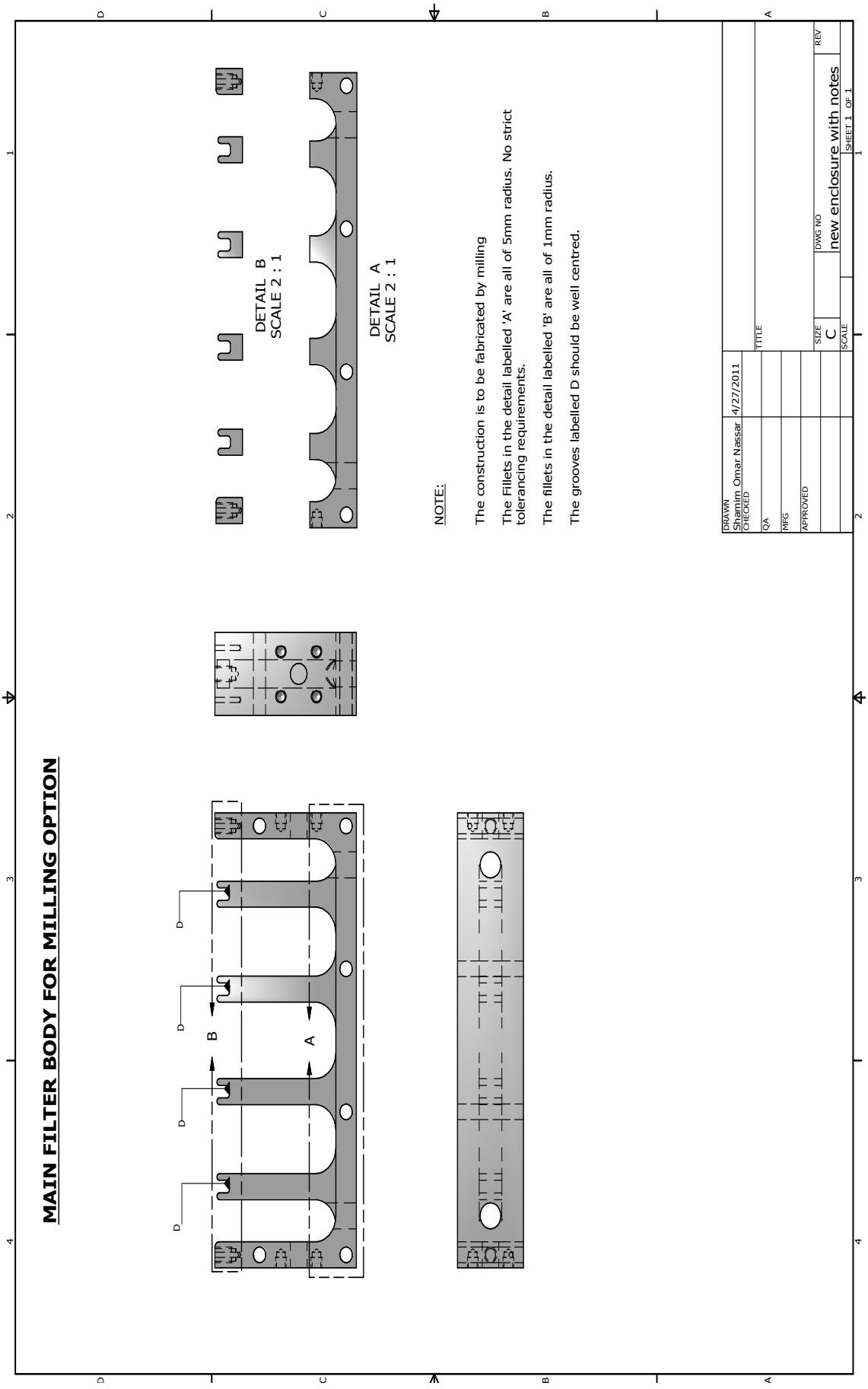

Figure A.14: 1.3GHz Combline Filter Instruction for Wirecutting Rounded Corners

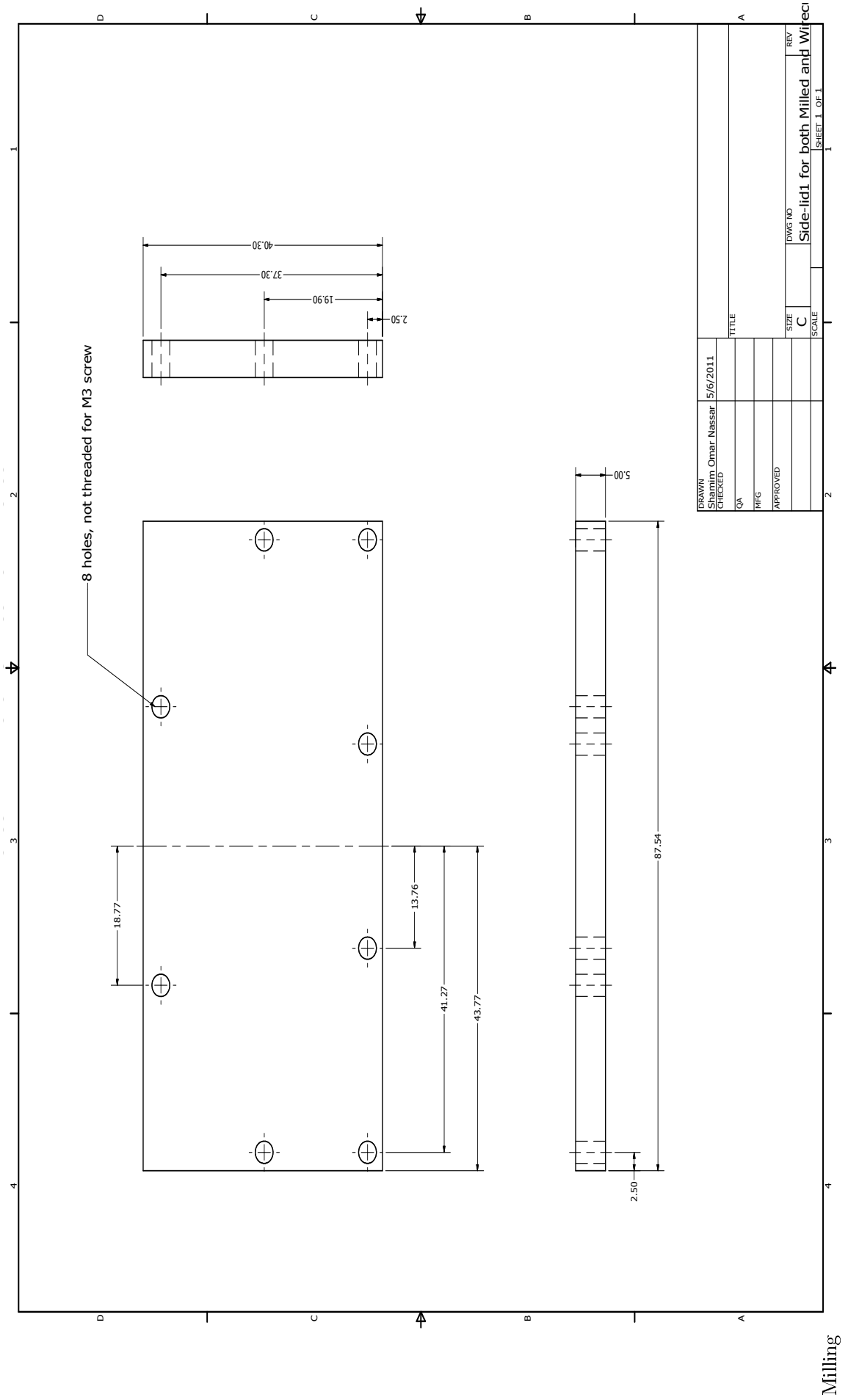

Figure A.15: 1.3GHz Combline Filter Sidelid Dimensions with Unthreaded Holes - Milling Option

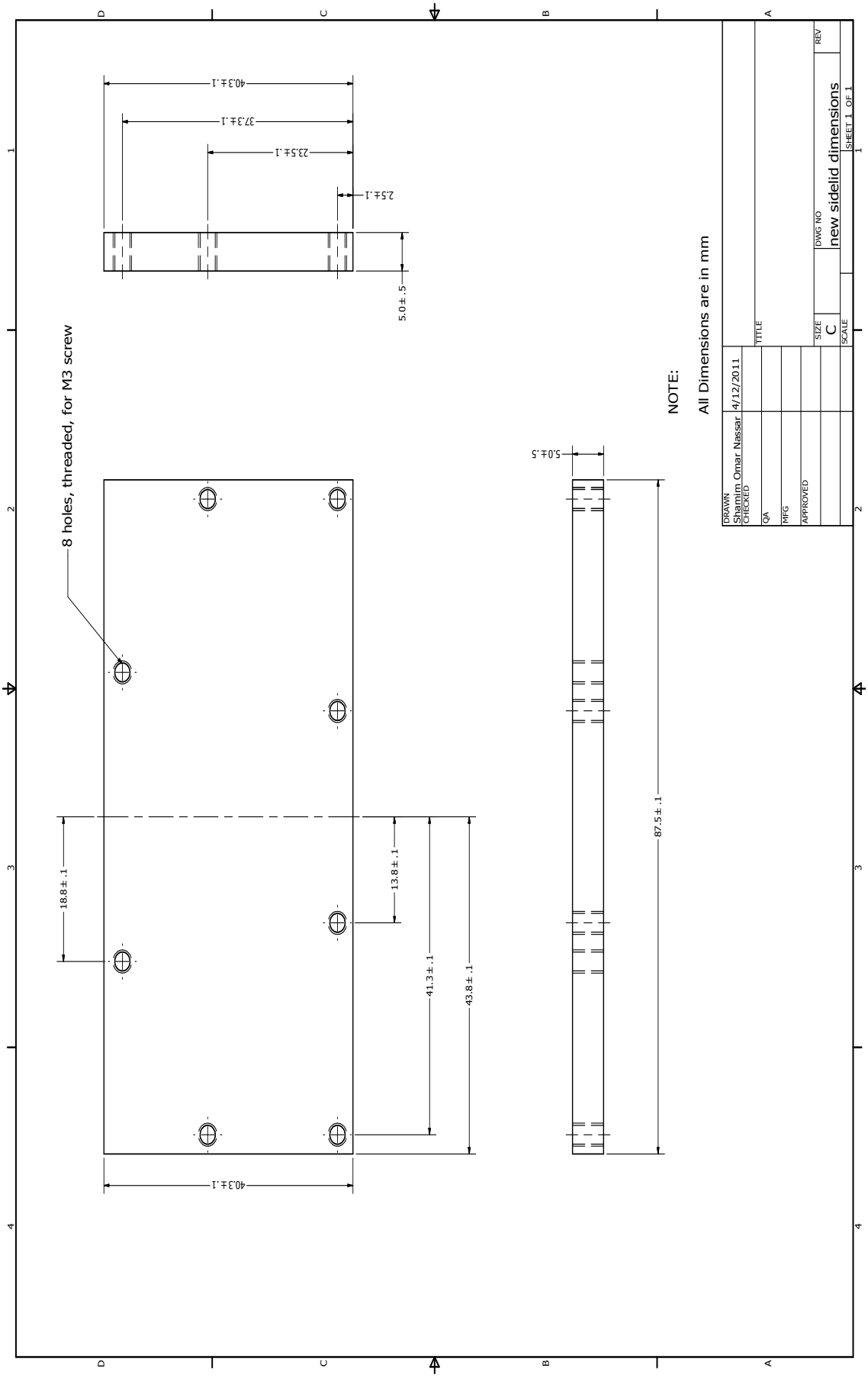

Figure A.16: 1.3GHz Combline Filter Sidelid Dimensions with threaded Holes - Milling Option

A.5 2.125GHz Filter

A.5.1 Schematics

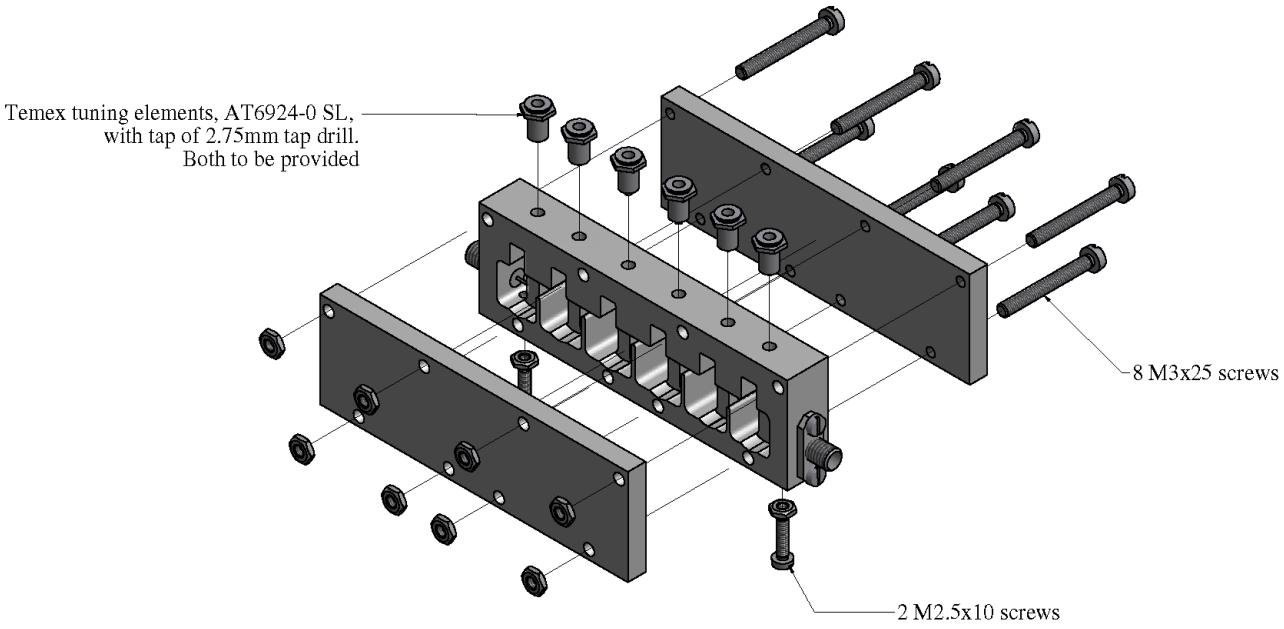

Figure A.17: Exploded View of 2.125GHz Combline Filter

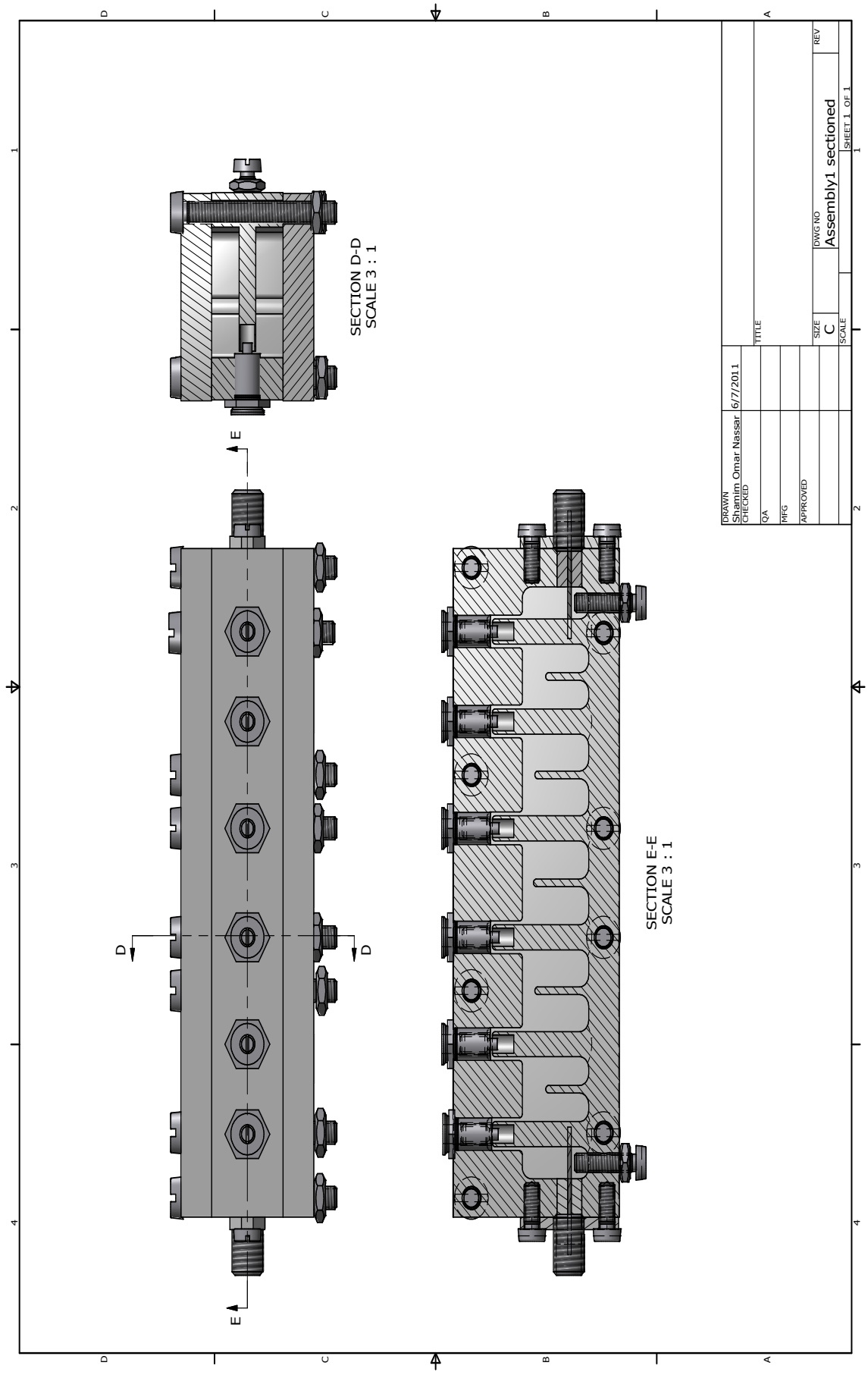

Figure A.18: Sectioned View of 2.125GHz Combline Filter

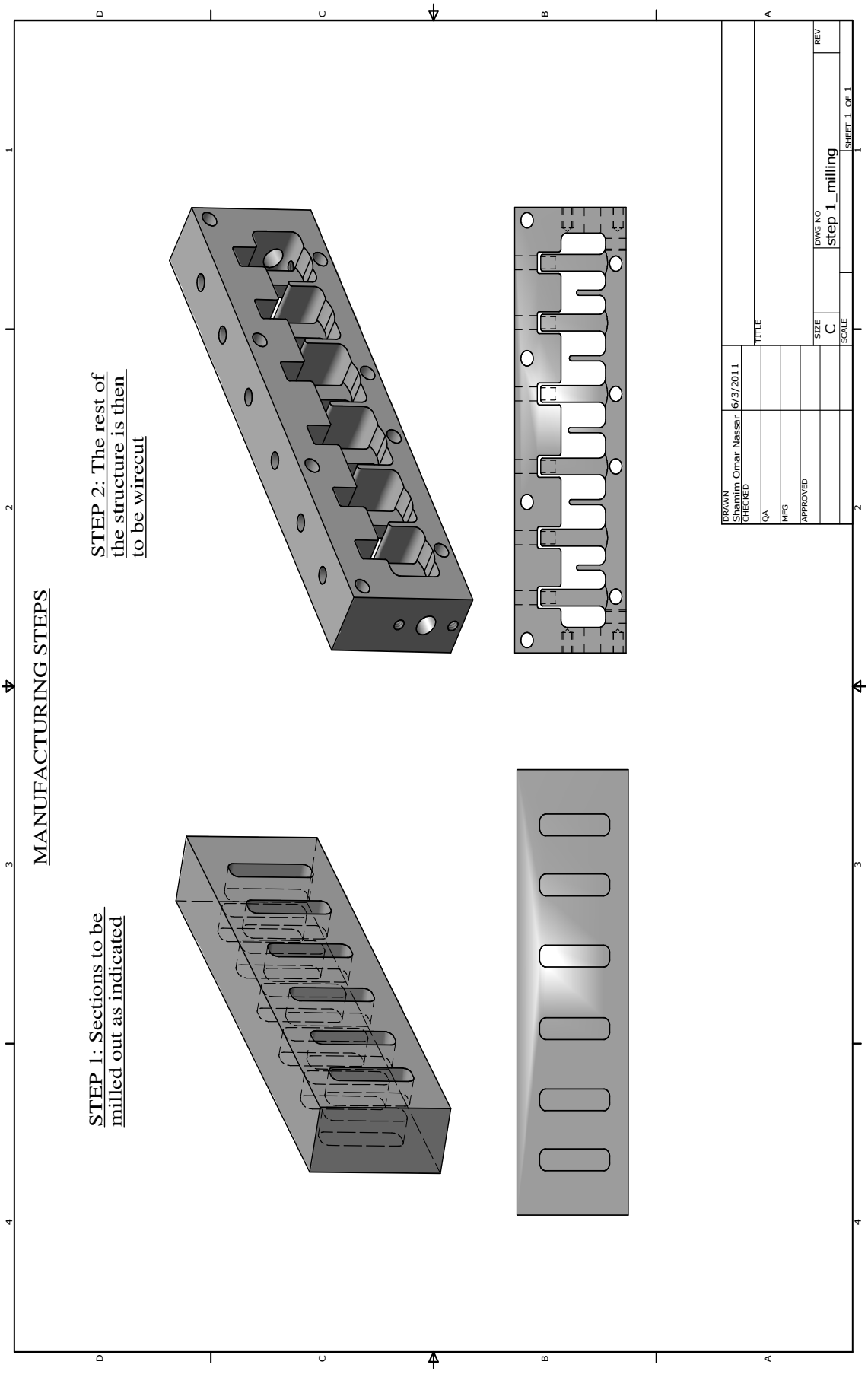

Figure A.19: 2.125GHz Combline Filter Manufacturing Steps

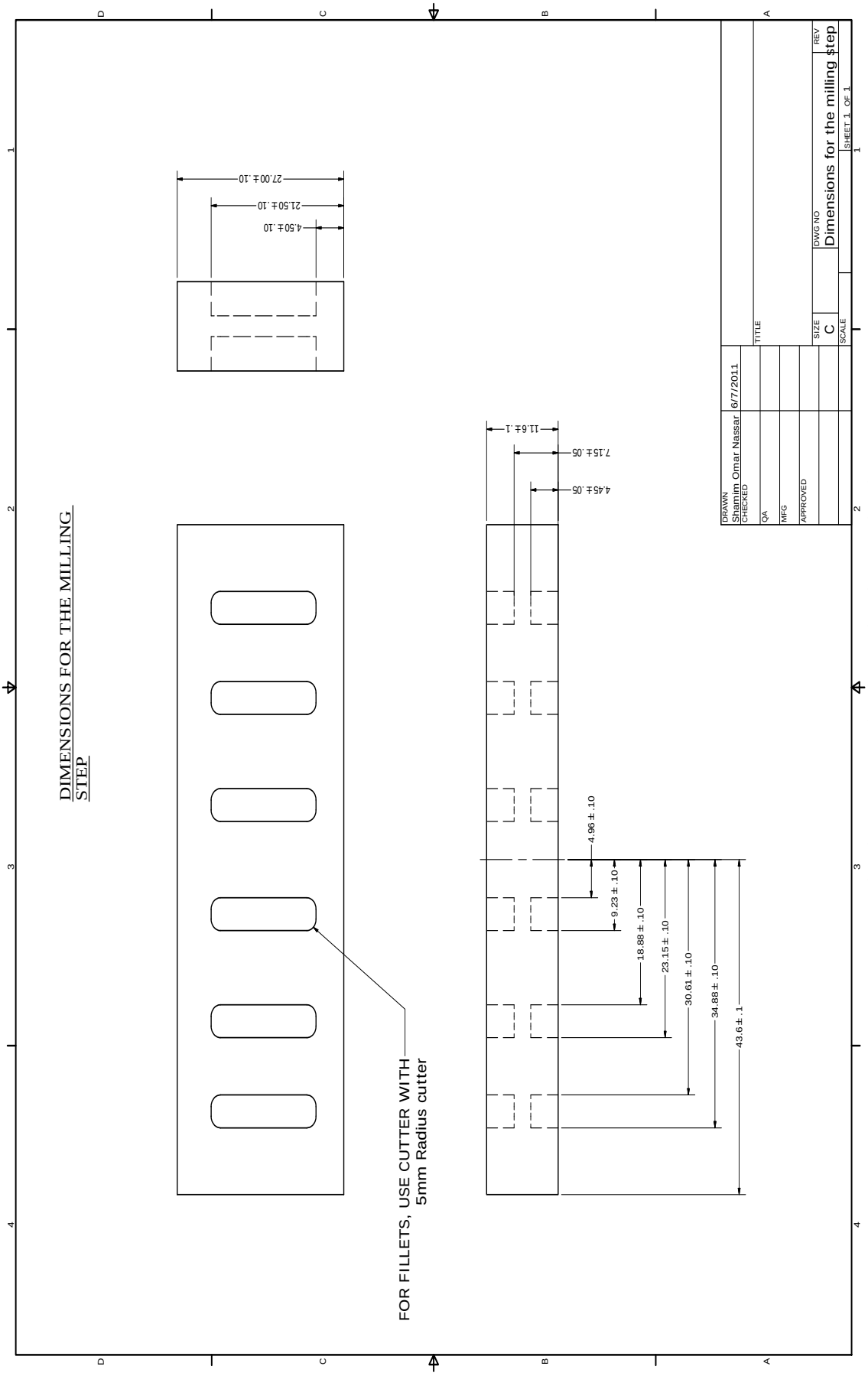

Figure A.20: 2.125GHz Combline Filter Dimensions for Milling Step

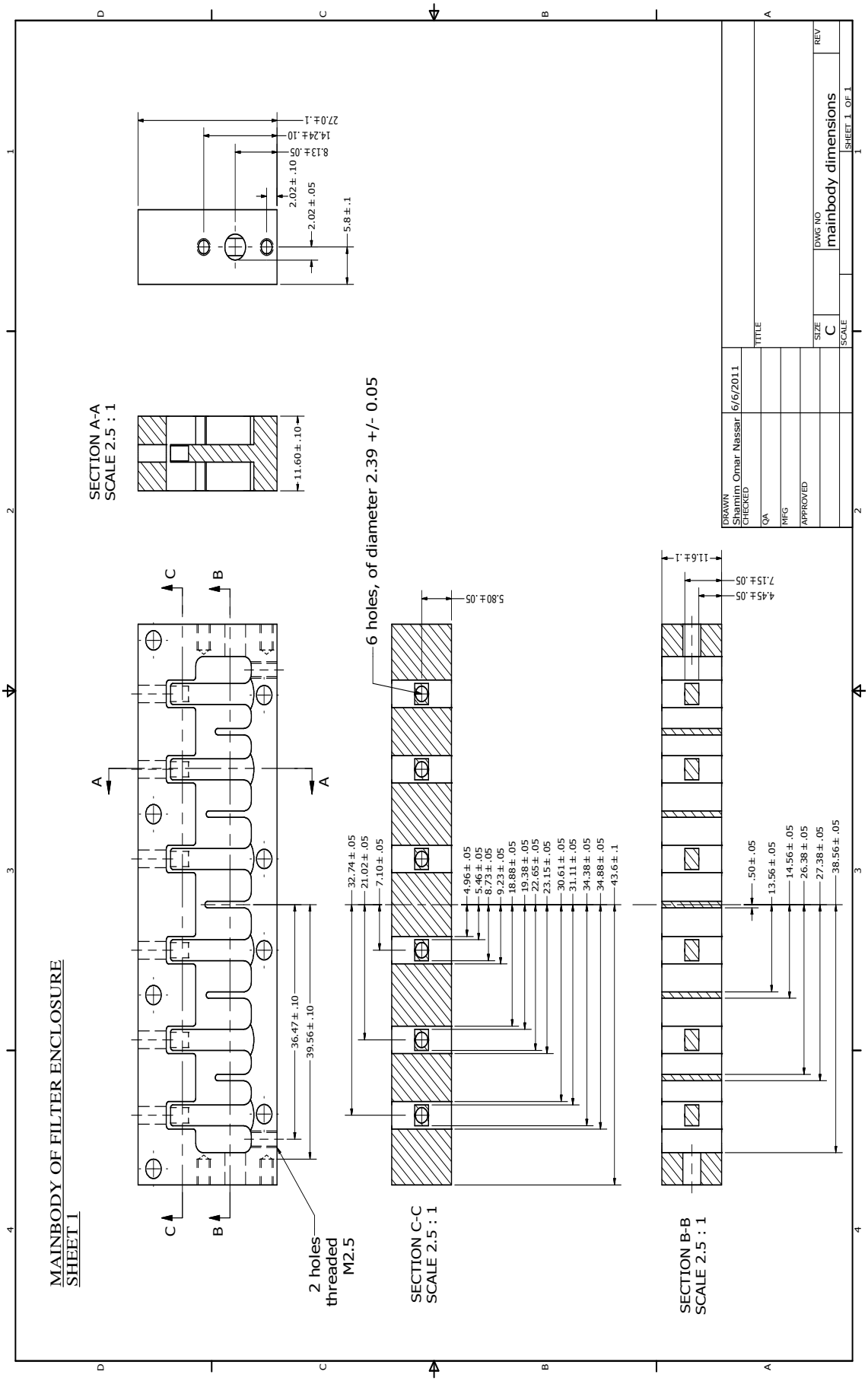

Figure A.21: 2.125GHz Combline Filter Main Body Dimensions - Sheet 1

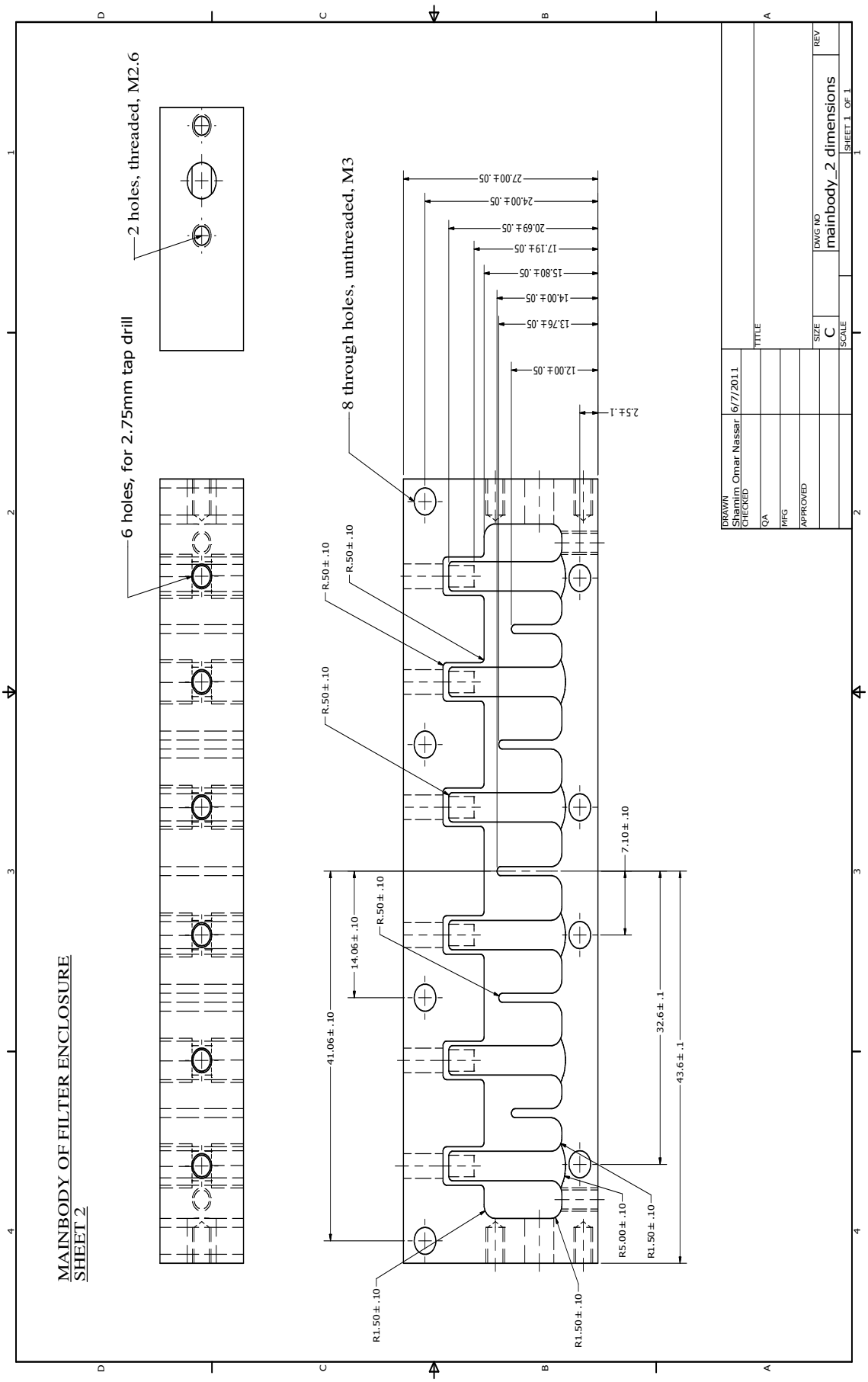

Figure A.22: 2.125GHz Combline Filter Main Body Dimensions - Sheet 2

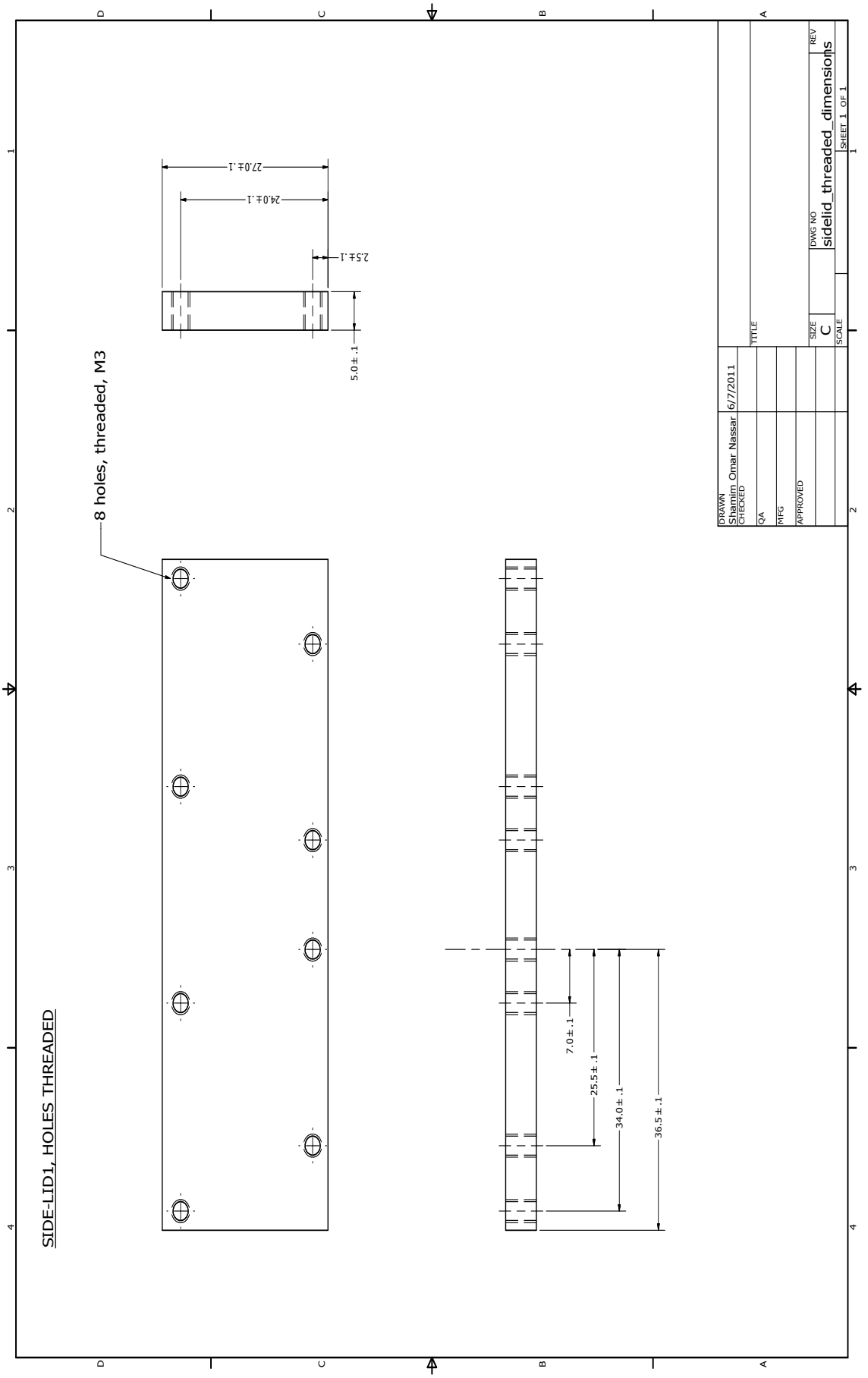

Milling

Figure A.23: 2.125GHz Combline Filter Sidelid Dimensions with Threaded Holes

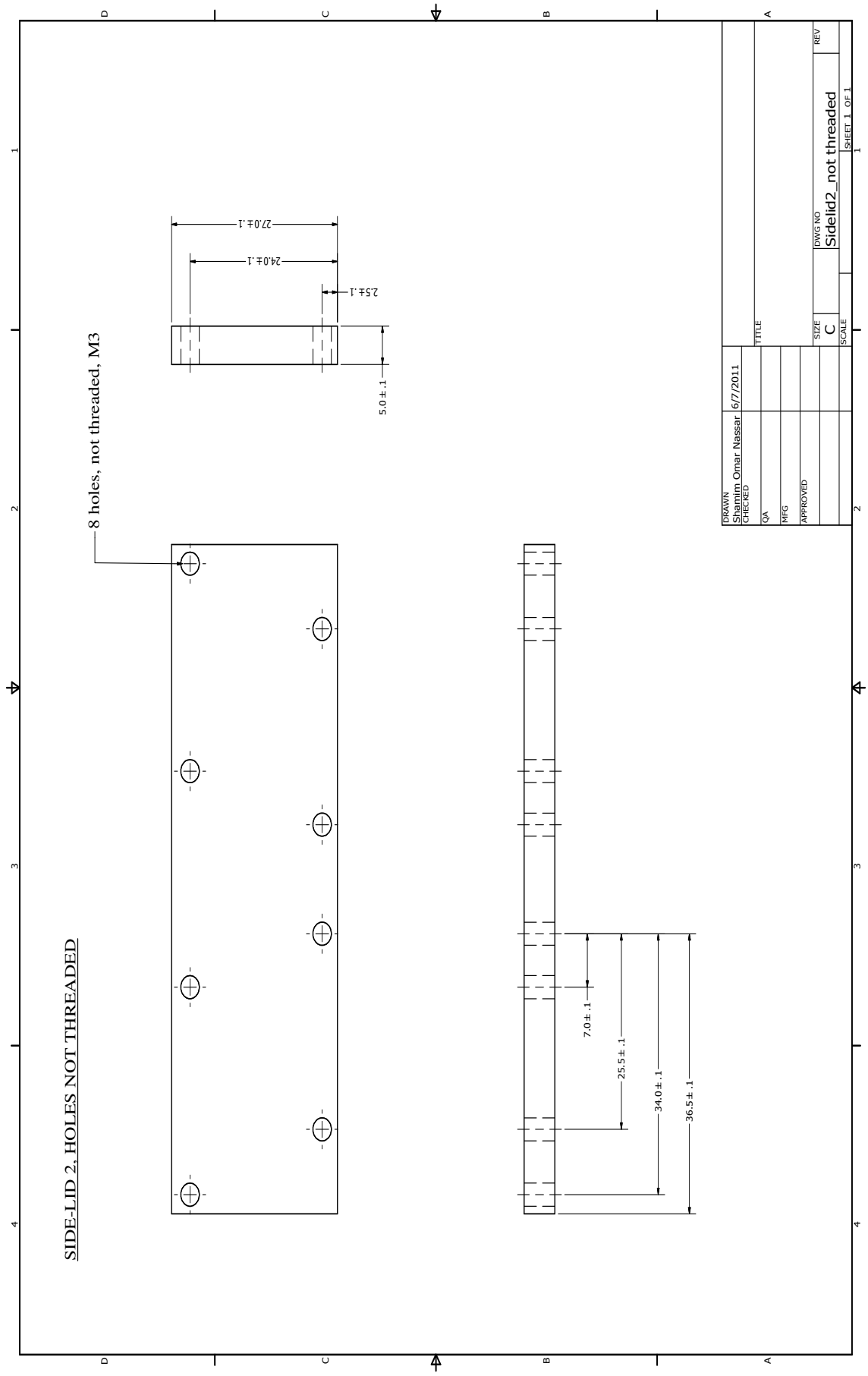

Figure A.24: 2.125GHz Combline Filter Sidelid Dimensions with Unthreaded Holes

Appendix B

Waterjet Cutting

Waterjet cutting refers to a process that uses a high pressure stream of water forced through a small hole (typically called the "*orifice*" or "*jewel*") to concentrate an extreme amount of energy in a small area, hence cutting through a piece of material. *Abrasive waterjet cutting* is a subcategory of waterjet in which abrasive is introduced to enhance the material removal rate and to increase the cutting speeds during the process.

Waterjet cutters can work with a wide variety of materials because they cut using water and abrasive. Some of these materials include: Copper, brass, aluminum, pre-hardened steel, mild steel, exotic materials such as titanium, Inconel and stainless steel.

Some of the advantages associated with the process are: Fast setup and programming, little fixturing for most parts and almost no heat generated on your part. The process also allows for the machining of thick material up to 4" (10 cm) [66]. However, the thicker the material, the longer it will take to cut. Parts made from material twice as thick take more than twice as long to cut. Some companies make low tolerance parts out of metal that is up to 5" to 10" thick (12.5 cm-25 cm), but it takes a long time and tends to be an occasional operation. Typically, most waterjet parts are made from metal that is 2" (5 cm) or thinner [66]. The process is also generally very safe; one of the largest hazards is cuts from the sharp edges of material created by the waterjet. Otherwise, water itself is safe and non-explosive and the abrasive is inert and non-toxic. Generally, a leak in a high-pressure water system tends to result in a rapid drop in pressure to safe levels [66].

During the process of abrasive waterjet cutting, a thin stream of water leaves the jewel and then the abrasive is added to the the stream and mixed to it; the high-velocity water exiting the jewel creates a vacuum which pulls abrasive from the abrasive line, which then mixes with the water in the mixing tube. The beam of water accelerates abrasive particles to speeds fast enough to cut through much harder materials. A diagram of an abrasive waterjet nozzle is shown below in figure B.1.

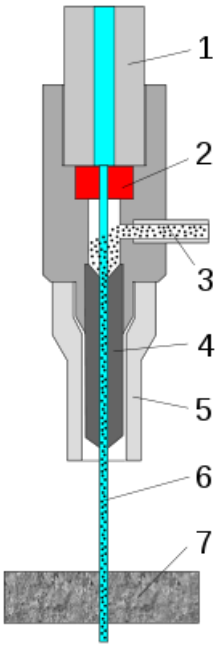

Figure B.1: Abrasive Waterjet Nozzle [66]

The cutting action of an abrasivejet is in two steps. First, the force of the water initially pierces the material while the jet is stationary and then abrasive erodes the material. In the second step the abrasivejet stream is moved across the material enhancing the cutting action. The ideal speed of movement depends on a variety of factors such as the material, the shape of the part, the water pressure and the type of abrasive used. For efficient and economical machining, it is crucial to control the speed of the abrasivejet nozzle during the process.

The level of accuracy associated with waterjet cutting is dependent on the speed with which the material is cut; a great detail of accuracy with very smooth edges can be achieved or a lower level of accuracy with rougher edges. New technology allows Abrasive jets to obtain tolerances of up to +/-.003" (0.075mm) or better [65, 66].If the tolerances required for your application are low, cutting speeds may be greatly increased to save money. Figure B.2 below shows different surface textures than can be obtained during the process depending on the cutting speed used.

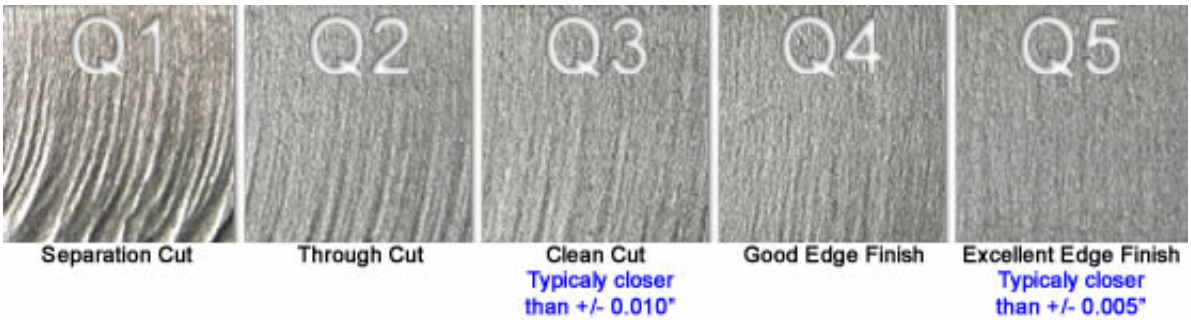

Figure B.2: Variation of surface finish due to different cutting speeds during waterjet cutting

Some of the advantages that waterjet cutting has over over wirecutting EDM are [66]:

Faster Abrasive jets are much faster than EDM, which slowly removes the metal.

- Can work with more materials.
- Waterjets can machine non-conductive materials that EDM cannot.
- Uniformity of material not important; a waterjet will retain much of its cutting power over uneven material.

- Waterjets make their own pierce holes; with wire-cut EDM, a hole needs to be first made in the material, which has to be done in a separate process.
- Waterjets do not change the properties of the material.
- Waterjets require less setup.

Its advantages over milling include [66]:

- The setup and fixturing with waterjets is much simpler.
- Waterjets can machine almost any material, including brittle materials, pre-hardened materials, and otherwise difficult materials such as Titanium, Hastalloy, Inconel, SS 304, and hardened tool steel.
- With a waterjet, there is also no tool changing.

Waterjets are frequently used for complimenting or replacing milling operations. They are used for roughing out parts prior to milling, for replacing milling entirely, or for providing secondary machining on parts that just came off the mill. For this reason, many traditional machine shops are adding waterjet capability to provide a competitive edge.

Appendix C

MWO Circuits for Chapter 6 Filters

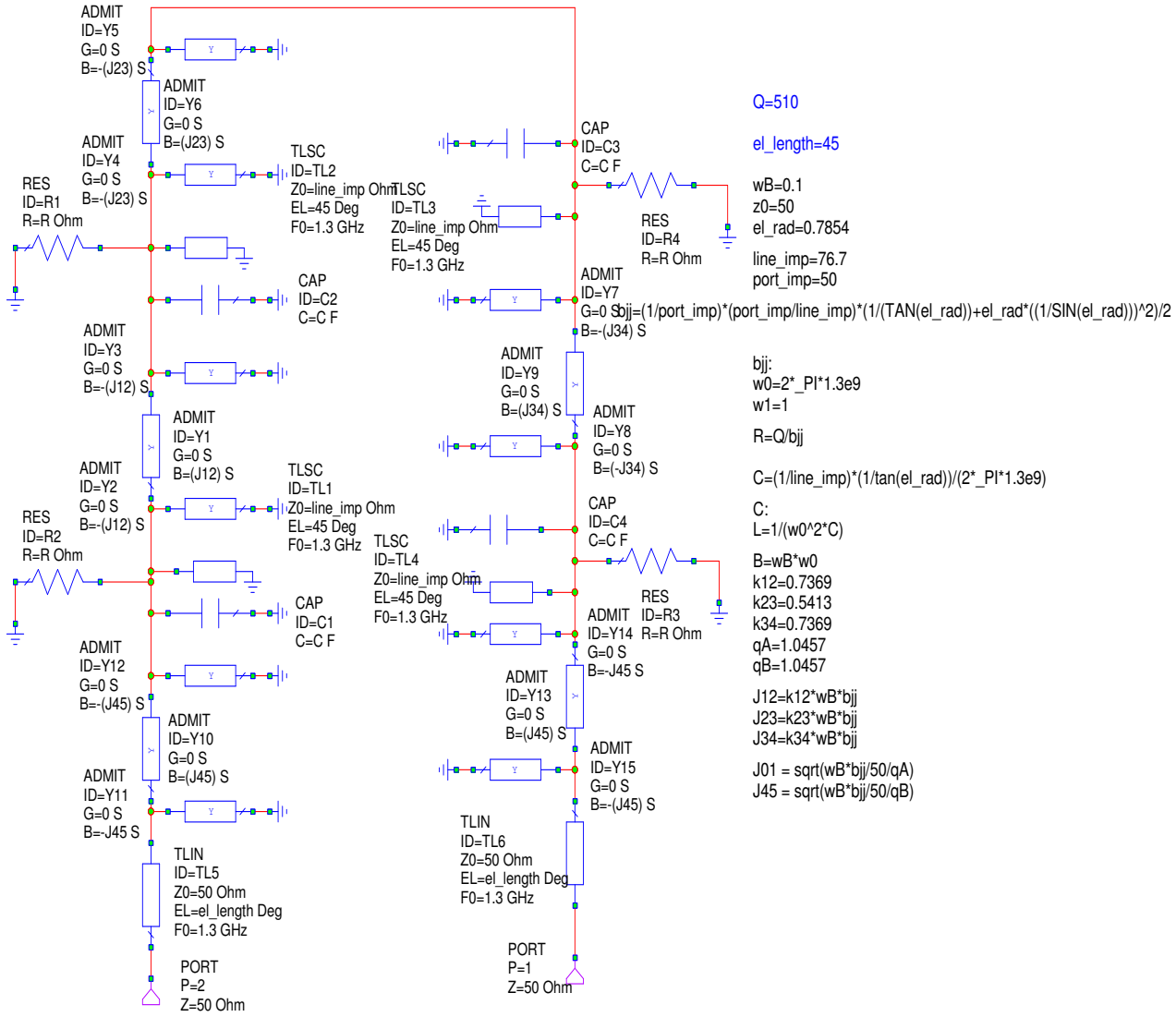

Figure C.1: 1.3 GHz 4th Order Chebyshev Filter

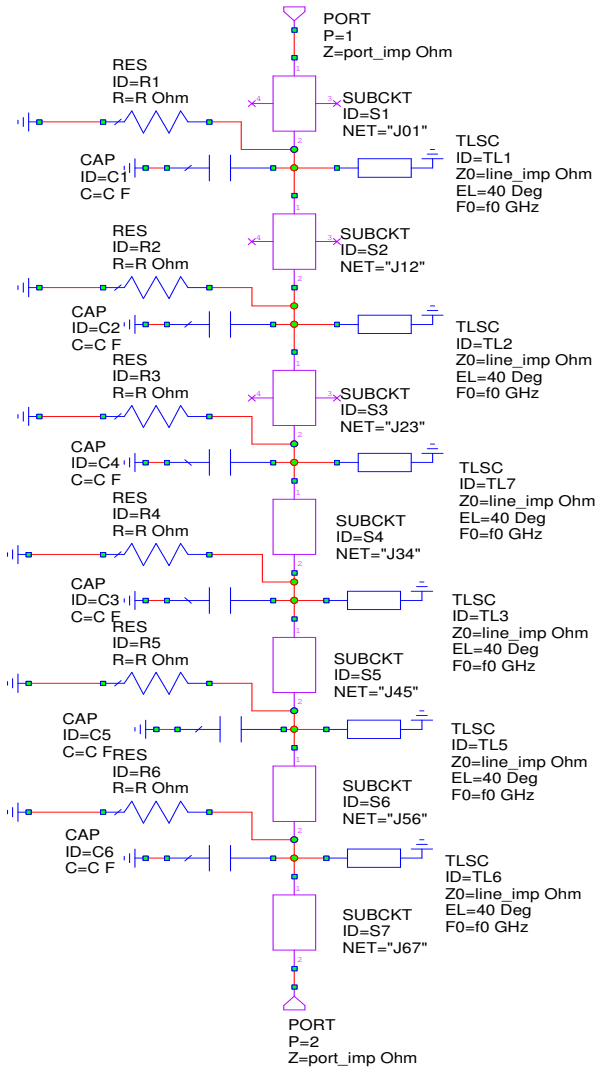

Q=800

el_radians=0.6981

line_imp=76.7
port_imp=50
f0=2.125
w0=2*_PI*f0*10^9
w1=1
wB=0.0188

A=(1/(TAN(el_radians))+el_radians*((1/SIN(el_radians)))^2)/2

bjj=(1/port_imp)*(port_imp/line_imp)*A

R=Q/ bjj

C=(1/line_imp)*(1/TAN(el_radians))/w0

L=1/(w0^2*C)

k12=0.8088
k23=0.55
k34=0.5177
k45=0.55
k56=0.8088

qA=0.9372
qB=0.9372

J01 = sqrt(wB*bjj/50/qA)
J12=k12*wB*bjj
J23=k23*wB*bjj
J34=k34*wB*bjj
J45=k45*wB*bjj
J56=k56*wB*bjj
J67 = sqrt(wB*bjj/50/qB)

Figure C.2: 2.125 GHz 6th Order Chebyshev Filter